Technische Universität München

Fakultät für Luftfahrt, Raumfahrt und Geodäsie

Lehrstuhl für Astronomische und Physikalische Geodäsie

Self-calibration of time-based localization systems in noisy environments with nonlinear optimization

Juri Sidorenko

Vollständiger Abdruck der von der Fakultät für Luftfahrt, Raumfahrt und Geodäsie der Technischen Universität München zur Erlangung des akademischen Grades eines

Doktor-Ingenieurs (Dr.-Ing.)

genehmigten Dissertation.

Vorsitzender:	Prof. Dr.-Ing. Uwe Stilla
Prüfer der Dissertation:	1. Prof. Dr.phil.nat. Urs Hugentobler
	2. Prof. Dr.rer.nat. Christian Schindelhauer
	3. Prof. Dr.-Ing. Johann Dambeck

Die Dissertation wurde am 25.09.2020 bei der Technischen Universität München eingereicht und durch die Fakultät für Luftfahrt, Raumfahrt und Geodäsie am 11.02.2021 angenommen.

"Scientific knowledge is a body of statements of varying degrees of certainty -- some most unsure, some nearly sure, none absolutely certain." — Richard P. Feynman

Abstract

Self-calibration is the ability of a measurement system to estimate system parameters without additional hardware. This can be the unknown coordinates of the positioning system or a fixed runtime delay caused by the hardware. The self-calibration is usually less time-consuming than manual calibration, does not require any additional measuring devices and can be performed during regular operations. This is not different with localization systems. The location of the reference stations must be known before the position of unknown station is estimated. A common mistake is that the position of the reference stations is not measured correctly, which leads to an incorrect position of the user receiver. This problem can be avoided by self-calibration. The only data required is the measurements themselves between the reference stations and the moving transponder. Therefore, no changes to the measurement technology are required. Self-calibration is a nonlinear non-convex problem, and the best solution is to use nonlinear optimization algorithms. The weak point of this solution is the risk to get trapped into a local minimum, if the initial parameters are unfavorable. Other not negligible aspects are errors caused by noise and outliers. Filtering requires transformation of the objective function in some cases. All of this must be taken into account to ensure robust self-calibration. This dissertation addresses the overall problem of the self-calibration for time-of-arrival (TOA) and time-difference-of-arrival (TDOA) based positioning systems. Real measurements are provided by two different positioning systems. In case of one system it is necessary to transform the raw measurements to apply pre-filtering. Two linear solutions are developed, which are able to use the pre-filtered data. The other positioning system does not require a transformation, but the precision of this system is affected by the received signal power and the clock drift. These effects are discussed in detail and compensated by two patents. It was shown that the signal power error can be obtained by self-calibration and the clock drift error by time stamp differences. The developed TOA and TDOA techniques are able to use these correction methods. In addition to the classical self-calibration, an alternative optimization is presented, in which the position of the transponders is obtained by the linear solutions in every iteration. Thereby the only optimized parameters are the coordinates of the reference stations. An important part of the dissertation deals with the dimension lifting and the proof that the additional dimension transforms the local minimum to a saddle point for non-trivial configurations. The proof only applies if the position of the reference stations are known. However, this approach has also a high impact on the TOA and TDOA self-calibration and reduces the risk to get trapped into a local minimum significantly.

Zusammenfassung

Unter einer Selbstkalibrierung wird die Fähigkeit eines Systems verstanden, unbekannte Parameter ohne die Zuhilfenahme externer Messinstrumente zu bestimmen, verstanden. Dabei ist der erforderliche Zeitaufwand im Vergleich zu manuellen Methoden geringer.

Im Bereich der Positionsbestimmung wird die Selbstkalibrierung unter anderem dazu verwendet, die Positionen der Referenzstationen zu bestimmen. Eine Änderung des regulären Messablaufs für die Selbstkalibrierung ist nicht notwendig.

Die Selbstkalibrierung ist ein nicht-lineares, nicht-konvexes Problem, welches sich am besten mittels einer nicht-linearen Optimierung lösen lässt. Ein entscheidender Nachteil dieses Lösungsverfahrens stellt das Risiko dar, in ein lokales Minimum zu konvergieren. Dieses Problem tritt insbesondere dann auf, wenn die Anfangswerte ungünstig gewählt wurden.

Ein weiterer nicht zu unterschätzender Aspekt ist der Einfluss von Ausreißern auf die Selbstkalibrierung. Die Anwendung von Filtern wird in diesem Fall unerlässlich, was unter Umständen eine Transformation der Zielfunktion erfordert.

Die vorliegende Dissertation behandelt die Problemstellung der Selbstkalibrierung von Laufzeit (TOA) und Laufzeit-differenz (TDOA) basierten Positionierungssystemen mit dem Ziel der Anwendung in bereits existierenden Systemen.

Die hierfür herangezogenen Positionierungssysteme wurden im Detail untersucht. Es stellte sich heraus, dass für ein System die Zielfunktion transformiert werden musste, um eine Vorfilterung zu realisieren. Das zweite Positionierungssystem erforderte keine Transformation, die Messungen sind jedoch unterschiedlichen Einflüssen, wie etwa der empfangenden Signalstärke, unterworfen. Diese Effekte werden im Weiteren analysiert und mittels einer eigens entwickelten und patentierten Selbstkalibrierung kompensiert.

Die Selbstkalibrierung der Referenzstationen wird in dieser Arbeit mit einer erweiterten und reduzierten Anzahl an Freiheitsgraden durchgeführt. Im Rahmen der Forschungsarbeit wird analytisch nachgewiesen, dass eine zusätzliche Dimension im Falle von bekannten Referenzstationen das lokale Minimum in einen Sattelpunkt umwandelt. Bei unbekannten Referenzstationspositionen wird das Risiko der Konvergenz in ein lokales Minimum durch die zusätzliche Dimension deutlich reduziert.

Structure

The dissertation is structured as follows. The first section describes the introduction and the second section describes the previous work. In the third section, the framework developed for both positioning systems is discussed. The fourth section contains a brief summary of each publication and highlights the key results. This section concludes with the remaining open questions and suggestions for further work. The functionality of the developed frameworks is explained in the appendix.

Contents

1. Introduction **15**
- 1.1. Taxonomy . . . 15
- 1.2. Techniques . . . 17
- 1.3. Self-calibration . . . 18
- 1.4. Scientific questions . . . 19

2. Preparation and state of the art **27**
- 2.1. Local Position Measurement system (LPM) . . . 27
- 2.2. DecaWave ultra-wideband (UWB) . . . 28
- 2.3. Self-calibration . . . 29

3. Methodology **31**
- 3.1. Local Position Measurement (LPM) . . . 31
- 3.2. Decawave UWB . . . 37

4. Content of publications **41**
- 4.1. P-I: Multilateration of the Local Position Measurement . . . 43
- 4.2. P-II: Improved linear direct solution for asynchronous radio network localization (RNL) . . . 54
- 4.3. P-III: Decawave UWB clock drift correction and power self-calibration 64
- 4.4. P-IV: DecaWave ultra-wideband warm-up error correction . . . 83
- 4.5. P-V: Error corrections for ultra-wideband ranging . . . 95
- 4.6. P-VI: Improved Time of Arrival measurement model for non-convex optimization . . . 109
- 4.7. P-VII: Improved Time of Arrival measurement model for non-convex optimization with noisy data . . . 123
- 4.8. P-VIII: Self-calibration for the time-of-arrival positioning . . . 130
- 4.9. P-IX: Self-Calibration for the Time Difference of Arrival Positioning . 141

5. Conclusions and outlook **159**
- 5.1. Conclusions . . . 159
- 5.2. Open questions . . . 160
- 5.3. Further work . . . 161

Acknowledgments **163**

A. Appendix **165**
A.1. GUI of the Local Position Measurement (LPM) 165
A.2. GUI of the Decawave UWB 169

Bibliography **173**

List of Abbreviations

Abbreviation	Explanation
AoA	Angle of arrival
BS	Base stations
CIR	Channel impulse response
FMCW	Frequency modulated continuous wave
GNSS	Global navigation satellite system
GUI	Graphical user interface
INS	Inertial navigation systems
LDE	Leading edge detection
LPM	Local position measurement
MCU	Microcontroller unit
MDS	Multidimensional scaling
ML	Maximum likelihood
NLOS	Non line of sight
PLL	Phase locked loop
RANSAC	Random sample consensus
Ref. S.	Reference station
RF	Radio frequency
RNL	Radio network localization
RSSI	Received signal strength indication
RX	Receiver
SCAPE	Self calibration and position estimation
SDP	Semi-definite programming
SPI	Serial peripheral interface
TCP	Transmission control protocol
TDOA	Time difference of arrival
TOA	Time of arrival
TWR	Two way ranging
TX	Transmitter
UDP	User datagram protocol
UWB	Ultra-wideband
WLAN	Wireless local area network

1. Introduction

In the last century, navigation systems have became omnipresent and universally useful in nearly every aspect of the daily life. Position estimation with respect to a reference system facilitates the exploration and cartography of our planet. Long before artificial navigation systems like satellites dominated the global navigation, seafarers used celestial bodies to navigate their ships for exploring and discovering our planet. The navigation was as good as the knowledge about the position of the reference target, like the stars or satellites. Nowadays, the reference systems are mostly artificial with the ability to change their position. This leads to the requirement that the new position of the reference system can be obtained quickly and precisely. This process must always be viewed in the context of the used localization system and the measurement technique.

1.1. Taxonomy

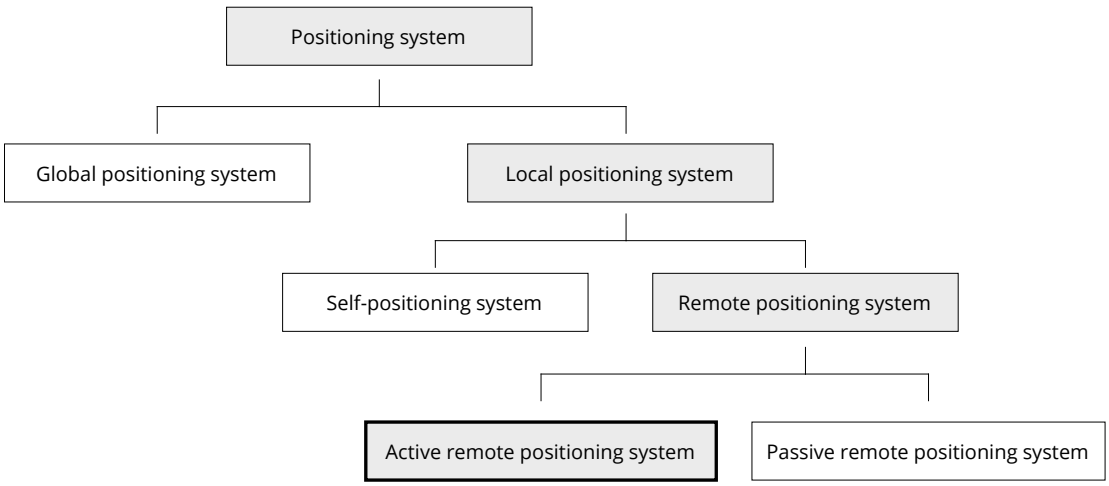

Figure 1.1.: Classification of the positioning system

Positioning as shown in Figure 1.1 can be classified into global and local positioning. Global positioning systems enable a mobile device to find its own position on the globe [1, 2]. Local positioning systems provide only location information and can be

classified into so-called self- and remote positioning systems. With self-positioning, the position is obtained with respect to a static point. An example of these systems is the inertial navigation systems (INS), which measure position changes. A remote positioning system provides a relative position with respect to external references. Depending on the extent to which the device to be localized is involved in the positioning, one speaks of active and passive remote positioning systems. In the last case, a passive remote positioning system often uses cameras or radar to determine the position of an object. In this work, we only deal with active remote positioning systems, where the system to be located is actively involved in determining the position. Some technical terms have a very specific meaning while others are often used as a synonym. In classical navigation, a distinction is made between stations at a known position and stations at an unknown position. Those at a known position are often referred to as base stations or anchors. The stations to be localized are called tags. Figure 1.2 presents an example of a typical active remote positioning system. The base stations BS 1, BS 2 and BS 3 are the reference targets. The unknown position of the tag is obtained with respect to three stations. Time synchronization is required in some areas of application. In practice, this is often achieved with an additional station which is referred to as a designated reference station. If the clocks are to be synchronized or the frequency difference is to be corrected in later sections of this work, the reference station is the time reference for all other stations. Not all stations have the ability to transmit data. If the base stations only receive and the tag only sends, then the base stations are referred to as receivers and the tag is a transmitter. If a station can send and receive, one speaks of a transceiver.

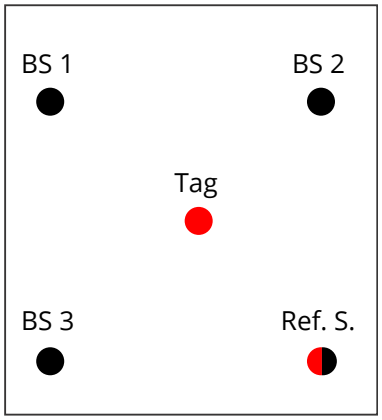

Figure 1.2.: Example for an active remote positioning system. The base stations (BS) have back dots, the tag a red dot and the reference station (Ref. S.) a mix of both colors.

1.2. Techniques

In contrast to optical positioning, radio frequency (RF) based systems are not affected by the visibility conditions and are therefore suitable for different non-line-of-sight (NLOS) applications, like imaging through walls [3]. In contrast, RF-based systems are more affected by interferences, also called fading, multipath and outliers [4, 5]. This leads to the necessity to develop robust filters, which are able to reduce the effect of noise and outliers. The used hardware does not only define the sensitivity of the system, but also the possibilities to use different measurement techniques like Time-of-Arrival (TOA) , Time-Difference-Of-Arrival (TDOA) , Angle-of-Arrival (AoA) [6] or Received Signal Strength Indicator (RSSI) [7, 8]. The most common measurement techniques that can be found in practice due to their high accuracy are TOA and TDOA. In the first measurement technique TOA, the absolute signal propagation time between the tag and the base stations is measured. This is depicted in the left plot of Figure 1.3. In combination with the known signal propagation speed in the medium, it is possible to calculate the distances D1, D2 and D3. The location of the tag corresponds to the coordinates, where the distance measurement equates the Euclidean norm between the three base stations BS1, BS2 and BS3 with respect to the tag. Geometrically speaking for the two-dimensional case, the tag is located at the intersection of the three circles, which represent the Euclidean distances between the tag and the base stations. In the three-dimensional case, one more base station is required to obtain a unique intersection between the spheres. Until now, it was assumed that the base stations and the tag are sharing the same time, which means that they are synchronized. In the case of NAVSTAR GPS, which is also based on the TOA measurement technique, the satellite are synchronized by atomic clocks [1, 2]. This does not apply to the receiver on the ground. Therefore, an additional satellite is required to determine the synchronization error between the satellites and the ground receiver. This is the reason why in satellite navigation, the distance measurement is not addressed as range but as pseudo range [1].
The synchronization of the base stations and the tag can also be avoided for TOA by using two-way-ranging (TWR) [9]. Thereby, the tag is not passive anymore, but responds to the signal of the base stations.
The location of the tag can only be obtained after all the distance measurements between the tag and the base stations are known. With an increasing number of stations the update rate decreases as more measurements are performed with more stations, provided that the measurements cannot be carried out in parallel and that the tag did not move significantly during the acquisition phase. A solution to this problem is provided by the TDOA measurement technique. In contrast to TOA, it uses the differences of the signal propagation times. While TOA does not require that the tag has to emit the signal, this changes with TDOA. The base stations are receiving the emitted signal without transmitting a response signal to the tag. The difference of the arrival time at the base stations, indicates the position of the tag.

The calculated distance difference for two base stations is constant on a hyperbola. This is shown in the right plot of figure 1.3. The intersection point of two hyperbolae defines the position of the tag in a two dimensional space.

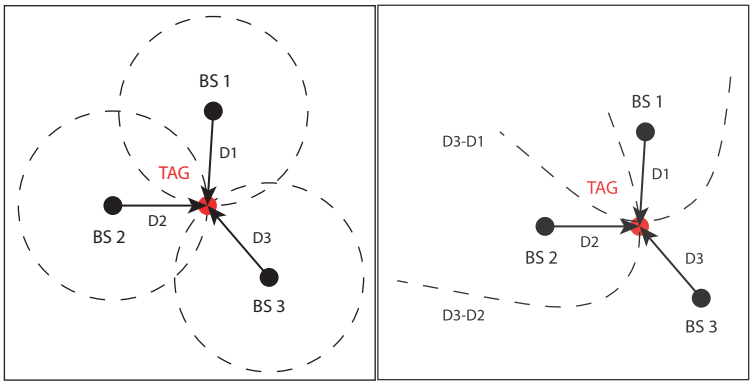

Figure 1.3.: Left plot: TOA. Right plot: TDOA. Distances between the base stations (back dots) and tag (red dot) have the notation D1, D2 and D3.

1.3. Self-calibration

Ground based localization systems like the Local Position Measurement (LPM) [10] use external localization systems to provide the location of the reference system.

In outdoor applications, satellite based systems are most frequently employed for the calibration of the LPM system, and laser distance measurements are used for indoor applications. These calibration methods have the disadvantage that the calibration relies on the accuracy of the external system. In general, the external systems should have a higher accuracy than the system to be measured. Alternatively, a so-called self-calibration method can be used to obtain the unknown parameters and geometrical configuration of the localization system, without additional measurement equipment. This method can be applied if the system of equations is determined or over-determined.

In many applications, as with the LPM system, it is not possible to obtain measurements between the base stations. This is mostly due to the fact that the main purpose of the hardware is to provide the unknown tag position. Therefore, the base stations are mostly passive and fixed at a certain location without a line of sight to each other. Figure 1.4 shows how one moving tag can be used for self-calibration while the base stations remain at their positions. The only available measurements are the distances between the base stations and the tag. With every position change, the amount of unknown variables increases by the coordinates of the new tag location. At the same time, the number of equations increases by the number of distance measurements. After a sufficient number of position changes and a minimum amount of base stations, it is possible to obtain a system of equations

that is solvable.
The path of the tag plays an important role for the self-calibration [11]. If the base stations positions differ along the z-axis but the tag movement taken place in a horizontal plane, then it is not possible to determine the vertical coordinate of the base station. It is not possible to obtain the coordinate of the base station in one specific dimension, if the tag is moving on a plane orthogonal to this dimension.

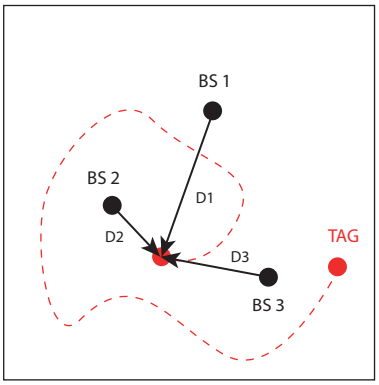

Figure 1.4.: TOA self-calibration

The objective functions for the TOA and TDOA self-calibration are non-linear, hence it is just natural to use non-linear solvers. This decision has the advantage that non-linear optimization is the most robust solution with missing data, outliers and noise [12]. On the other hand, non-linear optimization leads to two weaknesses. The first issue deals with the unknown initial estimates and this leads to the second problem, the convergence to a local minimum [13, 14, 15, 16]. The aim of this thesis is the development of a method, which is able to perform a non-linear TOA/TDOA self-calibration with real measurements. The constellation of the stations found can have any rotation or translation. The absolute coordinates require that the coordinates of at least two stations in the absolute coordinate system are known.

1.4. Scientific questions

The task of performing a self-calibration for the selected hardware with real measurements leads to the following scientific questions.

Questions based on the LPM system

- Q^1_{LPM}: Is it possible to pre-filter the LPM measurements?
- Q^2_{LPM}: Is there a closed-form solution with pre-filtered LPM measurements for the cases that base station positions are known?

Questions based on the Decawave UWB system

- Q^1_{UWB}: Can the UWB signal power correction be obtained by self-calibration?
- Q^2_{UWB}: Does the UWB clock drift error depend on on the signal power error? If so can it be obtained alternatively?
- Q^3_{UWB}: Is it possible to obtain TDOA measurement for the UWB without the offset?

Questions based on the TOA/TDOA self-calibration

- Q^1_{Self}: Has an additional dimension in the $l_2$norm an effect on the local minimum with known base stations?
- Q^2_{Self}: Which effect has the noise on the additional dimension?
- Q^3_{Self}: Has an additional dimension an effect on the TOA self-calibration?
- Q^4_{Self}: Has an additional dimension an effect on the TDOA self-calibration?
- Q^5_{Self}: Does it make sense to only adjust the positions of the base station and derive the location of the tag from it?
- Q^6_{Self}: Has the additional dimension an effect on the answer of the question Q^5_{Self}?
- Q^7_{Self}: How many measurements should be used for the self-calibration?

Publications

The publications P-III, P-V, P-VII, P-VIII are journal publications and P-I, P-II, P-IV, P-VI are conference publications. All of them are peer-reviewed. The notations of the first publication P-I were adjusted to fit the notation of the second publication P-II.

P-I

J. Sidorenko, N. Scherer-Negenborn, M. Arens and E. Michaelsen.
Multilateration of the Local Position Measurement. 2016 International Conference on Indoor Positioning and Indoor Navigation (IPIN), Alcala de Henares, Spain, Oct. 2016, pp. 1-8, DOI: 10.1109/IPIN.2016.7743625.

The Local Position Measurement system (LPM) is one of the most precise systems for 3D position estimation. It is able to operate in- and outdoor and updates at a rate of up to 1000 measurements per second. Previous scientific publications focused on the filtering

after the numerical position estimation. This paper investigates the advantages of the TOA over the time difference of arrival equation transformation (TDOA) and the signal smoothing prior to its fitting. The LPM was designed under the general assumption that the position of the base station and position of the reference station are known. The information resulting from this research can prove vital for the system's selfcalibration, providing data aiding in locating the relative position of the base station without prior knowledge of the transponder and reference station positions.

Keywords: time of arrival ✦ time-difference-of-arrival ✦ local position measurement.

P-II

J. Sidorenko, N. Scherer-Negenborn, M. Arens and E. Michaelsen.
Improved Linear Direct Solution for Asynchronous Radio Network Localization (RNL). Proceedings of the ION 2017 Pacific PNT Meeting, Honolulu, Hawaii, USA, May 2017, pp. 376-382, DOI: 10.33012/2017.15036.

The linear least square solution is frequently used in the field of localization. Compared to nonlinear solvers, this solution is more affected by noise but able to provide a position estimation without knowing any starting condition. The linear least square solution is able to minimize Gaussian noise by solving an overdetermined equation with the Moore-Penrose pseudoinverse. Unfortunately, this solution fails in the case of non-Gaussian noise. This publication presents a direct solution using prefiltered data for the LPM (RNL) equation. The input used for linear position estimation will not be the raw data but data filtered over time and for this reason this solution will be called the direct solution. It will be shown that the symmetrical direct solution presented is superior to the non-symmetrical direct solution and in particular to the non-prefiltered linear least square solution.

P-III

J. Sidorenko, V. Schatz, N. Scherer-Negenborn, M. Arens, U. Hugentobler.
Decawave UWB Clock Drift Correction and Power Self-Calibration. Sensors 2019, 19, 2942, DOI: 10.3390/s19132942

The position accuracy based on Decawave Ultra-Wideband (UWB) is affected mainly by three factors: hardware delays, clock drift, and signal power. This article discusses the last two factors. The general approach to clock drift correction uses the phase-locked loop (PLL) integrator, which we show is subject to signal power variations, and therefore, is less suitable for clock drift correction. The general approach to the estimation of signal power correction curves requires additional measurement equipment. This article presents a new method for obtaining the curve without additional hardware and clock drift correction without the PLL integrator. Both correction methods were fused together to improve two-way ranging (TWR).

Keywords: navigation ✦ time-of-arrival (TOA) ✦ ultra-wideband (UWB).

P-IV

J. Sidorenko, V. Schatz, N. Scherer-Negenborn, M. Arens, U. Hugentobler.
DecaWave ultra-wideband warm-up error correction. IEEE Transactions on Aerospace and Electronic Systems, DOI: 10.1109/TAES.2020.3015323.

In the field of indoor localization, ultra-wideband (UWB) technology is no longer dispensable. The market demands that the UWB hardware has to be cheap, precise and accurate. These requirements lead to the popularity of DecaWave UWB system. The great majority of the publications about this system, deals with the correction of the signal power, hardware delay or clock drift. It has traditionally been assumed that this error only appears at the beginning of the operation and is caused by the warm-up process of the crystal. In this article, we show that the warm-up error is influenced by the same error source as the signal power. To our knowledge, no scientific publication was the warm-up error explicit examined. This work aims to close this gap and, moreover, to present a solution which does not require any external measuring equipment and only has to be carried out once. It is shown, that the empirically obtained warm-up correction curve increases the accuracy for the two-way-ranging (TWR) significantly.

Keywords: Indoor localization ✦ two-way-ranging (TWR) ✦ DecaWave ✦ ultra-wideband (UWB).

P-V

J. Sidorenko, V. Schatz, N. Scherer-Negenborn, M. Arens, U. Hugentobler.
Fusion of time of arrival and time difference of arrival for ultra-wideband indoor localization. 2019 International Conference on Indoor Positioning and Indoor Navigation - Work-in-Progress Papers (IPIN-WiP 2019), Pisa, Italy, Sep. 2019, pp. 1-8.

Error corrections for ultra-wideband ranging. IEEE Transactions on Instrumentation and Measurement, DOI: 10.1109/TIM.2020.2996706.

Precise indoor localization is a major challenge in the field of localization. In this work we investigate multiple error corrections for the ultra-wideband (UWB) technology, in particular the DecaWave DW1000 transceiver. Both the time-of-arrival (TOA) and the time-difference-of-arrival (TDOA) methods are considered. Various clock-drift correction methods for TOA from the literature are reviewed and compared experimentally. The best performing method is extended to TDOA, corrections for the signal power dependence and the hardware delay are added, and two additional enhancements suggested. These are compared to each other and to TOA in positioning experiments.

Keywords: time-of-arrival (TOA) ✦ time-difference-of-arrival (TDOA) ✦ two-way-ranging (TWR) ✦ DecaWave ✦ ultra-wideband (UWB)

P-VI

J. Sidorenko, V. Schatz, L. Doktorski, N. Scherer-Negenborn, M. Arens, U. Hugentobler.
Improved Time of Arrival measurement model for non-convex optimization. Journal Institute of Navigation -ION: Online First, 25 pp. ISSN: 2161-4296 ISSN: 0028-1522, DOI: 10.1002/navi.277.

The quadratic system provided by the Time of Arrival technique can be solved analytically or by nonlinear least squares minimization. An important problem in quadratic optimization is the possible convergence to a local minimum, instead of the global minimum. This problem does not occur for global navigation satellite system (GNSS), due to the known satellite positions. In applications with unknown positions of the reference stations, such as indoor localization with self-calibration, local minima are an important issue. This article presents an approach showing how this risk can be significantly reduced. The main idea of our approach is to transform the local minimum to a saddle point by increasing the number of dimensions. In addition to numerical tests we analytically prove the theorem and the criteria that no other local minima exists for non-trivial constellations.

Keywords: time-of-arrival (TOA)✦ nonlinear optimization ✦ localisation ✦ navigation.

P-VII

J. Sidorenko, V. Schatz, N. Scherer-Negenborn, M. Arens, U. Hugentobler.
Improved Time of Arrival measurement model for non-convex optimization with noisy data. 2018 International Conference on Indoor Positioning and Indoor Navigation, Nantes, France, Sep. 2018, pp. 206-212, DOI: 10.1109/IPIN.2018.8533839.

The quadratic system provided by the Time of Arrival technique can be solved analytically or by nonlinear least squares minimization. In real environments the measurements are always corrupted by noise. This measurement noise affects the analytical solution more than nonlinear optimization algorithms. On the other hand it is also true that local optimization tends to find the local minimum, instead of the global minimum. This article presents an approach how this risk can be significantly reduced in noisy environments.

Keywords: localization ✦ navigation ✦ time-of-arrival (TOA)✦ nonlinear optimization.

P-VIII

J. Sidorenko, V. Schatz, D. Bulatov, N. Scherer-Negenborn, M. Arens, U. Hugentobler. **Self-calibration for the time-of-arrival positioning.** IEEE Access Journal, DOI: 10.1109/ACCESS.2020.2985353.

Self-calibration of time-of-arrival positioning systems is made difficult by the non-linearity of the relevant set of equations. This work applies dimension lifting to this problem. The objective function is extended by an additional dimension to allow the dynamics of the optimization to avoid local minima. Next to the usual numerical optimization, a partially analytical method is suggested, which makes the system of equations overdetermined proportionally to the number of measurements. Results with the lifted objective function are compared to those with the unmodified objective function. For evaluation purposes, the fractions of convergence to local minima are determined, for both synthetic data with random geometrical constellations and real measurements with a reasonable constellation of base stations. It is shown that the lifted objective function provides improved convergence in all cases, often significantly so.

Keywords: dimension lifting ✦ self-calibration ✦ time-of-arrival.

P-IX

J. Sidorenko, V. Schatz, D. Bulatov, N. Scherer-Negenborn, M. Arens, U. Hugentobler. **Self-Calibration for the Time Difference of Arrival Positioning.** Sensors 2020, 20, 2079, DOI: 10.3390/s20072079.

The time-difference-of-arrival (TDOA) self-calibration is an important topic for many applications, such as indoor navigation. One of the most common methods is to perform nonlinear optimization. Unfortunately, optimization often gets stuck in a local minimum. Here, we propose a method of dimension lifting by adding an additional variable into the l2 norm of the objective function. Next to the usual numerical optimization, a partially-analytical method is suggested, which overdetermines the system of equations proportionally to the number of measurements. The effect of dimension lifting on the TDOA self-calibration is verified by experiments with synthetic and real measurements. In both cases, self-calibration is performed for two very common and often combined localization systems, the DecaWave Ultra-Wideband (UWB) and the Abatec Local Position Measurement (LPM) system. The results show that our approach significantly reduces the risk of becoming trapped in a local minimum.

Keywords: dimension lifting ✦ self-calibration ✦ time-difference-of-arrival (TDOA).

Research questions answered by the publications

The following figure shows the relationship between the open questions and the publications. If the direction of the arrow points away from a publication, a question is answered. The arrows leading away from the questions are intended to illustrate how the knowledge gained from the publications was used for further work. This is to represent the chronological structure of the work. The chart can be divided into three areas. The first part deals with the Abatec LPM system, the second part with the DecaWave UWB system and the third part with the self-calibration of TOA and TDOA.

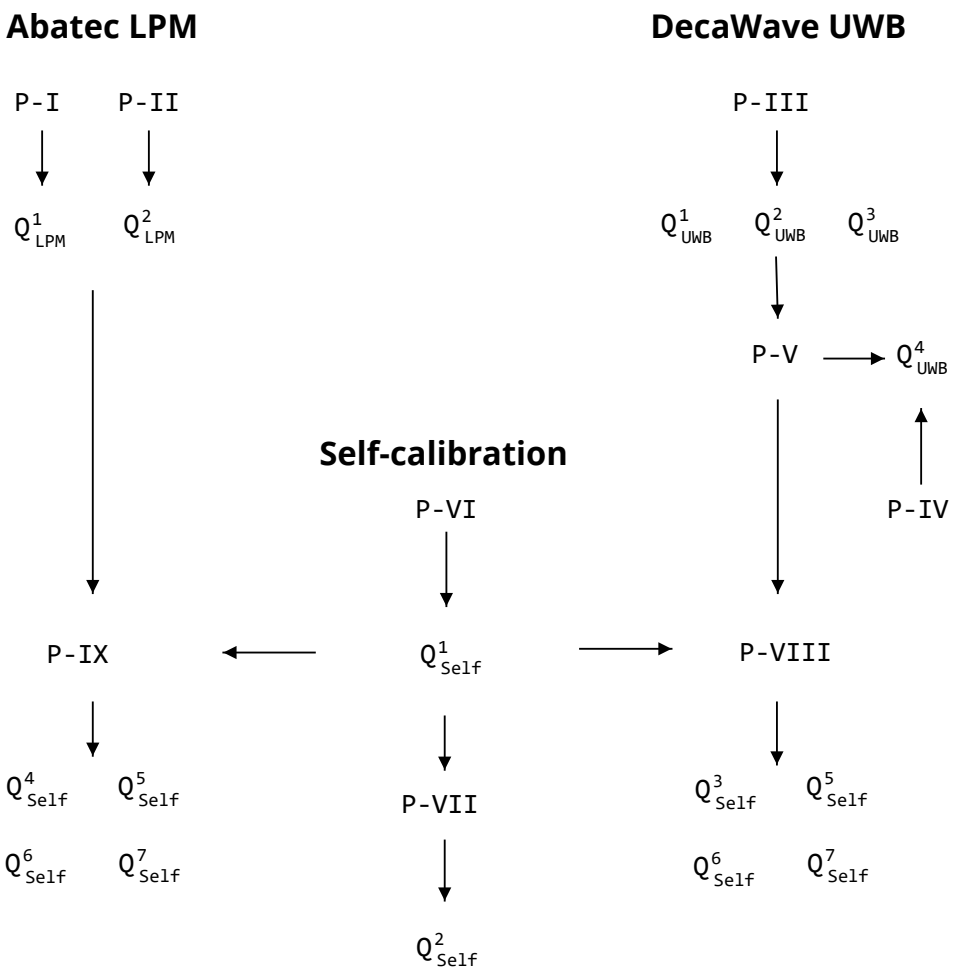

2. Preparation and state of the art

In the following, two localization systems are the subject of the investigation. Both systems are based on radio frequencies, with different measurement principles and objective functions. The Local Position Measurement system (LPM) is based on the TDOA measurement technique, while the UWB EVK1000 is able to operate with both measurements techniques TOA and TDOA.

2.1. Local Position Measurement system (LPM)

The LPM system was originally developed by inmotiotec GmbH, which belonged to the Abatec group. The LPM system is currently sold at https://inmotio.eu/technology/.

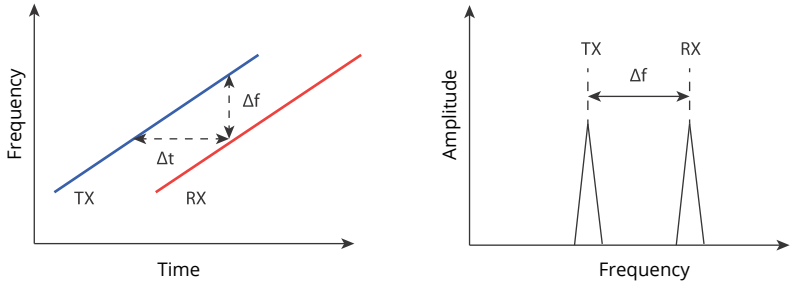

Figure 2.1.: LPM System

The LPM system uses a frequency chirp with a bandwidth of 150 MHz and a ramp duration of 500 μs on a frequency band with 5.725 GHz to 5.875 GHz [17]. In each step the transponder (TX) is emitting a signal with a certain frequency. The base stations are receiving the signal (RX) and comparing the received frequency with the internal frequency. The difference of both frequencies Δf in combination with the known slope of the chirp is equivalent to the time of flight between the transponder and the base station. This method is basically the extension of the frequency modulated continuous wave (FMCW) radar. Figure 2.1 shows the frequency chirp of the sending and receiving station. In practice analog mixers are used before the fast Fourier transformation (FFT) to produce a signal with a mean frequency $(f(TX) + f(RX))/2$ of the TX and RX frequency and the half of the frequency differences $(f(TX) - f(RX))/2$. This method allows using an analog to digital

converter with a smaller sampling rate after a low pass filtering. Until now it was assumed that the base stations are synchronized. The LPM solves the synchronization problem with an additional emitter station at a known position, so called reference station. More information about the specifics of the LPM system can be found in [18]. The main focus of the publications about the LPM are data filtering, sensor fusion and outlier detection [19, 20, 21]. The calibration of the system was performed by default with external measurement equipment without the possibility to use self-calibration.

2.2. DecaWave ultra-wideband (UWB)

The EVK1000 UWB transceivers used were developed by DecaWave limited. DecaWave has been wholly owned by Qorvo since 2020. The stations will continue to be distributed via https://www.decawave.com. Decawave offers a solution for the position self-calibration under the condition that the base stations are able to obtain the distances to each other. Otherwise external measurement equipment is necessary. The same applies for the antenna offset and signal power calibration.

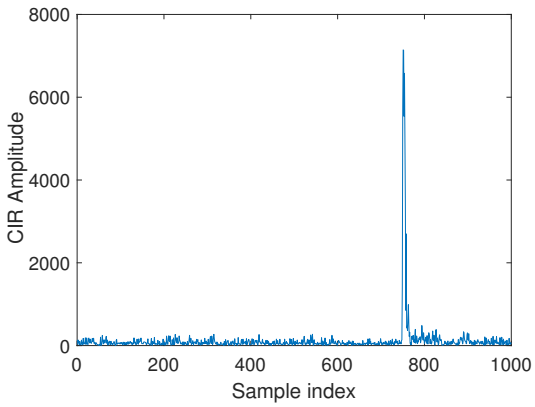

Figure 2.2.: UWB Impulse response

The measurement principle is based on the ultra wide-band (UWB) technology and is compliant with the IEEE802.15.4-2011 standard [22]. The EVK1000 supports six frequency bands from 3.5 GHz to 6.5 GHz with a bandwidth from 500 up to 1000 MHz, depending on the selected channel. The EVK1000 is using an estimation of the channel impulse response (CIR) to provide the time stamps. This estimation is obtained by correlating a known preamble sequence against the received signal and accumulating the result over a period of time. Figure 2.2 shows the output of the sampled signal. The sampling is performed by a 64 GHz chip with 15 ps event timing precision. The highest peak at 751 ns represents the direct path of the signal. In contrast to narrow band signals is UWB more resistant to fading, due to the low

probability that peaks from direct and reflected signals interfere with each other. The high bandwidth could disturb other radio frequency based signals, therefore the transmit power density is limited to -41.3 dBm/MHz.

2.3. Self-calibration

The ability to perform a time-based self-calibration has been the target of investigations for many years. From the theoretical point of view, it does not matter if the system is using acoustic, vision or radio frequencies to obtain the measurements as long as the objective functions are the same. The observations of our environment leads to models which allows us to predict the behavior of a system. The better the model predicts the reality the more it becomes non-linear. Therefore the general objective function for the self-calibration is non-linear. The solution which comes closest to the correct values in presence of Gaussian noise is the least square optimization [12]. Different non-linear optimization algorithms exist to provide an estimation of the correct solution. Global optimization algorithms are less suitable due to the amount of possible combinations, therefore local optimizations are the method of choice. Wendeberg et al. [23, 24] have used an iterative Cone Alignment algorithm to solve a non-linear TDOA self-calibration by a physical spring-mass simulation. TOA self-calibrations with Gauss-Newton optimization and a maximum likelihood (ML) estimator has been investigated in [25, 26]. R. Biswas and S. Thrun redefined the problem into a probabilistic model based on a Bayesian network and estimated the unknown constraints with a gradient descent algorithm [27]. All these approaches are based on non-linear optimization algorithms, with the risk to converge to a local minimum.

Therefore non-linear optimization algorithms are often used in combination with linear approximations of the model. Simplifications like an identical direction vector for all base stations also known as far-field approximation [28, 24] or that one base station position coincides with the position of one of the transponders [29, 30] are used to provide initial estimates. Other approaches are using linear equality and inequality constraints to transform the non-convex problem into a convex one with semi-definite programming (SDP) [26, 31]. Linear rank constraints in combination with nuclear norm minimization have been used to re-formulate the TDOA to a TOA problem in [32]. A non-iterative algorithm with rank constraints was presented in [33]. The transformation from TOA to TDOA has no effect on the error characteristics [34]. Multidimensional scaling (MDS) is also a very common method to obtain the initial estimates [14]. This technique was originally developed to process information contained in a distance matrix by non-linear dimension reduction [35]. Closed-form algebraic solutions for TOA self-calibration are the subject of the investigation in [36, 37, 30] and for TDOA self-calibration [38, 39, 37, 40, 41]. Some of these closed-form solutions are obtained by using the Groebner basis method [42] and the Macaulay2 software [43]. The disadvantage of this method is the necessity

to deal with polynomials of higher degrees.

In general analytical solutions are only valid for small noise conditions, due to the need to square the non-linear measurement equations [44]. The effect of dimension lifting [45, 46, 47] for the self-calibration has not been studied yet. The additional variable introduced by dimension lifting should not be confused with a slack variable or the time offset, especially because it is part of the l_2 norm. The only publication about the self-calibration, which was dealing with the effect of dimensions, was [48]. However, the topic was not the effect of an additional dimension to reduce the possibility to convert to a local minimum but the difference in dimensions between the affine subspaces spanned by the base stations and transponders.

3. Methodology

At the beginning of the scientific investigation it was necessary to develop a framework, which is able to provide real measurement data. This section intends to close the gap between the theoretical concepts discussed in the publications and the practical implementation. The development of the software for the sensors and the PC (ground station) was done with the programming language C and C++.

In addition to the computational algorithms was a Graphical User Interface (GUI) designed to simplify the communication between the ground station and the sensors. The interface, network and the thread management was performed by the QT library.

All measurements obtained by the ground station have been logged and analyzed with MATLAB.

3.1. Local Position Measurement (LPM)

The LPM system is using Wireless Local Area Network (WLAN) to exchange information between the base stations and the ground station. It allows the user to connect with a regular personal computer to the LPM-server, which broadcast the information to other stations. The ground station is the station where all data come together and where evaluation takes place. The user communicates with the LPM server via the ground station. The company software 'LightTool' can be used for this. It transmits the user commands to the LPM-Server. In return, the server receives information about system parameters, necessary for the position estimation. In the next step, the filtered position is sent with the User Datagram Protocol (UDP) to the visualization software. Self-calibration in combination with the ability to pre-filter the data requires the information about raw time stamps. Therefore a framework was created, which is independent of the "LightTool" software. The architecture of the framework is illustrated in Figure 3.1.

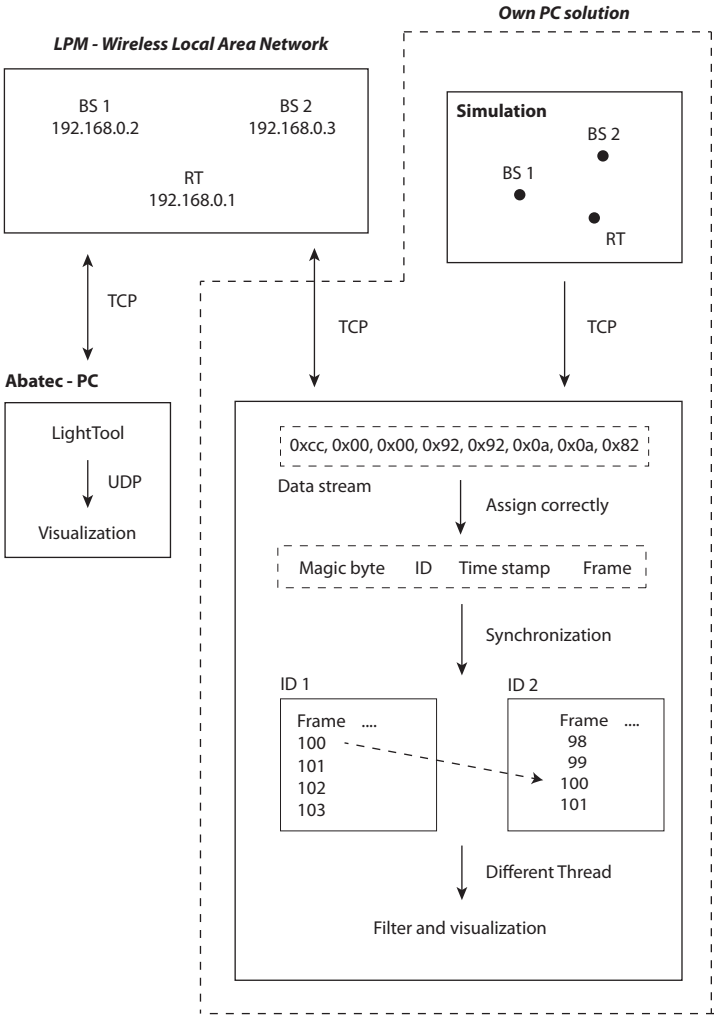

Figure 3.1.: LPM framework architecture

At the beginning of the reverse engineering, it was necessary to decipher the TCP data stream between the LPM system and the LPM client. This communication stream was intercepted with a network sniffer. It is common to use so called magic bytes, to separate information inside a stream.

Once it was clear which bytes belong to one message the next step was the correct interpretation. The ID of one station requires one byte and the time stamp measured in picoseconds at least four. With reverse engineering, it was possible to assign the bytes to the correct information and program an own interface between the ground station and the LPM system.

It was essential that the new interface is able to process the data stream as fast as possible, to be cross-platform compatible and to offer a user interface. These requirements lead to the decision to use the programming languages C++ in combination with the QT library. The developed software has two threads that operate

independently on each other. The first thread deals with the data stream and the correct synchronization of the data. The second thread processes the data and visualizes the results. The update rate of the LPM system is about 1,000 measurements per second and the visualization should not affect the decoding of the data stream.

The information about the time stamp, telemetry, signal strength etc. was stored for every station. Every emitted signal from the tag has a frame number. This frame number was used to obtain the synchronization between the vectors with respect to one base station. The synchronization has to be repeated if the frames become inconsistent. After the synchronization, the second thread is used to pre-filter the data and to perform a self-calibration.

Figure 3.2 shows an experimental setup to test the LPM system for indoor localization.

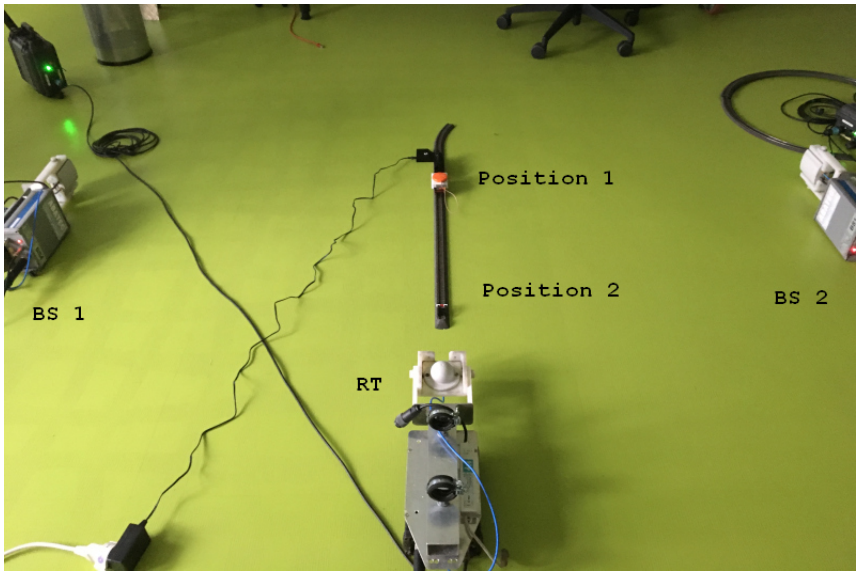

Figure 3.2.: Hardware test of the LPM

Two base stations are located at the same distance to the reference station position and a rail track, which transports a tag from Position 1 to Position 2 and vice versa. Every measurement at base station one and two is the time difference of the emitted signal from the tag, reference station and an unknown offset. This offset is equal for both stations and arises through the time difference between the tag and the reference station. It can be assumed, that the difference between the measurements for base station one and two should be zero along the rail track due to symmetry. However, Figure 3.3 shows that the assumption is incorrect for some positions along the track. This pattern of variation depends on the location and repeats if the tag is moving backward. This leads to the hypothesis that the pattern is the result of interference caused by reflections.

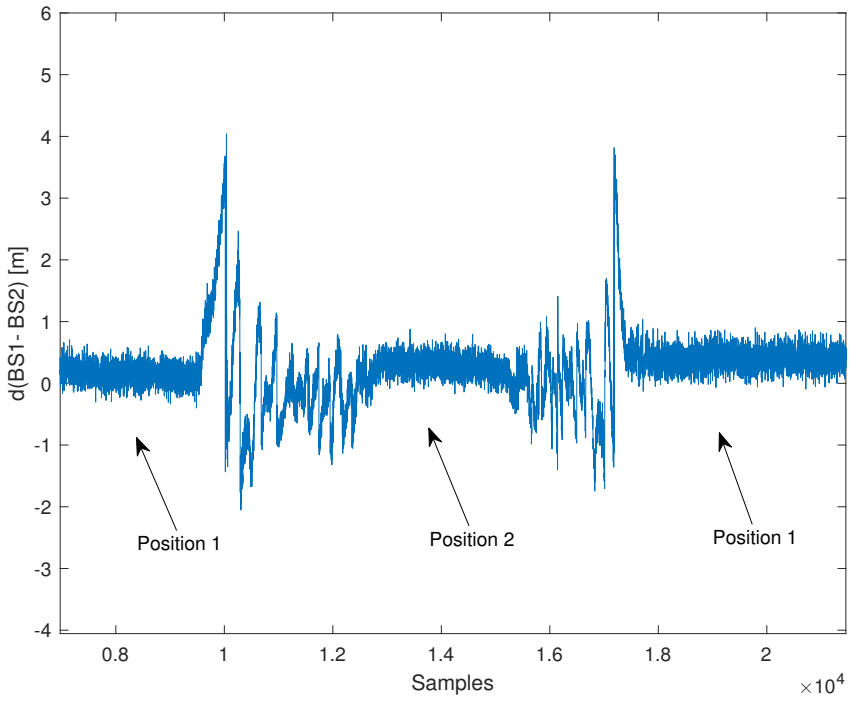

Figure 3.3.: Hardware test of the LPM

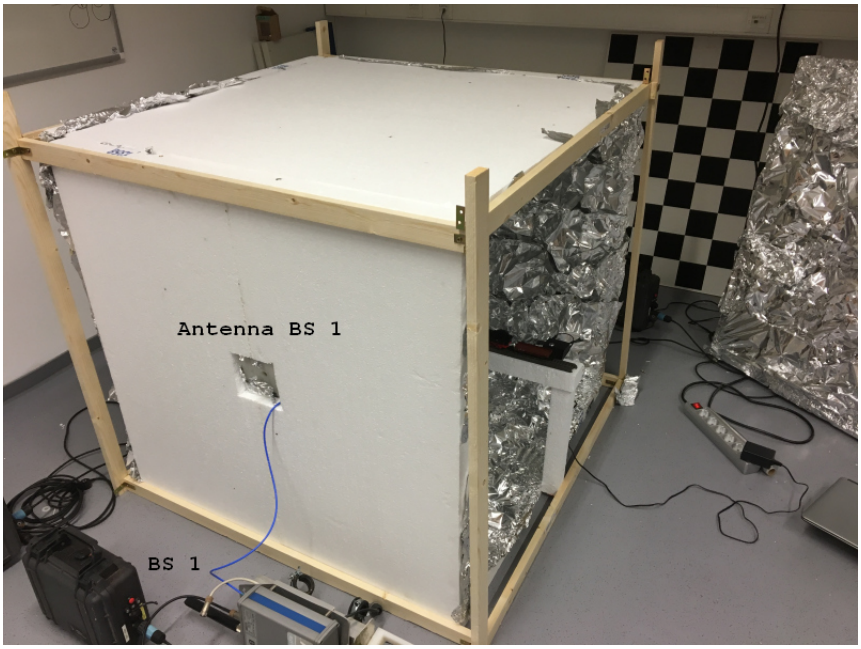

Figure 3.4.: Interference test box one

It is, unfortunately, not possible to reduce the emitted signal strength by software,

therefore a test box was constructed to create a more controllable environment. Figure 3.4 shows the open test box from the outside and Figure 3.5 from the inside. The walls of the box are coated with aluminum with a surface roughness higher than the emitted wave length, to create diffuse reflections.

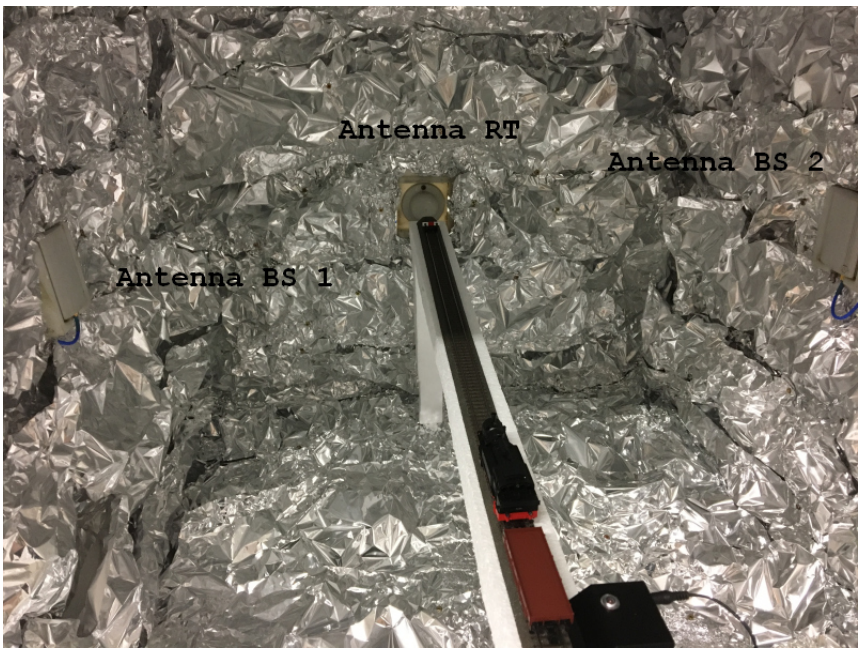

Figure 3.5.: Inside of the interference test box one

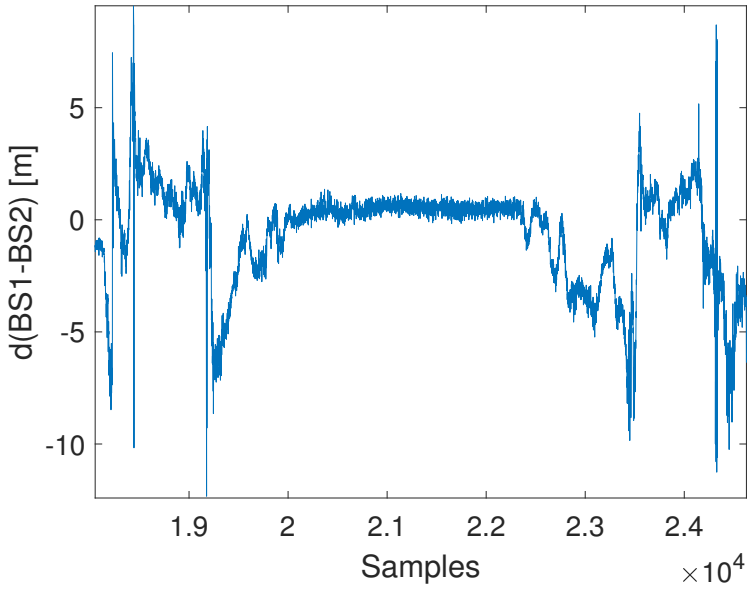

Figure 3.6.: Interference test box one results

The assumption was that the new measurement would not produce a pattern, but a flat line. The result was different than expected, as shown in Figure 3.6. It is likely that the signal strength is still too strong and the pattern is caused by the outside of the test box, like the the walls and the ceiling.

Therefore, the testbox design had to be changed significantly. The inside of the second test box are egg carton instead of aluminum. Due to the high attenuation (energy losses during wave propagation through a medium) of water compared to the air for electromagnetic waves with GHz frequencies [49] water was used as insulation for the second test box. Figure 3.7 presents the second test box without the insulation. In the right image of Figure 3.7, there are 1.5 liter water bottles and wet bedspreads used as insulation.

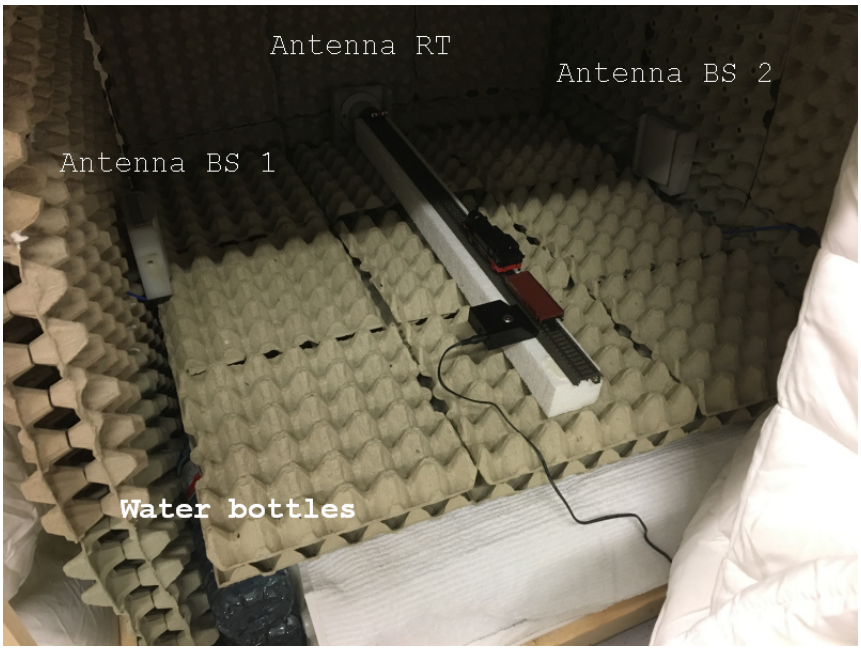

Figure 3.7.: Interference test for the second box

The transponder was again moved on the rail track from position one to two and vice versa. Figure 3.8 shows that the pattern is now much lower compared to the previous test. This underpins the hypothesis that the pattern is the result of inferences caused by reflections. In general narrow band signals are always affected by fading, as the result of multi-path in indoor applications, and the LPM system is no exception.

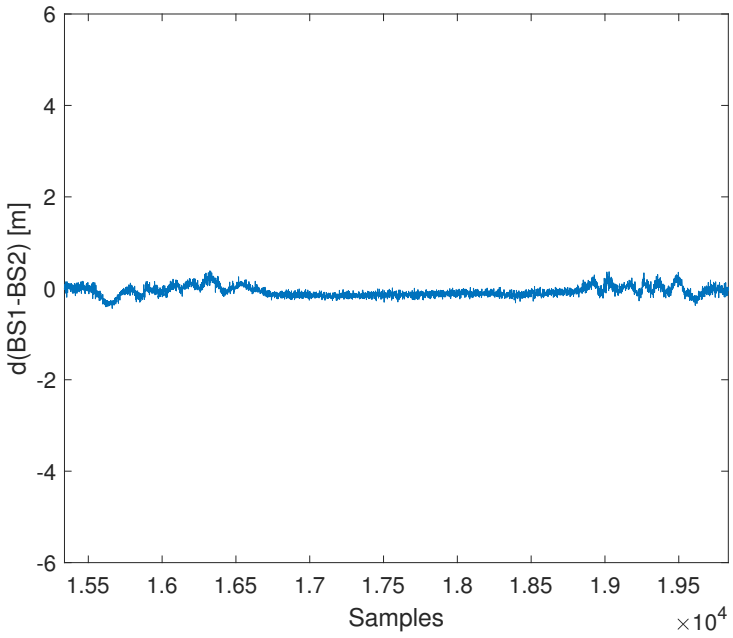

Figure 3.8.: Results of the interference test for the second box

The developed GUI of the LPM system can be found in the appendix A.1. In the following section an alternative system is presented, which is less affected by fading due to usage of ultra wide band technology.

3.2. Decawave UWB

In case of the Decawave UWB system it is possible to use the TOA measurement technique. At the beginning of the framework development, it was necessary to understand how to communicate with the DW1000 chip. The right-hand side of Figure 3.9 shows the Decawave DW1000 evaluation kit and on the left-hand side the STM32 evaluation kit. It consists mainly of the Decawave DW1000 and a microcontroller unit (MCU). The protocol of the operation is implemented in the MCU, which triggers the DW1000 to send information or to provide data about the time stamps and signal strength. The MCU and the DW1000 communicate through the Serial Peripheral Interface (SPI). Debugging or flashing of the MCU can be done with the JTAG adapter. If the pins S1 and S2 are disabled, it is possible to enable an SPI communication between the DW1000 and an external MCU. The correct communication between both units can be verified by a data analyzer, shown in the bottom of Figure 3.9.

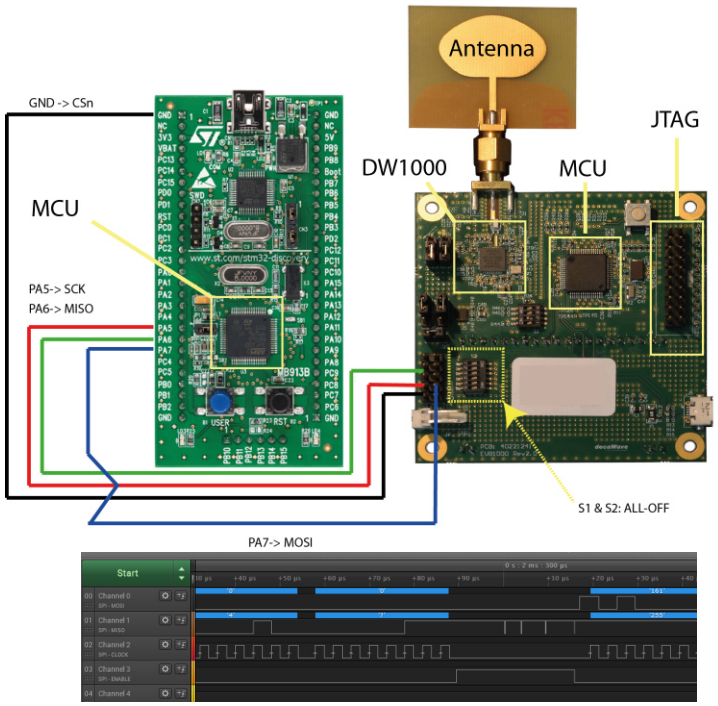

Figure 3.9.: Decawave EVK1000 connection to a STM32 developer kit by the SPI interface

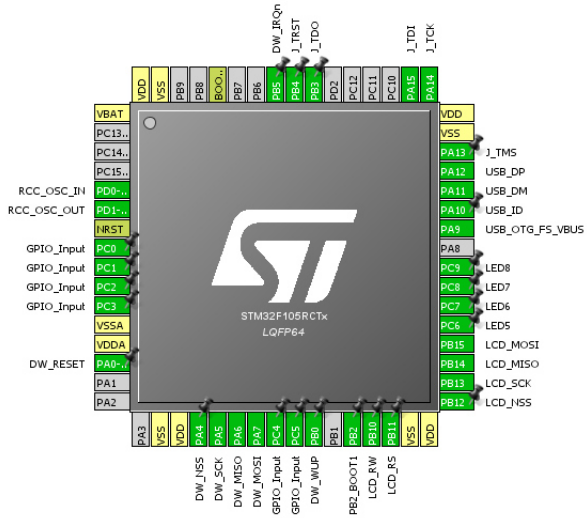

Figure 3.10.: CubeMX GPIO configuration

As the next step the MCU is configured. The STM32 offers a good interface, called CubeMX for the RCC (Reset and clock control) Configuration, GPIO Configuration and Clock Configuration, as seen in Figure 3.10.

After gaining the understanding of the communication and the correct data extraction from the registers with the evaluation kit, it was possible to use the DW1000 modules in the next step. This modules are based on the DW1000 IC (under the rf shield) and a small antenna. The evaluation kit (EVK1000) from the previous example does not offer an access to the GPIO (General Purpose Input/Output) pins. With the DW1000 module and an external MCU (with a development board) the system was extended by additional modules like the ESP32 for WLAN communication. The data exchange between the PC and the sensors could now be done with UWB or WLAN.

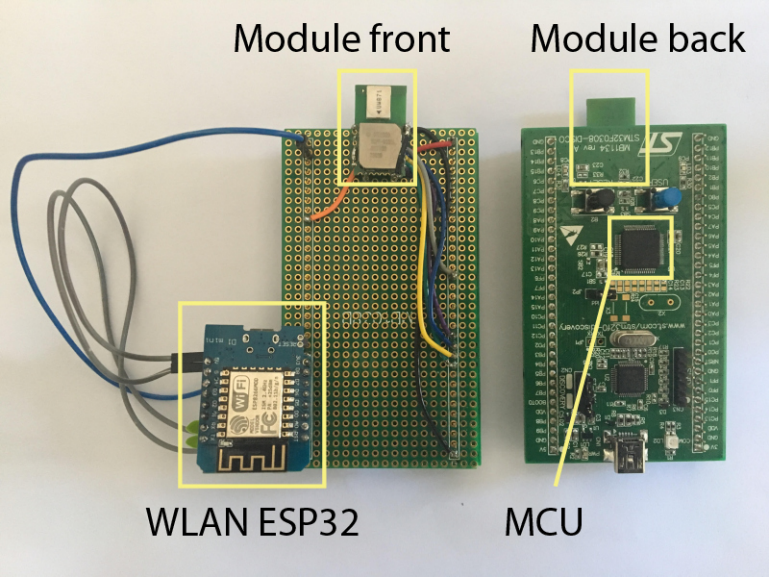

Figure 3.11.: Decawave Module connected by the SPI interface

The precision of the measurements is affected by two errors, namely, the signal power and the clock drift. The general approach to correct the clock drift is to use the integrator of the PLL (phase locked loop). In P-III, it is shown that the PLL is affected by the signal power. To eliminate this dependency, an alternative clock drift correction algorithm was developed. The general approach for the signal power correction requires the information of the ground truth distance provided by additional measurement systems. This disadvantage was eliminated by the development of an own signal power self-calibration algorithm. For a better communication between the sensors and the PC a graphical user interface was implemented, described in the Appendix A.2. The interface communicates only with one sensor, denoted as master station. This station coordinates the operation mode and the data transfer between the sensor stations. During the operation, the master station is responsible for the traffic control by telling the other sensors to send the data and which role the sensors have to take in the sensor network.

The stations can be set for different operation modes. Power calibration offers two roles denoted by TX and RX. The station with the TX role has only the aim to emit

signals, while the calibrated RX station is passive. The master station can be one of these two stations or even a third station. The same roles apply for the impulse response operation mode. Alternatively, operation modes are self-calibration, TOA or TDOA available. Depending on one of these three selected modes and the chosen settings the roles of the tag, reference station and passive mode are available to the user.

After finishing the configuration and connection to the master station, the settings are sent to every sensor. The ground station has always the possibility to tell the master station to emit a stop or a restart signal with new settings. It is essential that every station has the most up-to-date settings because otherwise it is likely that one station operates with a different channel than the master station. This would lead to the problem that this station is not anymore able to receive messages from the master station. To minimize this risk of false settings, an echo signal is used for verification.

4. Content of publications

All figure numbers in this chapter refer to the publications.

IEEE permission grant:

Requirements to be followed when using an entire IEEE copyrighted paper in a thesis:

1) The following IEEE copyright/ credit notice should be placed prominently in the references: © [year of original publication] IEEE. Reprinted, with permission, from [author names, paper title, IEEE publication title, and month/year of publication]

2) Only the accepted version of an IEEE copyrighted paper can be used when posting the paper or your thesis on-line.

ION permission grant:

Dear Mr. Sidorenko, The copyrights for the NAVIGATION paper belong to ION, but yes, you may use it in your dissertation. Please use the standard citation crediting ION as the publisher. For the second paper published in the PNT 2017 proceedings, you are the right owner of the copyright rights so you do not need the permission from ION to publish it anywhere else. However, the proper citation must be used crediting ION as the first publisher.

MDPI permission grant:

Both publications are open access.

4.1. P-I: Multilateration of the Local Position Measurement

Authors

Juri Sidorenko, Norbert Scherer-Negenborn, Michael Arens, Eckart Michaelsen

Conference paper

2016 International Conference on Indoor Positioning and Indoor Navigation (IPIN), Alcala de Henares, Spain, Oct. 2016, pp. 1-8, DOI: 10.1109/IPIN.2016.7743625.

The notation of P-I differs from that of this thesis, as it was adjusted to that of the second publication.

Introduction

The first publication describes the LPM positioning system and the advantages of a coordinate transformation with the aim to pre-filter the measurements. This system is highly affected by reflections and the previous publications about the LPM are focused on the filtering after the lateration. However, the lateration by a optimization algorithm is a nonlinear process, hence the previously Gaussian noise could turn into non-Gaussian noise, see Figure 5.
Filtering before the lateration is therefore more suitable. Unfortunately, the measurements of the LPM system are affected by an offset. This unknown offset is changing with every measurement and is by a factor of 10^7 higher than the distance itself.
The first two questions Q^1_{LPM} and Q^2_{LPM} have been answered in this publication.

Summary

The simplest and most robust solution is the subtraction of the measurements with respect to one station, leading to a transformation from TOA to TDOA. This method is only possible if the offset is the same for every station for the same measurement. The second part of the publication deals with the linear solution, which applies for the case that the positions of the base stations $\overrightarrow{B}$ and the reference station $\overrightarrow{R}$ are known. This solution is able to use the filtered data and provides the unknown position of the transponder $\overrightarrow{M}$. It is shown that due to the transformation the outliers become visible and easy to detect, as seen in Figure 6. The core idea of the

presented linear solution is that every measurement is corrupted by the measurement error α, hence the real measurement can be written as $L = \tilde{L} + \alpha$. The connection between the measurement error α_i and α_j can be found if the unfiltered measurement difference $((L_i + \alpha_i) - (L_j + \alpha_j))$ is subtracted from the filtered values $\Delta_{i,j}$. It is assumed that the filter is able to filter out the noise perfectly $(\tilde{L}_i - \tilde{L}_j) \approx \Delta_{i,j}$, this leads to the term $F_{ij} = ((\tilde{L}_i + \alpha_i) - (\tilde{L}_j + \alpha_j)) - \Delta_{i,j}$. The measurement error α_j of one measurement is replaced by $-F_{ij} + \alpha_i$. The direct solution, with the unknown variables $\overrightarrow{M}$, O and α_k then reads:

$$(\overrightarrow{B_i} - \overrightarrow{B_j}) \cdot \overrightarrow{M} - (\tilde{L}_i - \tilde{L}_j + F_{ij}) \cdot (O + \alpha_k) = \frac{1}{2}\left((\overrightarrow{B_i}^2 - \overrightarrow{B_j}^2) - \tilde{L_i}^2 - \tilde{L_j}^2 - F_{ij}^2\right)$$

An experiment with synthetic data and a Gaussian noise of 0.1 m standard deviation underpins the high effect of noise on the unfiltered linear solution, shown in Figure 7. In contrast, Figure 8 presents the results of the filtered linear solution. Afterwards, a weighted least square procedure was tested to reduce the effect of false results on the localization. It was observed that these methods works well as long as the matrix is not close to be singular. In the last part the nonlinear optimization was compared with the linear solution, while both are using the filtered data. The positioning error of the nonlinear solution was slightly lower compared to the linear solution.

Conclusions and outlook

The LPM self-calibration would require many more measurements, this increases also the risk to include an outlier. With the transformation and the pre-filtering, outliers becomes visible and can be eliminated. The answer for the questions Q^1_{LPM} is the presented transformation and the answer for Q^2_{LPM} is the linear solution. The presented linear solution is not symmetrical, due to the fact that it depends on one station more than on the others.
The aim of the next publication is to find a symmetrical linear solution for the LPM system, which is also able to use the pre-filter data as an input.

Declaration of own contribution

The idea of the transformation, pre-filtering and the development of the linear solution was done by the first author. This also applies for the software development to obtain the measurements and to perform the experiments, more information about the developed framework can be found in the Appendix. The co-authors improved the paper through their comments and corrections about the layout and the obtained results. **The overall own contribution is estimated at 88 %.**

Criteria	Estimated own contribution
Paper concept	90 %
Computations and software development	100 %
Data analysis and interpretation of results	80 %
Design and creation of figures	100 %
Manuscript structure and writing	70 %

Table 4.1.: Apportionment of own contributions for P-I

Multilateration of the Local Position Measurement

Juri Sidorenko, Norbert Scherer-Negenborn, Michael Arens, Eckart Michaelsen
Fraunhofer Institute of Optronics, System Technologies and Image Exploitation IOSB
Gutleuthausstrasse 1, 76275 Ettlingen, Germany.
Juri.Sidorenko@iosb.fraunhofer.de

***Abstract*—The Local Position Measurement system (LPM) is one of the most precise systems for 3D position estimation. It is able to operate in- and outdoor and updates at a rate up to 1000 measurements per second. Previous scientific publications focused on the time of arrival equation (TOA) provided by the LPM and filtering after the numerical position estimation. This paper investigates the advantages of the TOA over the time difference of arrival equation transformation (TDOA) and the signal smoothing prior to its fitting. The LPM was designed under the general assumption that the position of the base station and position of the reference station are known. The information resulting from this research can prove vital for the system's self-calibration, providing data aiding in locating the relative position of the base station without prior knowledge of the transponder and reference station positions.**

Keywords: time of arrival, time difference of arrival, local position measurement

I. Introduction

In the past, a wide range of different methods and sensors have been developed to obtain the exact position of an object of interest. The most common are radio frequency based methods, like NAVSAT GPS. This technology is often used as an example for the time of arrival equation (TOA). The traveling time between the satellite and the sensor on the ground can be used to estimate the sensor's position, neglecting the position estimation by phase. Both, the satellite's position in its orbit and the signal's send time, are known. Combining this information with the time signal arrival on the ground and the speed of light, it is then possible to estimate the range between the satellite and the sensor. This range is called pseudo range. If we neglect the time offset, three satellites are required to estimate the sensor's 3D position.
Unfortunately, the data update is quite slow and unsuitable for urban territory. During WWII, TDOA systems like DECCA became very popular. The TDOA method does not require knowledge of emission times. In contrast to the TOA, all possible locations for one measurement are located on a hyperbola. Other methods, like the angle of arrival, will not be addressed in this paper. All examples used from here on out will be based on the Abatec LPM. This system has potential, due to the fact that it is able to operate both in- and outdoors and provide an update rate of 1000 measurements per second.

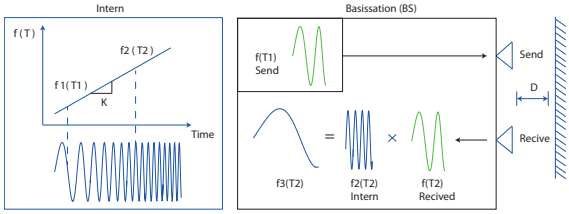

Fig. 1. FMCW: Left increasing frequency chirp with slope K. Right: mixed frequencies

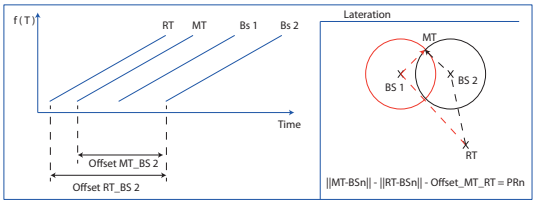

Fig. 2. LPM Left: Offset difference between transponder MT, basis station BS and reference station RT. Right: LPM euclidian equation

The LPM was highly inspired by the FMCW frequency modulated continues wave radar (FMCW) and systems based on TOA, such as GPS. Figure 1 illustrates the functionality of a FMCW. The internal system is generating an increasing frequency chirp with a fixed slope K. This chirp is sent and reflected by an object. The received signal does not change its frequency, but during this time $(T2 - T1)$ the internal frequency changed from $f1$ to $f2$. The radar can use an additive or multiplicative mixer to obtain the sum of the two frequencies and their differences. As only the frequency difference is required at this point, the frequency sum can be filtered by a low pass filter. The LPM is using this principle already, but in contrast to the FMCW radar, the send frequency chirp is getting compared with the frequency chirp of the other base station $KBS1 = KBS2$ (figure 2). If the chirps are synchronized (started at the same time) there is no offset, but since the base stations and transponder are not synchronized, a reference station is required. Every frequency measurement the LPM provides is based on the difference between the transponder and one of the base stations with respect to the reference station at the same base station. Due to this fact, the time offset O is equal for every base station for the same measurement as demonstrated in fig. 2. This all

leads to the LPM equation (1), with R: Pseudo Range, O: Offset, M: Transponder- and T: Reference station for different measurements i.

$$R_i = O + \|M - B_i\| - \|T - B_i\| \tag{1}$$

$$\|M - B_i\| = \sqrt{(x_i - x_M)^2 + (y_i - y_M)^2} \tag{2}$$

$$\|T - B_i\| = \sqrt{(x_i - x_T)^2 + (y_i - y_T)^2} \tag{3}$$

II. Previous Work

The measurement principal of the Abatec LPM and its hardware implementation have been presented in [6] [9]. Previously published work about the LPM predominantly focused on the usage of Kalman filters to detect an outlier[3] or to track the position of the transponder [7]. An approach to outlier detection can be found in [3], were the linear Kalman filter in combination with the χ^2 test was used to detect outliers within the offset corrupted data. Nonlinear equation solving with Bancroft is analyzed in [8][11] and compared with the least median of squares (LMS) in [2].

Abatec LPM (state-of-the-art):

- Solving of nonlinear TOA equation with a numerical solver.
- Unknown variables are coordinates of the transponder and the offset.
- Filtering after nonlinear multilateration.

New approach:

- TOA to TDOA transformation.
- The TDOA data is filtered before the multilateration.
- Both a linear TDOA solution and a nonlinear TDOA solution may be used to filter data before the lateration.

Advantages of new approach:

- Filtering before solving has the advantage that Gaussian noise inside of measurement data does not change due to numerical solver.
- The linear solution is faster than the nonlinear solution.
- The nonlinear solution does not have to fit the offset.
- Without the offset, outlier detection is enabled.

Disadvantage of new approach:

- The TDOA solution requires an additional base station
- The linear solution is more easily affected by unfavorable conditions .

III. Methodology

The previous section introduced the LPM and the following focuses on its position estimation. In general, the exact positions of the reference station and base stations are known. In this way, four base stations are required to obtain the x, y, and z coordinates of the transponder. The euclidean form for this equation can be solved using either the Gauss-Newton method, or another non-linear solver. Alternatively, the equation may be linearized with a Taylor-series expansion [4] within a starting position. Unfortunately, in that case, the solution depends heavily on a good estimation of the starting condition. In order to detect the outlier and to obtain a strong starting conditions, one needs to analyze the data. The general approach for the LPM to detect an outlier was using Chi-test within a linear Kalman filter (LKF) [3] on raw data. Figure 3 shows that the offset (O) is 10^6 times higher than the measurement itself. Furthermore, the offset is changing from one measurement to the next, due to the difference in oscillator clocks of reference station and transponder [3].The elimination of the offset allows us to see the relative range changing between the transponder and base station. This can be done by subtracting one base station from another at the same measurement. In figure 4 the result of this transformation on real measurements can be seen. The outliers are now visible with their typical characteristic of reflected data. At this point the TOA equation is changing to the TDOA. In [10] it was proven that the error propagation of the TDOA is equal to that of the TOA. This transformation can be done for two purposes: first, one may obtain the relative range between the base station and eliminate the offset; in this way we are able to filter data and outliers; second, one can rearrange the TOA equation to get the linear form of the transponder x, y, and z coordinates.

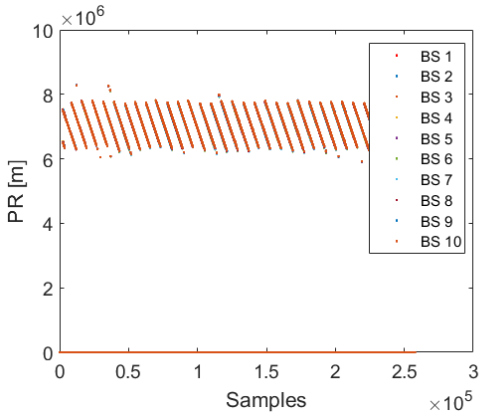

Fig. 3. LPM real raw data with offset Z at different measurements

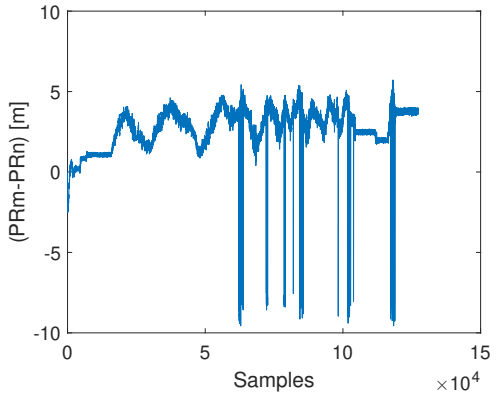

Fig. 4. Pseudo range of the real data after the transformation

TOA to TDOA

A. Linearization

Approaches such as the Taylor-series expansion [4] or other nonlinear solvers can be used to linearize the (1) equations. These methods require start information for the unknown variables. Alternatively one may use a reference station to obtain linear terms for the unknown position of the transponder. The offset will still be a part of the equation, but, just like the coordinates of the transponder, will be linear. This technique is also known as linear least squares multilateration. The main LPM equation (1) can be simplified by adding the known reference transponder range to the measurement term R (pseudo range).

$$L_i = R_i + \|T - B_i\| \tag{4}$$

$$\|M - B_j\|^2 - \|M - B_i\|^2 = (L_j - O)^2 - (L_i - O)^2 \tag{5}$$

The known quadratic terms of the transponder are eliminated, hence the linear solution for the transponder position at the known base station and reference station position is:

$$\left(\overrightarrow{B_i} - \overrightarrow{B_j}\right) \cdot \overrightarrow{M} - (L_i - L_j) \cdot O =$$

$$= \frac{1}{2}\left(\left(\left(\overrightarrow{B_i}\right)^2 - \left(\overrightarrow{B_j}\right)^2\right) - \left(L_i^2 - L_j^2\right)\right) \tag{6}$$

with

$$\overrightarrow{M} = \begin{pmatrix} x_M \\ y_M \end{pmatrix} \quad \overrightarrow{B} = \begin{pmatrix} x_B \\ y_B \end{pmatrix}$$

The state-of-the-art Abatec LPM software uses a damped Newton iteration for nonlinear regression [11], requiring some start positions are required. The solution here presented, does not require any start position or nonlinear solvers. The method's result, however, depends on the condition of the coefficient matrix (A). Should the pivots (diagonal elements of the coefficient matrix) be close to zero the condition is bad.

B. Filtering

The transformation of the TOA to TDOA by subtracting one base station from a reference station can also be used to filter data. If equation 1 is not getting solved for T and squared before subtracted from a reference station, the term will still be nonlinear for the unknown position of the transponder, but the offset will be eliminated.
As mentioned above, every measurement has its offset, which is usually 10^6 times higher than the location itself. If the numerical solver does not take this into account and the start conditions for the offset are unfavorable, then the changing in x, y, and z coordinates have almost no effect on the residuals. The higher the difference between $||M - B||$ and offset O the higher the deviation between local optima and global optimum. Another problem could appear $R + ||T–B|| > O$ in this case, the minimum of the numerical optimization becomes the maximum. The most suitable starting value for the offset would be the mean for every measurement, but we are still not able to set any start condition for the coordinates of the transponder or to interpret the measurements. In addition, the offset is changing from one measurement to the next, hence it promises suitable to use the difference between the base stations with respect to one reference station for the same measurement for further calculations. This method is known as the hyperbolic method [8] , due to the fact that the pseudorange is not maintained from the perspective of the transponder, if moving with a fixed radius on a circle around the basisstion, but in order to maintain the same pseudorange movement has to remain on a hyperbola. Changing the base station's instead the of transponder's position would provide a hyperbolic shape from the beginning. This shape is typical for TDOA, however, now the multidimensional damped Newton is utilized to solve the minimization of the equation [11]. Data may be filtered before position estimation, without the offset. The general approach for the LPM was to use the extended Kalman Filter, (EKF)[7] on the data provided by the numerical solver. But even if the data of the measurements has a gaussian noise, it does not necessarily mean that numerical output has a gaussian distribution as well. The least squares method to minimize the residuals $min \sum_{i=1}^{n} \frac{1}{2}(f(x,y,z) - y_i)^2$is effected by outliers, but is able to deal with gaussian noise. A bad matrix condition or poorly chosen starting condition could lead to a result, which does not have a gaussian distribution anymore and therefore makes filtering the data before solving an advantage accompanied by a solver that does not have to estimate the offset. The solver converges faster and filtering can be one dimensional instead of three dimensional. The difference between the base stations to one reference station causes a dependency between the equations due to noise [1]. Based on empirical measurements, the variance of the noise (figure 5) for every base station differs from $0.003\,m^2$ to $0.0036\,m^2$ for an immobile transponder. Thus one can assume that the variance is equal for every base station. This is an important fact for iterative solving. There are several filters applicable to filtering the data in question. A very

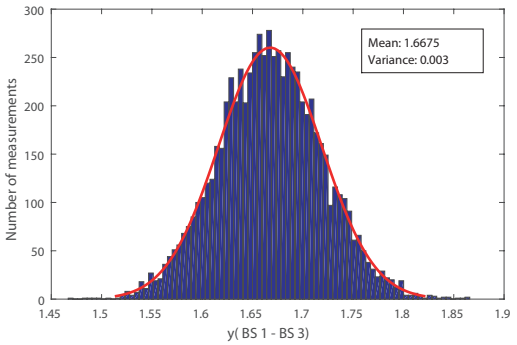

Fig. 5. BS_{1-3}, Real data based gaussian distribution of the pseudo range difference for a not moving transponder

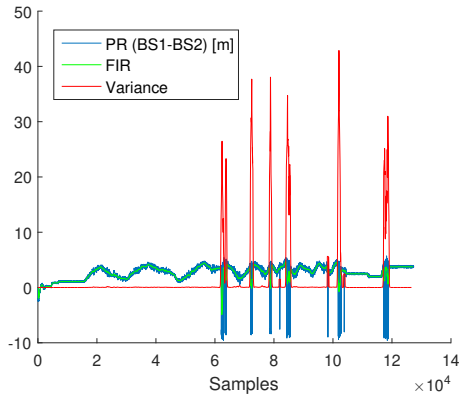

Fig. 6. Example of reflection inside real data. Red curve represents variance, blue measurements and the green the filtered data

fast and simple filter is the moving average filter. This filter proves helpful when the focus lies on the time domain instead of the frequency domain. Its filter kernel (impulse response of the filter) does not require a convolution with a signal, instead, processing can be reduced to subtracting the oldest measurement and adding one of the latest measurements. Due to the central limit theorem, running the filter several times would lead to a similar result as using a convolution with a gaussian kernel. In this way the over and under oscillations of the frequency domain are reduced. The method is faster than the convolution with a Gaussian kernel. In figure 6 the result of the moving average filter, which is a Finite Impulse Response filter (FIR) illustrating the moving variance on real data after the transformation. All outliers have a high variance with respect to the other measurements. This information can be used not just to detect the transponder, but also the source of the reflection. The disadvantage of this method is a delay $(N-1)/2$, which is increasing with the number of samples N. As an alternative, one could use the linear one dimensional Kalman filter instead. The difference between TOA and TDOA is visible (fig.7) Green circles represent the probability of the transponder location. Every circle represents one euclidean equation at a certain measurement. The correct location fits all the equations, therefore the residuals are the smallest. Smaller residuals are produced where just two equations fit, compared to other positions, hence the found coordinates are the local optimum (LO). The transformation results in simplified, hyperbola and triangles. The position of the transponder can be found by two hyperbola, but three hyperbola can be produced. The third can be represented by the other two, this hyperbola has no further information compared to the other two, but different local optima and another intersection angle. Due to this fact, numerical solving may influence, just by transforming, the probability to find a local optimum .

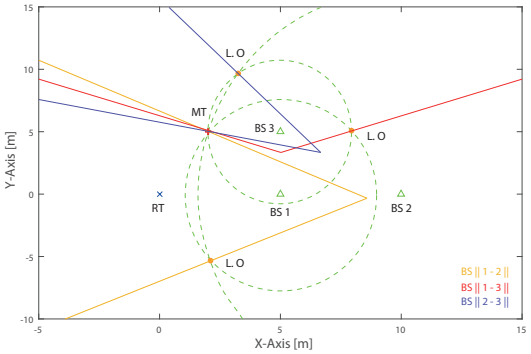

Fig. 7. Difference between TOA and TDOA . The triangles are the simplified hyperboloids of TDOA and the green circles the euclidean form of TOA

Combination of the linear equation with filtered data

The linear equation has some advantages over the nonlinear solution. This section presents a method of pre-filtering, which can be used to correct the linear solution. Tests showed that the noise is ten times higher than an immobile transponder, possibly due to the Doppler effect and the micro movements of the carrier. Therefore, we increased the random noise up to a maximum value of $0.1\,m$. The mean error of the estimated path with respect to the real path is $0.506\,m$ (fig. 8). The measurement L1 cannot be filtered as the time offset change with respect to time is 10^6 times higher than the range change itself. Therefore, the offset is eliminated by subtracting one base station measurement from the other $(L_i - L_j)$. In the next step this data is filtered over time. At this point it does not matter what kind of filter is used, it is only important that filtering takes place before position estimation and that the filter uses the measurement difference $(L_i - L_j)$ as an input. For the following calculations we only assume that for

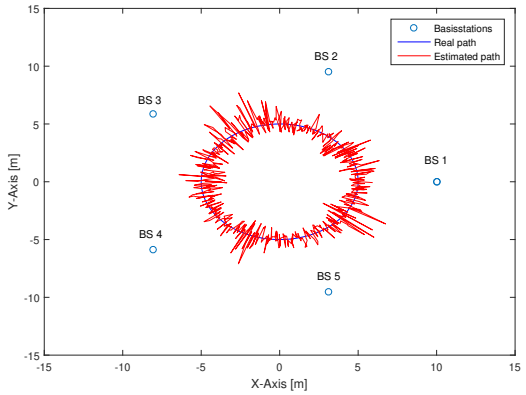

Fig. 8. Synthetic data: Real path of transponder is located around the reference station with a radius of 5 m. The base stations have a distance of 10 m from the center and same distance to each other. Measurement data is corrputed by gaussian noise.

every measurement we already have difference $(L_i - L_j)$ the filtered values $F(L_i - L_j)$ the main aim is to use the filtered values instead of the measurement differences between the base stations. The $(L_i^2 - L_j^2)$ term is nonlinear but the filtered values consist of the linear difference between the measurement ranges. One solution to using the filtered values would be to make every base station dependent on the same measurement error term α_i. Every measurement is corrupted by the measurement error αi, hence the real measurement can be written as $L = \tilde{L} + \alpha$. The connection between the measurement errors αi and αj can be found if the unfiltered measurement difference $(L_i + \alpha_i) - (L_j + \alpha_j)$ is subtracted from the filtered values $F(L_i - L_j)$.

$$F_{ij} = \left(\left(\tilde{L_i} + \alpha_i\right) - \left(\tilde{L_j} + \alpha_j\right)\right) - F\left(L_i - L_j\right) \quad (7)$$

$$\left(\tilde{L_i} - \tilde{L_j}\right) \approx F\left(L_i - L_j\right) \quad (8)$$

The assumption that the noise can be neglected after the filtering, this leads to the term F_{ij} being the difference between the noises of both signals.

$$F_{ij} = \alpha_i - \alpha_j \quad (9)$$

$$\alpha_j = -F_{ij} + \alpha_i \quad (10)$$

The measurement error is replaced by eq. 10.

$$\left(\overrightarrow{B_i} - \overrightarrow{B_j}\right) \cdot \overrightarrow{M} - \left(\tilde{L_i} - \tilde{L_j} + F_{ij}\right) \cdot O =$$

$$= \frac{1}{2}\left(\overrightarrow{B_i}^2 - \overrightarrow{B_j}^2 - \tilde{L_i}^2 - \tilde{L_j}^2 - F_{ij}^2 + \right.$$

$$\left. +2 \cdot \alpha_k \left(\tilde{L_i} - \tilde{L_j} + F_{ij}\right)\right)$$

It can be observed that the time offset O, depends on the same parameters as the measurement error

$$\left(\overrightarrow{B_i} - \overrightarrow{B_j}\right) \cdot \overrightarrow{M} - \left(\tilde{L_i} - \tilde{L_j} + F_{ij}\right) \cdot (O + \alpha_k) =$$

$$= \frac{1}{2}\left(\overrightarrow{B_i}^2 - \overrightarrow{B_j}^2 - \tilde{L_i}^2 - \tilde{L_j}^2 - F_{ij}^2\right)$$

With at least four base stations, the unknown coordinates of the transponder can be estimated. With the filtered values the linear direct solution provides better results, than with the unfiltered equation $Ax = b$. This equation can be solved as:

$$\begin{pmatrix} x_M \\ y_M \\ O \end{pmatrix} = \left(A^T A\right)^{-1} A^T b$$

Figure 9 presents the results of the new equation with noise. The mean error with a perfect filter is now below $10^{-11}\, m$. The experiment was repeated with synthetic data and a real moving average filter to investigate the behavior of outliers. Simulating a second base reflection the sample was set from 3500 to 3600 an outlier of 10 meters.

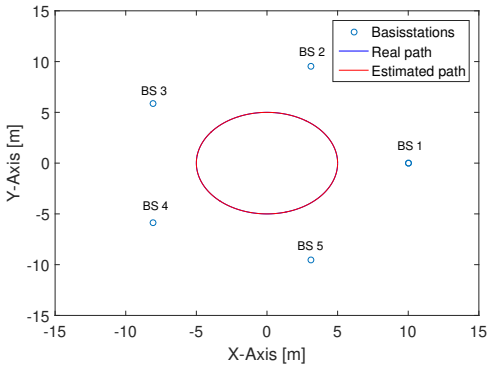

Fig. 9. Noise correction

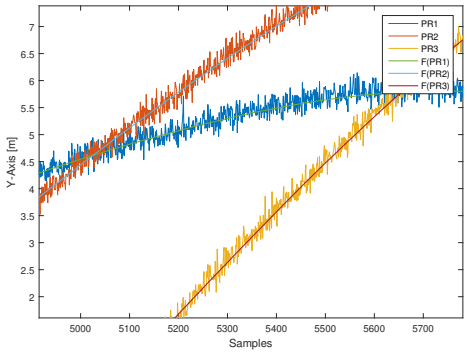

Fig. 10. Synthetic data (PR) with gaussian noise and moving average filter F(PR)

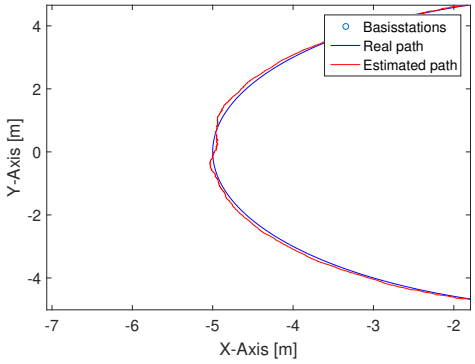

Fig. 13. Result of the weighting on synthetic data with outlier

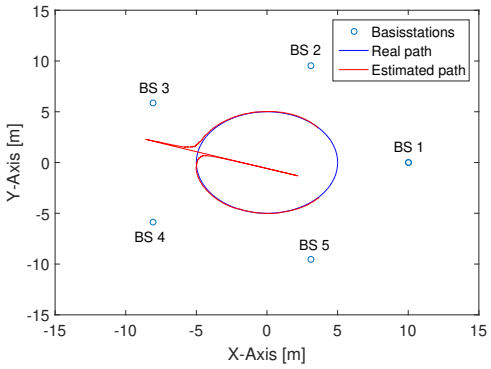

Fig. 14. Result of weighting at unfavorable geometric condition

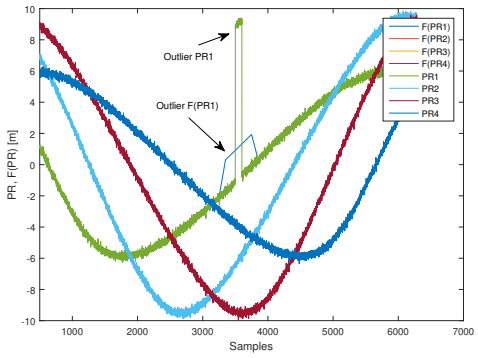

Fig. 11. Filter error due to outlier: Such measurements are typical for signal reflections

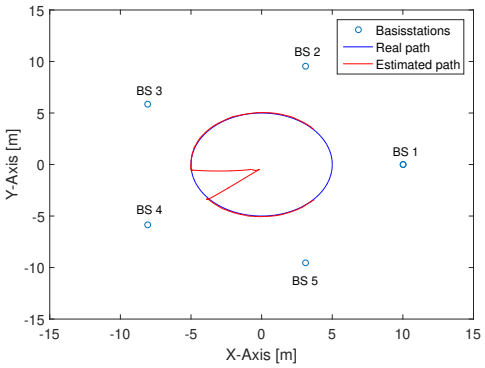

Fig. 12. Outlier position estimation

Figure 11 shows the results of the transformed signal and the filtered one (figure 10). The outlier causes some disturbance in the filtered output, which leads to an error in the position estimation (figure 12). This filter error can be minimized by taking variance into account. It is important to remember that the delay of the FIR filter to the signal is $(N-1)/2$ and of the moving variance $(N-1)/2$ plus the delay of the FIR, therefore we need some samples for the initialization and have no position estimation at the beginning (fig. 12). The provided variance is now used to obtain the weighting vector $w = 1/var$.

$$\begin{pmatrix} w_1 \\ \vdots \\ w_n \end{pmatrix} Ax = \begin{pmatrix} w_1 \\ \vdots \\ w_n \end{pmatrix} b$$

The result of the weighting is visible in figure 13, the measurement with the highest error now has the smallest weight in the minimizing of the least squares problem. That being said, in applying a working filter eliminates the need for weights. Applying weighting at the position where the equation is sensitive to perturbations like $(PR_m - PR_n + RT_m - RT_n) \approx 0$ or $B_x, B_y, B_z \approx 0$ the result of the position estimation will be highly inaccurate, due to corruption of the statistical meaning (fig. 14). In conclusion, we need to compare the nonlinear and the linear solution. Both methods have been transformed and filtered before the lateration. As a nonlinear solver we have used a Levenberg Marquardt method (LVM) [5]. The starting condition for the solver was the result of the previous fit beginning from the starting condition $x, y, z = 0$ and fit parameter (table I). Due to the TOA to TDOA equation transformation, there is no need to fit the offset, for every step LVM x, y, and z coordinates of the transponder need to be estimated.

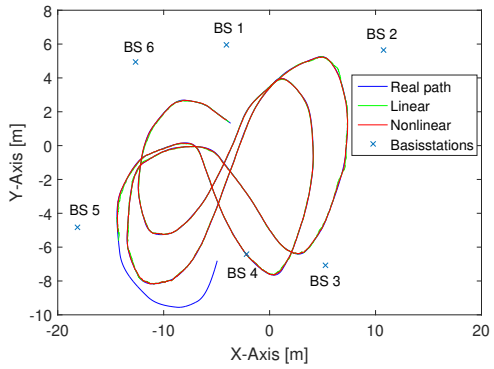

Fig. 15. Linear and Nonlinear

TABLE I
NEW LINEAR PARAMETER

Parameter	Value
Scaled gradient	0.000001
Relative function improvement	0.00001
Scaled step	0.001
Maximum iterations	20

Figure 15 presents the results of both methods. The linear solution has a slightly higher error rate compared to the nonlinear solution in some positions. The linear calculation, however, took $2596\,ms$ versus the nonlinear's $4677\,ms$ on a i7-4600u CPU 2.10GHz and 16 GB Ram. It follows that if prefiltering would be a 'perfect' approach, both solutions would have the same result as the real path.

IV. CONCLUSIONS

The transformation from the TOA equation to the TDOA brings several advantages for the LPM. Section 3 demonstrated that the transformation leads to a linear equation, which can be solved without initialization and numerical iterations. Admittedly, the linear solution as compared to the nonlinear TDOA solution is more sensitive to perturbations given specific geometric settings. Obtaining the condition of the coefficient matrix, though, allows detection of these settings, and permitting use of the faster linear solution for every other position. The latter part of section 3 dealt with the TOA to TDOA transformation with the aim to eliminate the offset and to filter the data before the multilateration. Filtering the data before the position estimation, because non-linear function estimation leads to violation of normal distribution, made more sense, however. Furthermore, the transformation allowed the detection of outliers, reducing the number of local optima and decreasing the computational time due to the elimination of the offset. In the end, the linear solution was expanded with the possibility to use pre-filtered data and provide a solution at in half the time that a non-linear solution can.

REFERENCES

[1] Lukasz Zwirello et al. Uwb localization system for indoor applications: Concept, realization and analysis,. In *Journal of Electrical and Computer Engineering*, 2012.

[2] Pfeil R et al. A robust position estimation algorithm for a local positioning measurement system. In *Wireless Sensing, Local Positioning, and RFID, 2009. IMWS 2009. IEEE MTT-S International Microwave Workshop on*, pages 1–4, Sept 2009.

[3] R. Pfeil et al. Distributed fault detection for precise and robust local positioning. In *In Proceedings of the 13th IAIN World Congress and Exhibition*, 2009.

[4] W. H. FOY. Position-location solutions by taylor-series estimation. *IEEE Transactions on Aerospace and Electronic Systems*, AES-12(2):187–194, March 1976.

[5] Jorge J. MorThe levenberg-marquardt algorithm: Implementation and theory. Numerical Analysis. Dundee, 1977.

[6] K. Pourvoyeur, A. Stelzer, Alexander Fischer, and G. Gassenbauer. Adaptation of a 3-D local position measurement system for 1-D applications. In *Radar Conference, 2005. EURAD 2005. European*, pages 343–346, Oct 2005.

[7] K. Pourvoyeur, A. Stelzer, T. Gahleitner, S. Schuster, and G. Gassenbauer. Effects of motion models and sensor data on the accuracy of the LPM positioning system. In *Information Fusion, 2006 9th International Conference on*, pages 1–7, July 2006.

[8] K. Pourvoyeur, A. Stelzer, and G. Gassenbauer. Position estimation techniques for the local position measurement system LPM. In *Microwave Conference, 2006. APMC 2006. Asia-Pacific*, pages 1509–1514, Dec 2006.

[9] A. Resch, R. Pfeil, M. Wegener, and A. Stelzer. Review of the LPM local positioning measurement system. In *Localization and GNSS (ICL-GNSS), 2012 International Conference on*, pages 1–5, June 2012.

[10] Dong-Ho Shin and Tae-Kyung Sung. Comparisons of error characteristics between TOA and TDOA positioning. *Aerospace and Electronic Systems, IEEE Transactions on*, 38(1):307–311, Jan 2002.

[11] A. Stelzer, K. Pourvoyeur, and A. Fischer. Concept and application of lpm - a novel 3-d local position measurement system. *IEEE Transactions on Microwave Theory and Techniques*, 52(12):2664–2669, Dec 2004.

4.2. P-II: Improved linear direct solution for asynchronous radio network localization (RNL)

Authors

Juri Sidorenko, Norbert Scherer-Negenborn, Michael Arens, Eckart Michaelsen

Conference paper

Proceedings of the ION 2017 Pacific PNT Meeting, Honolulu, Hawaii, USA, May 2017, pp. 376-382, DOI: 10.33012/2017.15036.

Introduction

In the previous publication P-I a linear solution for the LPM system was presented. This solution provides the unknown position of the transponder under the assumption that the location of the reference stations are known. The special aspect about the linear solution is the ability to operate with transformed LPM measurements and pre-filtered data. The weak point of the linear solution of P-I, is that it is not symmetric. This drawback is corrected in the following publication P-II and the question Q^2_{LPM} is answered.

Summary

The difference between two measurements $(L_i - L_j)$ can be replaced by results of the filter $\Delta_{i,j}$, due to the fact that the offset O is equal for the same measurement. Only the sum between two measurements $L_i + L_j$ is unknown. The core of this publication is the replacement of the sum of two measurements $L_i + L_j$ by the measurement differences Δ_{ij} and the sum of all measurements denoted by the variable S. The symmetrical solution has in contrast to the non-symmetrical solution from P-I the unknown variable $S = \sum_{i=1}^{n} L_i$ instead of the measurement error α_j . After some steps, explained in detail in P-II, the final symmetrical direct solution with the unknown variables $\overrightarrow{M}$, O and S can be written as:

$$(\overrightarrow{B_i} - \overrightarrow{B_j}) \cdot \overrightarrow{M} - \Delta_{i,j} \cdot (O - \frac{1}{n} \cdot S) = \frac{1}{2}(\overrightarrow{B_i}^2 - \overrightarrow{B_j}^2) - \Delta_{i,j} \cdot \frac{1}{2 \cdot n} \cdot (\sum_{k \neq i,j} \Delta_{ik} + \sum_{k \neq i,j} \Delta_{jk})$$

Every base station is equally represented in the final equation, but the filtering has now to be applied for all $(n^2 - n)/2$ differences between the measurements of all stations. This leads to a higher amount of required filters instead the previous

solution $n-1$. In the last part of the publication P-II, the symmetrical linear solution was compared with the non-symmetrical linear solution. It could be observed that the distribution of the localization error is symmetrical, as shown in Figure 2, unlike the results of the non-symmetrical solution from P-I, shown in Figure 1.

Conclusions and outlook

The symmetrical solution has the advantage that the noise of every station is equally weighted during the solution finding process. Especially, in case of unfavorable geometrical constellations and in presence of noise the symmetrical solution is by at least 10 % better than its non symmetrical counterpart. The developed symmetrical linear solution is used later on for the self-calibration.

Declaration of own contribution

The paper conception has been proposed by the second author Norbert Scherer-Negenborn, the development of the final symmetrical solution took many discussions between the first author and Norbert Scherer-Negenborn. The idea of a pre-filtered linear solution has its source in the previous work of the first author. The software development and the experiments were done by the first author, more information about the developed framework can be found in Appendix. The co-authors improved the paper through their comments and corrections about the layout and the obtained results. **The overall own contribution is estimated at 82 %.**

Criteria	Estimated own contribution
Paper concept	90 %
Computations and software development	80 %
Data analysis and interpretation of results	80 %
Design and creation of figures	90 %
Manuscript structure and writing	70 %

Table 4.2.: Apportionment of own contributions for P-II

Improved linear direct solution for asynchronous radio network localization (RNL)

Juri Sidorenko, Norbert Scherer-Negenborn, Michael Arens, Eckart Michaelsen
Fraunhofer Institute of Optronics, System Technologies and Image Exploitation IOSB
Gutleuthausstrasse 1, 76275 Ettlingen, Germany

BIOGRAPHY (IES)

Juri Sidorenko received the diploma in mechanical engineering from the Technical University Braunschweig, Germany and the Master of Science from the Cranfield University, UK in 2012 and 2014.

Norbert Scherer-Negenborn received the diploma and PhD degree in physics from the University of Freiburg, Germany, in 1996 and 2000, respectively.

Michael Arens received his diploma in Computer Science and his PhD (Dr.rer.nat.) from the University of Karlsruhe in 2001 and 2004, respectively.

Eckart Michaelsen graduated from the University of Innsbruck (Austria) in 1987 with diploma on Mathematics. In 1998 Eckart Michaelsen received Dr.-Ing. from the University of Erlangen, Germany.

ABSTRACT

The linear least square solution is frequently used in the field of localization. Compared to nonlinear solvers, this solution is more affected by noise but able to provide a position estimation without knowing any starting condition. The linear least square solution is able to minimize Gaussian noise by solving an overdetermined equation with the Moore–Penrose pseudoinverse. Unfortunately, this solution fails in the case of non-Gaussian noise. This publication presents a direct solution using prefiltered data for the LPM (RNL) equation. The input used for linear position estimation will not be the raw data but data filtered over time and for this reason this solution will be called the direct solution. It will be shown that the symmetrical direct solution presented is superior to the non-symmetrical direct solution and in particular to the non-prefiltered linear least square solution.

INTRODUCTION

Radio network-based localization is a radio wave-based positioning method, whereby a set of sensors at known positions (base stations) estimate the unknown sensor position (M). Range measurement can be accomplished using different principles, such as 'Round Trip Time of Flight (RTT, RTToF)'. With this approach, the base stations send the signal and it is sent back by M. This technique is very similar to radar, hence every measurement can be referred to as 'Time Of Arrival (TOA) '. Alternatively, the base stations can be passive and only the M emits the signal, referred to as 'Local Position Measurement (LPM)'. The base stations have to be synchronized, which can be achieved with a second transponder (T) at a known position. In contrast to the elliptical TDOA method [14], M and T do not communicate with each other, thus every measurement has a time offset. The unknown sensor position can be estimated using the direct linear (closed loop) solution instead of Taylor-series expansion [4] or nonlinear solvers. The direct solution has the advantage that no starting conditions are required compared to the nonlinear or Taylor solution. However, every real measurement is affected by noise, which is in the best Gaussian case. Unfortunately, reflections and other non-Gaussian disturbances can also be found in the measurements. The best approach is to filter this data before lateration, since even raw data with Gaussian noise can become non-Gaussian after a non-linear operation, caused by nonlinear optimization. This measurement principal requires data transformation to eliminate the time offset, filter the data and use it as an input for the linear solution. The Inmotiotec LPM system [6] [10] is an example of this kind of system and is able to provide an update rate of 1000 Hz with high three-dimensional position accuracy.

PREVIOUS WORK

A linear algebraic solution (direct solution) is frequently used in the field of position estimation. One of those most commonly used is Bancroft's method [2], which is well analyzed and described in [1],[3]. Furthermore, it has been shown that the nonlinear solvers, such as the Gauss–Newton algorithm, provide more accurate solutions for overdetermined cases than the linear solution solved by the Moore–Penrose pseudoinverse [12]. In our paper [11] we show an approach to using filtered measurements for the linear direct solution of the TOA-LPM equation. This solution is not symmetrical and less numerically stable, therefore an improved solution will be presented in this work. The Abatec LPM system itself is well described in [6], [10]. Previous publications about the Abatec LPM are mainly based on measurement principles [6], [10] and how the sensor data can be fused and filtered to detect outliers [9] and obtain the most accurate position [7] after multilateration. The latest publications on LPM focus on the numerical solvers. In general, LPM uses a Bancroft algorithm [8],[13],[5] to estimate the position of the transponder.

METHODOLOGY

The general LPM equation is:

Equation 1

$$R_i = O + ||M - B_i|| - ||T - B_i||$$

The pseudo range measurement (R), consists of the flight time between the first transponder and one base station subtracted from the reference transponder to the same base station. In this case, every time offset (O=time offset*speed of light) remains the same for every base station at one measurement but changes rapidly over time. The Euclidian distance between the reference station equates with T indices eq.(2) and transponder with M indices eq.(3) to the base stations B with indices number (i=1 → n).

Equation 2

$$||T - B_i|| = \sqrt{(x_i - x_T)^2 + (y_i - y_T)^2}$$

Equation 3

$$||M - B_i|| = \sqrt{(x_i - x_M)^2 + (y_i - y_M)^2}$$

The coordinates of the base stations and reference station are known. Only the transponder position and the offset have to be estimated.

Not symmetrical direct solution

In contrast to approaches such as Taylor-series expansion [4], for which starting information for the unknown variables is required, it is possible to obtain the linear components x,y,z of the transponder without derivation. The main LPM equation (1) can be simplified by adding the known reference transponder range to the measurement term R.

Equation 4

$$L_i = R_i + ||T - B_i||$$

Equation 5

$$||M - B_j||^2 - ||M - B_i||^2 = (L_j - O)^2 - (L_i - O)^2$$

The known quadratic terms of the transponder are eliminated, hence the linear solution for the transponder position at the known base station and reference station position is:

Equation 6

$$(\overrightarrow{B_i} - \overrightarrow{B_j}) \cdot \overrightarrow{M} - (L_i - L_j) \cdot O = \frac{1}{2}(((\overrightarrow{B_i})^2 - (\overrightarrow{B_j})^2) - (L_i^2 - L_j^2))$$

With:

$$\overrightarrow{M} = \begin{pmatrix} x_M \\ y_M \end{pmatrix} \quad \overrightarrow{B} = \begin{pmatrix} x_B \\ y_B \end{pmatrix}$$

In [11] it is shown that the linear solution for the LPM is highly affected by noise. The measurement L_1 cannot be filtered as the time offset change with respect to time is 1000 times higher than the range change itself. Therefore, the offset is eliminated by subtracting one base station measurement from the other (L_i-L_j). In the next step this data is filtered over time. At this point it does not matter what kind of filter is used, it is only important that filtering takes place before position estimation and that the filter uses the measurement difference (L_i-L_j) as an input. For the following calculations we only assume that for every measurement we already have difference (L_i-L_j) the filtered values F(L_i-L_j), the main aim is to use the filtered values instead of the measurement differences between the base stations. The (Li^2-Lj^2) term is nonlinear but the filtered values consist of the linear difference between the measurement ranges. One solution to using the filtered values would be to make every base station dependent on the same measurement error term α_i. Every measurement is corrupted by the measurement error α_i, hence the real measurement can be written as $L = \tilde{L} + \alpha$. The connection between the measurement errors α_i and α_j can be found if the unfiltered measurement difference ($(L_i+\alpha_i) - (L_j+\alpha_j)$) is subtracted from the filtered values F(L_i-L_j).

Equation 7

$$F_{ij} = ((\tilde{L}_i + \alpha_i) - (\tilde{L}_j + \alpha_j)) - F(L_i - L_j)$$
$$(\tilde{L}_i - \tilde{L}_j) \approx F(L_i - L_j)$$

The assumption that the noise can be neglected after the filtering, this leads to the term F being the difference between the noises of both signals.

Equation 8

$$F_{ij} = \alpha_i - \alpha_j$$

Equation 9

$$\alpha_j = -F_{ij} + \alpha_i$$

The measurement error α_j is replaced by $\alpha_j = -F_{ij} + \alpha_i$.

Equation 10

$$(\overrightarrow{B_i} - \overrightarrow{B_j})\cdot\overrightarrow{M} - (\tilde{L}_i - \tilde{L}_j + F_{ij})\cdot O = \tfrac{1}{2}(((\overrightarrow{B_i})^2 - (\overrightarrow{B_j})^2) - \tilde{L_i}^2 - \tilde{L_j}^2 - F_{ij}^2 + 2\cdot\alpha_k(\tilde{L}_i - \tilde{L}_j + F_{ij}))$$

It can be observed that the time offset Z, depends on the same parameters as the measurement error

Equation 11

$$(\overrightarrow{B_i} - \overrightarrow{B_j})\cdot\overrightarrow{M} - (\tilde{L}_i - \tilde{L}_j + F_{ij})\cdot(O + \alpha_k) = \tfrac{1}{2}(((\overrightarrow{B_i})^2 - (\overrightarrow{B_j})^2) - \tilde{L_i}^2 - \tilde{L_j}^2 - F_{ij}^2)$$

With at least four base stations, the unknown coordinates of the transponder can be estimated. With the filtered values the linear direct solution provides better results, than with the unfiltered equation.

Equation 12

$$Ax = b$$

This equation can be solved as:

Equation 13

$$\begin{pmatrix} x_M \\ y_M \\ O \end{pmatrix} = (A^T * A)^{-1} A^T * b$$

Symmetrical direct solution

The main disadvantage of the previous equation is that every base station measurement depends on one and the same base station, hence the solution is not symmetrical. Therefore, a more robust approach whereby every base station is used will be presented in the next part. In contrast to the not symmetrical direct solution, the nonlinear difference between the measurements will be rewritten as.

Equation 14

$$(L_i^2 - L_j^2) = (L_i - L_j)\cdot(L_i + L_j)$$

This leads to the term

Equation 15

$$(\overrightarrow{B_i} - \overrightarrow{B_j})\cdot\overrightarrow{M} - (L_i - L_j)\cdot(O - \tfrac{L_i+L_j}{2}) = \tfrac{1}{2}((\overrightarrow{B_i})^2 - (\overrightarrow{B_j})^2)$$

The difference between two measurements can be replaced by the results of the filter.

Equation 16

$$\Delta_{ij} = (L_i - L_j)$$

Filtering uses the differences between two measurements, as offset O is equal for the same measurement for every base station. Therefore, every measurement difference (L_i-L_j) can be replaced by the filtered values. Only the sum between two measurements (L_i+L_j) is unknown.

Equation 17

$$(\overrightarrow{B_i} - \overrightarrow{B_j})\cdot\overrightarrow{M} - \Delta_{i,j}\cdot(O - \frac{L_i + L_j}{2}) = \frac{1}{2}((\overrightarrow{B_i})^2 - (\overrightarrow{B_j})^2)$$

Equation 18

$$\Delta_{ji} = -\Delta_{ij},\ \Delta_{ii} = 0$$

In the following example, it will be shown how the sum of two measurements (L_i+L_j) is represented by the Differences of two measurements (L_i-L_j).

Symmetrical direct solution: Example with 5 base stations:

For five base stations the filtered measurement differences required are

Table 1 Base station measurement differences

	BS_{1-j}	BS_{2-j}	BS_{3-j}	BS_{4-j}
j=2	1-2	2-3	3-4	4-5
j=3	1-3	2-4	3-5	
j=4	1-4	2-5		
j=5	1-5			

The sum of measurements (L_i+L_j) for five base stations can be represented by the filtered measurement differences:

$$L_1 + L_3 = (L_1 + L_2) - (\Delta_{23})$$
$$L_1 + L_4 = (L_1 + L_2) - (\Delta_{24})$$
$$L_1 + L_5 = (L_1 + L_2) - (\Delta_{25})$$
$$L_2 + L_3 = (L_1 + L_2) - (\Delta_{13})$$
$$L_2 + L_4 = (L_1 + L_2) - (\Delta_{14})$$
$$L_2 + L_5 = (L_1 + L_2) - (\Delta_{15})$$
$$L_3 + L_4 = (L_1 + L_2) - (\Delta_{13}) - (\Delta_{24})$$
$$L_3 + L_5 = (L_1 + L_2) - (\Delta_{13}) - (\Delta_{25})$$
$$L_4 + L_5 = (L_1 + L_2) - (\Delta_{25}) - (\Delta_{34})$$

Now every base station depends on the unknown sum component (L_1+L_2) instead of (L_1+L_2) it is also possible to use any combination of (L_i+L_j). Our aim is to make the equation equally dependent on all the base stations and not only on fixed base station combinations (L_i+L_j). For this reason, the sum (L_i+L_j) between two base stations will be replaced by the sum of all base stations. If we stay with the example with five base stations, the sum S would be.

Equation 19

$$S = \sum_{i=1}^{n} L_i$$

This unknown sum S should now fit for every (L_i+L_j).If the indices are i=1 and j=2, the sum S need to be transformed in such a way that L_3+L_4+L_5 are eliminated by only using the differences between the L_i and L_j. For

Equation 20

$$L_1 + L_2 \neq S + (L_1 - L_3) + (L_1 - L_4) + (L_1 - L_5)$$

the components L_3, L_4 and L_5 are eliminated but now L_1 is represented four times instead of once. If the equation is changed to

Equation 21

$$L_1+L_2 \neq S+(L_1-L_3)+(L_1-L_4)+(L_1-L_5)+(L_2-L_3)+(L_2-L_4)+(L_2-L_5)$$

the measurements L_1 and L_2 are now overrepresented four times and L_3, L_4 and L_5 are overrepresented twice. By multiplying the measurement differences by 0.5 and adding them to the sum S, the L_3, L_4 and L_5 are eliminated but L_1 and L_2 now have the factor 5/2 instead of one. The numerator represents the number of base stations used, in this example five. The term (L_i+L_j) can now be expressed as

Equation 22

$$L_1+L_2 = \frac{2}{5}\cdot(S+\frac{1}{2}((L_1-L_3)+(L_1-L_4)+(L_1-L_5)+(L_2-L_3)+(L_2-L_4)+(L_2-L_5)))$$

The general equation for every (Li+Lj) becomes

Equation 23

$$L_i + L_j = \frac{2}{n}\cdot S + \frac{1}{n\cdot 2}\cdot(\sum_{k\neq i,j}(\Delta_{ik}) + \sum_{k\neq i,j}(\Delta_{jk}))$$

with the variable n, which stands for the number of base stations. The sum of the measurements between two base stations can now be replaced by the following term, whereby every other base station is used equally.

Equation 24

$$\frac{L_i + L_j}{2} = \frac{1}{n}\cdot S + \frac{1}{n\cdot 2}\cdot(\sum_{k\neq i,j}\Delta_{ik} + \sum_{k\neq i,j}\Delta_{jk})$$

The final symmetrical direct solution, with the unkown variables xM ,yM ,zM ,O and S:

Equation 25

$$(\overrightarrow{B_i} - \overrightarrow{B_j})\cdot\overrightarrow{M} - \Delta_{i,j}\cdot(O - \tfrac{1}{n}\cdot S) = \tfrac{1}{2}((\overrightarrow{B_i})^2 - (\overrightarrow{B_j})^2) - \Delta_{i,j}\cdot\tfrac{1}{2\cdot n}\cdot(\textstyle\sum_{k\neq i,j}\Delta_{ik} + \sum_{k\neq i,j}\Delta_{jk})$$

RESULTS

In the following two methods (symmetrical and non-symmetrical) filtering the direct solution will be compared. The five base station positions are located on a circle with a radius of 10 metres and the transponder position measurement is calculated for every metre in the 60 m^2 square area. Furthermore, the measurements have been corrupted by Gaussian noise with a variance of 0.064 m^2. This noise represents the filtering error not the measurement noise.

Table 2 Base station position

Base station	1	2	3	4	5	6
X-Axis [m]	10	5	-5	-10	-5	5
Y-Axis [m]	0	8.66	8.66	0	-8.66	-8.66

The position error of the previous method is subtracted from the new one at any position in the square area. Positive error differences indicate that the error with the second method is smaller. On the other hand, negative error difference shows that the error with the second approach is higher compared to the non-symmetrical solution. In the set-up presented, 56.11% have a positive error difference and 43.88% a negative one. Therefore, the second approach is 13% superior to the first one. In some test scenarios, where the geometrical constellation of the base stations is difficult for the lateration of the transponder position, the difference between the non-symmetrical and symmetrical approach increases by 30%. The first approach (non-symmetrical) always uses the same base station (base station one) from which the others are subtracted. If this transformation station is selected by the best condition of the coefficient matrix ||A||*|| A -1 ||, the error difference between the new and previous approach is almost always a value between 50.44 % and 49.55 %. The increase in noise when selecting difficult geometrical constellations of the base stations leads to a higher difference between the symmetrical and non-symmetrical approach, with better results for the symmetrical approach. The condition of the coefficient matrix at different transponder positions can be seen in figure 1 and 2.

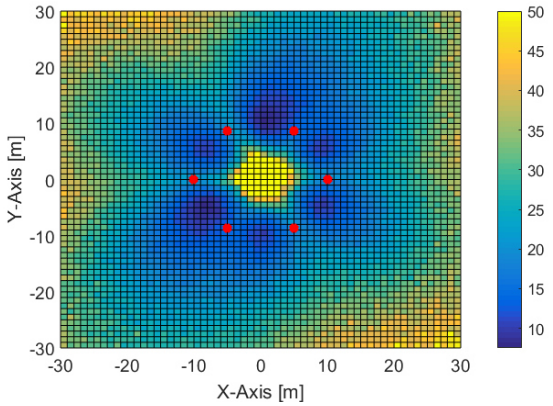

Figure 1: Matrix condition with BS 1 as reference. Colours from yellow to blue: condition at the specific position. The red dots: base station positions.

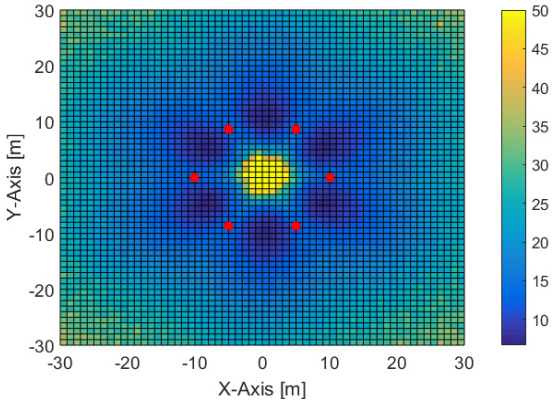

Figure 2 Matrix condition symmetric approach. Colours from yellow to blue: condition at the specific position. The red dots: base station positions.

It can be observed that the coefficient matrix condition with the previous method, figure (1) is not symmetrical compared to the new approach 2. Base station selection with the best condition slightly changes the results but still underlies the symmetrical approach. The condition appears to be best in the area between the base stations. This is not always the case and depends on the base station constellation.

CONCLUSION

'LPM' is a nonlinear offset corrupted equation, whereby any transformation to a linear solution leads to a high noise impact on the outcome. We present a new numerically more stable direct solution, which is able to work with prefiltered data. In contrast to a non-filtered linear least square solution, this filtered direct solution is statically not correct, as not the data corrupted by Gaussian noise is used but the output of the filter. The results of this filtered direct solution are less influenced by the noise and therefore more suitable for use as starting values for the nonlinear solver. Furthermore, the symmetrical approach does not require a specific base station that is used for filtering, but instead all base stations play an equal part in finding a solution. The results of the new approach are at least 10 % better, compared to approaches whereby only the same base station is used. The best result for the first solution appears if the reference station that causes the best condition matrix is selected. In the new solution, there is no need to find the base station which causes the best matrix condition since every base station is used equally. Especially when the noise increases or the geometrical set-up is unfavourable, the results of the symmetrical approach are superior to its non-symmetrical counterpart.

REFERENCES

[1] J. S. Abel and J. W. Chaffee. Existence and uniqueness of gps solutions. IEEE Transactions on Aerospace and Electronic Systems, 27(6):952–956, Nov 1991.
[2] S. Bancroft. An algebraic solution of the gps equations. IEEE Transactions on Aerospace and Electronic Systems, AES-21(1):56–59, Jan 1985.
[3] J. Chaffee and J. Abel. On the exact solutions of pseudorange equations. IEEE Transactions on Aerospace and Electronic Systems, 30(4):1021–1030, Oct 1994.
[4] W. H. FOY. Position-location solutions by taylor-series estimation. IEEE Transactions on Aerospace and Electronic Systems, AES 12(2):187–194,March 1976.
[5] R. Pfeil, S. Schuster, P. Scherz, A. Stelzer, and G. Stelzhammer. A robust position estimation algorithm for a local positioning measurement system. In Wireless Sensing, Local Positioning, and RFID, 2009. IMWS 2009. IEEE MTT-S International Microwave Workshop on, pages 1–4, Sept 2009.
[6] K. Pourvoyeur, A. Stelzer, Alexander Fischer, and G. Gassenbauer. Adaptation of a 3-D local position measurement system for 1-D applications. In Radar Conference, 2005. EURAD 2005. European, pages 343–346, Oct 2005.
[7] K. Pourvoyeur, A. Stelzer, T. Gahleitner, S. Schuster, and G. Gassenbauer. Effects of motion models and sensor data on the accuracy of the LPM positioning system. In Information Fusion, 2006 9th International Conference on, pages 1–7, July 2006.
[8] K. Pourvoyeur, A. Stelzer, and G. Gassenbauer. Position estimation techniques for the local position measurement system LPM. In Microwave Conference, 2006. APMC 2006. Asia-Pacific, pages 1509–1514, Dec 2006.
[9] A. Stelzer R. Pfeil, K. Pourvoyeur and G. Stelzhammer. Distributed fault detection for precise and robust local positioning. In Proceedings of the 13th IAIN World Congress and Exhibition, 2009.
[10] A. Resch, R. Pfeil, M. Wegener, and A. Stelzer. Review of the LPM local positioning measurement system. In Localization and GNSS (ICLGNSS), 2012 International Conference on, pages 1–5, June 2012.
[11] J. Sidorenko, N. Scherer-Negenborn, M. Arens, and E. Michaelsen. Multilateration of the local position measurement. In 2016 International Conference on Indoor Positioning and Indoor Navigation (IPIN), pages 1–8, Oct 2016.
[12] N. Sirola. Closed-form algorithms in mobile positioning: Myths and misconceptions. In 2010 7th Workshop on Positioning, Navigation and Communication, pages 38–44, March 2010.
[13] A. Stelzer, K. Pourvoyeur, and A. Fischer. Concept and application of lpm - a novel 3-d local position measurement system. IEEE Transactions on Microwave Theory and Techniques, 52(12):2664–2669, Dec 2004.
[14] Y. Zhou, C. L. Law, Y. L. Guan, and F. Chin. Indoor elliptical localization based on asynchronous uwb range measurement. IEEE Transactions on Instrumentation and Measurement, 60(1):248–257, Jan 2011.

4.3. P-III: Decawave UWB clock drift correction and power self-calibration

Authors

Juri Sidorenko, Volker Schatz, Norbert Scherer-Negenborn, Michael Arens, Urs Hugentobler.

Journal paper

Sensors 2019, 19, 2942, DOI: 10.3390/s19132942

Introduction

The precision of the Decawave UWB system is mainly affected by the received signal power and the clock drift. The classical approach to obtain the signal power dependency is to measure the distances between two transceivers for a range of some meters and comparing the results with the ground truth data. This approach requires additional measurement equipment for the ground truth distance measurements. Clock drift correction is obtained by the integrator of the phase locked loop (PLL) . Unfortunately, the integrator of the PLL is affected by the signal power.
In this publication an approach is presented allowing to obtain the signal power error curve by self-calibration and the clock drift without the PLL. This also answers the questions $Q^1_{UWB}$and Q^2_{UWB}

Summary

The developed clock drift correction method is using the information about the difference of the transmitted and received timestamps. It can be assumed, that the difference of two timestamps for the transmitted signal is equal the time difference at the receiving station. If not, one station has a higher clock frequency than the other. The same applies for three messages, as long as the relative speed is negligible. Experiments have shown that for short time intervals it is possible to assume a constant clock drift, see Figure 9. With three messages it is possible to estimate the clock drift error of the second signal. This assumption leads to a clock drift error approximation by linear interpolation.

Figure 12, shows that a change of the transmitted signal strength of the second signal would result in a time stamp error of the received signal. This dependency between the signal power and time stamp shift can be used to obtain the correction curve presented in Figure 15. A byproduct of this self-calibration is also the correction curve for the measured signal power and the correct signal power. This correction

is not required for the TOA or TDOA positioning but could be used for other localization principles, based on position estimation on signal power like Received Signal Strength Indication (RSSI). In the last part of the publication the developed clock drift correction and signal power curve is verified by two way ranging (TWR) with different distances. The TWR is performed between two stations R and T. Equation 4.1 shows how the correction terms for the signal power E_i and the clock drift $C_{n,m}$ error are applied, to obtain the time of flight between the station R and T, $0.5 \cdot \left(\Delta T^R_{1,2} - \Delta T^T_{1,2}\right)$. The unknown hardware delay is represented by the variable Z.

$$T_{TOA} = 0.5 \cdot \left(\Delta T^R_{1,2} - \Delta T^T_{1,2} - \left(\frac{C^{RT}_{1,3}}{\Delta T^T_{1,3}} \cdot \left(\Delta T^T_{1,2} + E_1\right)\right) - E_2 - E_1\right) + Z \quad (4.1)$$

The small standard deviation error of $0.015\,m$ indicates that both corrections are well-performing.

Conclusions and outlook

The signal power correction curve obtained by self-calibration is individual for every station, seen in Figure 16. This method eliminates the need for additional measurement equipment. On the other hand, the offset of this curve is unknown, defined by the signal strength with zero time stamp shift. However, this offset is constant and can be obtained like the antenna delay. The next step is the development of a TDOA method with the ability to use the correction methods presented in this publication.

Declaration of own contribution

The idea for the power self-calibration algorithm as well as the clock drift correction comes from the first author. Moreover, the software and hardware was prepared by the first author, more information about the framework development can be found in the Appendix. The co-authors improved the paper through their comments and corrections about the layout, content and the obtained results. **The overall own contribution is estimated at 94 %.**

Criteria	Estimated own contribution
Paper concept	100 %
Computations and software development	100 %
Data analysis and interpretation of results	90 %
Design and creation of figures	100 %
Manuscript structure and writing	80 %

Table 4.3.: Apportionment of own contributions for P-III

sensors

MDPI

Article

Decawave UWB Clock Drift Correction and Power Self-Calibration

Juri Sidorenko [1,2,*,†], Volker Schatz [1], Norbert Scherer-Negenborn [1], Michael Arens [1] and Urs Hugentobler [2]

[1] Fraunhofer Institute of Optronics, System Technologies and Image Exploitation IOSB, 76275 Ettlingen, Germany
[2] Institute of Astronomical and Physical Geodesy, Technical University of Munich, 80333 Munich, Germany
* Correspondence: juri.sidorenko@iosb.fraunhofer.de; Tel.: +49-7243-992-351
† Current address: Gutleuthausstraße 1, 76275 Ettlingen, Germany.

Received: 21 May 2019; Accepted: 2 July 2019; Published: 4 July 2019

Abstract: The position accuracy based on Decawave Ultra-Wideband (UWB) is affected mainly by three factors: hardware delays, clock drift, and signal power. This article discusses the last two factors. The general approach to clock drift correction uses the phase-locked loop (PLL) integrator, which we show is subject to signal power variations, and therefore, is less suitable for clock drift correction. The general approach to the estimation of signal power correction curves requires additional measurement equipment. This article presents a new method for obtaining the curve without additional hardware and clock drift correction without the PLL integrator. Both correction methods were fused together to improve two-way ranging (TWR).

Keywords: ultra-wideband (UWB); time of arrival (TOA); navigation

1. Introduction

In the last century, autonomous systems became omnipresent in almost every field of the industry. One of the most important tasks in robotics is the interaction between a robot and its environment. This task can only be accomplished if the location of the robot with respect to its environment is known. Visual sensors are very common for localization [1,2]. In some cases, estimating the position in non-line-of-sight conditions is required. Radio-frequency-based (RF) sensors are able to operate in such conditions, but the outcome depends highly on measurement principles, such as received signal strength indicator (RSSI) [3], fingerprinting [4], FMCW [5] and UWB [6], as well as on techniques such as the angle of arrival [7], time of arrival [8] or time difference of arrival [9]. Indoor positioning is, in general, a challenge for RF-based localization systems. Reflections could cause interference with the main signal. In contrast to narrowband signals are ultra-wideband (UWB) signals, which are more robust to fading [10,11]. A common UWB system is the Decawave UWB transceiver [12], which is low cost and provides centimeter precision. The accuracy and precision of this chip are affected by three factors: hardware delays, clock drift, and signal power [13,14]. This article discusses clock drift correction and signal power error, which is specific to the Decawave UWB transceiver and affects the accuracy of the position significantly. The general approach to estimating signal power dependency is to use ground truth data, which are provided by additional measurement equipment [15]. The clock drift error is caused by the different frequencies of the transceiver clocks. The general approach to Decawave UWB clock drift correction is to use the integrator of the phase-locked loop (PLL) [16–19]. In the following section, we explain that the general approach to clock drift correction is not suitable because the PLL is also affected by the signal power. Therefore, a more accurate method for clock drift correction is presented. The middle sections of this article discuss the estimation of the signal power

correction curve without the need for additional hardware. As far as we know, nobody has obtained a signal power correction curve by self-calibration before. The last part of this article presents a two-way ranging (TWR) method that is able to use the correction methods for distance estimation.

2. Decawave UWB

Decawave transceivers are based on UWB technology and are compliant with IEEE802.15.4-2011 standards [20]. They support six frequency bands with center frequencies from 3.5 GHz to 6.5 GHz and data rates of up to 6.8 Mb/s. The bandwidth varies with the selected center frequencies from 500 up to 1000 MHz. With higher bandwidth, the send impulse becomes shorter. The timestamps for the positioning are provided by an estimation of the channel impulse response, which is obtained by correlating a known preamble sequence against the received signal and accumulating the result over a period of time. In contrast to narrowband signals, UWB is more resistant to multipath fading. Reflections would cause an additional peak in the impulse response. The probability that two peaks interfere with each other is small. The sampling of the signal is performed by an internal 64 GHz chip with 15 ps event-timing precision (4.496 mm). Because of general regulations, the transmit power density is limited to -41.3 dBm/MHz. These regulations are due to the high bandwidth occupied by the UWB transceiver. The following experiments were carried out with the Decawave EVK1000. This board mainly consists of a DW1000 chip and an STM32 ARM processor.

3. Clock Drift Correction

In practice, it is not possible to manufacture exactly the same clock generators, so every transceiver has a different clock frequency. Clock drift correction represents the difference between clock frequencies but not current time values.

3.1. General Approach

The general approach to clock drift correction is to use the PLL integrator [16–19]. Figure 1 shows an example of frequency demodulation by a PLL. The voltage-controlled oscillator (VCO) is set to the mid-position and the loop is locked in at the frequency of the carrier wave. Modulations on the carrier would cause the VCO frequency to follow the incoming signal, so changes in the voltage correspond to the applied modulations. The difference between the received carrier frequency (VE) and the internal loop frequency (VI) can be observed in the integrator of the loop filter. In Figure 2, the integrator output is presented. The test scenario is based on measurements obtained at every 50 ms between two stationary transceivers. The difference between the two frequencies is about five parts per million. Reaching the final condition took up to 15 min. The tests were repeated four times with another two stationary stations. Figure 3 shows the filtered results of the obtained curves provided by a 500-point moving average filter. The curve progression is deterministic. Decawave indicates that the logarithmic increase of the integrator at the beginning is due to the warm-up when the crystal oscillator is activated, graphically represented in Figure 4. This oscillator follows from the combination of a quartz crystal and the circuitry within the DW1000-based design.

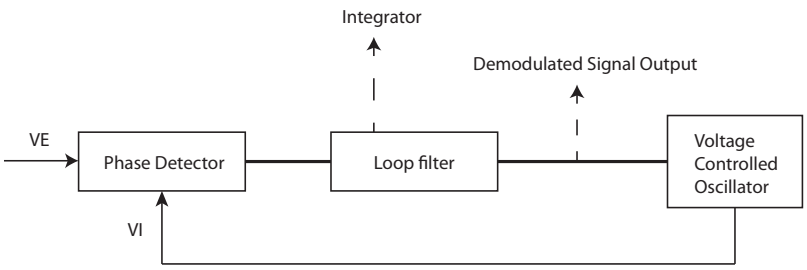

Figure 1. Example of the phase locked loop (PLL).

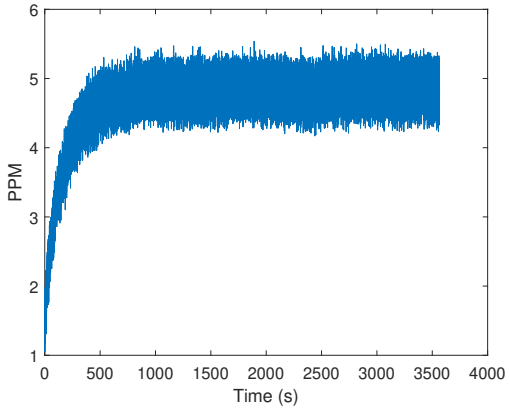

Figure 2. Frequency difference between the received carrier and the internal phase locked loop (PLL) in parts per million (PPM). The curve is obtained by reading the carrier integrator value of the DW1000 chips. The logarithmic increase of the curve is due to the warm-up of the crystal oscillator.

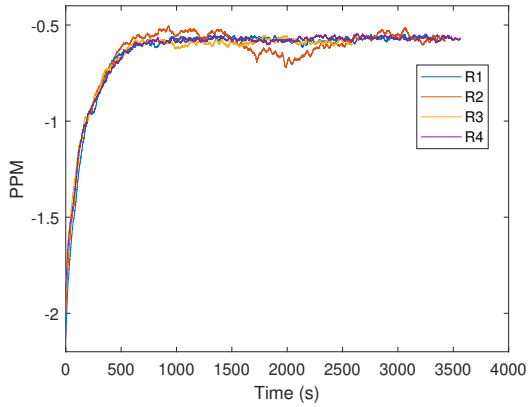

Figure 3. Filtered frequency difference between the received carrier and the internal phase locked loop (PLL) in parts per million (PPM). The colors represent different measurement obtained successively. It can be seen that the curves are deterministic.

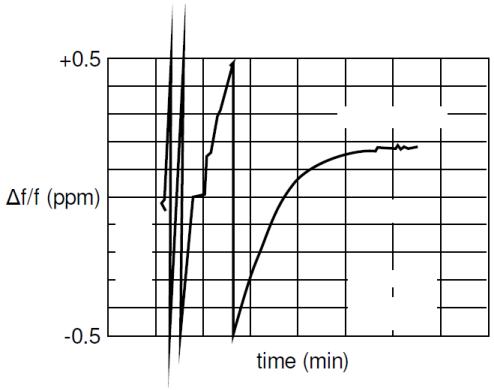

Figure 4. Frequency difference during the warm-up phase of the DW1000 crystal oscillator in parts per million (PPM) with respect to the time in minutes [15]. The figure is used with permission [15].

In the following test scenario, the effect of the signal power on the integrator was investigated. Both the transmitter and receiver stations were stationary. Figure 5 shows the measured signal strength at the receiving station. After about 2340 s, we arranged the transmitter to reduce the signal power. The integrator of the receiver jumped after the signal power changed to a new level (Figure 6), indicating that distance changes between the transmitter and receiver would affect the integrator, and so, affect the clock drift correction as well.

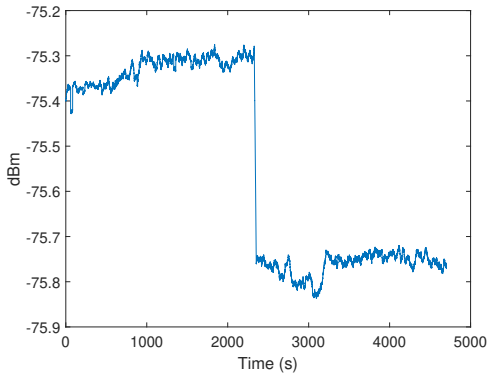

Figure 5. Signal power in dBm of the received blink message. The curve shows the filtered results of the received signal power over time, measured by the DW1000 chip. After 4600 measurements the transmitting signal power was reduced.

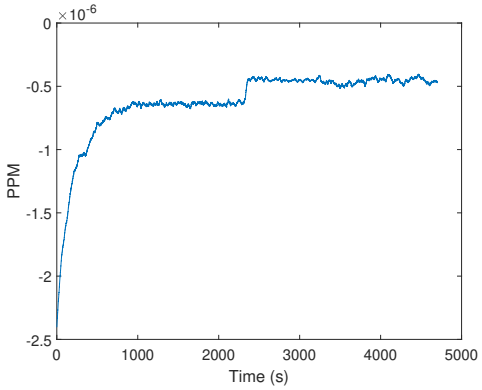

Figure 6. Filtered frequency differences between the received carrier and the internal phase locked loop (PLL) in parts per million (PPM) after changing the transmitting signal power after about 2340 s.

The reason for this dependency could be the analog phase detectors of the PLL, in which the loop gain K_D is a function of amplitude, which affects the error signal $v_e(t) = K_D[\Phi_{Out}(t) - \Phi_{In}(t)]$, and so, affects the pull-in time (total time taken by the PLL to lock) as well.

3.2. Proposed Approach for the Clock Drift Correction

In this section, we present an alternative method for the clock drift correction, which is independent of the signal power. The measurement setup is presented in Figure 7. All measurements and calibrations were conducted with Decawave EVK1000 boards. The station with the identification number (id) 2 is the transmitting station (TX). The receiving station (RX) has the identification number 1. The receiving signal power, as well as the timestamps, were obtained by reading the register provided

by the transceivers [14,15]. The general settings for the hardware setup can be found in Table 1 and the notations in Table 2.

Figure 7. The measurement setup consist of two transceivers (EVK100) with the identification number 1 and 2.

Table 1. Test settings.

Parameter	Value
Center Frequency	3993.6 MHz
Bandwidth	499.2 MHz
Pulse repetition frequency	64 MHz
Preamble length	128
Data rate	6.81 Mbps

Table 2. Notations used.

Notations	Definition
T_i	Timestamp
$\Delta T_{n,m}$	Clock drift with respect to the timestamps n and m
E_i	Timestamp error due to signal power
Z	Hardware delay and signal power correction offset

Figure 8 shows a schematic diagram of the approach. TX is sending three signals at times T_1, T_2, and T_3. The clocks of the transmitter and receiver are not synchronous. If the clocks have no drift, then both clocks should have the same frequency and the difference between $\Delta T_{1,2} = T_2 - T_1$ should be the same for the transmitter and the receiver; otherwise, $\Delta T_{1,2}^{RX} \neq \Delta T_{1,2}^{TX}$. The same applies to $\Delta T_{1,3}$. If the clock of RX is running faster than that of TX, then $\Delta T_{1,3}^{RX} > \Delta T_{1,3}^{TX}$ and the clock drift error becomes $C_{1,2} = \Delta T_{1,2}^{RX} - \Delta T_{1,2}^{TX}$.

Previously, the frequency difference between the two clocks was presented by the integrator of the PLL. After the warm-up time, the clocks reached their final frequencies. The clock error now increased linearly. For short measurement periods the clock drift error can be assumed to be linear even during the the oscillator's warm-up.

The main idea is for the clock drift error $C_{1,3} = \Delta T_{1,3}^{RX} - \Delta T_{1,3}^{TX}$ to be used for correcting the timestamp T_2 by simple linear interpolation. In Figure 9, three messages, P1, P2, and P3, with constant signal powers have been sent. The delay between every message was about 2 ms. The values are already filtered; hence, every point consists of the mean of 2000 measurements. The Figure 10 shows the clock drift error $C_{1,2} = \Delta T_{1,2}^{RX} - \Delta T_{1,2}^{TX}$. Because of the long delay, the distance error resulting from the clock drift is about 1 m.

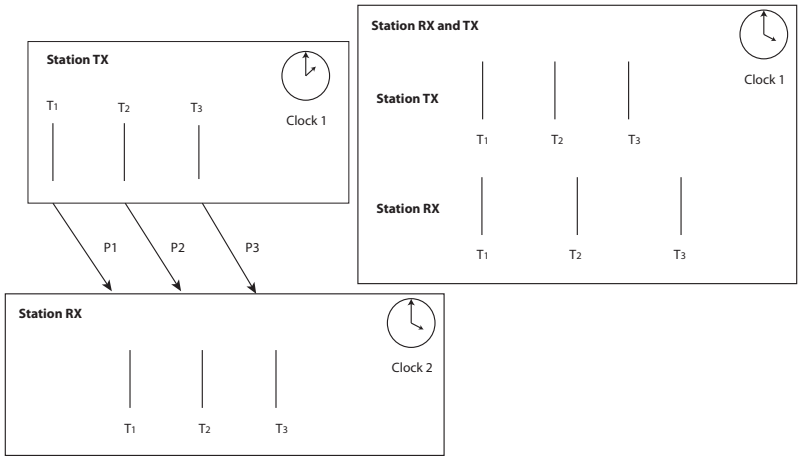

Figure 8. Schematic for the presented clock drift correction based on three transmitting messages. See text for explanation.

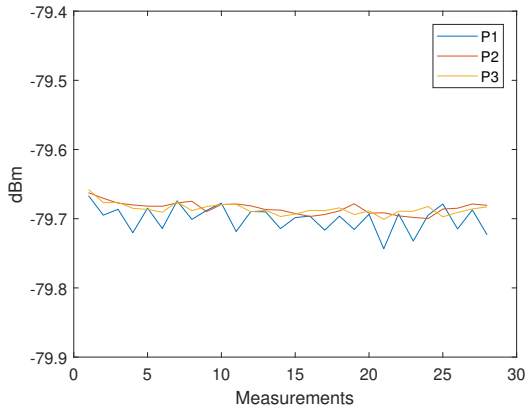

Figure 9. Filtered received signal power measurements of the three messages: P1, P2 and P3.

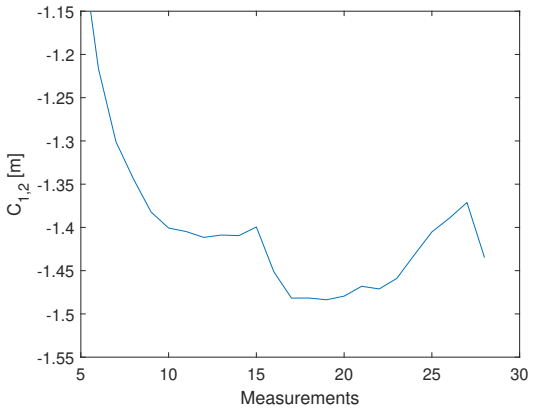

Figure 10. The error in meters caused by the clock drift. The curve is changing, due to the clock warm-up.

In the next step, the clock drift error $C_{1,2}$ is corrected by the linear interpolation of $C_{1,3}$.

$$C'_{1,2} = C_{1,2} - \frac{C_{1,3}}{\Delta T^{TX}_{1,3}} \cdot \Delta T^{TX}_{1,2} \tag{1}$$

The results are shown in Figure 11. The correction requires only three messages and the remaining average offset is about $-1.915 \cdot 10^{-5}$ m. The linear interpolation is also suitable for the warm-up phase. The implementation of the presented clock drift correction for the TWR is presented in the last section. A position error caused by a constant velocity of the object is also corrected by the linear interpolation, due to the linear increase of the position error (pseudo clock drift). In practice, it is possible to obtain $\Delta T^{TX}_{1,3}$ = 1 ms. An acceleration high enough to cause an error greater than 5 mm would require almost 1000 g $\left(10^4 \frac{m}{s^2}\right)$.

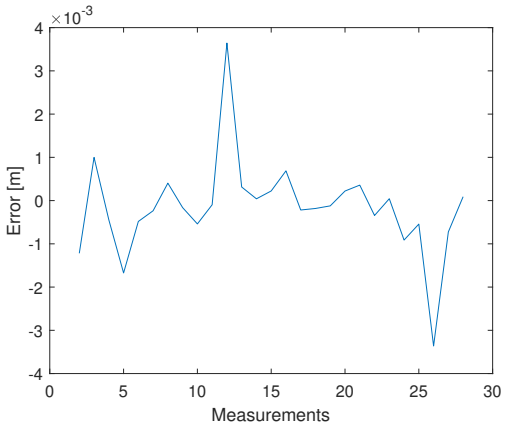

Figure 11. The error in meters after the clock drift correction. $C'_{1,2}$.

4. Signal Power Correction

The next section discusses the signal power correction. It is known that the time stamp of the DW1000 is affected by the signal power, in which an increase causes a negative shift of the time stamp and vice versa.

4.1. General Approach

Figure 12 illustrates the reported distance error with respect to the received signal power. At a certain signal strength, the range bias effect should be zero. In Figure 12 the bias vanishes between -80 and -75 dBm. The correction curve is affected by the system design elements, such as printed circuit boards, antenna gain, and pulse repetition frequency (PRF). The general approach to correction curve estimation is to compare the distance measurements with the ground truth distances. This method has two disadvantages. First of all, additional measurement equipment is necessary. Second, every created curve applies to two stations but not every individual station.

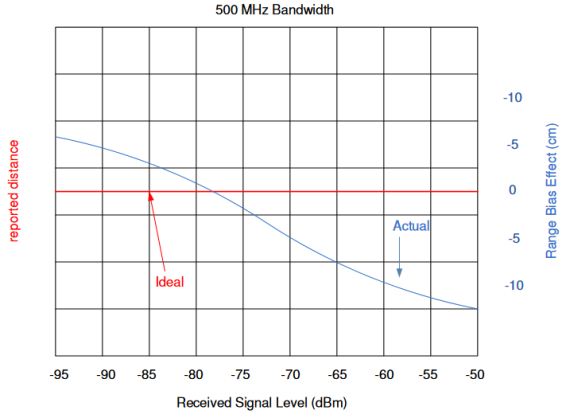

Figure 12. The effect of the received signal power on the distance measurement [15], used with permission. The red line represents the correct distance measurements. The blue line shows the range bias caused by different signal powers [15].

Figure 13 shows the relationship between the measured and correct signal strengths for different PRF. The measured signal power is correct only for measurements smaller than −85 dBm. The knowledge of the difference between the measured and correct signal strengths can be used for additional measurement techniques, such as the RSSI, for distance estimation.

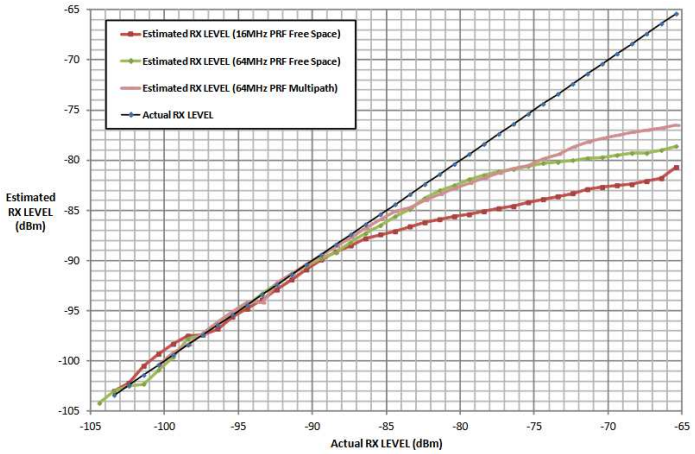

Figure 13. Measured received signal power at the DW1000 chip, with respect to the correct signal power. The blue line represent the reference line, every value of the x-axis has the same value on the y-axis. The other lines are the results of the estimated received signal power with different settings. The estimated received signal power equates the correct signal power for low signal strength [14].

4.2. Proposed Approach for the Signal Power Correction

In the previous section, we discussed an alternative approach to clock drift correction with three messages (P1, P2, and P3). The following method is based on this concept, but the TX station changes the signal strength of the second message (P2). Figure 14 shows how the signal strengths of the first and last messages (P1 and P3) remain constant and only the signal strength of the second signal (P2) decreases after 1000 measurements. Every measurement point is the result of the mean of 2000 signals. The tests were conducted with a cable connection of 10 cm and the transmitter decreased the signal gain with a step size of 3 dB. The transmit power settings can be adjusted by changing the gain of the

transmit Driver Amplifier (DA) and the transmit Mixer. These changes are not equivalent to the output power. Figure 11 shows that, after the clock drift correction, the remaining error of $C'_{1,2}$ (1) is close to zero. With the decreasing signal strength of P2, the error of $C_{1,2}$ is increasing, see Figure 15. Hence, it is possible to create a dependency between the measured signal strength and the timestamp error.

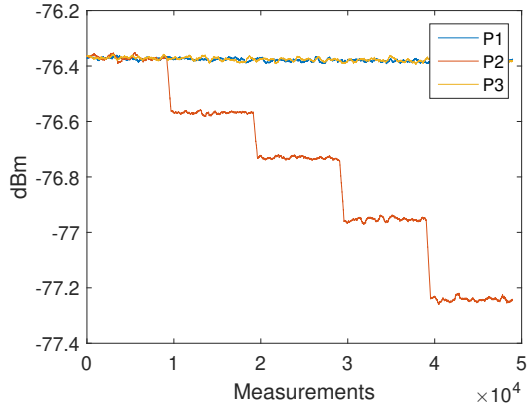

Figure 14. Filtered received signal power measurements of the three messages P1, P2 and P3. The measurements have been obtained with a cable connection between the transceivers. The transmitted signal power of the second signal P2 is reduced with a step size of 3 dB, while the signal power for P1 and P3 remains constant.

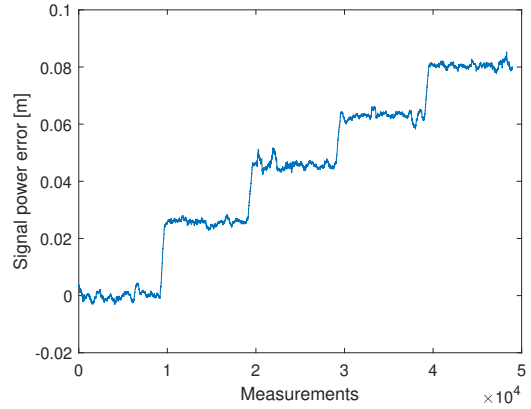

Figure 15. Filtered timestamp error changes due to the received signal power. The measurements have been obtained with a cable connection between the transceivers. The error is changing systematically with decreasing signal power.

In the following test scenario, the power calibration was repeated with an antenna and a distance of 1.5 m between the RX and TX stations. The gain step size was reduced to 0.5 dB. Figures 16 and 17 shows the results of the filtered signal power calibration curve. The main difference between Decawave's curve, as shown in Figure 12, and our curve is that the zero line is unknown. This line marks the signal power at which the timestamp error is zero. The step size of the decreasing transmitting signal power gain was constant, but the measured decreasing signal power curve for P2 was nonlinear because the measured signal power did not equate to the correct signal power for high signal strength, as shown in Figure 12.

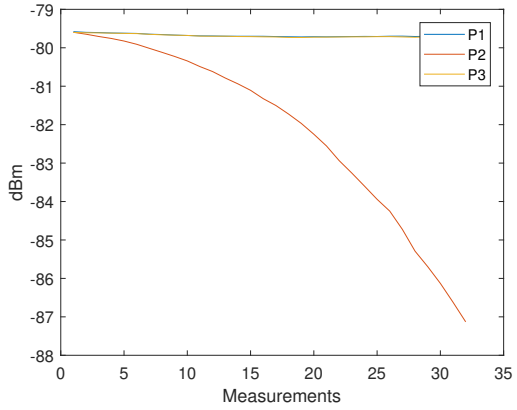

Figure 16. Filtered received signal power measurements of the three messages P1, P2 and P3. The measurements have been obtained with a wireless connection between the transceivers. The transmitted signal power of the second signal P2 is reduced with a step size of 0.5 dB, while the signal power for P1 and P3 remains constant.

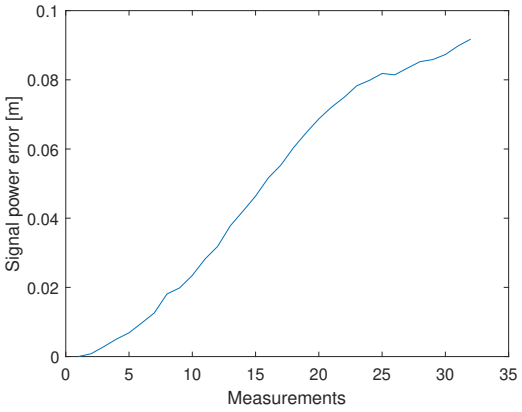

Figure 17. Filtered timestamp error changes due to the received signal power. The measurements have been obtained with a wireless connection between the transceivers. The error is changing with decreasing signal power.

It is necessary to pay attention to the timing between the messages. With short delays between the messages, it is possible that they affect each other. This effect can be seen by the offset between P1 and P3 in Figure 18. In Figure 16 a delay of 2 ms was used between the messages and in Figure 18 a delay of 150 µs was used.

It was previously mentioned that the measured signal strength equals the correct signal power only for small signal powers. Therefore, it is possible to use the very first measurements with small signal strengths to estimate the slope. Figure 19 shows an estimated line based on the estimated slope. The results are the same as the curve obtained by Decawave except that no additional measurement equipment is required and our curves can be obtained individually for every station. Figure 20 illustrates the correction curve with respect to the signal power.

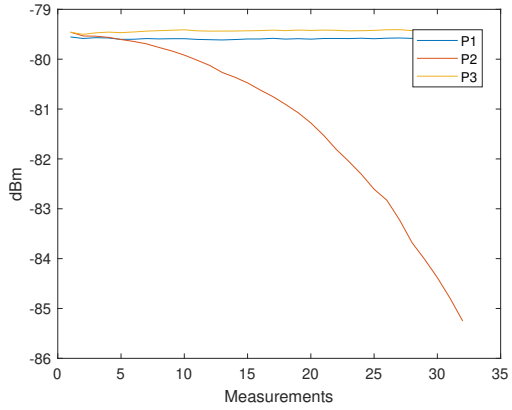

Figure 18. Interference between the received messages P1, P2 and P3. The transmitted signal power of the message P1 and P3 are the same. Due to the short update time are the signals interfering.

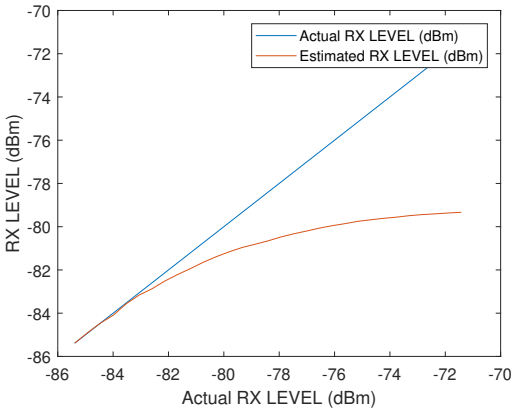

Figure 19. Estimated correction curve between the measured received signal power and the ideal signal power curve.

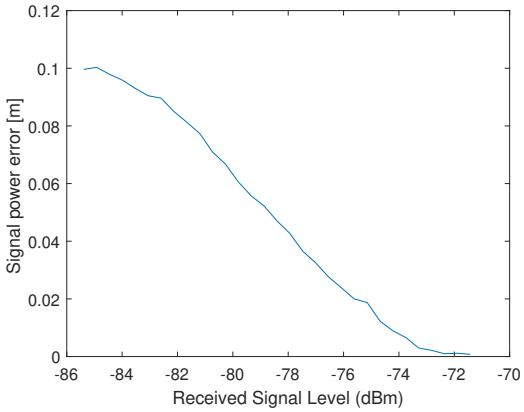

Figure 20. Correction value of the error caused by the signal power as a function of the received signal power.

Even for the same hardware design, it is possible that the shape of the correction curve differs. In Figures 21 and 22, the final results of the power correction curve are obtained from another station. The calibration was repeated six times. The shapes of the curves are deterministic but different from those of the station above. Therefore, it makes sense to repeat the calibration for every individual station.

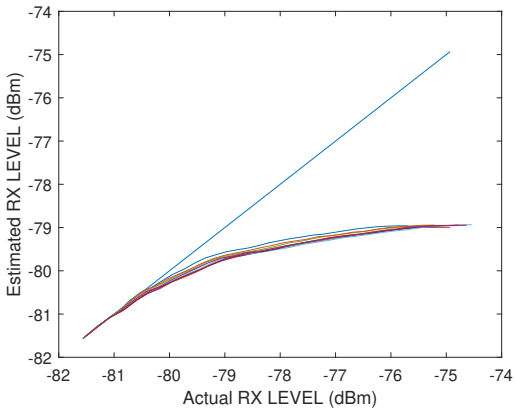

Figure 21. Power correction curve for the received signal power.

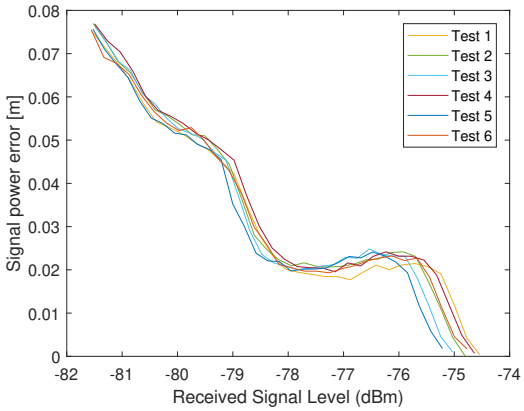

Figure 22. Correction value of the error caused by the signal power as a function of the received signal power for a different station with six restarts.

5. Two Way Ranging

The following section describes how the presented clock drift and signal power correction can be used for precise TWR. Figure 23 shows the concept for the TWR. The initial message is sent by the reference station at T_1^R and received by the tag. The timestamp T_2^T is affected by the signal power and causes an error E1. After some delay caused by internal processing, the tag sends a response message at T_2^T. The reference station receives the response from the tag and saves the timestamp T_2^R, which is affected by the signal power error E2. In this example, the delay due to the hardware offset is not considered.

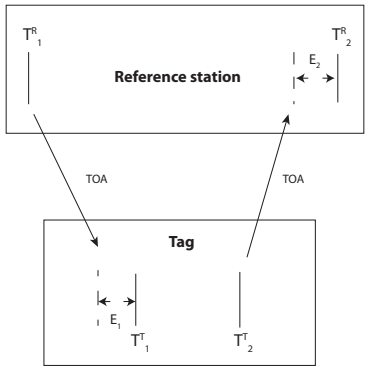

Figure 23. Schematic for the signal power correction for two-way ranging.

The time of flight between the reference station and the tag can be determined by the following formula. It is assumed that the distance between the two devices does not change between time stamp T_2^R and T_1^R.

$$T_{TOA} = \frac{\left(T_2^R - T_1^R\right) - \left(T_2^T - T_1^T\right) - E_2 - E_1}{2} \tag{2}$$

The values E1 and E2 can be obtained from the signal power correction curve. It should be taken into account that the signal power affects the tag and reference station differently. The time difference $\Delta T_{1,2}^R$ increases with decreasing signal power. The zero lines for both the signal power and hardware offset are unknown but constant; hence, both values are represented by the variable Z. In the previous section, we explained that the clock drift could be corrected by three messages. Figure 24 shows how this principle can be adapted for TWR. The last message was used to obtain the clock drift error $C_{1,3} = \Delta T_{1,3}^R - \Delta T_{1,3}^T$. The signal power E1 had no effect on the time stamp difference $\Delta T_{1,3}^T$. The final time of the flight equation with the clock drift correction becomes:

$$T_{TOA} = 0.5 \cdot \left(\Delta T_{1,2}^R - \Delta T_{1,2}^T - \frac{C_{1,3}^{RT}}{\Delta T_{1,3}^T} \cdot \left(\Delta T_{1,2}^T + E1\right)\right) + 0.5 \cdot \left(-E_2 - E_1\right) + Z$$

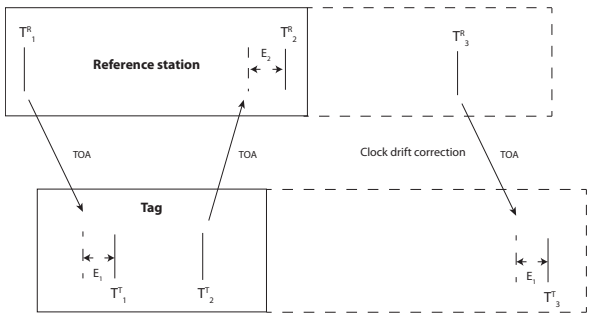

Figure 24. Two-way ranging with clock drift correction between reference station and tag.

The results of the TWR with signal power and clock drift correction are illustrated in Figure 25. The blue line represents the difference between laser distance measurements (ground truth) and distances provided by the TWR. The 11 distances extend from 3.515 m to 0.562 m. Every point results from the mean of 2000 measurements. The unknown hardware offset, which causes the 0.3 m offset, is not relevant in this example. The signal power error depends on the distance and the clock drift on time. If both effects are corrected properly, the resulting difference between the mean

error and every measurement error should be as small as possible. The standard deviation of the error is 0.015 m. The small error difference between the blue and red line shows that the signal power and clock drift correction are both sufficient. The antenna area was 0.0012 m^2; therefore, it is not possible to obtain ground truth data with a precision higher than a few centimeters.

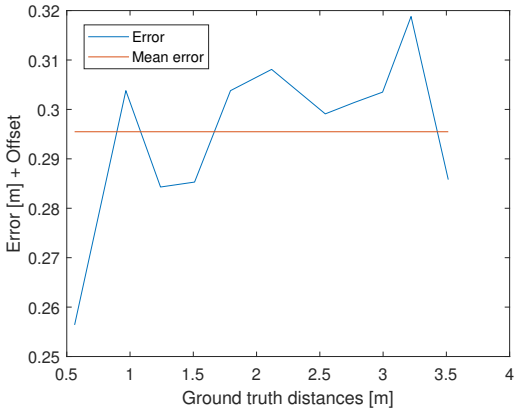

Figure 25. Difference between the measured distances obtained by two-way ranging and the ground truth distances in meter. The constant offset caused by the hardware delay is not compensated but is represented by the red line. The near most constant errors for different distances shows the power correction is correct.

6. Conclusions

This article presents a new method for signal power and clock drift correction. It was shown that the curves obtained for the signal power correction could be highly accurate and deterministic, as well as provide individual results for every station. The signal power correction procedure can be performed once as a factory calibration. In addition to the estimation of the signal power correction curve, it was also possible to obtain the relationship between the measured and real signal powers. Knowing the relationship allows for better distance estimations with methods based on the signal strength. In contrast to the general approach, our clock drift correction is independent of the signal power and promises results with centimeter accuracy. The last part of the article explained how the signal power and clock drift correction are fused together to provide highly accurate TWR.

7. Patents

Patent pending.

Author Contributions: The idea for the power self-calibration algorithm as well as the clock drift correction was done by J.S.; The coauthors V.S., N.S.-N., M.A. and U.H. improved the paper through their comments and corrections about the layout, content and the obtained results. Conceptualization, methodology, software, validation, visualization, formal analysis, investigation and writing-original draft preparation was done by J.S.; Supervision, project administration was done by N.S.-N. and U.H.; Funding acquisition was done by M.A.

Funding: This research was funded by Fraunhofer Institute of Optronics, System Technologies and Image Exploitation IOSB.

Conflicts of Interest: The authors declare no conflict of interest.

Abbreviations

The following abbreviations are used in this manuscript:

UWB	Ultra-wideband (UWB)
TOA	Time of Arrival (TOA)
PLL	Phase-locked loop
TWR	Two-way ranging
FMCW	Frequency modulated continuous wave
VCO	Voltage-controlled oscillator
VE	Received carrier frequency
VI	Internal loop frequency
PPM	Parts per million
TX	Transmitting station
RX	Receiving station
PRF	Pulse repetition frequency
RSSI	Received signal strength indication

References

1. Liu, C.; Wang, J.; Zhang, Z.; Bian, X.; Mei, X. SLAM for planar mobile robot. In Proceedings of the 2nd IEEE Advanced Information Management, Communicates, Electronic and Automation Control Conference (IM-CEC), Xi'an, China, 25–27 May 2018; pp. 1239–1242.
2. Wang, Z.; Jia, Q.; Ye, P.; Sun, H. A depth camera based lightweight visual SLAM algorithm. In Proceedings of the 4th International Conference on Systems and Informatics (ICSAI), Hangzhou, China, 11–13 November 2017; pp. 143–148.
3. Shen, X.; Yang, S.; He, J.; Huang, Z. Improved localization algorithm based on RSSI in low power bluetooth network. In Proceedings of the 2nd International Conference on Cloud Computing and Internet of Things (CCIOT), Dalian, China, 22–23 October 2016; pp. 134–137.
4. Zhu, J.Y.; Xu, J.; Zheng, A.X.; He, J.; Wu, C.; Li, V.O.K. WIFI fingerprinting indoor localization system based on spatio-temporal (s-t) metrics. In Proceedings of the International Conference on Indoor Positioning and Indoor Navigation (IPIN), Busan, Korea, 27–30 October 2014; pp. 611–614.
5. Resch, A.; Pfeil, R.; Wegener, M.; Stelzer, A. Review of the LPM local positioning measurement system. In Proceedings of the International Conference on Localization and GNSS, Starnberg, Germany, 25–27 June 2012; pp. 1–5.
6. Zwirello, L.; Schipper, T.; Jalilvand, M.; Zwick, T. Realization limits of impulse-based localization system for large-scale indoor applications. *IEEE Trans. Instrum. Meas.* **2015**, *64*, 39–51. [CrossRef]
7. Dotlic, I.; Connell, A.; Ma, H.; Clancy, J.; McLaughlin, M. Angle of arrival estimation using decawave DW1000 integrated circuits. In Proceedings of the 14th Workshop on Positioning, Navigation and Communications (WPNC), Bremen, Germany, 25–26 October 2017; pp. 1–6.
8. Barua, B.; Kandil, N.; Hakem, N. On performance study of TWR UWB ranging in underground mine. In Proceedings of the Sixth International Conference on Digital Information, Networking, and Wireless Communications (DINWC), Beirut, Lebanon, 25–27 April 2018; pp. 28–31.
9. Zhou, Y.; Law, C.L.; Guan, Y.L.; Chin, F. Indoor elliptical localization based on asynchronous UWB range measurement. *IEEE Trans. Instrum. Meas.* **2011**, *60*, 248–257. [CrossRef]
10. Gerrits, J.F.M.; Farserotu, J.R.; Long, J.R. Multipath behavior of FM-UWB signals. In Proceedings of the IEEE International Conference on Ultra-Wideband, Singapore, 24–26 September 2007; pp. 162–167.
11. Saeed, R.A.; Khatun, S.; Ali, B.M.; Khazani, M.A. Ultra-wideband (UWB) geolocation in NLOS multipath fading environments. In Proceedings of the 13th IEEE International Conference on Networks Jointly held with the 2005 IEEE 7th Malaysia International Conf on Communic, Kuala Lumpur, Malaysia, 16–18 November 2005; pp. 1068–1073.
12. Ruiz, A.R.J.; Granja, F.S. Comparing ubisense, bespoon, and decawave UWB location systems: Indoor performance analysis. *IEEE Trans. Instrum. Meas.* **2017**, *66*, 2106–2117. [CrossRef]

13. McElroy, C.; Neirynck, D.; McLaughlin, M. Comparison of wireless clock synchronization algorithms for indoor location systems. In Proceedings of the IEEE International Conference on Communications Workshops (ICC), Sydney, NSW, Australia, 10–14 June 2014; pp. 157–162.
14. DECAWAVE. DW1000 User Manual, Version 2.15, p. 45. Available online: https://www.decawave.com (accessed on 3 July 2019).
15. DECAWAVE. APS011 APPLICATION NOTE: Sources of Error in TWR Schemes, Version 1.0, p. 10. Available online: https://www.decawave.com (accessed on 3 July 2019).
16. Fofana, N.I.; Van Den Bossche, A.; Dalcé, R.; Val, T. An original correction method for indoor ultra wide band rangingbased localisation system. In *Ad-Hoc Mobile and Wireless Networks, Proceedings of the International Conference on Ad-Hoc Networks and Wireless, Lille, France, 4–6 July 2016;* Springer: Berlin, Germany, 2016; Volume 9724, pp. 79–92.
17. Van Den Bossche, A.; Dalce, R.; Fofana, N.I.; Val, T. DecaDuino: An ppen framework for wireless time-of-flight ranging systems. In Proceedings of the IFIP Wireless Days (WD), Toulouse, France, 23–25 March 2016; pp. 1–7.
18. Martel, F.M.; Sidorenko, J.; Bodensteiner, C.; Arens, M. Augmented reality and UWB technology fusion: Localization of objects with head mounted displays. In Proceedings of the 31st International Technical Meeting of The Satellite Division of the Institute of Navigation (ION GNSS+), Miami, FL, USA, 24–28 September 2018; pp. 685–692.
19. Dotlic, I.; Connell, A.; McLaughlin, M. Ranging methods utilizing carrierfrequency offset estimation. In Proceedings of the 15th Workshop on Positioning, Navigation and Communications (WPNC), Bremen, Germany, 25–26 October 2018; pp. 1–6.
20. Haluza, M.; Vesely, J. Analysis of signals from the DecaWave TREK1000 wideband positioning system using AKRS system. In Proceedings of the International Conference on Military Technologies (ICMT), Brno, Czech Republic, 31 May–2 June 2017; pp. 424–429.

4.4. P-IV: DecaWave ultra-wideband warm-up error correction

Authors

Juri Sidorenko, Volker Schatz, Norbert Scherer-Negenborn, Michael Arens, Urs Hugentobler.

Journal paper

IEEE Transactions on Aerospace and Electronic Systems,
DOI: 10.1109/TIM.2020.2996706.

Introduction

The clock drift and power correction were presented in the publication P-III. Neither method was able to correct the distance error during the warm-up phase.

This work should find out where this error comes from and how it can be corrected by self-calibration.

Summary

Various experiments have been carried out to determine whether this error is deterministic and can be reproduced. It was found that the frequency difference not only had an impact on the clock drift, but also on the time stamp. We assumed that there is a direct connection to the LDE algorithm (Leading Edge Detection), which sets the time stamp. By setting a trim value, a frequency difference can be set. This was originally intended to set the stations to a target frequency after production to compensate for imperfections in production. Especially with small frequency differences, it was observed that the rate of change was greatest in the distance measurement.

Conclusions and outlook

The system can create a correction table itself. This process requires changing the trim value and the transmitted signal strength. This makes it possible to reduce the error from 10 cm to less than 1 cm. In contrast to publication P-III, this table is created by TWR and therefore valid only for two stations. An alternative method would be to achieve a certain non-zero frequency drift when determining the position. This means that the self-calibration according to P-III can be carried out individually for each station and therefore is also suitable for TDOA.

Declaration of own contribution

The first author came up with the idea for the self-calibration algorithm and the warm-up correction. Moreover, the software and hardware was prepared by the first author. More information about the framework development can be found in the Appendix. The co-authors improved the paper through their comments and corrections about the layout, content and the obtained results. **The overall own contribution is estimated at 95 %.**

Criteria	Estimated own contribution
Paper concept	100 %
Computations and software development	100 %
Data analysis and interpretation of results	95 %
Design and creation of figures	100 %
Manuscript structure and writing	80 %

Table 4.4.: Apportionment of own contributions for P-IV

This article has been accepted for publication in a future issue of this journal, but has not been fully edited. Content may change prior to final publication. Citation information: DOI 10.1109/TAES.2020.3015323, IEEE Transactions on Aerospace and Electronic Systems

DecaWave ultra-wideband warm-up error correction

Juri Sidorenko, Volker Schatz, Norbert Scherer-Negenborn, Michael Arens, and Urs Hugentobler

***Abstract*—In the field of indoor localization, ultra-wideband (UWB) technology is no longer dispensable. The market demands that the UWB hardware has to be cheap, precise and accurate. These requirements lead to the popularity of the DecaWave UWB system. The great majority of the publications about this system deals with the correction of the signal power, hardware delay or clock drift. It has traditionally been assumed that this error only appears at the beginning of the operation and is caused by the warm-up process of the crystal. In this article, we show that the warm-up error is influenced by the same error source as the signal power. To our knowledge, no scientific publication has explicitly examined the warm-up error before. This work aims to close this gap and, moreover, to present a solution which does not require any external measuring equipment and only has to be carried out once. It is shown that the empirically obtained warm-up correction curve increases the accuracy for the two-way-ranging (TWR) significantly.**

***Index Terms*—Indoor localization, two-way-ranging (TWR), DecaWave, ultra-wideband (UWB)**

I. Introduction

LOCALIZATION based on ultra-wideband (UWB) technology is able to operate in indoor environments, where narrow-band systems are mostly failing due to fading [1], [2]. In recent years, this technology has gained more attention and will play a significant role in the future [3]. This is mostly due to the declining price and size of the devices. One of the market leaders is DecaWave Limited [4], whereby since 2019 the UWB device is part of the new generation Apple products [5] and will spark a revolution for augmented reality, smart home, mobile payments, keyless car entry and indoor navigation [6]. The devices distributed by DecaWave are compliant with the IEEE802.15.4-2011 standard [7] and support six frequency bands with center frequencies from $3.5\,\text{GHz}$ to $6.5\,\text{GHz}$ with data rates of up to $6.8\,\text{Mb/s}$. Depending on the selected center frequency, the bandwidth ranges from 500 to $1000\,\text{MHz}$. The sampling of the signal is performed by an internal $64\,\text{GHz}$ chip with $15\,\text{ps}$ event-timing precision ($4.496\,\text{mm}$). Due to general regulations, the transmit power density is limited to $-41.3\,\text{dBm/MHz}$. These regulations are due to the high bandwidth occupied by the UWB transceiver. The vast majority of all publications on the DecaWave system are focused on the correction of the hardware delay [8], the influence of the signal power on the timestamp [9], [10] and the clock drift [11], [12], [13], [14]. Correcting these errors is very common for ultra-wideband systems [15]. Only few publications mention the warm-up error, which is attributed to the temperature fluctuation arising at power-up [16], [17], [18]. The influence of this error is reduced by waiting some time before the measurements are obtained [19] or by adapting the measurement error within the clock drift correction model [17], [20]. In practice, the accuracy obtained by the DecaWave device is about $10\,\text{cm}$ for line-of-sight (LOS) applications [7]. In this article, we present a self-calibration method to obtain a correction curve for two-way-ranging (TWR) and show how it is possible to obtain an accuracy better than $1\,\text{cm}$. The higher accuracy would allow further fields of application like tomography, where signal power and flight time information can be used to determine the material between two transceivers. The remainder of this paper is structured as follows. The first part of this article deals with the Two-way-ranging and how it is affected by the clock drift. Afterwards come the experiments, which are used to gain new information about the source of the warm-up error. Finally, the conclusion is provided.

J. Sidorenko, V. Schatz, N. Scherer-Negenborn and M.Arens are with the Fraunhofer Institute of Optronics, System Technologies and Image Exploitation IOSB, Ettlingen, 76275 Germany, e-mail: (juri.sidorenko@iosb.fraunhofer.de).

J. Sidorenko and U. Hugentobler are with the Institute of Astronomical and Physical Geodesy, Technical University of Munich, 80333 Germany.

Manuscript received September 04, 2019; revised September 04, 2019.

II. Two-way-ranging protocol

The two-way-ranging (TWR) protocol counts as a time-of-arrival measurement technique (TOA)[21]. Its purpose is to provide distance measurements between two transceivers, even if they are not synchronized. In Figure 1 plot (a), the concept of TWR between two stations, the reference and the tag, is presented. The reference station initiates the ranging process by transmitting a message at the local time T_1^R. The tag receives the message at its local time T_1^T and, at the time T_2^T, it sends a response message back to the reference station. The time-of-flight (TOF) $TOF = 0.5 \cdot \left(\Delta T_{1,2}^R - \Delta T_{1,2}^T\right)$ can be obtained by subtracting the response time $\Delta T_{1,2}^T = \left(T_2^T - T_1^T\right)$ from the transmitting and receiving time difference of the reference station $\Delta T_{1,2}^R = \left(T_2^R - T_1^R\right)$. Due to small imperfections, the frequencies of their clock crystals are not identical. In [14], a three-message-based clock drift correction protocol was presented, the so-called AltDS-TWR. This protocol has a small residual error, which only depends on the TOF. For the sake of completeness, it should be mentioned that an alternative protocol also exists with the same residual error [11]. However, this alternative protocol is strongly connected to the phase-locked-loop (PLL) and in [22], we have shown that the PLL is affected by the signal power. In order to avoid cross-dependencies between the errors, we used the AltDS-TWR protocol. Figure 1 plot (b) illustrates the way this protocol works. The first steps are equivalent to Figure 1 plot (a), whereby the only difference is that the reference station transmits a third message at its local time T_3^R, which is also received by the tag at its local time T_3^T. Without a clock drift between the two stations, the time difference $\Delta T_{1,3}^R = \left(T_3^R - T_1^R\right)$ is equal to $\Delta T_{1,3}^T = \left(T_3^T - T_1^T\right)$. If this is not the case, it is possible to interpolate linearly the clock

This article has been accepted for publication in a future issue of this journal, but has not been fully edited. Content may change prior to final publication. Citation information: DOI 10.1109/TAES.2020.3015323, IEEE Transactions on Aerospace and Electronic Systems

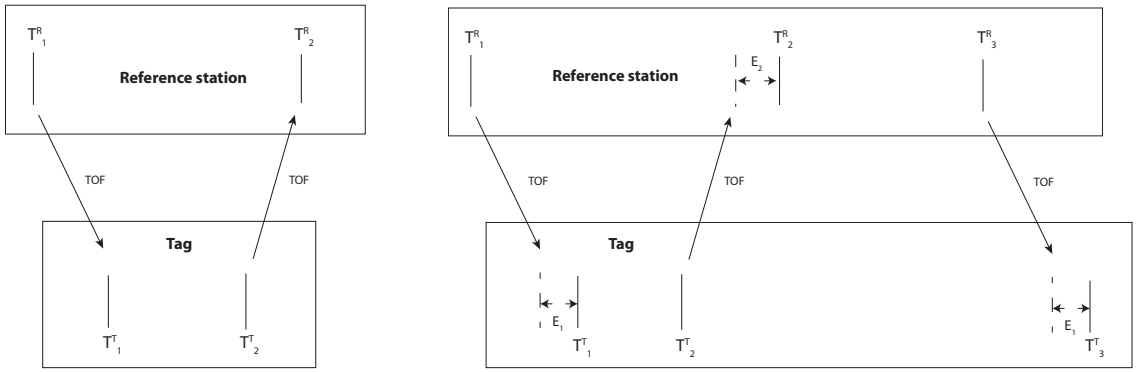

Fig. 1. Schematics of the two-way ranging between the reference station and the tag. The timestamps of the reference station have the superscript index R and the tag the index T. The shift of the timestamp caused by the signal power is labeled by E_1 and E_2. In (a) the two-way ranging with two messages is presented and in plot (b) the case with three messages.

offset to correct the ranging time stamps. Another difference between Figures 1 plot (a) and plot (b) is the shift E_1 and E_2 of the timestamp caused by signal power. In [22], we have shown that it is possible to create automatically a correction curve between the received signal power and the timestamp shift. Previously, it was the state of the art to use a correction curve based on the distance measurement and the ground truth distance [9]. The shift of the timestamp affects the timestamps T_1^T and T_3^T equally, under the assumption that the stations do not move during this message exchange of approximately one millisecond. The equal shift of both timestamps has the advantage that the signal power does not affect the clock drift correction. The hardware delay mainly depends on the temperature and can be estimated before the ranging [8], whereby this parameter is neglected for this article, due to the fact that the ambient temperature was almost constant during the experiments.

III. Experiments

In the previous section, we have discussed the well-studied clock drift correction. In this section, it is time to focus on the often neglected warm-up error. At this point, we deviate from the classical structure and immediately come to the experiments. The reason for this is that the experiments form the core element of our assumptions about the source of the warm-up error. The following experiments were carried out with the Decawave EVK1000 and an update rate of 80 Hz. This board mainly comprises a DW1000 chip and an STM32 ARM processor.

The experiments are structured as follows.

1) The experiment presented in III-B examines whether there is a dependency between the distance and the warm-up error.
2) The experiment described in III-C examines whether the changing transmitter gain affects the warm-up error.
3) In the experiment described in III-D the frequency difference is trimmed, to analyse the effects of the frequency difference on the received signal power and the warm-up error.
4) In the last experiment presented in III-E the frequency difference as well as the transmitter gain are trimmed, to show how both parameters affect the warm-up error.

Section III-F summarizes the results and offers an explanation for the observations. This section does not appear before the experiments, because if the obtained dependencies are deterministic and measurable, it is possible to provide an empirical correction curve that can be generated by self-calibration, as shown in the section IV-B. This also applies to the case when not all observations can be theoretically explained.

Fig. 2. Experimental setup with two stations mounted on a tripod.

This article has been accepted for publication in a future issue of this journal, but has not been fully edited. Content may change prior to final publication. Citation information: DOI 10.1109/TAES.2020.3015323, IEEE Transactions on Aerospace and Electronic Systems

A. Setup and typical distance measurement

In Figure 2, the experimental setup with two stations is presented. Unless otherwise stated, the stations have a distance of 1.5 m to each other. In the upcoming figures, the filtered values are presented, and unless otherwise stated, a moving average filter with a filter size of 500 measurements was used. The selected filter width is suitable to reduce the noise of the system without impairing the dynamics of the system too much. The distance measurements were all obtained with the AltDS-TWR protocol described in section II. The signal power was measured at the reference station for the upcoming experiments. In Figure 3, a typical curve of the distance measurements as a function of time is presented. Repeating the experiment with the same stations and same setup would lead to the same shape of the curve. In the Figure 4, the distance measurement was repeated three times for two other stations. The filtered data show that the curve is deterministic under the same conditions, such as signal strength, pulse repetition rate, preamble length and hardware structure. It can be observed that it takes up to 15 minutes before the curve reaches a constant value. The difference between the final value reached and the ground truth distance of 1.5 m is due to the hardware delay. This difference is irrelevant in this publication, due to the fact that it can be assumed to be constant. A possible explanation why the curve in Figure 3 is not straight could be due to the change of the reference station frequency. The residual error of the AltDS-TWR protocol depends on the TOF multiplied by the frequency change of the reference station. The DecaWave EVK1000 used is driven by a RSX-10 Rakon SMD crystal oscillator with a tolerance up to 50 ppm [23]. However, the TOF multiplied with the maximum change of the crystal oscillator offset is too small to cause an error of 3 cm. Therefore, it can be assumed that the source of this error is not the AltDS-TWR protocol. In [10], it is stated that the error at the beginning is due to the warm-up of the crystal oscillator after it is activated. This means that this error should not appear later on in the ranging process and is independent of the distance. This question justifies the first experiment, shown in the next section.

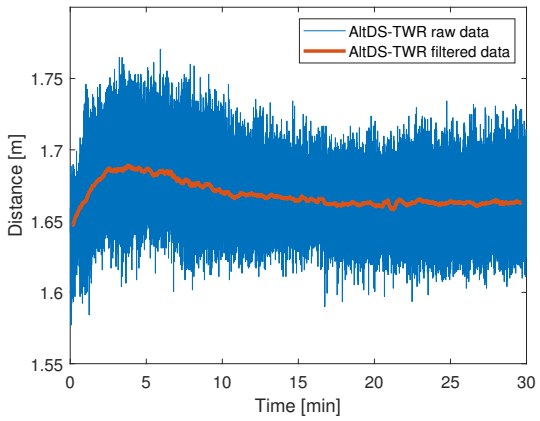

Fig. 3. Filtered typical distance measurement [m] over the time [min] provided by the AltDS-TWR protocol.

B. First experiment: Distance and distance error

In the first experiment, the distance between the reference station and the tag is changed stepwise from one meter up to three meters. Data are acquired for thirty minutes, and the last value in the sequence is subtracted from every distance measurement, because the focus is on the change over time. The subtracted distance measurements are labeled as distance errors for now. After every measurement, the device is unplugged from the power for ten minutes to restore the initial condition. Figure 5 shows the results of the first experiment. The blue curve is the distance error with a one-meter distance, the red line two meters and the yellow three meters, respectively. It can be observed that the error at the

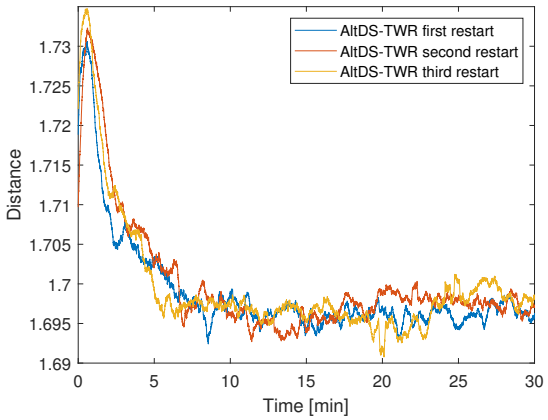

Fig. 4. Filtered typical distance measurement [m] over the time [min] provided by the AltDS-TWR protocol with alternative stations. The range measurements were repeated three times after a pause of 10 minutes.

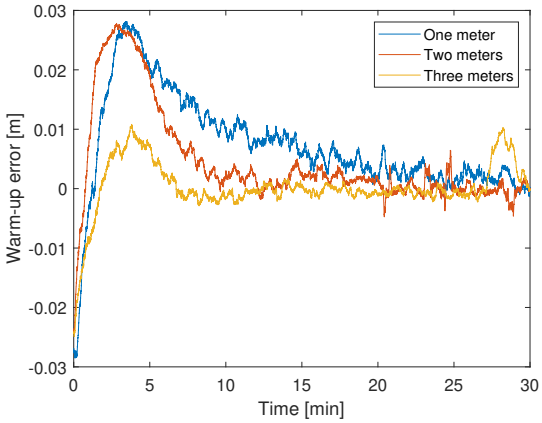

Fig. 5. Results of the first experiment with distance changes between the stations from one to three meters. The curves represent the distance error over the time for different distances.

This article has been accepted for publication in a future issue of this journal, but has not been fully edited. Content may change prior to final publication. Citation information: DOI 10.1109/TAES.2020.3015323, IEEE Transactions on Aerospace and Electronic Systems

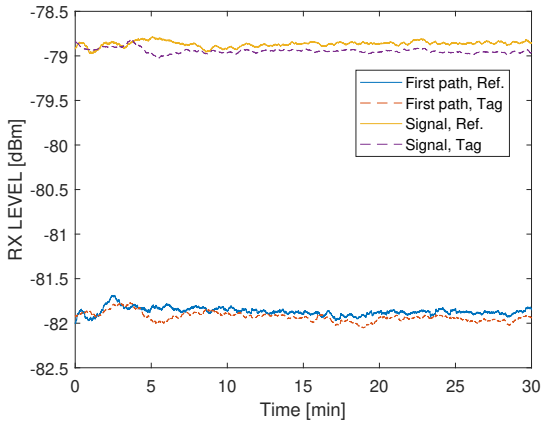

Fig. 6. Results of the first experiment with first path and total received signal power in [dBm] of the reference station (Ref.) and the tag. The dashed lines represent the received power measured at the tag station and the regular line at the reference station. The distance between the stations was 1.5 m

beginning of the measurement depends on the distance. This contradicts the assumption that this error is simply due to the warm-up of the crystal oscillator. One explanation could be the influence of the signal power, due to the change over time. Figure 6 shows the first path and total received signal power of the reference station and the tag. It cannot be observed that the measured first path as well as signal power are affected by the crystal warm-up. The TOF is too short to cause this difference, especially because the error at five minutes is the same for one and two meters. Therefore, the outcome is connected to the signal power.

C. Second experiment: Transmitter gain and warm-up error

In this experiment, the distance between the reference station and the tag is kept constant at 1.5 m, where only the transmitted signal power is changed. The received signal power can be read from a register at the receiving station. The frequency difference was determined as described in section II. As in the previous experiment, the stations are unplugged from the power for ten minutes after every experiment and the last value is subtracted from every measurement. The frequency difference between the stations is provided by $\left(1-\frac{\Delta T^T_{1,3}}{\Delta T^R_{1,3}}\right)$ in parts-per-million (PPM). The transmitter gain was reduced from 12 dB to 0 dB, with a step size of 3 dB. The transmitter gain should not be confused with the actual transmitted signal power. The measured signal power differs from the actual signal power received with increasing signal strength [10]. The resulting frequency difference and the distance error is shown in Figure 7. It can be observed that the signal strength has an influence on the frequency difference measured and the warm-up error. The question is whether this mutual dependence only arises in the first 15 min.

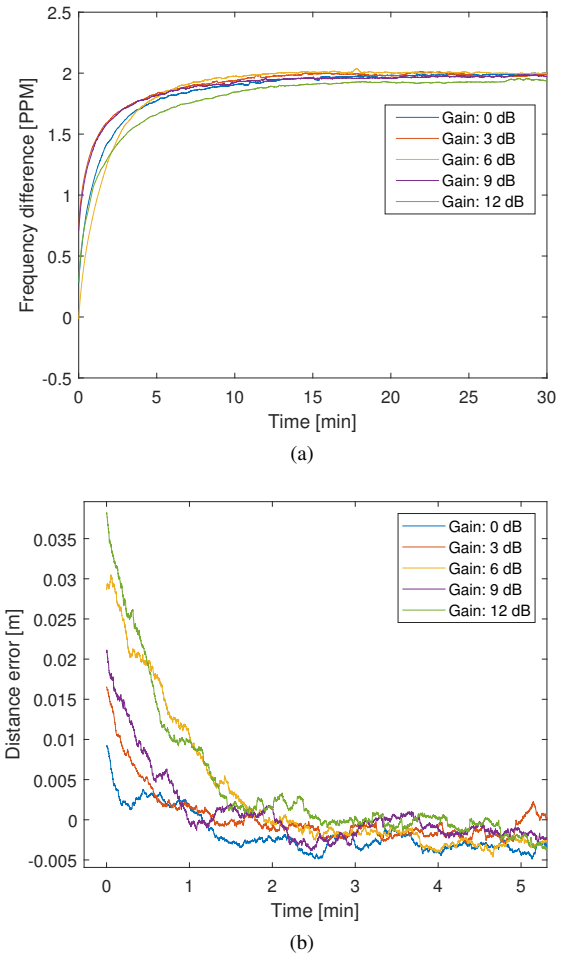

Fig. 7. Results of the second experiment. The curves represent the measurements of the (a) frequency difference and (b) distance error for different transmitter gains.

D. Third experiment: Frequency difference, received signal power and distance error

The DecaWave DW1000 IC allows centering the carrier frequency by adjusting the loading capacitance on the crystal oscillator [9]. The trimming is used to increase the receiver sensitivity by minimizing the frequency difference between the devices. In this experiment, the trimming is used to check whether the frequency difference affects the distance error. The ranging is performed with the transmitter gain of 12 dB. Figure 8 shows that the trim value is changed stepwise until the final value is reached. In the plot (a), it can be observed that the signal power increases the closer the frequency difference approaches zero, due to the increased sensitivity of the transceiver. The distance error as shown in Figure 8 plot (b) is the highest at this point. It can be observed that the change over time is the higher, the closer the frequency difference is to zero.

This article has been accepted for publication in a future issue of this journal, but has not been fully edited. Content may change prior to final publication. Citation information: DOI 10.1109/TAES.2020.3015323, IEEE Transactions on Aerospace and Electronic Systems

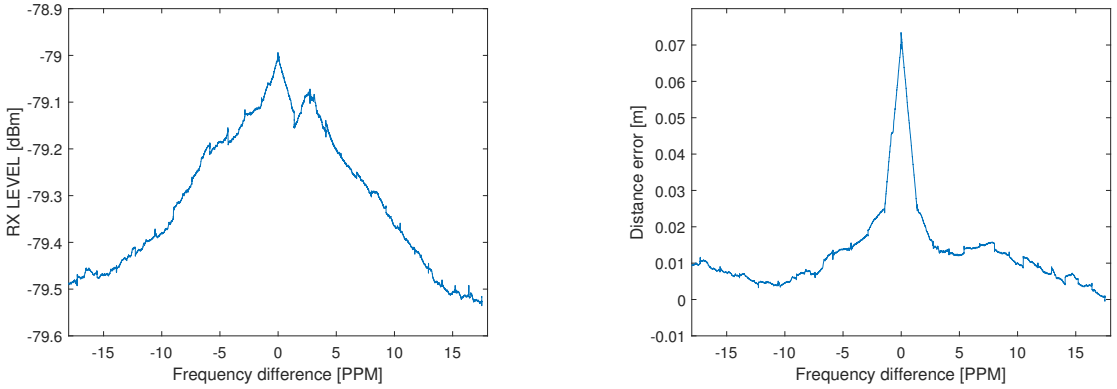

(a) (b)

Fig. 8. Results of the third experiment with changing crystal trim over time. In plot (a) the measured signal power is presented, in plot (b) the distance error.

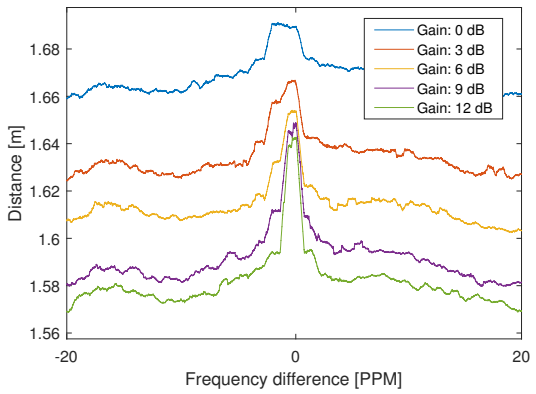

(a)

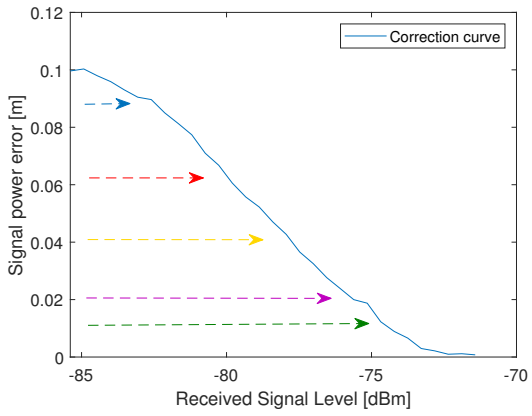

(b)

Fig. 9. Results of the fourth experiment. Relation between the signal power correction curve shown in plot (b) and the distance measurements shown in plot (a).

E. Fourth experiment: Frequency difference, changing transmitter gain and distance error

The III-D experiment is repeated with decreasing gain from 12 dB to 0 dB, with a step size of 3 dB. The signal gain is changed after the trim value reached its final value. This can be especially observed for the measurements with 9 dB to 12 dB signal gain at different times. In [22], we have shown how the correction curve between the received signal power and the timestamp shift can be obtained automatically. In the plot (b) of Figure 9, this curve is exemplarily presented. In the plot (a), the distance measurements of this experiment are presented. It can be observed that this correction curve only applies for a certain frequency difference, which is not constant.

F. Interpretationen of the results

In Table I, the observations of the previous experiments are summarized. The first experiment states that the transmit power affects the frequency difference. The reason for this dependency is most likely because the analog phase detectors of the phase-locked-loop (PLL), in which the loop gain is a function of amplitude, affects the error signal, and thus it also affects the pull-in time (total time taken by the PLL to lock). The results of the experiment III-D state that the transmit power and frequency difference affect the received signal power. It is obvious that a higher transmitting power also causes a higher measured power received. This allows transferring more energy and therefore, the measured signal power received is higher. The results of the III-D and III-E are the most interesting for the ranging, because they affect the timestamp. The reason for the influence of the signal power and the frequency difference on the timestamp could be due to the LDE algorithm. This algorithm is a microcode loaded in the random-access memory (RAM) of the DW1000 IC. It is executed on every frame reception to calculate the frame time-of-arrival (TOA) [9]. It is not possible for the end user to change the code of this algorithm. After the digital sampling of the signal received, the LDE algorithm searches for the

This article has been accepted for publication in a future issue of this journal, but has not been fully edited. Content may change prior to final publication. Citation information: DOI 10.1109/TAES.2020.3015323, IEEE Transactions on Aerospace and Electronic Systems

TABLE I
OBSERVED DEPENDENCIES

Experiment-Sections	Cause	Effect
III-D	Transmit power and frequency difference	Received power
III-D and III-E	Transmit power and frequency difference	Timestamp

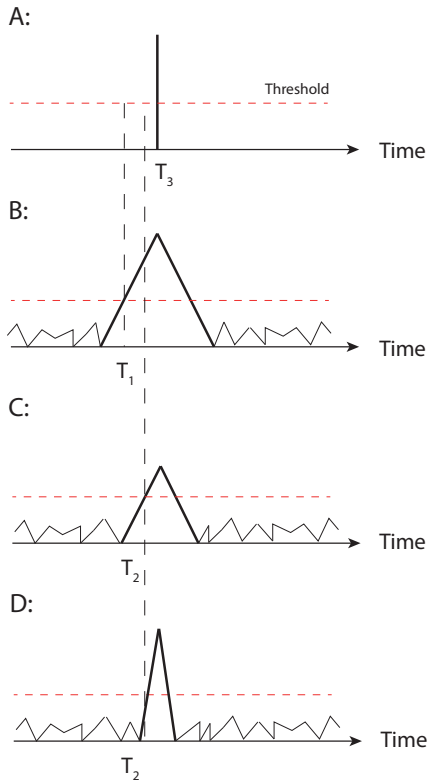

Fig. 10. LDE algorithm. A: Ideal case, B: High signal power, C: Low signal power, D: High signal power and low frequency difference.

leading edge. The detected edge is ideally infinitely steep and higher than a certain threshold, as shown in case A of Figure 10. In reality, the impulse is not infinitely steep and looks more like in case B. This leads to the threshold being passed earlier, and the set timestamp is not set at T_3 but at T_1. If the received signal power is now reduced, the new timestamp T_2 is closer to T_3 than T_1. With a smaller frequency difference between the transceivers, the PLL can better lock on to the received signal. With a higher signal spectrum or bandwidth, the impulse becomes sharper, as shown in case D of figure 10. This also has an impact on the timestamp, which is now the same as in case C with a reduced signal power.

IV. CORRECTION

From the previous sections, we obtained the knowledge that the frequency difference has an influence on the measured signal power received. Furthermore, the received signal power and the frequency difference lead to a shift of the timestamp. In this section, we show how the timestamp can be corrected.

The principle of the correction method is shown in diagram 11. The distance between two stations is determined using TWR. The tag varies the Mixer/DA gain and the trim value. More detailed information on how this is done can be found in [9]. This variation can be realized with two loops. The reference station calculates the frequency difference, the distance and the received signal strength. At this point, the calculated distance should be cleared of the influence of the clock drift. In section II and III-C we show how the distance and the frequency difference can be determined and source [9] explains in detail how the signal strength is obtained. During the ranging application it is necessary that the calculated distance does not change over time, even if the frequency difference and the signal strength change. For this purpose, a reference value is determined in F and P, at this point the correction value D is zero. With a regular distance measurement, the frequency difference and signal strength are determined that come closest to a value in F and P. The corresponding value for D is subtracted from the distance measurement.

A. Dynamic trim

The first presented approach is based on the implementation of a trimming routine during the ranging process at the reference station. The measured frequency offset between the two stations is used to trim the frequency with the aim of minimizing the difference. Figure 12 shows the warm-up error during the dynamic trim. Due to two reasons, it was not possible to correct the warm-up error by dynamic trim: first, the PLLs of both devices tend to automatically reduce the frequency difference; and second, the step size of the trim is too high, at about 1.5 ppm. In the next section, it is shown that a step size of 1.5 ppm is too high to properly correct this error by dynamic trimming.

B. Correction curves

In the fourth experiment from section III-E, we have modified the signal power and trimmed the frequency difference to obtain the impact on the distance measurement. To obtain data for use in a correction, the step size for the transmitter gain was reduced to 0.5 dB. Moreover, a moving average filter for smoothing the data is not used. The data is collected until the trim value or gain changes. This happens after 1,000 measurements have been received. The mean of these 1,000 measurements represents one data point. The results are shown in Figure 13. A certain value of this plot can be used as a reference measurement. If the signal power or frequency difference changes, it is possible to correct the distance measured to maintain a constant value. The correction curve can be obtained automatically for two stations without additional measurement equipment. Unfortunately, the step

This article has been accepted for publication in a future issue of this journal, but has not been fully edited. Content may change prior to final publication. Citation information: DOI 10.1109/TAES.2020.3015323, IEEE Transactions on Aerospace and Electronic Systems

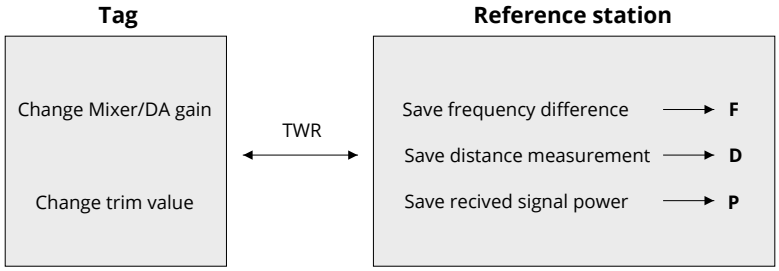

Fig. 11. Diagram for creating the correction values. The estimates of the frequency difference, the distance measurement and the received signal power are stored in the vectors F, D and P.

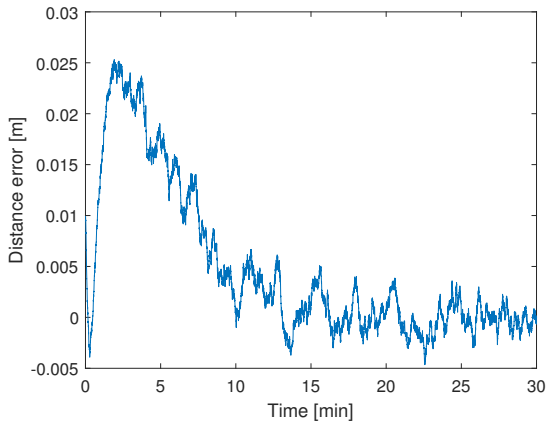

Fig. 12. Distance error during the dynamic trim.

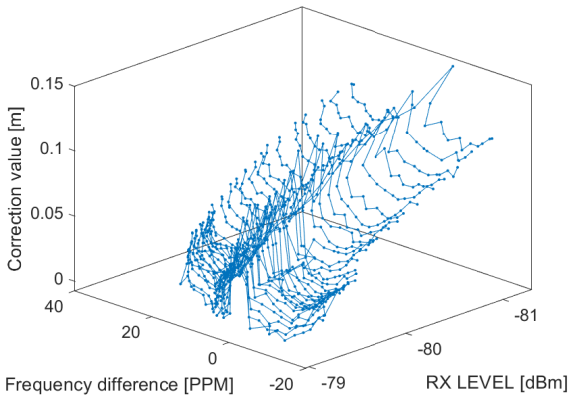

Fig. 13. Correction curve. Measured distance [m] with respect to the frequency difference [PPM] and the signal power received [dBm].

size of the crystal trim is too high to sample the region close to zero frequency difference with sufficient accuracy, as shown in Figure 14. The linear interpolation in this region is too inaccurate and it is also possible that the value at zero is even higher. Alternatively, it is also possible to restart the device

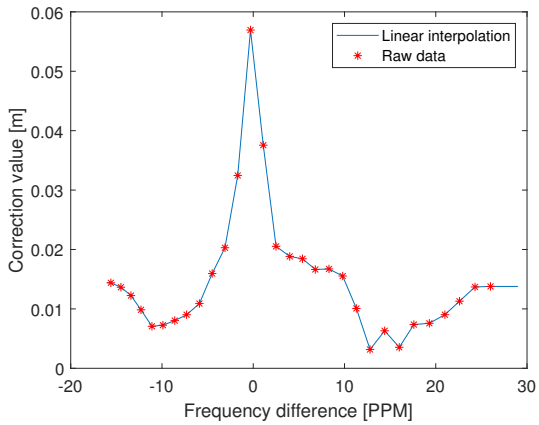

Fig. 14. Correction curve. Interpolation of the curve with the transmitted signal gain of 0 dB.

several times to obtain the dependency between the frequency difference and the distance measurement close to zero PPM. However, it is not practical and the dependency between the frequency difference and the signal power is too complex to perform this kind of correction. It is better to sample the error for every combination of the signal power and frequency difference.

C. Validation of the correction curve

In the previous parts, it has been shown which parameter has an impact on the TWR and how a correction curve can be assembled. This section is dedicated to the validation of the correction curve. The measurement setup such as the station distance and filter size is equivalent to that of section III.
The measurements take place at small and large frequency differences. The assumption is that due to the low sampling capability close to zero, the low frequency difference experiments become less accurate.

1) Small frequency difference: In the first test case, we do not use frequency trimming to reduce the frequency difference. Only the transmitter gain between both stations has been changed in this experiment. During the first 30 min, the gain

This article has been accepted for publication in a future issue of this journal, but has not been fully edited. Content may change prior to final publication. Citation information: DOI 10.1109/TAES.2020.3015323, IEEE Transactions on Aerospace and Electronic Systems

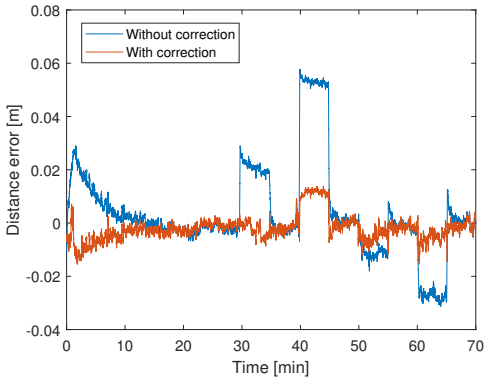

(a)

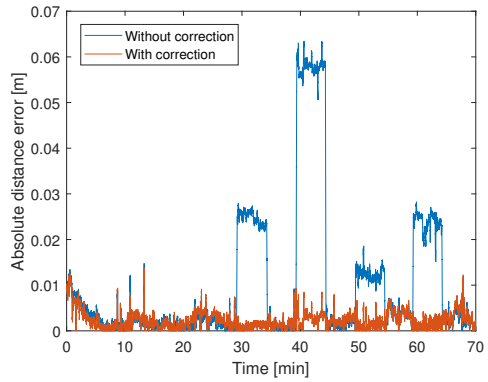

(b)

Fig. 15. Validation of the correction curve with small (a) and large (b) frequency difference.

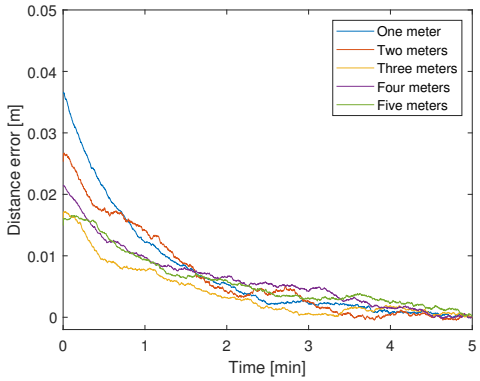

(a)

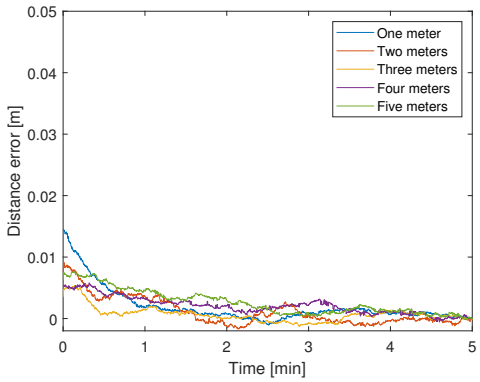

(b)

Fig. 16. Validation of the correction curve with small frequency difference for other stations and different distances. Plot (a) shows the distance error without using the correction curve and (b) with using the correction curve.

was at 6 dB, while in the following, the gain was reduced to 3 dB and 0 dB, before it increased again to 9 dB and 12 dB. Between the power changes, the gain was set back to the initial value of 6 dB. After the first 30 min, every gain was measured for 5 min.

The frequency difference and the received signal power have been used to find the corresponding correction values in the correction curve. In Figure 15 plot (a), the results of the TWR with and without correction are presented. It can be observed that the corrected values perform much better compared with the results without the correction. In particular, the distance error at the beginning is reduced by one-third. In some regions, such as between 40 and 45 min, the correction was not perfect. The reason is most likely that the frequency difference is very close to zero. In this area, it is not possible to obtain good correction values, due to the high step size of 1.5 ppm. Table II summarizes the mean of the absolute value and the maximum peak of the absolute value. The corrected values have a three times smaller error compared with the uncorrected values.

To validate the results, we repeated this experiment for other stations with an alternative correction curve. It was not the signal strength that was changed, but the distance of the stations. After each change of position, the stations were restarted to initiate a warm-up phase. Figure 16 (a) shows the distance error of the uncorrected and (b) of the corrected stations. Without the warm-up the solution with changing distances is equivalent to the one presented in reference [22]. It can be clearly seen that the corrected values have a significantly smaller distance error than the uncorrected ones.

2) Large frequency difference: The setup of the second test case is equivalent to the previous test case. The only difference is that the system is trimmed from the beginning on, to obtain a higher offset. Further away from the frequency difference zero, we expect a smaller rate of change in the distance error. This should also decrease the uncorrected warm-up error. As observed in Figure 14, the change of the error curve with respect to the input parameters is smaller. In Figure 15 plot (b), it can be seen that the distance error is smaller at the beginning, as expected. Moreover, the remaining error of the corrected curve is smaller compared with the first test case, especially between 40 and 45 minutes. The absolute mean and maximum distance errors are shown in Table II. Large frequency difference is great for applications where accurate

This article has been accepted for publication in a future issue of this journal, but has not been fully edited. Content may change prior to final publication. Citation information: DOI 10.1109/TAES.2020.3015323, IEEE Transactions on Aerospace and Electronic Systems

measurements are required. In addition, small differences have a much smaller influence on the measurement. With dynamic trimming it is possible to have a fixed frequency difference. This means that only the signal strength is required for the correction. The correction curves are no longer created via TWR but for each station individually. They are therefore also suitable for TDOA applications. More information on this topic can be found in [22].

TABLE II
THE FOLLOWING TABLE SHOWS THE ABSOLUTE MEAN AND MAXIMUM VALUE OF THE DISTANCE ERROR WITH SMALL FREQUENCY DIFFERENCES (SF) AND LARGE FREQUENCY DIFFERENCES (LF).

	Mean [m]	Max [m]
SF without correction:	0.0108	0.0577
SF with correction:	0.0039	0.0155
LF without correction:	0.0103	0.0634
LF with correction:	0.0023	0.0137

V. CONCLUSION

In this paper, we performed different practical experiments to identify the influence of the signal power and the frequency difference on the timestamp shift. It was shown that the error, known as the warm-up error, is strongly connected to the frequency difference between the devices. We showed that the warm-up error has the strongest impact at the beginning, but also appears later on in the ranging process. We presented a method that automatically creates a correction curve that can be used as a lookup table. This method can be used for any DecaWave chip-based station to correct TWR measurements. After the clock drift correction, the DecaWave DW1000 device has an accuracy of 10 cm for the two-way-ranging. If the impact of the signal power and the frequency difference is properly corrected, it is possible to obtain an accuracy smaller than 1 cm. The higher accuracy allows to use this system in other technology fields like tomography, with the aim of detecting the time delay caused by a penetrated material or the material itself. This would not be possible if the time-of-flight measurements depended on the signal strength or frequency difference between the devices.
In order to accomplish this task, we presented a self-calibration solution that does not require additional measurement equipment or any change of the hardware. The correction look-up table can be created and saved independently on the devices. In the later course this table can then be used for the correction of the distance measurements. Alternatively, it is also possible to change the hardware to reduce the step size for the clock frequency trim by additional capacitors. The dynamic trim with a smaller step size allows obtaining the correction curve for every station individually. At this point, the correction curve can be used for time-of-arrival as well as time-difference-of-arrival measurement techniques. In future work, the effect of temperature and voltage on frequency difference will be studied in more detail.

VI. ACKNOWLEDGMENT

The authors would like to thank Dr. Dimitri Bulatov from the Fraunhofer Institute of Optronics, System Technologies and Image Exploitation IOSB as well as two anonymous reviewers for reading the manuscript and providing ideas for its improvement.

GLOSSARY OF ABBREVIATIONS

The following abbreviations are used in this article:

AltDS-TWR	Alternative double-sided TWR
LOS	Line of sight
PLL	Phase-locked-loop
RAM	Random-Access Memory
SMD	Surface mounted device
TDOA	Time-difference-of-arrival
TOA	Time-of-arrival
TOF	Time of flight
TWR	Two-way-ranging
UWB	Ultra-wideband

mds
July 05, 2020

REFERENCES

[1] J. F. M. Gerrits, J. R. Farserotu and J. R. Long, *Multipath behavior of FM-UWB signals*, In IEEE International Conference on Ultra-Wideband, pp. 162-167, Sept. 2007.
[2] R. A. Saeed, S. Khatun, B. M. Ali and M. A. Khazani, *Ultra-wideband (UWB) geolocation in NLOS multipath fading environments*, In 13th IEEE International Conference on Networks Jointly held with the IEEE 7th Malaysia International Conf on Communications, pp. 6, Nov. 2005.
[3] D. Dardari, N. Decarli, A. Guerra and F. Guidi, *The future of ultrawideband localization in RFID*, In IEEE International Conference on RFID, pp. 1-7, May. 2016.
[4] A. R. Jiménez Ruiz and F. Seco Granja, *Comparing ubisense, bespoon, and decawave uwb location systems: Indoor performance analysis*, In IEEE Transactions on Instrumentation and Measurement, vol. 66, no. 8, pp. 2106-2117, Aug. 2017.
[5] *Online article*, [Online]. Available: https://sixcolors.com/post/2019/09/the-u1-chip-in-the-iphone-11-is-the-beginning-of-an-ultra-wideband-revolution, [Accessed: 09-Oct.-2019].
[6] *DecaWave markets*, [Online]. Available: https://www.decawave.com/markets-applications/, [Accessed: 09-Oct.-2019].
[7] M. Haluza and J. Vesely, *Analysis of signals from the DecaWave TREK1000 wideband positioning system using AKRS system*, In International Conference on Military Technologies (ICMT), pp. 424-429, June 2017.
[8] *Decawave APS014 APPLICATION NOTE: Antenna delay calibration DW1000-Based products and systems*, Version 1.2 , [Online]. Available: https://www.decawave.com, pp. 10. [Accessed: 09-Oct.-2019].
[9] *DW1000 User Manual*, Version 2.15, [Online]. Available: https://www.decawave.com, pp. 45. [Accessed: 09-Oct.-2019].
[10] *Decawave APS011 APPLICATION NOTE: Sources of error in TWR*, Version 1.0, [Online]. Available: https://www.decawave.com, pp. 10. [Accessed: 09-Oct.-2019].
[11] I. Dotlic, A. Connell and M. McLaughlin, *Ranging Methods Utilizing Carrier Frequency Offset Estimation*, In 15th Workshop on Positioning, Navigation and Communications (WPNC), pp. 1-6, Oct. 2018.
[12] R. Hach, *Symmetric double sided two-way ranging*, [Online]. Available: http://www.ieee802.org/15/pub/TG4a.html, doc: IEEE 15-05-0334-00-004a, June 2005
[13] Y. Jiang and V. C. M. Leung, *An Asymmetric Double Sided Two-Way Ranging for Crystal Offset*, In International Symposium on Signals, Systems and Electronics, pp. 525-528, July 2007.
[14] D. Neirynck, E. Luk and M. McLaughlin, *An alternative double-sided two-way ranging method*, In 13th Workshop on Positioning, Navigation and Communications (WPNC), pp. 1-4, Oct 2016.
[15] J. Sidorenko, V. Schatz, N. Scherer-Negenborn, M. Arens and U. Hugentobler, *Error corrections for ultra-wideband ranging*, In IEEE Transactions on Instrumentation and Measurement, Early Access, May 2020.

This article has been accepted for publication in a future issue of this journal, but has not been fully edited. Content may change prior to final publication. Citation information: DOI 10.1109/TAES.2020.3015323, IEEE Transactions on Aerospace and Electronic Systems

[16] R. Zandian and U. Witkowski, *Robot self-localization in ultra-wideband large scale multi-node setups*, In 14th Workshop on Positioning, Navigation and Communications (WPNC), pp. 1-6, 2017.
[17] V. Navrátil, J. Krška, F. Vejražka and V. Koreček, *Chained wireless synchronization algorithm for UWB-TDOA positioning*, In IEEE/ION Position, Location and Navigation Symposium (PLANS), pp. 149-157, 2018.
[18] R. Zandian and U. Witkowski, *Implementation Challenges of Synchronisation of UWB Nodes in TDoA Structures*, International Conference on Indoor Positioning and Indoor Navigation (IPIN), pp. 1-8, 2018.
[19] J. Cano, S. Chidami and J. L. Ny, *A Kalman Filter-Based Algorithm for Simultaneous Time Synchronization and Localization in UWB Networks*, In International Conference on Robotics and Automation (ICRA), pp. 1431-1437, 2019.
[20] A. Ledergerber, M. Hamer and R. D'Andrea, *A robot self-localization system using one-way ultra-wideband communication*, In IEEE/RSJ International Conference on Intelligent Robots and Systems (IROS), pp. 3131-3137, 2015.
[21] D. L. Adamy, *EW 102: A Second Course in Electronic Warfare*, Boston, London: Artech House, July 2004.
[22] J. Sidorenko, V. Schatz, M. Arens, N. Scherer-Negenborn and U. Hugentobler, *Decawave UWB clock drift correction and power self-calibration*, In Sensors, pp. 16, July 2019.
[23] *Product manual RSX-10*, [Online]. Available: http://www.rakon.com, [Accessed: 09-Oct.-2019].

Juri Sidorenko received a diploma in mechanical engineering from the Technical University Braunschweig, Germany and a Masters of Science from the Cranfield University, the UK in 2012 and 2014. He is currently a Research Assistant with the Fraunhofer Institute of Optronics, System Technologies and Image Exploitation IOSB and pursuing the Ph.D. degree in engineering at the Technical University of Munich. His research interests include the localization and self-calibration of sensor networks.

Dr. Volker Schatz received his diploma in physics from the Ruperto Carola University, Heidelberg, Germany, in 2000, developing trigger circuits for high-energy physics experiments. He obtained his PhD, also at Heidelberg University, in theoretical particle physics, in 2003. After a year of post-doctoral research in theoretical geophysics, he started workat what is now Fraunhofer IOSB in Ettlingen, Germany, in 2005. Volker Schatz's current occupations and research interests are developing multi-sensor data acquisition systems, synchronising imaging sensors for sensor fusion applications and measuring the timing behaviour of commercial cameras.

Dr. Norbert Scherer-Negenborn Dr. Norbert Scherer-Negenborn received the diploma and PhD degree in physics from the University of Freiburg, Germany, in 1996 and 2000, respectively. He is currently the group leader of the Tracking and Tracking Assessment Group in the department of the Object Recognition (OBJ) at the Fraunhofer Institute for Optronics, System Technology and Image Exploitation IOSB.

Dr. Michael Arens received his diploma in Computer Science and his PhD (Dr.rer.nat.) from the University of Karlsruhe in 2001 and 2004, respectively. He is currently head of the department Object Recognition (OBJ) at Fraunhofer Institute for Optronics, System Technology and Image Exploitation IOSB.

Prof. Dr. Urs Hugentobler studied theoretical physics at the University of Bern and received a doctorate in astronomy from the same university in 1997. After working as a postdoctoral researcher at the European Space Agency (ESA), he joined the University of Bern in 1999 as head of the GPS Research Group. He has headed TUM's Department of Space Geodesy and TUM's Space Geodesy Research Unit since 2006. He is Secretary General of the Project Geodesy (DGK) of the Bavarian Academy of Science.

4.5. P-V: Error corrections for ultra-wideband ranging

Authors

Juri Sidorenko, Volker Schatz, Norbert Scherer-Negenborn, Michael Arens, Urs Hugentobler.

Work-in-Progress paper

2019 International Conference on Indoor Positioning and Indoor Navigation - Work-in-Progress Papers (IPIN-WiP 2019), Pisa, Italy, Sep. 2019, pp. 1-8.

Journal paper

IEEE Transactions on Instrumentation and Measurement,
DOI: 10.1109/TIM.2020.2996706.

Introduction

In the publication P-III and P-IV, a signal power error and a clock drift correction method was presented. Both approaches differ from the usual solutions, hence it is a prerequisite to develop TDOA positioning approaches, which are able to use the presented correction methods. The developed algorithm is also answering the question Q^3_{UWB}.

Summary

In contrast to TWR the TDOA method requires a synchronization between the base stations. Similar to the LPM system, an additional emitter station R is used to provide a synchronization between the base stations. The time difference between both signals received at the station S can be used to get the unknown position of the tag $T_{TDOA_K} = \left(\Delta T^S_{1,2} + E_3 - E_4\right)\left(\frac{\Delta T^R_{1,3}}{\Delta T^S_{1,3}}\right) - K$. In contrast to LPM the Decawave UWB system allows to read the raw timestamps. This attribute is used to get the unknown offset $K = T_{TOF} + \left(\Delta T^S_{1,2} + E_1\right)\left(\frac{\Delta T^R_{1,3}}{\Delta T^S_{1,3}}\right) + 2B$. The offset is caused by the different transmission times of the tag T and synchronization station. The TDOA equation without the offset K and with all correction terms can be written as.

$$T_{TDOA} = \Delta T^R_{1,3}\left(\frac{\Delta T^S_{1,2} + E_3 - E_4}{\Delta T^S_{1,3}} - \frac{0.5\cdot\left(\Delta T^T_{1,2} + E_1\right)}{\Delta T^T_{1,3}}\right) - 0.5\cdot\left(\Delta T^R_{1,2} - E_2\right) + A - B$$

(4.2)

In addition to the elimination of the offset K, it is also possible to combine the TOA and TDOA measurements without losing the advantages of the TDOA measurement technique.

Conclusions and outlook

The presented TDOA solution without the offset and TOA fusion provides more equations compared to the regular solution. The precision of the TOA position is about 0.02 m and 0.03 m for the fused TDOA measurement technique. The advantages of the higher update rate of the TDOA measurement technique outweigh the slightly lower precision. With the developed TOA and TDOA methods it is now possible to begin the next step, the position self-calibration.

Declaration of own contribution

The first author came up with the idea for the TDOA algorithm, the TOA and TDOA fusion as well as the offset estimation. Moreover, was the software and hardware prepared by the first author, more information about the framework development can be found in the Appendix. The co-authors improved the paper through their comments and corrections about the layout, content and the obtained results. **The overall own contribution is estimated at 94 %.**

Criteria	Estimated own contribution
Paper concept	100 %
Computations and software development	100 %
Data analysis and interpretation of results	90 %
Design and creation of figures	100 %
Manuscript structure and writing	80 %

Table 4.5.: Apportionment of own contributions for P-V

This article has been accepted for publication in a future issue of this journal, but has not been fully edited. Content may change prior to final publication. Citation information: DOI 10.1109/TIM.2020.2996706, IEEE Transactions on Instrumentation and Measurement

Error corrections for ultra-wideband ranging

Juri Sidorenko, Volker Schatz, Norbert Scherer-Negenborn, Michael Arens, and Urs Hugentobler

***Abstract*—Precise indoor localization is a major challenge in the field of localization. In this work we investigate multiple error corrections for the ultra-wideband (UWB) technology, in particular the DecaWave DW1000 transceiver. Both the time-of-arrival (TOA) and the time-difference-of-arrival (TDOA) methods are considered. Various clock-drift correction methods for TOA from the literature are reviewed and compared experimentally. The best performing method is extended to TDOA, corrections for the signal power dependence and the hardware delay are added, and two additional enhancements suggested. These are compared to each other and to TOA in positioning experiments.**

***Index Terms*—time-of-arrival (TOA), time-difference-of-arrival (TDOA), two-way-ranging (TWR), DecaWave, ultra-wideband (UWB)**

I. Introduction

LOCALIZATION systems have become indispensable in everyday life. Satellite navigation [1], [2] has replaced paper maps and is now essential for self-driving cars. As the requirements of logistics and manufacturing processes increase, access to precise positional information is becoming a necessity. Depending on the operating conditions for the localization application, different measurement principles [3], [4], [5] and techniques [6], [7], [8] are available. Two of the most common measurement techniques are based on the time-of-arrival (TOA) [6] and the time-difference-of-arrival (TDOA) [7]. TOA calculates the distance between two stations from the signal traveling time, whereas TDOA considers the travel time differences between the stations. The measuring equipment is just as important as the measurement technique itself. This article focuses on indoor radio frequency (RF)-based localization systems. In general, indoor positioning applications are a challenge for RF-based localization systems. Reflections can generate interference with the main signal and lead to fading. Compared to narrowband signals, ultra-wideband (UWB) signals are more robust against fading [9], [10]. The DecaWave transceiver [11] uses ultra-wideband (UWB) technology and is compliant with the IEEE802.15.4-2011 standard [12]. It supports six frequency bands with center frequencies from 3.5 GHz to 6.5 GHz and data rates of up to 6.8 Mb/s. Depending on the selected center frequency, the bandwidth ranges from 500 to 1000 MHz. The precision and accuracy of the DecaWave UWB depend primarily on three factors: the clock drift, the received signal power, and hardware delay.

J. Sidorenko, V. Schatz, N. Scherer-Negenborn and M.Arens are with the Fraunhofer Institute of Optronics, System Technologies and Image Exploitation IOSB, Ettlingen, 76275 Germany, e-mail: (juri.sidorenko@iosb.fraunhofer.de).

J. Sidorenko and U. Hugentobler are with the Institute of Astronomical and Physical Geodesy, Technical University of Munich, 80333 Germany.

Manuscript received September 04, 2019; revised September 04, 2019.

In the first part of this article, it is shown which two-way-ranging protocol is most suitable for correcting the effect of the clock drift. The results are then verified by experiments with the DecaWave UWB system.

The subsequent section deals with the extension of the best two-way-ranging (TWR) protocol for the time-difference-of-arrival (TDOA) application. In [13], it was shown how the signal power correction curve can be obtained automatically for every station individually. In the present publication, we demonstrate how to apply these corrections for TOA and TDOA localization. The last section of this paper describes how a synchronization signal from the reference station can be used to perform a range measurement between the reference station and a tag for every TDOA position estimation. This information increases the number of equations and also allows us to estimate the time offset between the reference station and the tag. Table I presents the notations used in this article.

TABLE I
NOTATIONS USED

Notation	Definition
A, B, C	Hardware delay
A_L	Linear parameter of the correction function
A_Q	First non-linear parameter of the correction function
B_Q	Second non-linear parameter of the correction function
$C_{n,m}$	Clock drift error, calculated from the timestamps n and m
F_C	Used clock drift error function correction term
F_L	Linear clock drift error function correction term
F_Q	Quadratic clock drift error function correction term
ϵ_{TWR}	Residual error
e_R	Frequency offset of the reference station (R.)
e_T	Frequency offset of the tag (T.)
$e_R - e_T$	Clock drift between the stations R. and T.
E	Timestamp error due to the signal power
K	Sending time difference between R. and T.
T_i^R	Timestamp at R.
T_i^T	Timestamp at T.
T_i^S	Timestamp at the anchor station S
$\Delta T_{n,m}$	Difference between two timestamps $T_m - T_n$
T_{TWR}	Time of flight without frequency drift
$\hat{T}_{TWR}$	Time of flight with frequency drift
T_{TOA}	Our TOA approach
T_{TDOA}	Our TDOA approach
T_{TDOA_K}	Our TDOA approach with the offset K
TWR	Index standing for the used TWR protocol
Z	Auxiliary results

Contribution

In this article, we review the most common two-way-ranging (TWR) protocols and present their residual error. The next part of this article deals with the evaluation of these protocols by practical experiments. The best TWR protocol is extended by the ability to use the signal power and hardware delay correction for every station individually. In previous

This article has been accepted for publication in a future issue of this journal, but has not been fully edited. Content may change prior to final publication. Citation information: DOI 10.1109/TIM.2020.2996706, IEEE Transactions on Instrumentation and Measurement

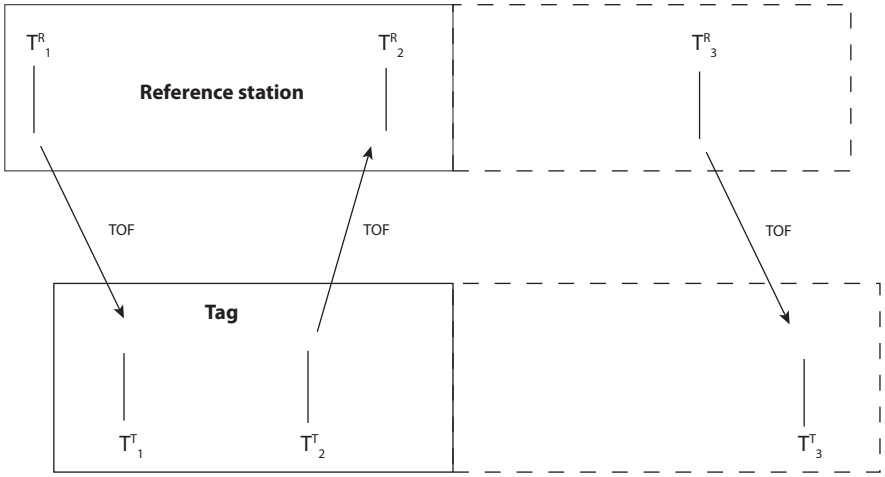

Fig. 1. Two-way-ranging in theory

works, it was only possible to use the signal power correction for two stations after the ranging.

The second part of this article combines the findings from the TWR part to create a robust TDOA approach. We successively present our own TDOA solution; it has an additional range measurement and does not require computation of the unknown time-offset between the reference station and the tag.

II. Time-of-arrival measurement technique

The time-of-arrival (TOA) measurement technique provides the distance between two stations from the signal traveling time. In a one-way-ranging application, it is necessary that both stations are time synchronous. This condition can be bypassed if two-way-ranging (TWR) is used instead. Figure 1 illustrates the concept of TWR between two stations, with two and three messages. The initial station, also called the reference station, emits a signal at the local time T_1^R. The second station, named tag, receives the signal at its local time T_1^T and sends a response at its time T_2^T back to the reference station. The double time-of-flight can now be obtained by subtracting the delay of the second station $\Delta T_{1,2}^T = \left(T_2^T - T_1^T\right)$ from the transmitting and receiving time difference of the reference station $\Delta T_{1,2}^R = \left(T_2^R - T_1^R\right)$. Equation 1 shows the time-of-flight provided by the ideal two-way-ranging protocol.

$$TOF = 0.5 \cdot \left(\Delta T_{1,2}^R - \Delta T_{1,2}^T\right) \tag{1}$$

In practice, the frequencies of the crystals are not identical, and small imperfections lead to the clock of one station operating faster or slower than the other. Since the two-way-ranging and the hardware becomes more commonly used, different approaches have been proposed to deal with the clock drift. Some of them like SS-TWR and CCSS-TWR use two messages while others require a third message, as shown in figure 1. In this section, the most common clock drift correction methods are analyzed in detail. We use the term clock drift error to refer to the integral of the clock drift. This error appears as the result of the clock drift and increases over time. We define that e_R and e_T denote the clock frequency offset of the reference station and tag, respectively. In the following it is assumed that the frequency drift is constant during the ranging.

A. Single-sided two-way ranging (SS-TWR)

The single-sided two-way ranging protocol is the basic protocol without the clock drift correction. Hence, the time-of-flight is shown in equation 2.

$$T_{SS} = 0.5 \cdot \left(\Delta T_{1,2}^R - \Delta T_{1,2}^T\right). \tag{2}$$

The time-of-flight with the frequency offsets is presented in equation 3.

$$\hat{T}_{SS} = 0.5 \cdot \left(\Delta T_{1,2}^R \left(1 + e_R\right) - \Delta T_{1,2}^T \left(1 + e_T\right)\right) \tag{3}$$

The residual error $\epsilon_{SS} = \hat{T}_{SS} - T_{SS}$ is the error caused by the frequency offset. Equation 4 states that the residual error depends mainly on the response time of the tag, $\Delta T_{1,2}^T$. Even if the clock difference is just few parts-per-million (ppm) are delays $\Delta T_{1,2}^T$ in order of some milliseconds long, hence the multiplication leads to a significant impact on the range estimation. The clock drift error caused by the time-of-flight T_{SS} can be neglected, due to the short-range limitations of the UWB system.

$$\epsilon_{SS} = T_{SS} e_R + 0.5 \cdot \Delta T_{1,2}^T \cdot \left(e_R - e_T\right) \tag{4}$$

This article has been accepted for publication in a future issue of this journal, but has not been fully edited. Content may change prior to final publication. Citation information: DOI 10.1109/TIM.2020.2996706, IEEE Transactions on Instrumentation and Measurement

B. CFO-Corrected Single-sided two-way ranging (CCSS-TWR)

Minimization of the residual error can be achieved by reducing the response time $\Delta T^T_{1,2}$ and using precise crystals. However, due to the real-life limitation, this is not always possible. In [17] a so-called carrier frequency offset (CFO) single-sided two-way ranging protocol was presented. It used the integrator of the phase-locked-loop (PLL) to obtain the clock drift difference between two DecaWave UWB transceivers. The information provided by the integrator of the PLL, allows us to compensate the effect of the clock drift during the message exchange. The residual error is computed as equation 5.

$$\epsilon_{CCSS} = T_{CCSS} \cdot e_R \tag{5}$$

The residual error is now independent of the response time, and only the time-of-flight T_{CCSS} is the limiting factor. This technique is widely used in the community [18], [19], [20]. The reason why we will not use this method later on is that in [13], we showed that the integrator of the PLL depends on the signal power, and therefore introduces additional inaccuracies.

C. Symmetric double-sided two-way ranging (SDS-TWR)

The symmetric double-sided two-way ranging protocol [21] is part of the 802.15.4a standard. It was also introduced to minimize the errors due to crystal imperfections. In contrast to the previously presented CCSS-TWR method, three messages are now required, as shown in figure 1. With $\Delta T^R_{2,3} = \left(T^R_3 - T^R_2\right)$ and $\Delta T^T_{2,3} = \left(T^T_3 - T^T_2\right)$, the time-of-flight with the SDS-TWR protocol is obtained by equation 6.

$$T_{SDS} = 0.25 \cdot \left(\Delta T^R_{1,2} - \Delta T^T_{1,2} + \Delta T^T_{2,3} - \Delta T^R_{2,3}\right) \tag{6}$$

The time-of-flight with the frequency offsets is shown in equation 7.

$$\begin{aligned} \hat{T}_{SDS} =& 0.25 \cdot \left(\Delta T^R_{1,2} - \Delta T^R_{2,3}\right)(1 + e_R) \\ &+ 0.25 \cdot \left(\Delta T^T_{2,3} - \Delta T^T_{1,2}\right)(1 + e_T) \end{aligned} \tag{7}$$

The residual error for the SDS-TWR is obtained analogously to SS-TWR, $\epsilon_{SDS} = \hat{T}_{SDS} - T_{SDS}$. This leads to equation 8.

$$\begin{aligned} \epsilon_{SDS} =& 0.5 \cdot T_{SDS}\left(e_R + e_T\right) \\ &+ 0.25 \cdot \left(\Delta T^T_{1,2} - \Delta T^R_{2,3}\right) \cdot \left(e_R - e_T\right) \end{aligned} \tag{8}$$

Again, it is possible to neglect the error caused by the time-of-flight. Therefore, the residual error of the SDS-TWR protocol depends mainly on the difference between the response time $\Delta T^T_{1,2}$ and $\Delta T^R_{2,3}$. In contrast to the CCSS-TWR protocol, the information about the clock drift is not used to correct the ranging, it is more of an averaging.

D. Asymmetric double-sided two-way ranging (ADS-TWR)

The asymmetric double-sided two-way ranging protocol [22] is also often used in the field of localization. In general, it is an SDS-TWR protocol with the additional constraint that the response time $\Delta T^R_{2,3}$ is zero. This can be only achieved if the reference station sends the ranging message back to the tag instantly. The residual error is shown in equation 9.

$$\epsilon_{ADS} = 0.5 \cdot T_{ADS}\left(e_R + e_T\right) + 0.25 \cdot \left(\Delta T^T_{1,2}\right) \cdot \left(e_R - e_T\right) \tag{9}$$

E. Alternative double-sided two-way ranging (AltDS-TWR)

The alternative double-sided two-way ranging protocol [23] uses the fact that the time differences of the first and last message should be the same for the transmitter and for the receiver $\Delta T^T_{1,3}\left(1 + e_T\right) = \Delta T^R_{1,3}\left(1 + e_R\right)$. The deviation between both time differences represents the clock drift error. This error can be linearly interpolated to correct the time difference $\Delta T^T_{1,2}$. The time-of-flight for the AltDS-TWR protocol is presented in equation 10.

$$T_{AltDS} = \frac{\Delta T^R_{1,2} \cdot \Delta T^T_{2,3} - \Delta T^T_{1,2} \cdot \Delta T^R_{2,3}}{2\left(\Delta T^T_{2,3} + \Delta T^T_{1,2}\right)} \tag{10}$$

The time-of-flight with the frequency offsets is presented in equation 11.

$$\hat{T}_{AltDS} = (1 + e_R)\frac{\Delta T^R_{1,2} \cdot \Delta T^T_{2,3} - \Delta T^T_{1,2} \cdot \Delta T^R_{2,3}}{2\left(\Delta T^T_{2,3} + \Delta T^T_{1,2}\right)} \tag{11}$$

The residual error for the AltDS-TWR with, $\epsilon_{AltDS} = \hat{T}_{AltDS} - T_{AltDS}$ equates

$$\epsilon_{AltDS} = e_R T_{AltDS} \tag{12}$$

The remaining error depends, equivalently to the CCSS-TWR protocol, on the time-of-flight. In some publications the AltDS-TWR distance is presented as in equation 13. It should be noted that this equation applies only if $\Delta T^T_{1,3} = \Delta T^R_{1,3}$, which means without clock drift between the stations.

$$T_{AltDS} = \frac{\Delta T^R_{1,2} \cdot \Delta T^T_{2,3} - \Delta T^T_{1,2} \cdot \Delta T^R_{2,3}}{\left(\Delta T^R_{1,2} + \Delta T^T_{2,3} + \Delta T^T_{1,2} + \Delta T^R_{2,3}\right)} \tag{13}$$

III. Experimental results: Two-way ranging

In this section, the previously introduced residual errors due to clock drift between two stations are verified by practical measurements. The experimental setup is presented in figure 2. In each of the presented variants, the distance between stations was 1.5 meters, with a measuring time of 30 minutes. The filtered values are, if not otherwise mentioned, using a moving average filter with a filter size of 500 measurements and an update rate of 25 measurements per seconds. This size was selected to remove the noise but preserve variations from the scale of a few ms. It should be noted that the best result is a straight line, which means that the measured distance between the both stations is always the same. The difference

This article has been accepted for publication in a future issue of this journal, but has not been fully edited. Content may change prior to final publication. Citation information: DOI 10.1109/TIM.2020.2996706, IEEE Transactions on Instrumentation and Measurement

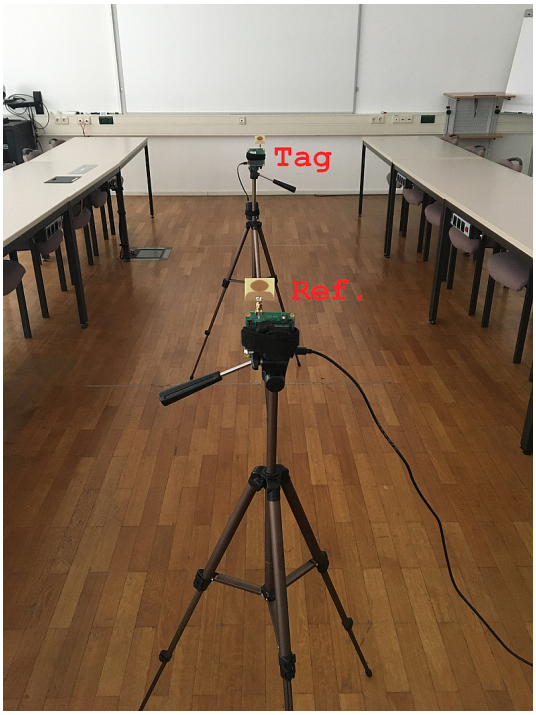

Fig. 2. Experimental setup of two DecaWave EVK1000 transceivers

between the measurement and the expected 1.5 meters is irrelevant for evaluating the clock drift correction, it is just important that this offset is constant. In experiment one and two are the results of the different ranging protocols based on the same measurement.
The ADS-TWR is not part of the upcoming plots since a zero response time is not feasible with our setup where response transmissions are triggered with a microcontroller external to the wireless transceiver. Even with the minimum possible response time, the distance determined with ADS-TWR is orders of magnitude larger than in reality [1]. However, we investigate the influence of the response time in the following section.

A. First TWR experiment: Two-way ranging with different ranging protocols

In this experiment the response times of both stations were set to be as close to each other as possible: $T^T_{1,2} = 1.5566\,\text{ms}$ and $T^R_{2,3} = 1.5530\,\text{ms}$. In figure 3, the results of the different TWR protocols are presented. It can be observed that the uncorrected SS-TWR has the highest change in distance over time. This curve is the warm-up process of the system [15]. The difference between the SDS-TWR and AltDS-TWR is on average $0.2331\,\text{mm}$. The results of the SDS-TWR are hidden by the AltDS-TWR. This changes for the next experiment.

[1]The method used by the DW1000 firmware is misidentified as ADS-TWR in the two-way ranging application note APS013 version 2.3 although it is in fact AltDS-TWR. This can be seen by comparison with [23], equation 17.

B. Second TWR experiment: Dependency on the response time

In this experiment the response delay $T^T_{1,2} = 1.5566\,\text{ms}$ is multiplied by an increasing factor over the time. The factor increase began after an hour to reduce the warm-up effect. Afterwards is the factor is increased by 0.2 after 1000 measurements. The response delay $T^R_{2,3} = 1.5530\,\text{ms}$ remains the same. In figure 4 the results of this experiment are presented. The left plot presents the raw distance measurements provided by the different ranging protocols. It can be observed that the noise of the CCSS-TWR case is rapidly increasing with a growing delay time. Moreover, the distance measurement of the SDS-TWR increases with a higher delay time. The right plot of figure 4 clearly shows that at the factor one, with equal response delays the SDS-TWR equates the AltDS-TWR. At this point the response times are nearly the same: $T^T_{1,2} \approx T^R_{2,3}$. The increase in the distance measurement of the CCSS-TWR was unexpected. This could be due to measurement imperfections of the clock drift error. Even if the remaining error was small, with increasing delay it becomes more significant. The best results are provided by the AltDS-TWR protocol.

The AltDS-TWR protocol provides the best results, with a nearly constant distance measurement over time even with changing delay times. The only deviation from the ideal case appears at the beginning. This problem is highlighted in figure 5, where only the filtered distance measurements of the AltDS-TWR case are presented.
The linear approximation of the error is completely suitable for the clock drift correction. Furthermore, a position error caused by a constant velocity of the object is corrected by the linear interpolation because of the linear increase of the position error (pseudo clock drift). An acceleration high enough to cause an error greater than $5\,\text{mm}$, would require almost 1,000g $\left(10^4 \frac{m}{s^2}\right)$. Another possible explanation of the warm-up error could be the change in the reference frequency. In the case of the AltDS-TWR, the residual error depends only on the reference frequency and the time of flight $\epsilon_{AltDS} = e_R T_{AltDS}$. The DecaWave DW1000 chip of the EVK1000 is driven by an RSX-10 Rakon SMD crystal oscillator with a tolerance of $10\,\text{ppm}$ up to $50\,\text{ppm}$ [24]. The short time-of-flight multiplied with the maximum change of the crystal oscillator offset is too small to cause a warm-up error of $3\,\text{cm}$. Therefore, the reason for the observed phenomenon is not the AltDS-TWR protocol.

C. Other sources of error

In practice the timestamp of the DecaWave UWB device is affected by the signal power [14], [15], see figure 6 (a). Increasing the signal power causes a negative shift of the timestamp and vice versa. In [13], we showed how the signal power correction curve can be determined for each DecaWave UWB transceiver individually, without requiring additional

This article has been accepted for publication in a future issue of this journal, but has not been fully edited. Content may change prior to final publication. Citation information: DOI 10.1109/TIM.2020.2996706, IEEE Transactions on Instrumentation and Measurement

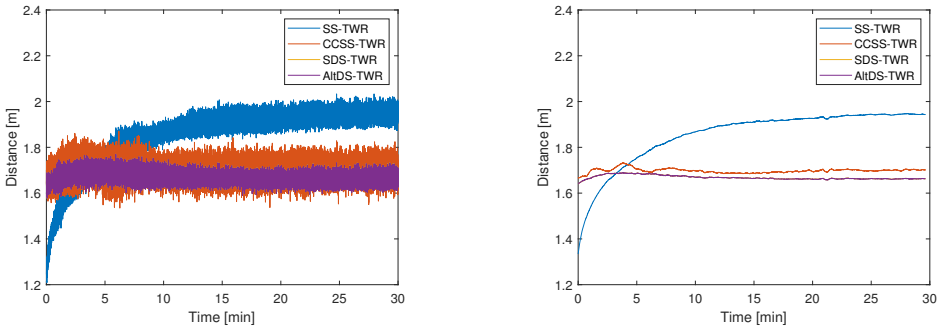

Fig. 3. Comparing the different two-way ranging protocols. Distance measurements with respect to the time. (a) raw distance measurements and (b) filtered distance measurement

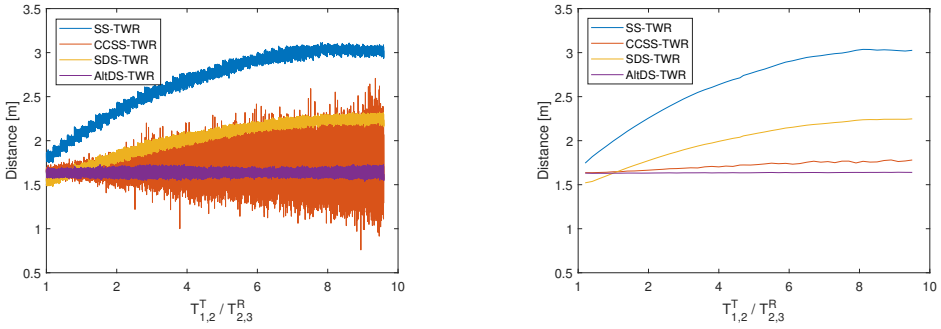

Fig. 4. Comparing the different two-way ranging protocols with increasing response time. (a): Raw distance measurements with respect to response time ratio, (b): Filtered distance measurement with respect to response time ratio.

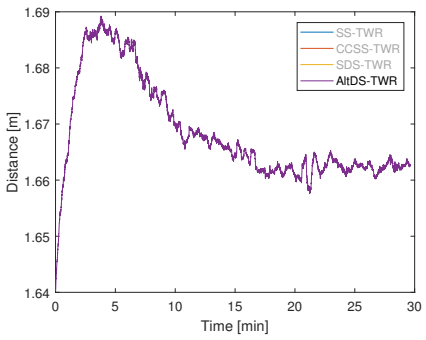

Fig. 5. Filtered distance measurement with respect to the time for the AltDS-TWR case. The plot is based on the measurement data from the first experiment.

measurement equipment. The developed algorithm is reducing the signal power to determine the dependence between the signal power and the timestamp shift. The presented technique allows us to correct the timestamp directly during the ranging procedure by considering the signal power correction terms E_1 and E_2. Note that the signal power may affect the tag and the reference station differently. At a lower signal power, the time difference $\Delta T^R_{1,2}$ increases.

The second important effect on the distance measurement is caused by the hardware delay. This time corresponds to the delay between the arrival of the signal on the antenna until the setting of the time stamp. The effect of the hardware delays A and B on the two-way-ranging, see figure 6 (b). This error depends mainly on the temperature and can be estimated before the ranging [16].

The corrected time-of-flight equation 14 considers the effect of the signal power and the hardware delay for SS-TWR

$$TOF = 0.5 \cdot \left(\Delta T^R_{1,2} - \Delta T^T_{1,2} - E_2 - E_1\right) - A - B \quad (14)$$

IV. Time-difference-of-arrival measurement technique

In applications with several moving targets (tags), TWR is less suitable due to its slow update rate. Trilateration in two-dimensional space requires at least three distance

This article has been accepted for publication in a future issue of this journal, but has not been fully edited. Content may change prior to final publication. Citation information: DOI 10.1109/TIM.2020.2996706, IEEE Transactions on Instrumentation and Measurement

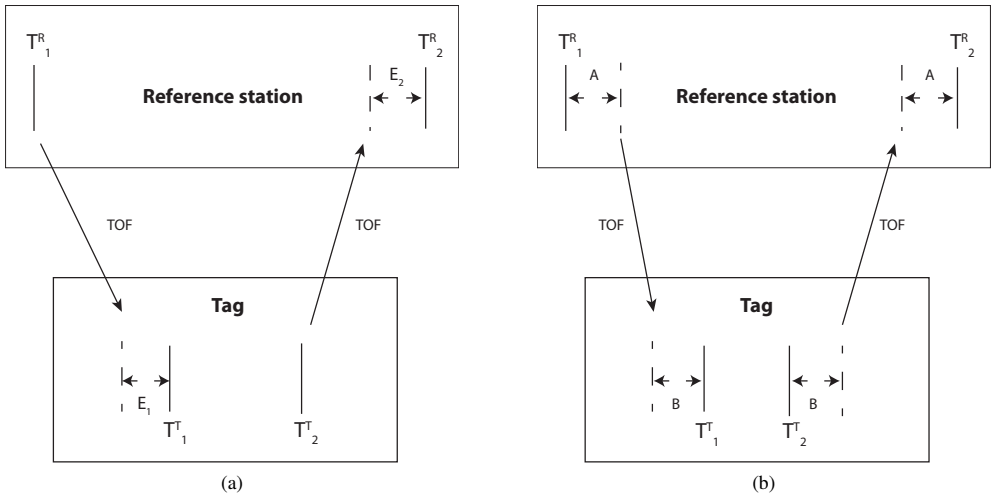

Fig. 6. Schematics for the TWR. (a) Effect of the power on the TOA and (b) effect of the hardware delay on TOA

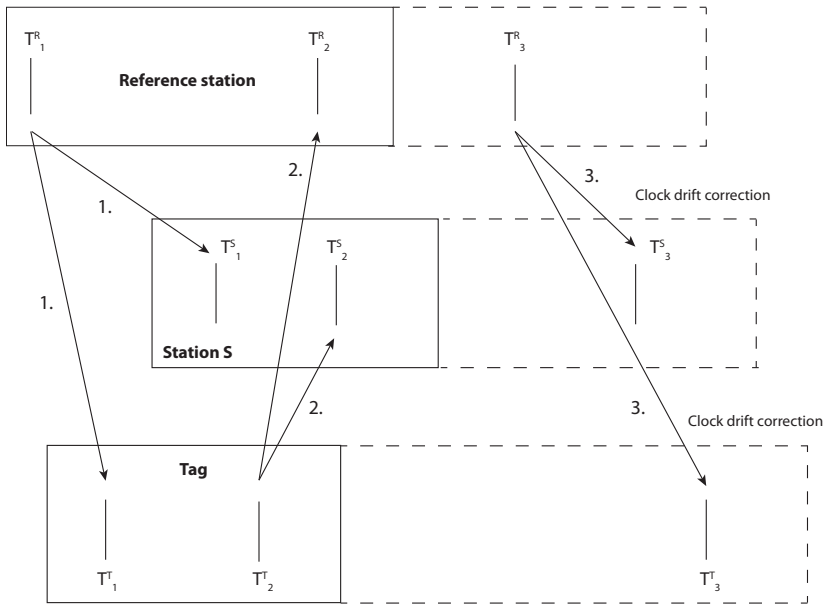

Fig. 7. TAO and TDOA ranging: The first two messages (1 and 2) are required for the ranging, and the third message (3) is for the clock drift correction. During the beginning of the ranging, the reference station sends the first message at its local time T_1^R. The tag and the passive station S receive the message and create timestamps T_1^S and T_1^T. In the next step, the tag sends a response message at its local time T_2^T . The reference station and station S receive this message at their local times T_2^R and T_2^S, respectively.

measurements. As the number of tags increases, the update rate decreases. In contrast to TOA, TDOA remains suitable for applications with large numbers of tags. In TDOA applications, the reference stations do not respond to the tags. Multilateration is performed by considering timestamp differences between anchors. Geometrically, TOA equations describe circles, whereas TDOA equations are hyperbolas in a two-dimensional space. Time synchronization between the base stations can be performed by wire [25] or with an additional station [3]. Various methods for wireless TDOA clock synchronization are presented in [26], [27], [28]. Without clock synchronisation, it is necessary to correct the clock drift for the TDOA application. In [17], Igor Dotlic et al. used the CCSS-TWR method (see. section II-B) to correct the clock drift for TOA and TDOA. They also suggested to extend the SS-TWR with TDOA.

This article has been accepted for publication in a future issue of this journal, but has not been fully edited. Content may change prior to final publication. Citation information: DOI 10.1109/TIM.2020.2996706, IEEE Transactions on Instrumentation and Measurement

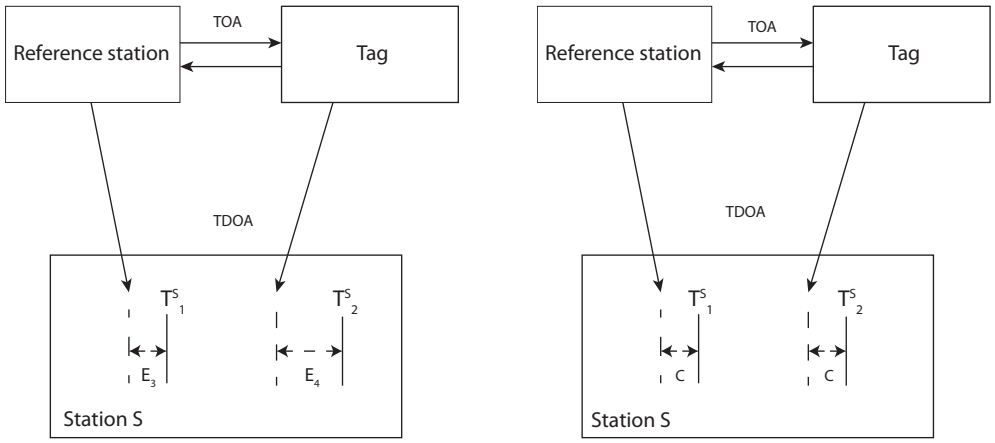

Fig. 8. The effect of signal power on TDOA ranging is shown in (a) and the effect of the hardware offset in (b). on the TDOA.

The results in section II indicate that the AltDS-TWR protocol is the best solution to correct the clock drift. This is the reason why we are going to upgrade the AltDS-TWR protocol for the TDOA application. The error caused by signal power and the influence of the hardware delay are different for the TDOA application compared to the TOA application. Both errors have been neglected in the previous section, but will now be corrected. In previous publications, the signal power error was corrected after obtaining the distance measurement. Using our presented method in [13], it is now possible to obtain the connection between the signal power and the timestamp shift. This allows us to correct the influence of the signal power as a part of the ranging protocol. First of all, the AltDS-TWR equation 10 is transformed into a more intuitive equation 17; it clearly shows that the clock drift error is corrected by linear interpolation. The time differences $T^T_{2,3}$ and $T^R_{2,3}$ are replaced by $\left(\Delta T^T_{1,3} - \Delta T^T_{1,2}\right)$ and $\left(\Delta T^R_{1,3} - \Delta T^R_{1,2}\right)$, respectively. The AltDS-TWR equation 10 becomes:

$$T_{AltDS} = \frac{\Delta T^R_{1,2} \cdot \left(\Delta T^T_{1,3} - \Delta T^T_{1,2}\right)}{\Delta T^T_{1,3}} - \frac{\Delta T^T_{1,2} \cdot \left(\Delta T^R_{1,3} - \Delta T^R_{1,2}\right)}{\Delta T^T_{1,3}} \tag{15}$$

This equation is transformed into equation 16.

$$T_{AltDS} = \Delta T^R_{1,2} - \frac{\Delta T^R_{1,2} \cdot \Delta T^T_{1,2}}{\Delta T^T_{1,3}} - \frac{\Delta T^T_{1,2} \cdot \left(\Delta T^R_{1,3} - \Delta T^R_{1,2}\right)}{\Delta T^T_{1,3}} \tag{16}$$

Without the signal power error and the hardware delay, the function for the time-of-flight T_{TOF} calculation between two stations becomes 17.

$$T_{AltDS} = 0.5 \cdot \left(\Delta T^R_{1,2} - \Delta T^T_{1,2}\left(\frac{\Delta T^R_{1,3}}{\Delta T^T_{1,3}}\right)\right) \tag{17}$$

With all the correction terms, equation 17 corresponds to 18.

$$T_{TOF} = 0.5 \cdot \left(\Delta T^R_{1,2} - \left(\Delta T^T_{1,2} + E_1\right)\left(\frac{\Delta T^R_{1,3}}{\Delta T^T_{1,3}}\right) - E_2\right) - A - B \tag{18}$$

Figure 7 shows the protocol for the TOA-TDOA ranging, without the influence of the signal power and the hardware delay. The first two messages (1 and 2) are required for the ranging, and the third message (3) is for the clock drift correction. During the beginning of the ranging, the reference station sends the first message at its local time T^R_1; this station is used for the time synchronization and the clock drift correction. The tag and the passive station S receive the message and create timestamps T^S_1 and T^T_1. In the TDOA application the stations S are the reference stations, which are located at known positions. In the next step, the tag sends a response message at its local time T^T_2 . The reference station and station S receive this message at their local times T^R_2 and T^S_2, respectively. Without the influence of clock drift, hardware delay and signal power, TOA equates $T_{TOF} = 0.5 \cdot \left(\Delta T^R_{1,2} - \Delta T^T_{1,2}\right)$ and TDOA equation $T_{TDOA_K} = \Delta T^S_{1,2} - K$. The unknown parameter K is the time offset between the transmission times of messages 1 and 2. If both messages are emitted at the same time, this offset is zero. Similarly to the AltDS-TWR, the third message is used for the clock drift correction. The reference station at its local time T^R_3 emits a message that is received by the tag and station S at T^S_3 and T^T_3, respectively. This leads to the clock drift corrected equations $T_{TOF} = 0.5 \cdot \left(\Delta T^R_{1,2} - \Delta T^T_{1,2}\left(\frac{\Delta T^R_{1,3}}{\Delta T^T_{1,3}}\right)\right)$ and $T_{TDOA_K} = \Delta T^S_{1,2}\left(\frac{\Delta T^R_{1,3}}{\Delta T^S_{1,3}}\right) - K$.

The influence of the signal power E_3, E_4 and the hardware delay C for TDOA compared to TOA is shown in figure 8.

This article has been accepted for publication in a future issue of this journal, but has not been fully edited. Content may change prior to final publication. Citation information: DOI 10.1109/TIM.2020.2996706, IEEE Transactions on Instrumentation and Measurement

The error caused by the signal power on the measurement is smaller for TDOA; this is due to the fact that both timestamps of station S are affected. The hardware delay can be assumed to be constant between receiving messages 1 and 2, and hence it has no effect on the time difference $\Delta T^S_{1,2}$.

Considering the clock drift, signal power, and hardware delay leads to the TDOA equation 19.

$$T_{TDOA_K} = \left(\Delta T^S_{1,2} + E_3 - E_4\right)\left(\frac{\Delta T^R_{1,3}}{\Delta T^S_{1,3}}\right) - K \qquad (19)$$

This time still depends on the offset K, as illustrated in figure 9. In general, this offset is simply the time-of-flight T_{TOF} of message 1 from the reference station to the tag plus the computation time $\Delta T^T_{1,2}$ at the tag before the signal 2 is emitted. The hardware delay A of the reference station has no effect on the offset K due to the fact that only the moment the signal leaves the transceiver matters. However, it is important to consider the hardware delay B of the tag two times: when the tag receives message 1 and when message 2 is emitted. At both times the message is delayed by B.

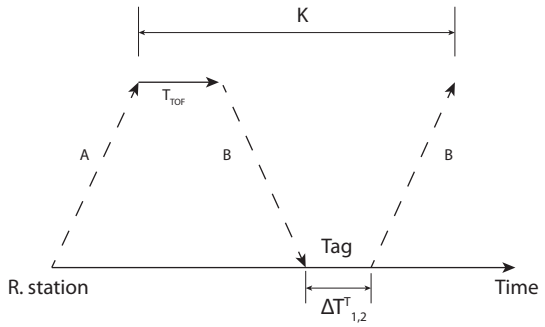

Fig. 9. Calculation of the offset K. A: Delay caused by the hardware of the reference station (T_{TOA}: time of flight between the reference station and the tag). B: Delay caused by the hardware of the tag ($\Delta T^T_{1,2}$: response time of the tag)

It may be calculated as stated in equation 20.

$$K = T_{TOF} + \left(\Delta T^T_{1,2} + E_1\right)\left(\frac{\Delta T^R_{1,3}}{\Delta T^T_{1,3}}\right) + 2B \qquad (20)$$

The new TDOA equation after eliminating the offset K and including all corrections is shown in equation 21 below.

$$T_{TDOA} = \Delta T^R_{1,3}\left(\frac{\Delta T^S_{1,2} + E_3 - E_4}{\Delta T^S_{1,3}} - \frac{0.5\cdot\left(\Delta T^T_{1,2} + E_1\right)}{\Delta T^T_{1,3}}\right) - 0.5\cdot\left(\Delta T^R_{1,2} - E_2\right) + A - B \qquad (21)$$

V. Experimental results: TOA and TDOA position estimation

The aim of this section is to apply the knowledge from the previous sections to estimate the unknown position of the tag with respect to several base stations at known positions. The experiments have been carried out only for the two-dimensional variant. The hardware delay as well as the signal power correction curve have been obtained before the multilateration. The real measurements have been performed with the DecaWave EVK1000. This device supports different message types, which are specified for the discovery phase, ranging phase, and final data transmission. Depending on the update rate and the preamble length, each message can vary from 190 μs to 3.4 ms. In our experiments, we only used 190 μs messages; the settings are listed in table II.

TABLE II
Test settings

Option	Value
Channel	2
Center Frequency	3993.6 MHz
Bandwidth	499.2 MHz
Pulse repetition frequency	64 MHz
Preamble length	128
Data rate	6.81 Mbps

Figure 10 and table III show the constellation of the stations. The ground truth data were obtained by laser distance measurements. The position of the tag with the identification number (ID) 2 is assumed to be unknown. The other stations with IDs 1, 3, 4, and 5 are used to estimate the position of this tag. The station identified as the reference station changes during TWR. This is because the distances between the tag and the other stations must be calculated before the lateration. Unlike TOA, the reference station remains the same for TDOA; in this example it is the reference station with the ID 1. This characteristic of the TDOA measurement technique and the fact that stations S remain passive leads to a much higher update rate compared to TOA trilateration.

Fig. 10. Constellation of the stations

This article has been accepted for publication in a future issue of this journal, but has not been fully edited. Content may change prior to final publication. Citation information: DOI 10.1109/TIM.2020.2996706, IEEE Transactions on Instrumentation and Measurement

TABLE III
POSITION OF THE STATIONS OBTAINED BY LASER DISTANCE MEASUREMENTS

Station ID	X-Axis [m]	Y-Axis [m]
1	0	0
2	0.75	0.75
3	0	1.5
4	1.5	1.5
5	1.5	0

Given the corrected time measurements and the propagation speed of the signal, positioning may be performed to deduce the position of the tag with respect to the anchors.

A. TOA lateration

In figure 11 the results of 2211 tag position estimations are presented; these results are provided by the TOA measurement technique. The base stations are illustrated by red crosses and the estimated tag positions by blue dots.

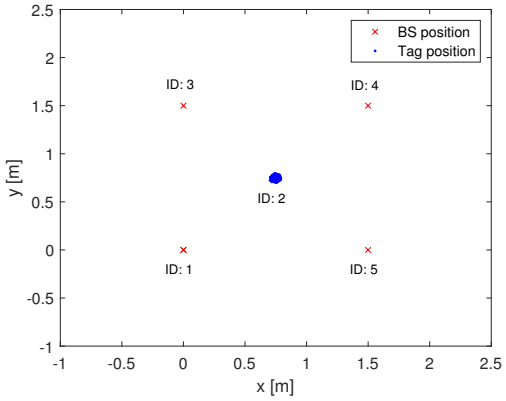

Fig. 11. TOA position estimation. The red crosses are the base stations (BS). The blue dots are the results of the tag position estimations.

The TOA precision equals $\sqrt{\sigma_x^2 + \sigma_y^2} = 0.0221$.

B. TDOA multilateration

Section IV introduced our TDOA ranging protocol. It has the ability to correct the impact of the signal power and the hardware delay for every station individually. It is also possible to obtain the TOF between the reference station and the tag. The variants where the TDOA measurements are combined with the additional TOF measurement will be called 'TOA fusion'. The offset K can be determined either analytically (equation 20) or included in the numerical optimization. The latter will be denoted with the subscript K. This results in four variants, which are defined in table IV.

The same geometric constellation of the base stations and the tag used in the TOA experiments in section V-A are used here. Figure 12 presents the results of 12587 tag position estimations provided by the TDOA measurements with and without offset K and TOA fusion. The base stations are illustrated by red crosses and the estimated tag positions by blue dots. The number of TDOA position estimations is much higher compared to TOA lateration (section V-A) due to the higher update rate. The covariance of the results for the different variants equals

TABLE IV
TDOA VARIANTS

TDOA variants	Definition
M_K	With K and without TOA fusion
M	Without K and without TOA fusion
$M_{K,F}$	With K and with TOA fusion
M_F	Without K and with TOA fusion

$$Cov(M_K) = \begin{pmatrix} 0.0015 & 0.0010 \\ 0.0010 & 0.0027 \end{pmatrix}$$

$$Cov(M) = \begin{pmatrix} 0.0018 & 0.0011 \\ 0.0011 & 0.0020 \end{pmatrix}$$

$$Cov(M_{K,F}) = \begin{pmatrix} 0.0005 & -0.0002 \\ -0.0002 & 0.0009 \end{pmatrix}$$

$$Cov(M_F) = \begin{pmatrix} 0.0005 & -0.0002 \\ -0.0002 & 0.0006 \end{pmatrix}$$

and the precision

TDOA variants:	M_K	M	$M_{K,F}$	M_F
Precision:	0.0644	0.0610	0.0376	0.0336

In contrast to station four, the distance from station five and three to the reference station is the same. The asymmetry of the position errors in M_K and M is expected due to station 1 being the reference station. The influence can be reduced by taking the additional distance measurement into account as shown in $M_{K,F}$ and M_F. For more information on the influence of geometry on positioning, also known as dilution of precision (DOP), see [29]. Furthermore, the ratio between the number of equations with respect to the unknown variables increasing is due to the TOA fusion, and hence, the overall noise is reduced. It can be observed that the best results are obtained for the variant M_F with TOA fusion and with analytical determination of K. The difference from the case M_K without TOA fusion and with offset K optimization is 3 cm. The difference from the variants to each other, M_K to $M_{K,F}$ and M to M_F compared to M_K to M and $M_{K,F}$ to M_F, shows that the TOA fusion has the highest impact on precision. The standard deviation for the best TDOA case M_F is 1 cm higher than that in the TOA lateration (section V-A). It can be observed that the TOA measurements have a better precision compared to TDOA multilateration, but a much slower update rate. This difference becomes even higher with more stations.

This article has been accepted for publication in a future issue of this journal, but has not been fully edited. Content may change prior to final publication. Citation information: DOI 10.1109/TIM.2020.2996706, IEEE Transactions on Instrumentation and Measurement

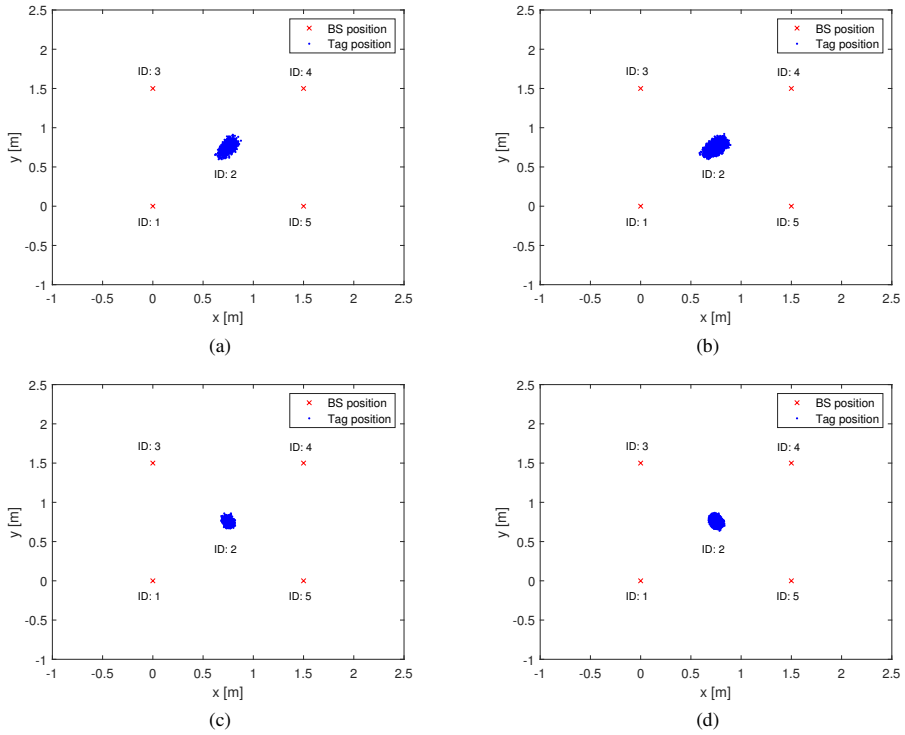

Fig. 12. TDOA position estimation. The red crosses are the base stations (BS). The blue dots are the results of the tag position estimations. In (a) are the position estimations obtained with offset K and without TOA fusion. In (b) without offset K optimization and without TOA fusion. In (c) with offset K and with TOA fusion. In (d) without offset K optimization and with TOA fusion.

VI. Conclusion

This article analyzed the most common two-way-ranging protocols for the DecaWave UWB system, with the aim to find the one most suitable for correcting the clock drift error. These protocols were evaluated experimentally for their ability to correct the clock drift between reference station and tag. It was shown that the AltDS-TWR provides the best results. This protocol was expanded by the ability to correct the signal power and hardware delay for every station individually. The AltDS-TWR equation was transformed to perform the TDOA multilateration with four variants. It was shown that the effect of signal power and hardware delay for the TDOA case has to be considered differently. The best results were obtained with our new approach, where the offset K is computed analytically and fused with an additional distance measured. This method provides almost the same precision as TOA with the high update rate of TDOA. We are very confident that this new method will become the method of choice for DecaWave TDOA positioning.

VII. Acknowledgment

The authors would like to thank Dr. Dimitri Bulatov from the Fraunhofer Institute of Optronics, System Technologies and Image Exploitation IOSB for his constructive criticism of the manuscript.

Glossary of abbreviations

The following abbreviations are used in this article:

ADS-TWR	Asymmetric double-sided TWR
AltDS-TWR	Alternative double-sided TWR
BS	Base stations
CCSS-TWR	CFO-Corrected TWR
CFO	Carrier frequency offset
ID	Identification number
PLL	Phase-locked-loop
RF	Radio frequency
SDS-TWR	Symmetric double-sided TWR
SMD	Surface mounted device
SS-TWR	Single-sided TWR
TDOA	Time-difference-of-arrival
TOA	Time-of-arrival
TWR	Two-way-ranging
UWB	Ultra-wideband

mds
September 04, 2019

This article has been accepted for publication in a future issue of this journal, but has not been fully edited. Content may change prior to final publication. Citation information: DOI 10.1109/TIM.2020.2996706, IEEE Transactions on Instrumentation and Measurement

REFERENCES

[1] D. Douglass and K. Monahan, *GPS instant navigation: A practical guide from basics to advanced techniques by kevin monahan*, Portland, U.S.A.: Fineedge.Com Llc, 1998.

[2] RB. Thompson, *Global positioning system: the mathematics of GPS receivers*, Mathematics Magazine, Published online, 1998.

[3] A. Resch, R. Pfeil, M. Wegener and A. Stelzer, *Review of the LPM local positioning measurement system*, In 2012 International Conference on Localization and GNSS, pp. 1-5, June 2012.

[4] X. Shen, S. Yang, J. He and Z. Huang, *Improved localization algorithm based on RSSI in low power Bluetooth network*, In 2nd International Conference on Cloud Computing and Internet of Things (CCIOT), pp. 134-137, Oct. 2016.

[5] L. Zwirello, T. Schipper, M. Jalilvand and T. Zwick, *Realization Limits of Impulse-Based Localization System for Large-Scale Indoor Applications*, In IEEE Transactions on Instrumentation and Measurement, vol. 64, no. 1, pp. 39-51, Jan. 2015.

[6] D. L. Adamy, *EW 102: A Second Course in Electronic Warfare*, Boston, London: Artech House, July 2004.

[7] Y. Zhou, C. L. Law, Y. L. Guan and F. Chin, *Indoor Elliptical Localization Based on Asynchronous UWB Range Measurement*, In IEEE Transactions on Instrumentation and Measurement, vol. 60, no. 1, pp. 248-257, Jan. 2011.

[8] I. Dotlic, A. Connell, H. Ma, J. Clancy and M. McLaughlin, *Angle of arrival estimation using decawave dw1000 integrated circuits*, In 14th Workshop on Positioning, Navigation and Communications (WPNC), pp. 1-6, Oct. 2017.

[9] J. F. M. Gerrits, J. R. Farserotu and J. R. Long, *Multipath behavior of FM-UWB signals*, In IEEE International Conference on Ultra-Wideband, pp. 162-167, Sept. 2007.

[10] R. A. Saeed, S. Khatun, B. M. Ali and M. A. Khazani, *Ultra-wideband (UWB) geolocation in NLOS multipath fading environments*, In 13th IEEE International Conference on Networks Jointly held with the IEEE 7th Malaysia International Conf on Communications, pp. 6, Nov. 2005.

[11] A. R. Jiménez Ruiz and F. Seco Granja, *Comparing ubisense, bespoon, and decawave uwb location systems: Indoor performance analysis*, In IEEE Transactions on Instrumentation and Measurement, vol. 66, no. 8, pp. 2106-2117, Aug. 2017.

[12] M. Haluza and J. Vesely, *Analysis of signals from the DecaWave TREK1000 wideband positioning system using AKRS system*, In International Conference on Military Technologies (ICMT), pp. 424-429, June 2017.

[13] J. Sidorenko, V. Schatz, M. Arens, N. Scherer-Negenborn and U. Hugentobler, *Decawave UWB clock drift correction and power self-calibration*, In Sensors, pp. 16, July 2019.

[14] *DW1000 User Manual*, Version 2.15, [Online]. Available: https://www.decawave.com, pp. 45. [Accessed: 04-Sep.-2019].

[15] *Decawave APS011 APPLICATION NOTE: Sources of error in TWR*, Version 1.0, [Online]. Available: https://www.decawave.com, pp. 10. [Accessed: 04-Sep.-2019].

[16] *Decawave APS014 APPLICATION NOTE: Antenna delay calibration DW1000-Based products and systems*, Version 1.2 , [Online]. Available: https://www.decawave.com, pp. 10. [Accessed: 04-Sep.-2019].

[17] I. Dotlic, A. Connell and M. McLaughlin, *Ranging Methods Utilizing Carrier Frequency Offset Estimation*, In 15th Workshop on Positioning, Navigation and Communications (WPNC), pp. 1-6, Oct. 2018.

[18] N. I. Fofana, A. van den Bossche, R. Dalcé and T. Val, *An original correction method for indoor ultra wide band rangingbased localisation system*, In Ad-hoc, Mobile, and Wireless Networks, Springer International Publishing. vol. 9724, pp. 79-92, June 2016.

[19] A. van den Bossche, R. Dalce, N. I. Fofana and T. Val, *DecaDuino: An Open Framework for Wireless Time-of-Flight Ranging Systems*, In IFIP Wireless Days (WD 2016), pp. 1-7, March 2016.

[20] F. Molina Martel, J. Sidorenko, C. Bodensteiner, M. Arens, *Augmented reality and uwb technology fusion: Localization of objects with head mounted displays*, In Proceedings of the 31st International Technical Meeting of The Satellite Division of the Institute of Navigation (ION GNSS+), pp. 685-692, Sep. 2018.

[21] R. Hach, *Symmetric double sided two-way ranging*, [Online]. Available: http://www.ieee802.org/15/pub/TG4a.html, doc: IEEE 15-05-0334-00-004a, June 2005

[22] Y. Jiang and V. C. M. Leung, *An Asymmetric Double Sided Two-Way Ranging for Crystal Offset*, In International Symposium on Signals, Systems and Electronics, pp. 525-528, July 2007.

[23] D. Neirynck, E. Luk and M. McLaughlin, *An alternative double-sided two-way ranging method*, In 13th Workshop on Positioning, Navigation and Communications (WPNC), pp. 1-4, Oct 2016.

[24] *Product manual RSX-10*, [Online]. Available: http://www.rakon.com. [Accessed: 05-Sep.-2019].

[25] *Decawave APS007 APPLICATION NOTE: Wired synchronizsation of anchor nodes in a TDOA real time location system*, Version 1.0, [Online]. https://www.decawave.com. [Accessed: 05-Sep.-2019].

[26] C. McElroy, D. Neirynck and M. McLaughlin, *Comparison of wireless clock synchronization algorithms for indoor location systems*, In IEEE International Conference on Communications Workshops (ICC), pp. 157-162, June 2014.

[27] V. Djaja-Josko and J. Kolakowski, *A new method for wireless synchronization and TDOA error reduction in UWB positioning system*, In 21st International Conference on Microwave, Radar and Wireless Communications (MIKON), pp. 1-4, May 2016.

[28] J. Tiemann, F. Eckermann and C. Wietfeld, *ATLAS - an open-source TDOA-based Ultra-wideband localization system*, In International Conference on Indoor Positioning and Indoor Navigation (IPIN), pp. 1-6, Oct 2016.

[29] N. Salman, H. K. Maheshwari, A. H. Kemp and M. Ghogho, *Effects of anchor placement on mean-CRB for localization*, In The 10th IFIP Annual Mediterranean Ad Hoc Networking Workshop, pp. 115-118, June 2011.

[30] J. Sidorenko, N. Scherer-Negenborn, M. Arens, E. Michaelsen, *Improved Linear Direct Solution for Asynchronous Radio Network Localization (RNL)*, Institute of Navigation ION Pacific PNT Meeting, May. 2017.

Juri Sidorenko received a diploma in mechanical engineering from the Technical University Braunschweig, Germany and a Masters of Science from the Cranfield University, the UK in 2012 and 2014. He is currently a Research Assistant with the Fraunhofer Institute of Optronics, System Technologies and Image Exploitation IOSB and pursuing the Ph.D. degree in engineering at the Technical University of Munich. His research interests include the localization and self-calibration of sensor networks.

Dr. Volker Schatz received his diploma in physics from the Ruperto Carola University, Heidelberg, Germany, in 2000, developing trigger circuits for high-energy physics experiments. He obtained his PhD, also at Heidelberg University, in theoretical particle physics, in 2003. After a year of post-doctoral research in theoretical geophysics, he started workat what is now Fraunhofer IOSB in Ettlingen, Germany, in 2005. Volker Schatz's current occupations and research interests are developing multi-sensor data acquisition systems, synchronising imaging sensors for sensor fusion applications and measuring the timing behaviour of commercial cameras.

Dr. Norbert Scherer-Negenborn Dr. Norbert Scherer-Negenborn received the diploma and PhD degree in physics from the University of Freiburg, Germany, in 1996 and 2000, respectively. He is currently the group leader of the Tracking and Tracking Assessment Group at the Fraunhofer Institute for Optronics, System Technology and Image Exploitation IOSB.

This article has been accepted for publication in a future issue of this journal, but has not been fully edited. Content may change prior to final publication. Citation information: DOI 10.1109/TIM.2020.2996706, IEEE Transactions on Instrumentation and Measurement

Dr. Michael Arens received his diploma in Computer Science and his PhD (Dr.rer.nat.) from the University of Karlsruhe in 2001 and 2004, respectively. He is currently the head of department of the Object Recognition (OBJ) Department at the Fraunhofer Institute for Optronics, System Technology and Image Exploitation IOSB.

Prof. Dr. Urs Hugentobler studied theoretical physics at the University of Bern and received a doctorate in astronomy from the same university in 1997. After working as a postdoctoral researcher at the European Space Agency (ESA), he joined the University of Bern in 1999 as head of the GPS Research Group. He has headed TUM's Department of Space Geodesy and TUM's Space Geodesy Research Unit since 2006. He is Secretary General of the Project Geodesy (DGK) of the Bavarian Academy of Science.

4.6. P-VI: Improved Time of Arrival measurement model for non-convex optimization

Authors

Juri Sidorenko, Volker Schatz, Leo Doktorski, Norbert Scherer-Negenborn, Michael Arens, Urs Hugentobler

Journal paper

Navigation (2018), Online First, 25 pp. ISSN: 2161-4296 ISSN: 0028-1522

Introduction

The time of arrival measurement technique leads to a nonlinear quadratic equation. It is just natural to use nonlinear optimization algorithms to obtain the unknown variables. The weak point of this solution finding process is the risk to get trapped into a local minimum. In the following an approach is presented which transforms a local minimum into a saddle point for the case that only the coordinates of the transponder are unknown. The presented approach is answering the question Q^1_{Self} and could also be used later on for the self-calibration for the case that the positions of the base stations are also unknown. The core of the following publication is the mathematical proof of the hypothesis.

Summary

The idea is that an additional dimension λ in the l_2 norm transforms the local minimum into saddle point leaving only the global minimum. This hypothesis was empirically proven with more than 10.000 tests for the objective function $F_1(x,y,z) \coloneqq \frac{1}{4}\sum_{i=1}^{N}\left[\sqrt{(x-a_i)^2+(y-b_i)^2+(z-c_i)^2+\lambda^2}-d_i\right]^2$ and also analytically for the squared objective function. The results for both objective functions are illustrated in Figure 6 and Figure 7. The transformation of the local minimum into a saddle point requires that the first derivative of the squared objective function with respect to the additional variable λ is zero and the second derivative is negative at the local minimum, see Table 2 and Table 3. First, it was necessary to define a new coordinate system centered at L (local minimum) with G (global minimum) on the positive x axis. After some steps only the inequality $2\sum_{i=1}^{N} a_i < N\, x_G$ had to be proven to fulfill the hypothesis. The Cauchy-Bunyakovsky-Schwarz inequality $|\langle\vec{x},\vec{y}\rangle| \leq \|\vec{x}\| \cdot \|\vec{y}\|$ provides the mathematical basis to prove the inequality. In Section 3.7 additionally the proof is given that no other local minimum can exist for non trivial configurations.

Conclusions and outlook

The visualization of the mathematical results can be performed if we assume that two circles intersect at two points for the two dimensional space. The radii of the circles represent the Euclidean distances with the local and global optimum at the intersections respectively. If the optimization algorithm starts close to the local minimum it is likely that a derivative based optimization algorithm converges into a local minimum. An additional dimension transforms the circle into a sphere and the optimization algorithm is now able to escape the local minimum into a higher dimension and converge to the global optimum. This example is explained in more detail in Section 3.8. It is important to mention that the initial estimates for the additional dimension should be nonzero for the derivative based optimization algorithm, otherwise the step size would be zero.

Declaration of own contribution

The first author came up with the idea for the additional dimension and also developed the example and performed the numerical tests and the calculation up to the final hypothesis. The co-author Leo Doktorski proposed to prove the hypothesis by using the Cauchy-Bunyakovsky-Schwarz inequality. Volker Schatz delivered the proof that no other local minima can exist for non trivial constellations. The co-authors improved the paper through their comments and corrections about the layout, content and the obtained results. **The overall own contribution is estimated at 72 %.**

Criteria	Estimated own contribution
Paper concept	70 %
Computations and software development	60 %
Data analysis and interpretation of results	80 %
Design and creation of figures	80 %
Manuscript structure and writing	70 %

Table 4.6.: Apportionment of own contributions for P-VI

Received: 8 January 2018 | Revised: 25 July 2018 | Accepted: 10 August 2018

DOI: 10.1002/navi.277

ORIGINAL ARTICLE

WILEY ION

Improved Time of Arrival measurement model for non-convex optimization

Juri Sidorenko[1,2] | Volker Schatz[1] | Leo Doktorski[1] | Norbert Scherer-Negenborn[1] | Michael Arens[1] | Urs Hugentobler[2]

[1]Fraunhofer Institute of Optronics, System Technologies and Image Exploitation IOSB, Ettlingen, Germany

[2]Institute of Astronomical and Physical Geodesy, Technical University of Munich, Munich, Germany

Correspondence
Juri Sidorenko, Fraunhofer Institute of Optronics, System Technologies and Image Exploitation IOSB, Ettlingen, Germany.
Email: juri.sidorenko@iosb.fraunhofer.de

Funding information
Fraunhofer IOSB

Abstract

The quadratic system provided by the Time of Arrival technique can be solved analytically or by nonlinear least squares minimization. An important problem in quadratic optimization is the possible convergence to a local minimum, instead of the global minimum. This problem does not occur for Global Navigation Satellite Systems (GNSS), due to the known satellite positions. In applications with unknown positions of the reference stations, such as indoor localization with self-calibration, local minima are an important issue. This article presents an approach showing how this risk can be significantly reduced. The main idea of our approach is to transform the local minimum to a saddle point by increasing the number of dimensions. In addition to numerical tests, we analytically prove the theorem and the criteria that no other local minima exist for nontrivial constellations.

1 | INTRODUCTION

In position estimation, the Time of Arrival (ToA)[1] technique is standard. The area of applications extends from satellite-based systems like GPS,[2] GLONASS,[3] Galileo,[4] mobile phone localization (GSM),[5] and radar-based systems such as UWB[6] and FMCW radar[7] to acoustic systems.[8]

The ToA technique leads to a quadratic equation. Optimization algorithms used to solve this system depend on the initial estimate. Unfortunately chosen initial estimates can cause the optimization algorithm to converge to the local minimum. With known reference station positions, it is possible to transform the quadratic to a linear system.[9-11] This linear system can be used to provide an initial estimate. On the other hand, the linear system is more affected by noise, compared with the quadratic system.[9,10] In general, local minima are not an issue in applications with known reference station positions such as GNSS. This changes if it is necessary to obtain the locations of the reference stations without additional measuring equipment, which is also known as self-calibration. The most robust self-calibration solution with noise is nonlinear optimization.[12] This solution suffers if the initial estimates are not close to the global minimum.[13-15] In Mekonnen and Wittneben[16] and Biswas et al,[17] it was proposed to use semi-definite relaxation (SDP) as an initialization for the maximum likelihood (ML) estimator. Nuclear norm-based methods[18-20] also reduce the risk of being trapped in a local minimum. Alternatively, non-iterative methods can be used. A two-dimensional non-iterative method was proposed for the case with three transponders and three receivers in Stewénius.[21] The solution for the three-dimensional case was the subject of the investigation in Kuang[22] and Pollefeys and Nister.[23] The authors

provided a non-iterative solution for the cases with (5, 5), (6,4), and (10,4) transponders and receivers. The roles of the base stations and the transponders are equivalent; hence, it does not matter if six base stations and four transponders are used or vice versa. In the case that one of the base station positions coincides with the position of one of the transponders, it is possible to obtain a closed form solution.[24,25] An alternative approach is called far field.[26] If the distances between the base stations and the transponders are considerably larger than those between the base stations, it is also possible to use a linear simplification. Real measurement data are highly non-convex and nonlinear optimization still provides the most robust solutions.[12]

We present a new approach which does not require an initial estimate at all. The idea is that an additional dimension in the l^2 norm transforms the local minimum of the ToA equation to a saddle point without adding more local minima. This is not equivalent to a receiver time offset, which would be added or subtracted outside the norm. Under the constraint that the position of the reference stations is known, we prove that with our approach, the local minimum becomes a saddle point and no further local minima exist for nontrivial constellations. This paper focuses on proving our approach. Further publications will be based on this concept and will investigate its practical use for self-calibration.

Our approach is based on introducing an additional dimension. It can be seen as a kind of lifting method, a generic term covering many numerical methods introducing an additional variable. Lifting methods have been used for solving nonlinear optimization problems,[27] machine learning problems,[28] optimal control problems,[29] boundary value problems,[30] and parameter estimation problems in ordinary differential equations (ODE).[31] To the best of our knowledge, our specific approach has not been applied before, in particular in the context of ToA localization. It does not work with every objective function, but we will show that it is suitable for ToA localization equations.

This paper is organized as follows. The next section introduces the objective functions F and the corresponding improved objective functions F_L. In Section 3, we use the Levenberg-Marquardt algorithm[32] to illustrate the optimization steps for F and F_L. The last section addresses the results of the optimization algorithm with randomly selected constellations.

2 | METHODOLOGY

Table 1 provides notations used throughout this paper.

Figure 1 shows three base stations B_i at known positions (a_i, b_i, c_i) and one object T at unknown position (x, y, z). The distance measurements d_i between base stations B_i and object T are known and derived from time of flight measurements. The unknown position of object T can be estimated by the known positions of the base stations B_i and the distance measurements d_i. Measurement errors are neglected in this paper; therefore, distance measurements can be referred to as distances.

TABLE 1 Used notations

Notations	Definition
x, y, z	Estimated position of object T
x_G, y_G, z_G	Ground truth position of object T
a_i, b_i, c_i	Ground truth position of base stations B_i, $1 \le i \le N$
d_i	Distance measurements between base stations B_i and object T
λ	Additional variable

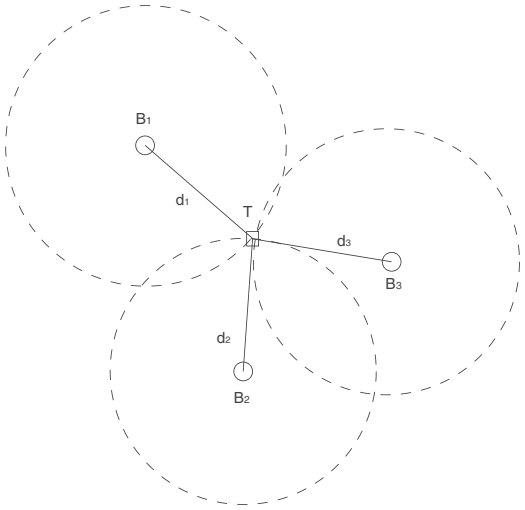

FIGURE 1 The dashed circles are the distances between the base stations B_i and object T. The object T is located at the intersection point between the three dashed circles

2.1 | Mathematical formulation

The distances between the base station B_i and object T are defined as follows:

$$d_i^2 = (x_G - a_i)^2 + (y_G - b_i)^2 + (z_G - c_i)^2. \qquad 1 \le i \le N.$$

- Objective function F_1:

$$F_1(x, y, z) := \frac{1}{4}\sum_{i=1}^{N}\left[\sqrt{(x-a_i)^2+(y-b_i)^2+(z-c_i)^2} - d_i\right]^2 \tag{1}$$

- Objective function F_2:

$$F_2(x,y,z) := \frac{1}{4}\sum_{i=1}^{N}\left[(x-a_i)^2+(y-b_i)^2+(z-c_i)^2-d_i^2\right]^2. \tag{2}$$

(see Douglass[2] and Thompson[33]). Finding the minimum of the objective function of (1) or (2) can be done by non-convex optimization.[34] Alternatively, the nonlinear system can be transformed into a linear system.[9,10] With the assumptions made in Section 2.1, it is possible to obtain a linear system. With regard to future extensions to determining the base station positions as well as the location of the object T, this article focuses on finding a solution with a non-convex optimization algorithm.

2.2 | Reason for the approach

The objective functions (1) and (2) are nonlinear and non-convex. Numerical optimization can cause convergence to a local minimum L instead of the global minimum G. In our approach, instead of F_1 (1) and F_2 (2), the improved objective functions F_{L1} and F_{L2} are used. Both have an additional variable λ compared with the F functions.

- Improved objective function F_{L1}:

$$F_{L1}(x,y,z,\lambda) := \frac{1}{4}\sum_{i=1}^{N}\left[\sqrt{(x-a_i)^2+(y-b_i)^2+(z-c_i)^2+\lambda^2}-d_i\right]^2. \tag{3}$$

- Improved objective function F_{L2}:

$$F_{L2}(x,y,z,\lambda) := \frac{1}{4}\sum_{i=1}^{N}\left[(x-a_i)^2+(y-b_i)^2+(z-c_i)^2+\lambda^2-d_i^2\right]^2. \tag{4}$$

In the next section, we prove that F_{L2} (4) has a saddle point at every position of the local minimum $L(x_L,y_L,z_L)$ of F_2 (2). Therefore, the Levenberg-Marquardt algorithm has a lower probability of converging to a local minimum. The additional variable λ is not equivalent to a receiver time offset in GNSS, which would be added or subtracted outside the norm.

2.3 | Characteristics of a local minimum

2.3.1 | Assumption

The objective function has a unique global minimum at $G(x_G,y_G,z_G)$ and at least one local minimum at $L(x_L,y_L,z_L)$.

2.3.2 | Criterion

It is known that the first derivative of F_L with respect to x, y, and z is zero at the local minimum. The criterion is that the second derivative of F_L at the same position is positive (Table 2).

2.4 | Assertion

The first derivative of F_L with respect to the additional variable λ is zero, and the second derivative is less than zero at the local minimum (Table 3). In combination with the assumption and the criterion, the local minimum becomes a saddle point. The Levenberg-Marquardt (derivative-based optimization algorithm) would not converge to a saddle point.

2.4.1 | Assertion for function F_1

Every local minimum of function F_1 (1) becomes a saddle point at the same coordinates with function F_{L1} (3). We have no analytical proof of this assertion, but the numerical results in Section 3 demonstrate its validity in practice.

2.4.2 | Assertion for function F_2

Every local minimum of function F_2 (2) becomes a saddle point at the same coordinates with function F_{L2} (4). This assertion is proven analytically in Appendix A and demonstrated numerically in Section 3.

TABLE 2 Criterion

First Derivative	Second Derivative
$\left(\frac{\partial}{\partial x}F_L\right)(x_L,y_L,z_L,0)=0$	$\left(\frac{\partial^2}{\partial x^2}F_L\right)(x_L,y_L,z_L,0)>0$
$\left(\frac{\partial}{\partial y}F_L\right)(x_L,y_L,z_L,0)=0$	$\left(\frac{\partial^2}{\partial y^2}F_L\right)(x_L,y_L,z_L,0)>0$
$\left(\frac{\partial}{\partial z}F_L\right)(x_L,y_L,z_L,0)=0$	$\left(\frac{\partial^2}{\partial z^2}F_L\right)(x_L,y_L,z_L,0)>0$

TABLE 3 Assertions of our approach

First Derivative	Second Derivative
$\left(\frac{\partial}{\partial \lambda}F_L\right)(x_L,y_L,z_L,0)=0$	$\left(\frac{\partial^2}{\partial \lambda^2}F_L\right)(x_L,y_L,z_L,0)<0$
	$\left(\frac{\partial^2}{\partial x\partial \lambda}F_L\right)(x_L,y_L,z_L,0)=0$
	$\left(\frac{\partial^2}{\partial y\partial \lambda}F_L\right)(x_L,y_L,z_L,0)=0$
	$\left(\frac{\partial^2}{\partial z\partial \lambda}F_L\right)(x_L,y_L,z_L,0)=0$

2.5 | The effect of an additional variable on the global minimum

At the global minimum, the additional variable λ must be zero, and the second derivative must be positive. The second derivative of F_{L2} (4) with respect to λ at the global minimum is the following:

$$\left(\frac{\partial^2}{\partial\lambda^2}F_{L2}\right)(x_G, y_G, z_G, \lambda_G) = 3\lambda_G^2 N = 0.$$

If the second derivative is zero, a higher-order derivative is required.

$$\left(\frac{\partial^3}{\partial\lambda^3}F_{L2}\right)(x_G, y_G, z_G, \lambda_G) = \sum_{i=1}^{N} 6\lambda_G N = 0.$$

The third derivative is also zero. Finally, the fourth derivative is greater than zero; hence, the additional variable has no effect on the global minimum.

$$\left(\frac{\partial^4}{\partial\lambda^4}F_{L2}\right)(x_G, y_G, z_G, \lambda_G) = 6N.$$

2.6 | No new local minima for F_{L2} with $\lambda \neq 0$

We have shown that the modified objective function F_{L2} (4) turns the local minima of F_2 (2) into saddle points and leaves the global minimum unaffected. It must still be proven that F_{L2} does not introduce new local minima that might adversely affect convergence to the global minimum.

In this section, we will show that in practically relevant base station arrangements, F_{L2} has no stationary points for $\lambda \neq 0$ and $\mathbf{x} \neq \mathbf{x}_G$, and therefore, no minima that would lead an optimization method astray. We will show that if the first derivative of F_{L2} with respect to λ vanishes when $\lambda \neq 0$, its gradient in the spatial directions is nonzero for $\mathbf{x} \neq \mathbf{x}_G$. This proof is best presented in vectorial notation. We will use $\mathbf{x} = (x, y, z)^T$ for the position argument and $\mathbf{a}_i = (a_i, b_i, c_i)^T$ for the base station locations.

$$\frac{\partial}{\partial\lambda}F_{L2}(\mathbf{x}, \lambda) = \lambda \sum_i \left((\mathbf{x} - \mathbf{a}_i)^2 + \lambda^2 - d_i^2\right) = 0, \qquad \lambda \neq 0$$

$$\Rightarrow \quad \sum_i \left((\mathbf{x} - \mathbf{a}_i)^2 + \lambda^2 - d_i^2\right) = 0, \tag{5}$$

$$\operatorname{grad}_{\mathbf{x}} F_{L2}(\mathbf{x}, \lambda) = \sum_i \left((\mathbf{x} - \mathbf{a}_i)^2 + \lambda^2 - d_i^2\right)(\mathbf{x} - \mathbf{a}_i). \tag{6}$$

Equation 5 allows us to add or subtract any term not dependent on the summation index i in the right-hand factor of (6). We subtract $\mathbf{x}$ and add $\mathbf{a}_* = \frac{1}{N}\sum_{i=1}^{N}\mathbf{a}_i$, the geometrical center of the base stations:

$$\begin{aligned}\operatorname{grad}_{\mathbf{x}} F_{L2}(\mathbf{x}, \lambda) &= \sum_i \left((\mathbf{x} - \mathbf{a}_i)^2 + \lambda^2 - d_i^2\right)(\mathbf{x} - \mathbf{a}_i - \mathbf{x} + \mathbf{a}_*) \\ &= -\sum_i \left((\mathbf{x} - \mathbf{a}_i)^2 + \lambda^2 - d_i^2\right)(\mathbf{a}_i - \mathbf{a}_*).\end{aligned}$$

By the construction of $\mathbf{a}_*$, we have $\sum_{i=1}^{N}(\mathbf{a}_i - \mathbf{a}_*) = 0$, so now we can add or subtract any term not depending on the summation index in the left-hand factor. We add $-\lambda^2 - \mathbf{x}^2 + \mathbf{x}_G^2$ and substitute $d_i = |\mathbf{x}_G - \mathbf{a}_i|$, expand the squares and simplify, obtaining the following:

$$\begin{aligned}\operatorname{grad}_{\mathbf{x}} F_{L2}(\mathbf{x}, \lambda) &= -\sum_i \left((\mathbf{x} - \mathbf{a}_i)^2 - \mathbf{x}^2 + \mathbf{x}_G^2 - d_i^2\right)(\mathbf{a}_i - \mathbf{a}_*) \\ &= -\sum_i \left((\mathbf{x} - \mathbf{a}_i)^2 - \mathbf{x}^2 + \mathbf{x}_G^2 - (\mathbf{x}_G - \mathbf{a}_i)^2\right) \\ &\quad (\mathbf{a}_i - \mathbf{a}_*) \\ &= \sum_i (2\mathbf{x}\mathbf{a}_i - 2\mathbf{x}_G\mathbf{a}_i)(\mathbf{a}_i - \mathbf{a}_*) \\ &= 2\,(\mathbf{x} - \mathbf{x}_G)^T \sum_i \mathbf{a}_i \otimes (\mathbf{a}_i - \mathbf{a}_*) \\ &= 2\,(\mathbf{x} - \mathbf{x}_G)^T\,\mathbf{M}.\end{aligned}$$

Here, $\mathbf{u}\otimes\mathbf{v}$ denotes the outer product, resulting in a matrix with the entries $u_i v_j$. The matrix $\mathbf{M}$ can be expressed in the following form:

$$\begin{aligned}\mathbf{M} &= \sum_i \mathbf{a}_i \otimes \mathbf{a}_i - \left(\sum_i \mathbf{a}_i\right) \otimes \mathbf{a}_* = \sum_i \mathbf{a}_i \otimes \mathbf{a}_i - N\,\mathbf{a}_* \otimes \mathbf{a}_* \\ &= \sum_i (\mathbf{a}_i - \mathbf{a}_*) \otimes (\mathbf{a}_i - \mathbf{a}_*).\end{aligned}$$

The last step is analogous to the well-known derivation of the variance of a data set. The result represents $\mathbf{M}$ as a sum of unnormalized projection matrices onto the directions to the base stations from their center.

The calculation above shows that the gradient of F_{L2} has the form of a vector times a sum of projection matrices at all local minima with $\lambda \neq 0$. Projection matrices are positive semidefinite by construction, and their null space is the subspace orthogonal to the projection direction. When adding several positive semidefinite matrices, the null space of the result is the intersection of the null spaces of the individual matrices, in our case the subspace orthogonal to all projection directions. For unambiguous location in n (2 or 3) dimensions, at least $n + 1$ base stations are needed, and they must be arranged in a nondegenerate way, ie, so that the $\mathbf{a}_i - \mathbf{a}_*$ are a spanning set of the whole space. This makes the matrix $\mathbf{M}$ positive definite, and the gradient of F_{L2} cannot be zero for $\mathbf{x} \neq \mathbf{x}_G$. Therefore, there are no local minima that prevent an optimization method from converging to the global minimum.

2.7 | Two-dimensional example

In Appendix A, it is proven that the F_{L2} (4) has a saddle point at the coordinates of the local minimum of F_2 (2) . In this section, an example is created with known coordinates of the global $G(1, 0)$ and local minimum $L(0, 0)$. The aim of this example is to illustrate the converging steps of the

Levenberg-Marquardt algorithm for F_2 and F_{L2}. The positions of the local minimum and global minimum leads to the coordinates of base stations B_i (see Table A3).

Figure 2 shows a top view perspective of the base stations B_i and object T positions inside a Cartesian coordinate system. The circles represent the distance measurements between the base stations B_i and the object T. In this example, the measurements are not corrupted by noise; hence, the ground truth position of object T is located at the intersection point between all circles. Nonlinear optimization algorithms can find the ground truth by minimizing the residues of the predefined objective function to obtain the global minimum. Under certain constellations of the base station, it is possible that the objective function used has a global minimum in addition to at least one local minimum. A more detailed description of the requirements for this kind of constellation can be found in the Appendix A.3. The local and global minima both have the commonality that the first derivative is zero and the second derivative is higher than zero. This attribute makes the local minimum a trap for derivative-based nonlinear optimization algorithms. In this example, the local minimum is located at $L(0,0)$ and the global minimum at $G(1,0)$.

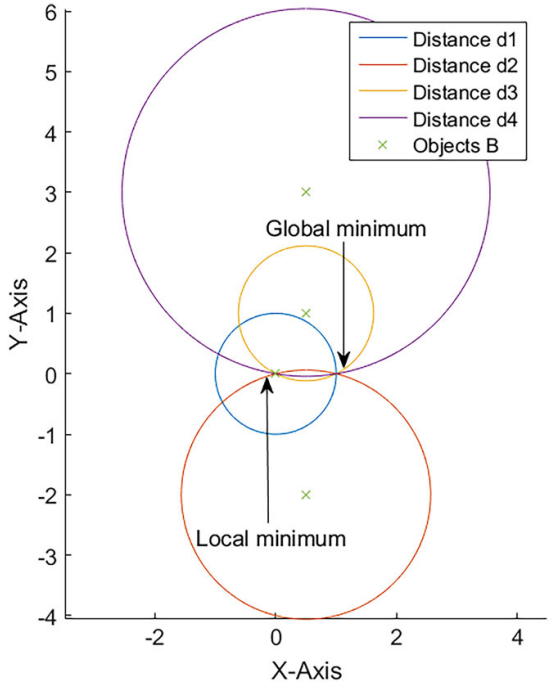

FIGURE 2 The circles represent the true distance between base stations B_i and the global minimum. The blue, red, yellow, and magenta circles are the distances between base stations B and object T, respectively [Color figure can be viewed at wileyonlinelibrary.com and www.ion.org]

Figure 3 shows the search space of objective function F_2 (2) and the zoom at the global minimum. The x-axis of Figure 3 is equivalent to the x-axis in Figure 2 and the y-axis represents the result of objective function F_2. It can be observed that the first derivative is zero, and the second derivative is higher than zero for the local minimum $L(0,0)$ and the global minimum $G(1,0)$. The only difference between both minima is the result of the objective function. At the ground truth position $G(1,0)$, the result of the objective function is zero and at the local minimum $L(0,0)$ it equates to one. In the case of bad initial estimates, close to the local minimum, it is possible that the derivative-based nonlinear optimization algorithm converges to the local minimum and remains there. The main aspect of our approach is to transform this local minimum to a saddle point and eliminate this trap.

2.7.1 | Local optimization

The Levenberg-Marquardt algorithm uses the derivative to obtain the stepsize; therefore, it is important that the initial estimate for the additional variable λ is nonzero. Otherwise, λ remains zero, and F_{L2} (4) is effectively reduced to F_2 (2). The initial estimates for the optimization are $x = -1$, $y = 2$ and $\lambda = 1$.

Figure 4 is equivalent to Figure 2. The x-y axes represent the positions of the base stations B_i and object T inside a Cartesian coordinate system. The circles are the two-dimensional euclidean distances between the base stations B_i and object T. The main difference between Figures 2 and 4 is the additional dimension λ with the initial estimate one. The stepsize of the optimization algorithm is obtained by the first derivative of the objective function. The first derivative for the additional dimension at $\lambda = 0$ is always zero and leads to a stepsize with the value zero. $\left(\frac{\partial}{\partial\lambda}F_2\right)(x,y,z) = \sum_{i=1}^{N}\left[(x-a_i)^2+(y-b_i)^2+\lambda^2-d_i^2\right]\lambda$.

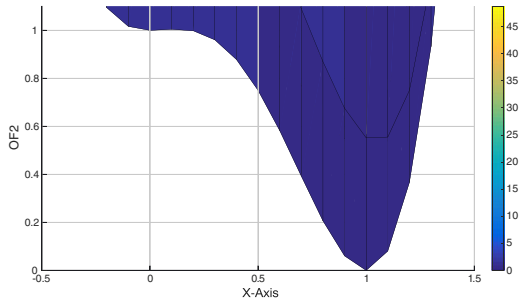

FIGURE 3 The Local minimum is at $L(0,0)$ and global minimum at $G(1,0)$. Colors ranging from blue to yellow show the residues of the objective function [Color figure can be viewed at wileyonlinelibrary.com and www.ion.org]

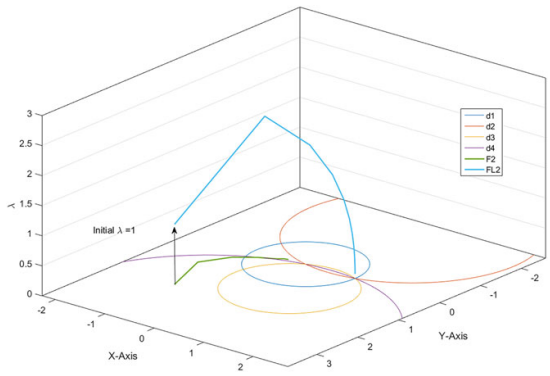

FIGURE 4 Iteration steps of the Levenberg-Marquardt algorithm for F_2 and F_{L2}. F2: Objective function F_2. FL2: Improved objective function F_{L2}. Blue line: Opimization steps of F_2. Green line: Optimization steps of F_{L2}. The circles blue, red, yellow and magenta are the distances between base stations B_i and object T [Color figure can be viewed at wileyonlinelibrary.com and www.ion.org]

Without using the additional dimension, the nonlinear optimization algorithm converges to the local minimum $L(0, 0)$. On the other hand, if the improved objective function F_{L2} is used, the same optimization algorithm converges to the global minimum $G(1, 0)$. The optimization steps with objective function F_2 are represented by the green line and, for the improved objective function F_{L2}, by the blue line. It can be seen that the improved objective function F_{L2} allows the optimization algorithm to use the additional dimension of freedom to bypass the local minimum.

Figure 5 is divided in to two plots. Both plots are based on the same coordinate system as Figure 2, with the same positions for base stations B_i, object T, the local $L(0, 0)$ and global minimum $G(1, 0)$. The colored lines represent the optimization steps. Blue lines indicate the convergence to the local minimum and the green lines to the global minimum. In the left plot, it can be observed that the correct convergence for the objective function F_2 highly depends on the initial estimate of the x-coordinate. With an initial estimate $x > 0$, the optimization algorithm converges to the global minimum, otherwise to the local minimum. In the right plot, the improved objective function F_{L2} is used. At this point, the initial estimates for the x axis are not relevant anymore. The optimization algorithm always converges to the global minimum $G(1, 0)$ if the initial estimate for the additional dimension λ is not equal to zero.

3 | NUMERICAL RESULTS

The base stations B_i, object T and initial estimates were randomly generated by the MATLAB "randn()" function. This function provides normally distributed random numbers in a predefined range. This range was limited to a $10 \times 10 \times 10$ cube. Randomly generated base station positions have the risk of creating collinear constellations with two solutions. These constellations have been avoided by considering the normalized singular value of the covariance matrix. These values provide information about how spread out the base stations are relative to each other. The threshold used for the normalized singular value was set to 0.1. Constellations with a higher value were rejected. The quality of the result is evaluated by the euclidean distance between the fitted value x_F, y_F and z_F and the ground truth position x_G, y_G, and z_G .

- Error term:

$$E = \sqrt{(x_F - x_G)^2 + (y_F - y_G)^2 + (z_F - z_G)^2}. \quad (7)$$

The tests were carried out with the MATLAB Levenberg-Marquardt algorithm using the default settings (Table 4). T4

3.1 | Results with the objective function F_1 and F_{L1}

In the following section, the results of the optimization with a two-dimensional F_1 and F_{L1} are presented.

Figure 6 shows the error term with different constellations of the four base stations B_i ($N = 4$). The x-axis indicates the number of tests carried out. Every scenario was done with random constellations and random initial estimates. The y-axis represents the error term (7). The blue dots are the error with the objective function F_1 and the red dots the improved objective function F_{L1}. It can be seen that F_{L1} has no outlier. It has yet to be proven that the local minimum of F_1 becomes a saddle point for F_{L1}. However, the results show a significant effect of the F_{L1} on the optimization process.

3.2 | Results with the objective function F_2 and F_{L2}

In the following section, the results of the optimization with a two-dimensional F_2 and F_{L2} are presented.

Figure 7 has the same axis notations as Figure 6. The x-axis indicates the number of tests carried out and the y-axis the error term (7). The main difference from Figure 6 is that the blue dots now indicate the error with objective function F_2 and the red dots the improved objective function F_{L2}. In this case, it was proven that the local minimum of F_2 becomes a saddle point with an additional variable. This fact is also underpinned by the error term of F_{L2} , which is always less than 0.5.

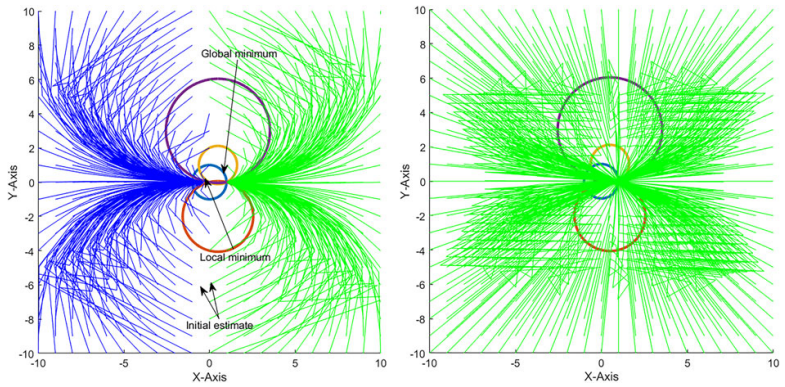

FIGURE 5 Left figure shows F_2 and the right figure shows F_{L2} with different initial estimates. Green: Convergence to global minimum. Blue: Convergence to local minimum [Color figure can be viewed at wileyonlinelibrary.com and www.ion.org]

TABLE 4 Default MATLAB "Levenberg Marquardt algorithm" parameters

	Value
Maximum change in variables for finite-difference gradients	Inf
Minimum change in variables for finite-difference gradients	0
Termination tolerance on the function value	1e-6
Maximum number of function evaluations allowed	100*numberOfVariables
Maximum number of iterations allowed	400
Termination tolerance on the first-order optimality	1e-4
Termination tolerance on x	1e-6
Initial value of the Levenberg-Marquardt parameter	1e-2

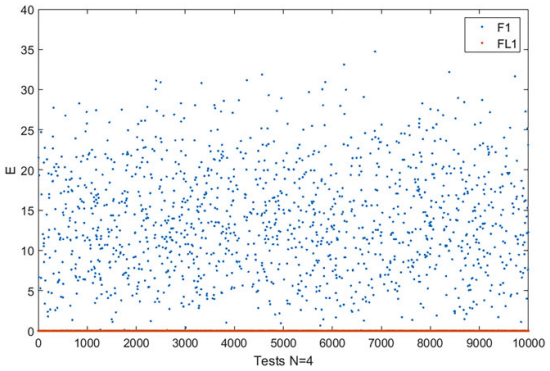

FIGURE 6 Blue dots: Objective function F_1. Red dots: Improved objective function F_{L1} [Color figure can be viewed at wileyonlinelibrary.com and www.ion.org]

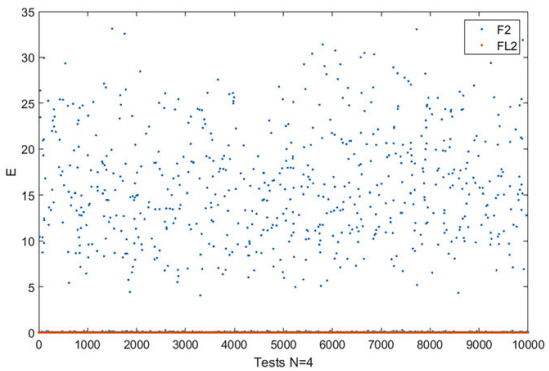

FIGURE 7 The blue dots are the results of the error term of F_2. The red dots are the results of F_{L2} [Color figure can be viewed at wileyonlinelibrary.com and www.ion.org]

3.3 | Summary of the results

Tables 5 and 6 summarize the obtained results. For each number of objects (N), 10 000 constellations have been created and tested with Levenberg-Marquardt. F_L never converges to a local minimum. It can be observed that the risk to converge to a local minimum is decreasing for the objective function F_1 and F_2 with higher number of base stations. This is probably due to the increase in the convergence radius with a higher amount of base stations.

TABLE 5 Examples are based on a 2-D model[a]

N	Objective Function	F_1: L	F_2: L
4	F	1357	634
4	F_L	**0**	**0**
5	F	982	399
5	F_L	**0**	**0**
6	F	810	286
6	F_L	**0**	**0**
7	F	586	182
7	F_L	**0**	**0**

[a]N, number of base stations B_i; F_1, objective function one; F_2, objective function two; L, number of convergences to local minima (Error greater than 0.5).

TABLE 6 Examples are based on a 3-D model[a]

N	Objective function	F_1: L	F_2: L
7	F	494	216
7	F_L	**0**	**0**

[a]N, number of base stations B_i; F_1, objective function one; F_2, objective function two; L, number of convergences to local minima (Error greater than 0.5).

4 | CONCLUSIONS

In the Section 2, it was proven that the improved objective function F_{L2} has no local minima for nontrivial constellations. In addition to the mathematical proof, a simple two-dimensional example was created with one local minimum and one global minimum. This example illustrates how the optimization algorithm uses the additional dimension to bypass the local minimum and converges to the global minimum. This was underpinned by more than 100 000 numerical tests with reasonable constellations. It still has to be proven that the local minimum of F_1 becomes a saddle point with F_{L1}. However, the results show a significant effect of F_{L1} on the optimization process. The objective function F_2 performed better than the objective function F_1. Furthermore, the number of false results L decreases with a higher number of base stations B_i .

5 | DISCUSSION

It is important that the initial estimate of the additional variable is not equal to zero. Otherwise, gradient-based optimization algorithms like Levenberg-Marquardt would not converge to the additional dimension. This is due to the fact that the optimization algorithm used is estimating the stepsize for every dimension by the first derivative of the objective function. With $\lambda = 0$, the derivatives for this additional dimension are always zero; thus, the stepsize also equals zero. The test scenarios were carried out with at least four base stations. This is due to the fact that the additional dimension requires one more measurement. In all test scenarios, the positions of base stations B_i were known. Under the condition that the reference stations are known, it is also possible to obtain the solution analytically. In the case of unknown positions of base stations B_i and objects T_j, with real measurements it is no longer feasible. At this point, our approach becomes extremely valuable.

ACKNOWLEDGMENTS

The first author would like to thank Sebastian Bullinger, Gregor Stachowiak, and Sebastian Tome for their inspiring discussion and the Fraunhofer IOSB for making this work possible. We would also like to thank the reviewers and the Editor for their helpful and constructive comments that greatly contributed to improving the paper.

ORCID

Juri Sidorenko https://orcid.org/0000-0003-0089-967X

REFERENCES

1. Adamy DL. *Ew 102: A Second Course in Electronic Warfare*. Boston London: Artech House; 2004.
2. Douglass D. *GPS instant navigation: a practical guide from basics to advanced techniques by Kevin Monahan*. Fine Edge Productions; 1998; Guildford.
3. Bogdanov PP, Druzhin AV, Tiuliakov AE, Feoktistov AY. GLONASS time and UTC(SU). *2014 31st URSI General Assembly and Scientific Symposium (URSI GASS)*; August 2014; Beijing:1-3.
4. Benevides P, Nico G, Catalão J, Miranda PMA. Analysis of galileo and GPS integration for GNSS tomography. *IEEE Trans Geosci Remote Sens*. April 2017;55(4):1936-1943.
5. Nambiar V, Vattapparamban E, Yurekli AI, Güvenç İ, Mozaffari M, Saad W. SDR based indoor localization using ambient WiFi and GSM signals. *2017 International Conference on Computing, Networking and Communications (ICNC)*; January 2017; Santa Clara:952-957.
6. Marquez A, Tank B, Meghani SK, Ahmed S, Tepe K. Accurate UWB and IMU based indoor localization for autonomous robots. *2017 IEEE 30th Canadian Conference on Electrical and Computer Engineering (CCECE)*; April 2017; Windsor:1-4.
7. Vossiek M, Roskosch R, Heide P. Precise 3-d object position tracking using FMCW radar. *1999 29th European Microwave Conference*, Vol. 1; October 1999; Munich:234-237.
8. Akiyama T, Sugimoto M, Hashizume H. Light-synchronized acoustic ToA measurement system for mobile smart nodes. *2014 International Conference On Indoor Positioning And Indoor Navigation (IPIN)*; October 2014; Busan:749-752.
9. Sidorenko J, Scherer-Negenborn N, Arens M, Michaelsen E. Improved linear direct solution for asynchronous radio network localization (RNL). *ION 2017 Pacific PNT*; Honolulu, HI, May 2017; Honolulu, Hawaii:376-382.
10. Sidorenko J, Scherer-Negenborn N, Arens M, Michaelsen E. Multilateration of the local position measurement. *2016 International Conference on Indoor Positioning and Indoor Navigation (IPIN)*; October 2016; Alcala de Henares:1-8.

11. Hmam H. Quadratic optimisation with one quadratic equality constraint. Electronic Warfare and Radar Division, Edinburgh, South Australia; 2010.
12. Batstone K, Oskarsson M, Åström K. Robust time-of-arrival self calibration with missing data and outliers. *2016 24th European Signal Processing Conference (EUSIPCO)*; August 2016; Budapest:2370-2374.
13. Birchfield ST, Subramanya A. Microphone array position calibration by basis-point classical multidimensional scaling. *IEEE Trans Speech Audio Process*. September 2005;13(5): 1025-1034.
14. Raykar VC, Kozintsev IV, Lienhart R. Position calibration of microphones and loudspeakers in distributed computing platforms. *IEEE Trans Speech Audio Process*. January 2005;13(1): 70-83.
15. Prieto J, Bahillo A, Mazuelas S, Fernández P, Lorenzo RM, Abril EJ. Self-calibration of TOA/distance relationship for wireless localization in harsh environments. *2012 IEEE International Conference On Communications (ICC)*; June 2012; Ottawa:571-575.
16. Mekonnen ZW, Wittneben A. Self-calibration method for toa based localization systems with generic synchronization requirement. *2015 IEEE International Conference On Communications (ICC)*; June 2015; London:4618-4623.
17. Biswas P, Lian T-C, Wang T-C, Ye Y. Semidefinite programming based algorithms for sensor network localization. *ACM Trans Sen Netw*. May 2006;2(2):188-220.
18. Candès EJ, Li X, Ma Y, Wright J. Robust principal component analysis. *J ACM*. June 2011;58(3):11:1-11:37.
19. Garg R, Roussos A, Agapito L. Dense variational reconstruction of non-rigid surfaces from monocular video. *2013 IEEE Conference On Computer Vision And Pattern Recognition*; June 2013; Portland:1272-1279.
20. Olsson C, Oskarsson M. A convex approach to low rank matrix approximation with missing data. *Proceedings of the 16th Scandinavian Conference on Image Analysis*, *SCIA '09*. Berlin, Heidelberg: Springer-Verlag; 2009:301-309.
21. Stewénius H. Gröbner Basis Methods for Minimal Problems in Computervision. *Ph.D. Thesis*: Lund Inst. for Technology, Centre for Mathematical Sciences, Lund Univ.; April 2005.
22. Kuang Y, Burgess S, Torstensson A, Åström K. A complete characterization and solution to the microphone position self-calibration problem. *2013 IEEE International Conference on Acoustics, Speech and Signal Processing*; May 2013; Vancouver:3875-3879.
23. Pollefeys M, Nister D. Direct computation of sound and microphone locations from time-difference-of-arrival data. *2008 IEEE International Conference on Acoustics, Speech and Signal Processing*; March 2008; Las Vegas:2445-2448.
24. Crocco M, Bue AD, Murino V. A bilinear approach to the position self-calibration of multiple sensors. *IEEE Trans Signal Process*. February 2012;60(2):660-673.
25. Crocco M, Bue AD, Bustreo M, Murino V. A closed form solution to the microphone position self-calibration problem. *2012 IEEE International Conference on Acoustics, Speech and Signal Processing (ICASSP)*; March 2012; Kyoto:2597-2600.
26. Kuang Y, Ask E, Burgess S, Åström K. Understanding TOA and TDOA network calibration using far field approximation as initial estimate. *International Conference on Pattern Recognition Applications And Methods*; 2012:590-596.
27. Matei I, Baras JS. Nonlinear programming methods for distributed optimization. Cornell University Library *arXiv:1707.04598*. 2017; Osaka.
28. Brafman RI, Engel Y. *Lifted optimization for relational preference rules*. Leuven, Belgium: ILP-MLG-SRL; 2009.
29. Bock HG, Plitt KJ. A multiple shooting algorithm for direct solution of optimal control problems. *9th IFAC World Congress: A Bride between control science and technology, Budapest, Hungary. IFAC Proceedings*, July 1984;17(2):1603-1608.
30. Osborne MR. On shooting methods for boundary value problems. *J Math Anal Appl*. 1969;27(2):417-433.
31. Peifer M, Timmer J. Parameter estimation in ordinary differential equations for biochemical processes using the method of multiple shooting. *IET Syst Biol*. March 2007;1(2):78-88.
32. Moré J. The Levenberg-Marquardt Algorithm: Implementation and Theory. *In Numerical Analysis*. Berlin, Heidelberg: Springer; 1978:105-116.
33. Thompson RB. Global positioning system: the mathematics of GPS receivers. *Math Mag*. 1998;71:260-269.
34. Stigler SM. Gauss and the invention of least squares. *Ann Stat*. May 1981;9(3):465-474.
35. Bityutskov VI. Bunyakovskii inequality. *Encyclopedia of Mathematics*. NY, USA: Springer, New York; 2001.

How to cite this article: Sidorenko J, Schatz V, Doktorski L, Scherer-Negenborn N, Arens M, Hugentobler U. Improved Time of Arrival measurement model for non-convex optimization. *NAVIGATION*. 2019;1-12. https://doi.org/10.1002/navi.277

APPENDIX A: PROOF OF THE ASSERTION FOR OBJECTIVE FUNCTION F_2

In Section 2.3, the assumption and the criterion was introduced. In this section, the assertion will be proven for the objective function F_2 (2) . The proof of the assertion for objective function F_1 (1) has yet to be found. The empirical results show that the approach works for both objective functions. First, a new coordinate system is defined. This coordinate system is centered at the local minimum with global minimum on the positive x-axis.

A.1 | Definition of the new coordinate system

Without loss of generality, the following coordinate system can be used

$$\boxed{y_G = z_G = x_L = y_L = z_L = 0,}$$

and

$$\boxed{x_G > 0.}$$

The distances between the base stations B_i and object T are defined in Section 2.1. With the new coordinate system the equation becomes

$$d_i^2 = (x_G - a_i)^2 + (b_i)^2 + (c_i)^2.$$

The second objective function can also be written as follows:

$$F_2(x,y,z) = \sum_{i=1}^{N} \varphi_i(x,y,z)^2,$$

with the auxiliary function $\varphi_i(x,y,z)$

$$\varphi_i(x,y,z) := (x-a_i)^2 + (y-b_i)^2 + (z-c_i)^2 - d_i^2.$$

At the position of the local minimum L, the auxiliary function becomes

$$\begin{aligned}\varphi_i(0,0,0) &= \left[{a_i}^2 + {b_i}^2 + {c_i}^2 - d_i^2\right] = \\ &= \left[{a_i}^2 + {b_i}^2 + {c_i}^2 - (x_G - a_i)^2 - {b_i}^2 - {c_i}^2\right] = \\ &= \left[{a_i}^2 - (x_G - a_i)^2\right] = \left[2a_i x_G - (x_G)^2\right] = x_G\left[2a_i - x_G\right].\end{aligned} \tag{A1}$$

Therefore, the second objective function at the local minimum can be written as follows:

$$F_2(0,0,0) = {x_G}^2 \sum_{i=1}^{N} [2a_i - x_G]^2. \tag{A2}$$

In Section 2.3, the assumption and the criterion for the approach were presented.

$$\left(\frac{\partial^2}{\partial\lambda^2} F_L\right)(x_L, y_L, z_L, 0) < 0. \tag{A3}$$

In the following, it will be shown that the assertion (A3) is always correct for the improved objective function F_{L2} (4). Equations A4 and A5 are the first and second derivatives of objective function F_{L2} with respect to λ.

$$\begin{aligned}\left(\frac{\partial}{\partial\lambda} F_{L2}\right)(x,y,z,\lambda) = \sum_{i=1}^{N} &\left[(x-a_i)^2 + (y-b_i)^2\right. \\ &\left.+(z-c_i)^2 + \lambda^2 - d_i^2\right]\lambda,\end{aligned} \tag{A4}$$

$$\begin{aligned}\left(\frac{\partial^2}{\partial\lambda^2} F_{L2}\right)(x,y,z,\lambda) = \sum_{i=1}^{N} &\left[(x-a_i)^2 + (y-b_i)^2\right. \\ &\left.+(z-c_i)^2 + \lambda^2 - d_i^2\right] + 2N\lambda^2.\end{aligned} \tag{A5}$$

At the local minimum $L(x_L, y_L, z_L)$,

$$\begin{aligned}\left(\frac{\partial^2}{\partial\lambda^2} F_{L2}\right)(0,0,0,0) &= \sum_{i=1}^{N}\left[a_i^2 + b_i^2 + c_i^2 - d_i^2\right] \\ &= \sum_{i}^{N} \varphi_i(0,0,0) = \\ &= x_G \sum_{i=1}^{N} [2a_i - x_G] = 2x_G \sum_{i=1}^{N} a_i - N x_G^2.\end{aligned}$$

We want to show that $\left(\frac{\partial^2}{\partial^2\lambda} F_{L2}\right)(x_L, y_L, z_L, 0) < 0$; hence, we have to prove the inequality (A6).

$$\begin{aligned}2x_G \sum_{i=1}^{N} a_i - N {x_G}^2 &< 0 \\ 2\sum_{i=1}^{N} a_i &< N x_G.\end{aligned} \tag{A6}$$

In the next step, the condition at the local minimum is analyzed. The first derivative of objective function F_2 (2) equates to (A7),

$$\begin{aligned}\left(\frac{\partial}{\partial x} F_2\right)(x,y,z) = \sum_{i=1}^{N} &\left[(x-a_i)^2 + (y-b_i)^2\right. \\ &\left.+(z-c_i)^2 - d_i^2\right](x-a_i) = \\ = \sum_{i}^{N} &\varphi_i(x,y,z)(x-a_i),\end{aligned} \tag{A7}$$

in combination with (A1), the first derivative becomes (A8).

$$\begin{aligned}\left(\frac{\partial}{\partial x} F_2\right)(0,0,0) &= \sum_{i=1}^{N} \varphi_i(0,0,0)(-a_i) \\ &= \sum_{i=1}^{N} x_G\left[2a_i - x_G\right](-a_i) = \\ &= \left[{x_G}^2 \sum_{i=1}^{N} a_i - 2x_G \sum_{i=1}^{N} a_i^2\right].\end{aligned} \tag{A8}$$

At the local minimum $L(x_L, y_L, z_L)$, the first derivative of objective function F_2 is equal to zero.

$$\begin{aligned}x_G^2 \sum_{i=1}^{N} a_i - 2x_G \sum_{i=1}^{N} a_i^2 &= 0 \\ x_G \sum_{i=1}^{N} a_i &= 2\sum_{i=1}^{N} a_i^2.\end{aligned} \tag{A9}$$

This leads to $\sum_{i=1}^{N} a_i > 0$. The objective function F_2 has a higher result at the local minimum compared with the global minimum. It is assumed that the objective functions have no errors; therefore, the result of F_2 at the global minimum must be zero.

$$F_2(0,0,0) > F_2(x_G, 0, 0) = 0, \tag{A10}$$

$$x_G{}^2 \sum_{i=1}^{N} (2a_i - x_G)^2 > 0 \tag{A11}$$

$$\sum_{i=1}^{N} (2a_i - x_G)^2 > 0$$

$$4\sum_{i=1}^{N} a_i^2 - 4x_G \sum_{i=1}^{N} a_i + N x_G^2 > 0$$

$$4x_G\sum_{i=1}^{N}a_i < 4\sum_{i=1}^{N}a_i^2 + Nx_G^2. \tag{A12}$$

The term $F_2(0,0,0)$ of (A10) is replaced by (A2). Equation A11 can be converted to A12. Combined with (A9), the new inequality equates to A13.

$$\begin{aligned} 8\sum_{i=1}^{N}a_i^2 &< 4\sum_{i=1}^{N}a_i^2 + Nx_G^2 \\ 4\sum_{i=1}^{N}a_i^2 &< Nx_G^2. \end{aligned} \tag{A13}$$

A.2 | Proof by Cauchy-Bunyakovsky-Schwarz inequality

The final step of the proof for the assertion requires the Cauchy-Bunyakovsky-Schwarz inequality[35] for $\mathbb{R}^N$.

Here, it is desired to prove that $2\Sigma_{i=1}^{N}a_i < Nx_G$.

The Cauchy-Bunyakovsky-Schwarz inequality states that $\left|\langle\vec{x},\vec{y}\rangle\right| \le \|\vec{x}\|\cdot\|\vec{y}\|$. In our case, the vectors are the following:

$$\vec{x} = \begin{pmatrix} 1 \\ \vdots \\ 1 \end{pmatrix} \text{ and } \vec{y} = \begin{pmatrix} a_1 \\ \vdots \\ a_n \end{pmatrix}.$$

Therefore, the left term $2\sum_{i=1}^{N}a_i$ of (A6) must be less than or equal to $2\sqrt{N}\sqrt{\sum_{i=1}^{N}a_i{}^2}$.

$$2\sum_{i=1}^{N}a_i \le 2\sqrt{N}\sqrt{\sum_{i=1}^{N}a_i^2}. \tag{A14}$$

From (A13), it is known that $\sum_{i=1}^{N}(a_i)^2 < \frac{1}{4}N\cdot(x_G)^2$; therefore, the right side of (A14) can be written as $2\sqrt{N}\sqrt{\frac{1}{4}Nx_G{}^2}$.

The inequality becomes

$$2\sum_{i=1}^{N}a_i < 2\sqrt{N}\sqrt{\frac{1}{4}Nx_G^2} = Nx_G.$$

A.3 | Possible constellations for the example

The coordinate system was described in Section A.1. We want to find base station constellations with a local minimum at x_L, y_L, z_L and a global minimum at x_G, y_G, z_G .

A.4 | Analysis of the first derivative

The first derivative of objective function F_2 has to be zero at the local minimum. This means

$$\left(\frac{\partial}{\partial x}F_2\right)(0,0) = \sum_{i=1}^{N}\left[(a_i^2-(x_G-a_i)^2)\cdot(-a_i)\right] = 0, \tag{A15}$$

$$\left(\frac{\partial}{\partial y}F_2\right)(0,0) = \sum_{i=1}^{N}\left[(a_i^2-(x_G-a_i)^2)\cdot(-b_i)\right] = 0. \tag{A16}$$

The simplest constellation that fulfills (A15) and (A16) is the following:

$$\begin{cases} \left[(a_i^2-(x_G-a_i)^2)\cdot(-a_i)\right] = 0 & 1 \le i \le N \\ \left[(a_i^2-(x_G-a_i)^2)\cdot(-b_i)\right] = 0 & 1 \le i \le N. \end{cases}$$

There are two obvious options that fulfill these equations. The first one is $a_i = b_i = 0$. The second one $a_i = \frac{1}{2}x_G$ with any b_i. The number of base stations using the first and second options are denoted as S_1 and S_2, respectively. Only sensible constellations are considered; therefore, S_1 can only be one or zero.

A.5 | Analysis of the second derivative

The second derivative of objective function F_2 (2) must be positive at the local minimum. This means,

$$\left(\frac{\partial^2}{\partial x^2}F_2\right)(0,0) = \sum_{i=1}^{N}\left[2a_i^2 + a_i^2 - (x_G-a_i)^2\right] > 0, \tag{A17}$$

and

$$\left(\frac{\partial^2}{\partial y^2}F_2\right)(0,0) = \sum_{i=1}^{N}\left[2b_i^2 - x_G^2 + 2a_ix_G\right] > 0. \tag{A18}$$

Inserting (A15) into (A17) leads to the first condition.

$$\sum_{i=1}^{N}3a_i > Nx_G. \tag{A19}$$

The second and third conditions are obtained by inserting the options S_1 and S_2 into (A17) and (A18), respectively. Therefore, the second derivative of objective function F_2 becomes

$$\left(\frac{\partial^2}{\partial x^2}F_2\right)(0,0) = -S_1x_G^2 + \frac{1}{2}S_2x_G^2 > 0,$$

and

$$\left(\frac{\partial^2}{\partial y^2}F_2\right)(0,0) = -S_1x_G^2 + 2\sum_{i=1}^{S_2}b_i^2 > 0.$$

All the conditions required for a local minimum at $L(0,0)$ are listed in Table A1.

TABLE A1 Conditions required for a local minimum at $L(0, 0)$

	Conditions
1	$3\sum_{i=1}^{N} a_i > Nx_G$
2	$0.5 \cdot S_2 > S_1$
3	$2\sum_{i=1}^{S_2} b_i^2 > x_G^2 S_1$

TABLE A2 Assumptions used for the example

Assumptions
$S_1 = 1$
$S_2 = 3$

TABLE A3 Coordinates of object B

Base Stations B_i With Index	X-Axis	Y-Axis
1	0	0
2	$0.5 \cdot x_G$	-2
3	$0.5 \cdot x_G$	1
4	$0.5 \cdot x_G$	3

A.6 | Constellations used in the example

The assumptions used in the example and the coordinates of the base stations B_i can be found in Tables A2 and A3.

4.7. P-VII: Improved Time of Arrival measurement model for non-convex optimization with noisy data

Authors

Juri Sidorenko, Volker Schatz, Norbert Scherer-Negenborn, Michael Arens, Urs Hugentobler

Conference paper

2018 International Conference on Indoor Positioning and Indoor Navigation, Nantes, France, Sep. 2018, pp. 206-212, DOI: 10.1109/IPIN.2018.8533839.

Introduction

The presented approach from P-VI transforms the local minimum of the TOA measurement to a saddle point, under the premise that the position of the base stations are known. In the following publication the final inequality from P-VI is proven with the variance instead of the Cauchy-Bunyakovsky-Schwarz inequality. Additionally to the alternative proof of the hypotheses also the question Q^2_{Self} the effect of noise on the lifted objective function is an aim of the investigation.

Summary

The nonlinear optimization of the transponder position at random locations and with increasing noise shows that the noise affects the lifted objective function more than the regular objective function. This is because the ratio between the amount of equations with respect to the number of unknown dimensions is better for the regular objective function. With increasing noise is it also possible that the optimization for the lifted objective function converges into a local minimum due to the fact that the inequality $2\sum_{i=1}^{N} a_i < N\, x_G$ does not apply any more, see Table 5.

Conclusions and outlook

The lifted objective function has reduced the risk to get trapped into a local minimum significantly, even in presense of noise as shown in Figure 5. A higher number of dimensions has no effect on the optimization, shown in Figure 6. However, the conventional objecive function has a better damping of the noise due to the better ratio between the number of equations to unkown dimension. The solution for

this problem is presented in Figure 7. It is recommended to restart the optimization with the regular objective functions and initial estimates provided by the lifted optimization. In this way the advantages of both objective functions are combined.

Declaration of own contribution

The first author came up with the idea for the implementation of the additional dimension also the example, the numerical tests and the combination of both objective function to combine the advantages of both methods. The co-author Volker Schatz proved the alternative final proof of the hypothesis by the variance of the base station location. The co-authors improved the paper through their comments and corrections about the layout, content and the obtained results. **The overall own contribution is estimated at 80 %.**

Criteria	Estimated own contribution
Paper concept	90 %
Computations and software development	70 %
Data analysis and interpretation of results	80 %
Design and creation of figures	80 %
Manuscript structure and writing	80 %

Table 4.7.: Apportionment of own contributions for P-VII

2018 International Conference on Indoor Positioning and Indoor Navigation (IPIN), 24-27 September 2018, Nantes, France

Improved Time of Arrival Measurement Model for Non-Convex Optimization with Noisy Data

Juri Sidorenko[1,2], Volker Schatz[1], Norbert Scherer-Negenborn[1], Michael Arens[1], Urs Hugentobler[2]
1. Fraunhofer Institute of Optronics, System Technologies and Image Exploitation IOSB, Ettlingen, Germany
2. Institute of Astronomical and Physical Geodesy, Technical University of Munich, Munich, Germany
juri.sidorenko@iosb.fraunhofer.de

***Abstract*—The quadratic system provided by the Time of Arrival technique can be solved analytical or by non-linear least squares minimization. In real environments the measurements are always corrupted by noise. This measurement noise effects the analytical solution more than non-linear optimization algorithms. On the other hand it is also true that local optimization tends to find the local minimum, instead of the global minimum. This article presents an approach how this risk can be significantly reduced in noisy environments. The main idea of our approach is to transform the local minimum to a saddle point, by increasing the number of dimensions. In addition to numerical tests we analytically prove the theorem and the criteria that no other local minima exists for non-trivial constellations.**

Keywords— localization, navigation, time of arrival, non-linear optimization

I. Introduction

In position estimation, the Time of Arrival (ToA) [2] technique is standard. The area of application extends from satellite-based systems like GPS [10], GLONASS [8], Galileo [5], mobile phone localization (GSM) [13], radar-based systems such as UWB [16], FMCW radar [23] to acoustic systems [8]. The ToA technique leads to a quadratic equation. Optimization algorithms used to solve this system depend on the initial estimate. Unfortunately, chosen initial estimates can increase the probability convergence to a local minimum. In some cases it is possible to transform the quadratic to a linear system [11, 20, 14]. This linear system can be used to provide an initial estimate. On the other hand, the linear system is more affected by noise, compared to the quadratic system [11, 20]. In practice, a combination of both methods is used to obtain the unknown position of an object [1, 4, 9].

We present a new approach that does not require an initial estimate at all. The idea is that an additional dimension in the l^2 norm transforms the local minimum of the ToA equation to a saddle point without adding more local minimum. This is not equivalent to a receiver time offset, which would be added or subtracted outside the norm. Our approach involves introducing an additional special dimension. It can be seen as a kind of lifting method, a generic term covering many numerical methods introducing an additional variable. Lifting methods have been used for solving non-linear optimization problems [15], machine learning [12], optimal control problems [7], boundary value problems [18] and parameter estimation problems in ordinary differential equations (ODE) [19]. To the best of our knowledge, our specific approach has not been applied before, in particular in the context of ToA localization. It does not work with every objective function but we will show that it is suitable for ToA localization equations. In the publication [21], it was shown that this approach, reduces the risk of convergence to a local minimum for measurements without noise. This elaboration is more focused on the effect of noise on our approach.

This paper is organized as follows. The next section, introduces the objective functions F and the corresponding improved objective functions F_L. In Section 4, we use Levenberg-Marquardt algorithm [17] to illustrate the optimization steps for F and F_L. The last section address the results of the optimization algorithm with randomly selected constellations and different amounts of white noise.

978-1-5386-5635-8/18/$31.00 ©2018 IEEE

II. Methodology

Figure 1 shows three base stations B_i at known positions (a_i, b_i, c_i), and one transponder T at unknown position (x,y,z). The distances measurements d_i between base stations B_i and the transponder T are known. The unknown position of the transponder T can be estimated by the known positions of the base stations B_i and the distance measurements d_i. This data is effected by Gaussian noise e_i.

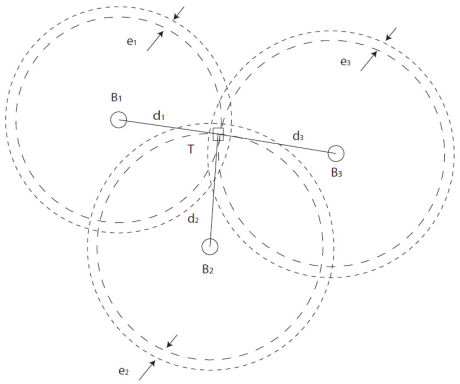

Fig. 1. The dashed circles with a smaller radius are the true distances between base stations B_i and transponder T. The dashed circles are the false measurements due to noise.

2018 International Conference on Indoor Positioning and Indoor Navigation (IPIN), 24-27 September 2018, Nantes, France

TABLE I. USED NOTATIONS

Notations	Definition
x, y, z	Estimated position of the transponder T
x_G, y_G, z_G	Ground truth position of the transponder T
a_i, b_i, c_i	Ground truth position of base stations B_i, $1 \leq i \leq N$
d_i	Distance measurements between B_i and T
λ	Additional variable

A. Mathematical formulation

The distance measurements between the base stations B_i and transponder T are defined as

$$d_i = \sqrt{(x_G - a_i)^2 + (y_G - b_i)^2 + (z_G - c_i)^2}. \qquad 1 \leq i \leq N$$

Objective function F_1:

$$F_1(x, y, z) \coloneqq \sum_{i=1}^{N} \left[\sqrt{(x - a_i)^2 + (y - b_i)^2 + (z - c_i)^2} - d_i + e_i\right]^2 \tag{1}$$

The solving of (1) can be done by non-convex optimization [22]. Alternatively, the non-linear system can be transformed into a linear system [11, 20]. With regard to future extensions to determining the base station positions as well as the location of the transponder T, this article focuses on finding a solution with a non-convex optimization algorithm.

B. Reason for the approach

The objective function (1) is non-linear and non-convex. The optimization of the objective function can cause the convergence to a local minimum L instead the global minimum G (see Table [1]). In our approach, instead F_1 the improved objective function F_{L1} is used. This function has an additional variable \lambda compared to the function F_1.

Improved objective function F_{L1}:

$$F_{L1}(x, y, z, \lambda) \coloneqq \sum_{i=1}^{N} \left[\sqrt{(x - a_i)^2 + (y - b_i)^2 + (z - c_i)^2 + \lambda^2} - d_i + e_i\right]^2 \tag{2}$$

$$F_{L2}(x, y, z, \lambda) \coloneqq \sum_{i=1}^{N} \left[(x - a_i)^2 + (y - b_i)^2 + (z - c_i)^2 + \lambda^2 - d_i^2\right]^2 \tag{3}$$

In [21], we have proven that the improved objective function (3) with an additional variable, transforms the local minimum to a saddle point at $\lambda = 0$. Furthermore, it was shown that no further local minima exist for $\lambda \neq 0$ at non trivial constellations. The same effect was demonstrated numerically for (1) and (3). The final proof of the hypothesis was provided with the help of the Cauchy-Bunyakovsky-Schwarz inequality [28]. Alternatively, (29) in [29] can also be obtained from the variance

$$Var(X) = \mathbb{E}\left((X - \mathbb{E}(X))^2\right) = \mathbb{E}(X)^2 - (\mathbb{E}(X))^2 \tag{4}$$

The base stations should have a variance in a position greater than or equal to zero

$$0 \leq Var(\{a_i\}) = \frac{1}{N}\sum_{i=1}^{N} a_i^2 - \left(\frac{1}{N}\sum_{i=1}^{N} a_i\right)^2 = \frac{1}{N}\sum_{i=1}^{N} a_i^2 - \frac{1}{N^2}\left(\sum_{i=1}^{N} a_i\right)^2 \tag{5}$$

This leads to the final term

$$\sum_{i=1}^{N} a_i \leq \sqrt{N}\sqrt{\sum_{i=1}^{N} a_i{}^2} \tag{6}$$

In this article, the measurement data is effected by white noise, therefore the objective function F_1 (1) is used. In contrast to objective function F_2, this function is statistically correct in presence of noise.

C. Two-dimensional example

In this section, an example is created with known coordinates of the global minimum at G(1,0) , local minimum L(0,0) without noise. The aim of this example is to illustrate the converging steps of the Levenberg-Marquardt algorithm for F_1 and F_{L1}. Other derivative based optimization algorithms like Gauss-Newton or damped Gauss-Newton would provide the same results but require different computational time. The positions of the local minimum and global minimum leads to the coordinates of base stations B_i (see Table 2). Figure 2 shows the coordinates of base stations B_i, which are located in the center of the circles. Figure 3 presents the search space of objective function F_1.

TABLE II. COORDINATES OF BASE STATION B_i

Base stations	Y-Position	X-Position
B_1	0.5	0
B_2	0	2
B_3	0	−2

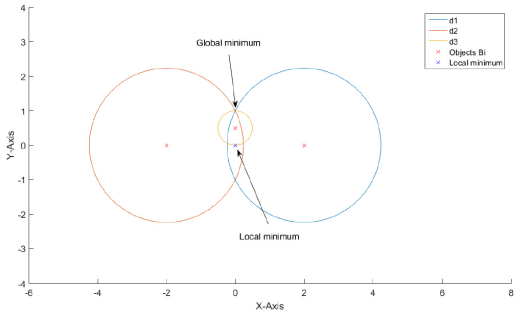

Fig. 2. The circles represents the true distance between base stations B_i and the global minimum. The blue circle is the distance between base station B_2 and the transponder. The red circle is the distance between base station B_3 and transponder. The yellow circle is the distance between base station B_1 and the transponder

2018 International Conference on Indoor Positioning and Indoor Navigation (IPIN), 24-27 September 2018, Nantes, France

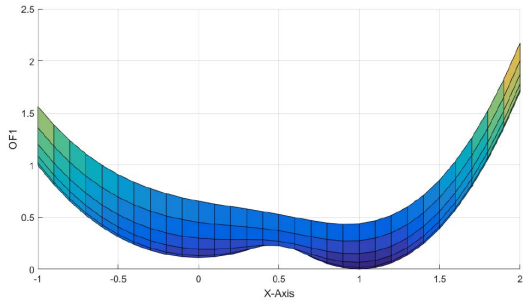

Fig. 3. Local minimum at L(0,0) and global optima at G(1,0). Ranging from blue to yellow showing the result of the objective function

D. Local optimization

The Levenberg-Marquardt algorithm uses the derivative to obtain the stepsize; therefore, it is important that the initial estimate for the additional variable λ is non-zero. Otherwise λ remains zero, and F_{L1} is effectively reduced to F_1. Table 3 shows initial estimates of the optimization.

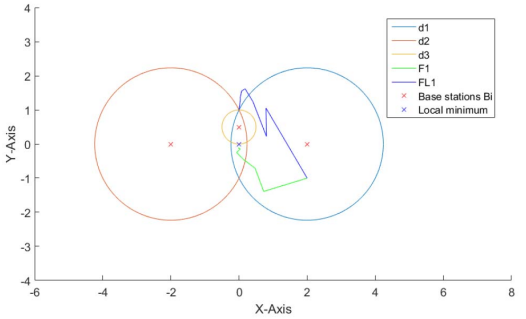

Fig. 4. Iteration steps of the Levenberg-Marquardt algorithm for F_1 and F_{L1}. F_1: Objective function F_1. F_{L1}: Improved objective function F_{L1}. Blue line: Opimization steps. Green line: Optimization steps improved function. The blue, red and yellow circles are the distances between base stations B_i and transponder T.

TABLE III. INITIAL ESTIMATE OF THE LEVENBERG-MARQUARDT ALGORITHM FOR F_1 AND F_{L1}

	x	y	λ
Initial estimate	2	-1	1

In Figure 4, the result of the optimization can be observed. The blue path shows the steps of the improved objective function F_{L1}, which converge to the global minimum G(1,0). On the other hand, the original objective function F_1 represented by the green line, converges to the local minimum L(0,0). If the measurement is effected by noise, the residues would be higher than zero at the global minimum. With more additional variables (8), the error splits up between the additional variables in the manner

$$\lambda = \sqrt{\sum_{i=1}^{N} \lambda_i{}^2} \tag{7}$$

$$F_{L2}(x, y, z, \lambda_2, \lambda_3) := \sum_{i=1}^{N} \left[\sqrt{(x-a_i)^2 + (y-b_i)^2 + (z-c_i)^2 + \lambda_2{}^2 + \lambda_3{}^2} - d_i - e_i\right]^2 \tag{8}$$

We assume that the proven hypothesis [21] for the improved objective function F_{L2} apply as well for the improved objective function F_{L1} (9).

$$\left(\frac{\partial^2}{\partial \lambda^2} F_{L1}\right)(0,0,0,0) = \sum_{i=1}^{N} \frac{\left(\sqrt{a_i{}^2 + b_i{}^2} - d_i + e_i\right)}{\sqrt{a_i{}^2 + b_i{}^2}} < 0 \tag{9}$$

III. NUMERICAL RESULTS

The tests were carried out with MATLAB Levenberg-Marquardt algorithm using the default settings. The base stations B_i, transponder T and initial estimates were randomly generated in a 10x10x10 cube. Unfavorable constellation close to collinearity have been avoided by the requirement that every normalized singular value of the covariance matrix should be greater than 0.1.

Error term:

$$E = \sqrt{(x - x_G)^2 + (y - y_G)^2 + (z - z_G)^2} \tag{10}$$

A. Results of the objective function and the improved objective function

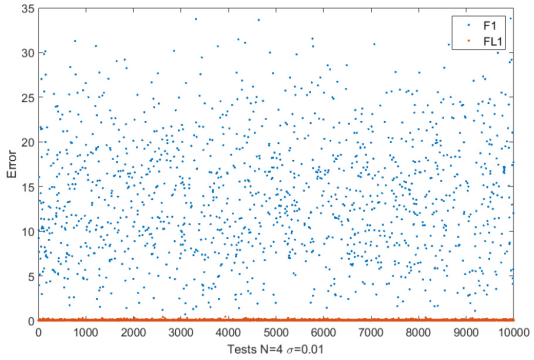

Fig. 5. Blue dots: Objective function F_1. Red dots: Improved objective function F_{L1}.

In the following section, the results of the optimization with a two dimensional F_1 are presented. Figure 5 shows the error term with different constellations of the four base stations B_i. It can be seen that F_{L1} has no outlier for measurement noise less than 0.01. The measurement noise e_i effects (9) and could lead to a local minima.

2018 International Conference on Indoor Positioning and Indoor Navigation (IPIN), 24-27 September 2018, Nantes, France

TABLE IV. THE EXAMPLES ARE BASED ON A 2-D MODEL WITH 4 BASE STATIONS B_i. F_1: OBJECTIVE FUNCTION ONE. F_{L1}: IMPROVED OBJECTIVE FUNCTION ONE. M: MEAN ERROR. SIGMA: STANDARD DEVIATION. L: NUMBER OF LOCAL MINIMA (ERROR GREATER THEN 0.5).

Noise σ	Objective function	$M \pm \sigma$	L	$M \pm \sigma$ without outlier
0.01	F_1	1.9139 ± 5.3541	1357	0.0344 ± 0.0286
0.01	F_{L1}	0.0357 ± 0.0304	0	0.0357 ± 0.0304
0.05	F_1	1.8155 ± 5.0454	1313	0.1306 ± 0.0810
0.05	F_{L1}	0.1746 ± 0.1505	362	0.1542 ± 0.0986
0.1	F_1	1.9939 ± 5.1490	1900	0.2250 ± 0.1133
0.1	F_{L1}	0.3426 ± 0.2920	1743	0.2419 ± 0.1191

Therefore, with higher noise, convergences to local minima are also possible for the improved objective function. The mean error without the outlier is higher for the improved objective function F_{L1}, due to the fact that with more dimensions the ratio between the number of equations with respect to the amount of unknown dimensions and is decreasing.

B. *Results with more than one additional variable*

In Figure 6, the results with more than one additional variable can be observed. In contrast to the results of Section 4.1 all possible constellations have been used for the lateration. Therefore, in some cases the optimization converges to a local minimum. Regardless, the number of additional variables, the results are the same; hence, it makes no sense to use more than one additional variable.

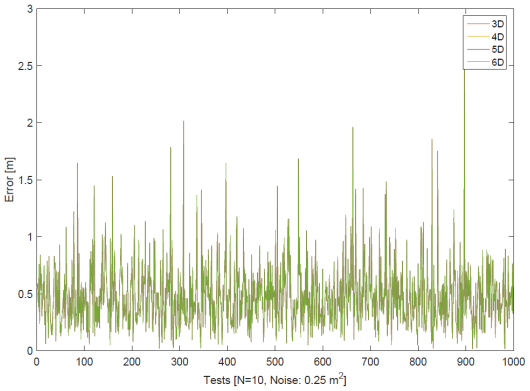

Fig. 6. Tests with 10 base stations and different number, of additional variables.

C. *Results with restart*

The improved objective function F_{L1} has the advantage that it is less effected by local minima. The general objective function has with less dimensions a better noise compensation.

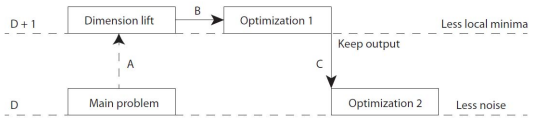

Fig. 7. Flow of the optimization process. D: Optimization with the exact number of dimensions of the model. D+1: Optimization with an additional dimension. A,B,C order of the flow.

TABLE V. THE EXAMPLES ARE BASED ON A 2-D MODEL WITH 4 BASE STATIONS B_i. F_1: OBJECTIVE FUNCTION ONE. F_{L1}: IMPROVED OBJECTIVE FUNCTION ONE. F_{L1} TO F_1: RESTART OF THE OPTIMIZATION F_{L1} WITH INITIAL ESTIMATES OBTAINED FROM OPTIMIZATION WITH F_1. M: MEAN ERROR, SIGMA: STANDARD DEVIATION. L: NUMBER OF LOCAL MINIMA (ERROR GREATER THEN 0.5).

Noise	$M \pm \sigma$	L	Noise σ without outlier
0.01	0.0260 ± 0.0175	0	0.0260 ± 0.0175
0.05	0.1302 ± 0.0900	61	0.1269 ± 0.0769
0.1	0.2582 ± 0.1924	697	0.2249 ± 0.1130

Therefore, it makes sense to combine the strength of both functions. In Figure 7, we present a method for using both effects. At the beginning of the optimization process, the objective function is increases by one additional variable λ (step A). In the next step B the optimization is done with the additional variable to minimize the risk of finding a local minimum. In step C, the outcome of the optimization is used as the initial estimate for the next optimization without the additional variable. Table 5 shows the results of the optimization process with restart. The number of outliers and the mean error are less than the objective function and the improved objective function.

IV. DISCUSSION

The presented method shows a huge advantage over the classic objective function. In [21], we have proven that the improved objective function F_2 has a saddle point at the local minimum of objective function F_2. In the test scenarios with no or little white noise, the improved objective function F_{L1} never converges into a local minimum. With increasing noise, the improved objective function F_{L1} loses its ability to avoid local minima. However, the amount of false convergences was ten times lower with F_{L1} compared to F_1. On the other side, the function F_1 has better noise dumping than F_{L1}. This is due to a better ratio between number of equations to unknown dimensions. The method presented in Section C shows that this disadvantage can be overcome by a restart of the optimization with F_1 and initial estimates provided by F_{L1}. In any case, it is not necessary to implement more than one additional variable. It is important that the initial estimate of the additional variable is unequal zero. Otherwise, gradient-based optimization algorithms like Levenberg-Marquardt algorithm would not converge to the additional dimension. Under the condition that the reference stations are known, it is also possible to obtain the solution analytically. In the case of unknown positions of base stations B_i and objects T_j, it is more

likely to converge to a local minimum instead the global minimum. At this point, our approach becomes extremely valuable.

References

[1] J. S. Abel and J. W. Chaffee. Existence and uniqueness of GPS solutions.

[2] David L. Adamy. EW 102: A Second Course in Electronic Warfare. Artech, House, Boston London, 2004.

[3] T. Akiyama, M. Sugimoto, and H. Hashizume. Light-synchronized acoustic ToA measurement system for mobile smart nodes. In 2014 International Conference on Indoor Positioning and Indoor Navigation (IPIN), pages 749-752, Oct 2014.

[4] S. Bancroft. An algebraic solution of the GPS equations. IEEE Transactions on Aerospace and Electronic Systems, AES-21(1):56-59, Jan 1985.

[5] P. Benevides, G. Nico, J. Catalão, and P. M. A. Miranda. Analysis of galileo and GPS integration for GNSS tomography. IEEE Transactions on Geoscience and Remote Sensing, 55(4):1936-1943, April 2017.

[6] V.I Bityutskov. Bunyakovskii inequality. Encyclopedia of Mathematics, 2001.

[7] H.G. Bock and K.J. Plitt. A multiple shooting algorithm for direct solution of optimal control problems*. IFAC Proceedings Volumes, 17(2):1603-1608, 1984. 9th IFAC World Congress: A Bridge Between Control Science and Technology, Budapest, Hungary, 2-6 July 1984.

[8] P. P. Bogdanov, A. V. Druzhin, A. E. Tiuliakov, and A. Y. Feoktistov. GLONASS time and UTC(SU). In 2014 XXXIth URSI General Assembly and Scientific Symposium (URSI GASS), pages 1-3, Aug 2014.

[9] J. Chaffee and J. Abel. On the exact solutions of pseudorange equations. IEEE Transactions on Aerospace and Electronic Systems, 30(4):1021-1030, Oct 1994.

[10] Don Douglass. GPS instant navigation : A practical guide from basics to advanced techniques by kevin monahan. Fine Edge Productions, 1998.

[11] Juri Sidorenko et. al. Improved linear direct solution for asynchronous radio network localization (RNL). In 2017 Pacific Positioning, Navigation and Timing technology (PNT), 2017.

[12] Ronen I. Brafman et al. Lifted optimization for relational preference rules. ILP-MLG-SRL, Leuven, Belgium, 2009.

[13] V. Nambiar et al. SDR based indoor localization using ambient WiFi and GSM signals. In 2017 International Conference on Computing, Networking and Communications (ICNC), pages 952-957, Jan 2017.

[14] H. Hmam. Quadratic optimisation with one quadratic equality constraint. Electronic Warfare and Radar Division, 2010.

[15] John S. Baras Ion Matei. Nonlinear programming methods for distributed optimization. arXiv:1707.04598, 2017.

[16] A. Marquez, B. Tank, S. K. Meghani, S. Ahmed, and K. Tepe. Accurate UWB and IMU based indoor localization for autonomous robots. In 2017. IEEE 30th Canadian Conference on Electrical and Computer Engineering (CCECE), pages 1-4, April 2017.

[17] J. Moré. The Levenberg-Marquardt Algorithm: Implementation and Theory. In In Numerical analysis, 1978.

[18] M.R Osborne. On shooting methods for boundary value problems. Journal of Mathematical Analysis and Applications, 27(2):417-433, 1969.

[19] M. Peifer and J. Timmer. Parameter estimation in ordinary differential equations for biochemical processes using the method of multiple shooting. IET Systems Biology, 1(2):78-88, March 2007.

[20] J. Sidorenko, N. Scherer-Negenborn, M. Arens, and E. Michaelsen. Multilateration of the local position measurement. In 2016 International Conference on Indoor Positioning and Indoor Navigation (IPIN), pages 1-8, Oct 2016.

[21] Juri Sidorenko, Leo Doktorski, Volker Schatz, Norbert Scherer-Negenborn, and Michael Arens. Improved time of arrival measurement model for nonconvex optimization. arXiv, 2018.

[22] Stephen M Stigler. Gauss and the invention of least squares. The Annals of Statistics, 1981.

[23] M. Vossiek, R. Roskosch, and P. Heide. Precise 3-d object position tracking using FMCW radar. In 1999 29th European Microwave Conference, volume 1, pages 234-237, Oct 1999.

4.8. P-VIII: Self-calibration for the time-of-arrival positioning

Authors

Juri Sidorenko, Volker Schatz, Dimitri Bulatov, Norbert Scherer-Negenborn, Michael Arens, Urs Hugentobler

Journal paper

IEEE Access Journal,
DOI: 10.1109/ACCESS.2020.2985353.

Introduction

The TOA position self-calibration has the aim to obtain the location of the base stations and the transponder just based on the distance measurements. In the presented publication the distance measurements only between the base stations and the transponder are available. This application is most related to real applications, with base stations without a line of sight condition to each other. In P-VI an approach was developed, where the additional dimension in the l_2 norm transform the local minimum into a saddle point, for the case that the positions of the base stations are known. In this publications the question Q^3_{Self} is answered, whether the additional dimension has an effect on the TOA self-calibration.
In addition to the lifted objective function also a partitally analytical optimization is presented. The optimization algorithm only determines the unknown base stations and the transponder positions are estimated by the linear solution in every iteration step.

Summary

A sufficient number of measurements is obtained by changing the position of the transponder, while the base stations remain stationary. In contrast to the lifted objective function with known base station positions requires the lifted objective function for the self-calibration a back transformation to the original dimensional space. This transformation reduces the additional dimensions λ back to zero and can be performed by the singular value decomposition or by a optimization algorithm, as shown in Section C. The self-calibration is performed for both synthetically generated random geometrical constellations and real measurements using an ultra-wideband positioning system. All experiments are carried out with and without the additional dimension for the fully numerical and partially analytical.

Conclusions and outlook

The conventional case without the additional dimension tends to get trapped into a local minimum more often with more measurements Q^7_{Self}, see Table 3. The partially analytical optimization method provides the best results for arbitrary geometrical constellations of base stations, while the fully numerical method can be more robust to noise for reasonable constellations, see Table 7. Hence, the answer for question Q^3_{Self} is that the additional dimension has a huge impact on the TOA self-calibration.

Declaration of own contribution

The first author came up with the idea for the additional dimension for the self-calibration, the examples with synthetic and real measurements. The co-authors improved the paper through their comments and corrections about the layout, content and the obtained results. **The overall own contribution is estimated at 87%.**

Criteria	Estimated own contribution
Paper concept	80 %
Computations and software development	100 %
Data analysis and interpretation of results	90 %
Design and creation of figures	85 %
Manuscript structure and writing	80 %

Table 4.8.: Apportionment of own contributions for P-VIII

IEEE Access
Multidisciplinary ⋮ Rapid Review ⋮ Open Access Journal

Received February 13, 2020, accepted March 31, 2020. Date of publication xxxx 00, 0000, date of current version xxxx 00, 0000.

Digital Object Identifier 10.1109/ACCESS.2020.2985353

Self-Calibration for the Time-of-Arrival Positioning

JURI SIDORENKO[1,2], VOLKER SCHATZ[1], DIMITRI BULATOV[1], NORBERT SCHERER-NEGENBORN[1], MICHAEL ARENS[1], AND URS HUGENTOBLER[2]

[1]Fraunhofer Institute of Optronics, System Technologies, and Image Exploitation IOSB, 76275 Ettlingen, Germany
[2]Institute of Astronomical and Physical Geodesy, Technical University of Munich, 80333 Munich, Germany

Corresponding author: Juri Sidorenko (juri.sidorenko@iosb.fraunhofer.de)

ABSTRACT Self-calibration of time-of-arrival positioning systems is made difficult by the non-linearity of the relevant set of equations. This work applies dimension lifting to this problem. The objective function is extended by an additional dimension to allow the dynamics of the optimization to avoid local minima. Next to the usual numerical optimization, a partially analytical method is suggested, which makes the system of equations overdetermined proportionally to the number of measurements. Results with the lifted objective function are compared to those with the unmodified objective function. For evaluation purposes, the fractions of convergence to local minima are determined, for both synthetic data with random geometrical constellations and real measurements with a reasonable constellation of base stations. It is shown that the lifted objective function provides improved convergence in all cases, often significantly so.

INDEX TERMS Dimension lifting, self-calibration, time-of-arrival (TOA).

I. INTRODUCTION

Knowledge about the position has always been a key technology for exploring unknown territories. Without reference points like stars or the Earth's poles, it would not be feasible to cross the ocean. In the last century, more precise and nature-independent base stations have been developed. In some cases, it is necessary to obtain the locations of the base stations just by distance measurements without further measuring equipment. This method receives the name of self-calibration. In the case of the time-of-arrival measurement technique (TOA), it is possible to obtain the geometrical constellation of the base stations only by the distance measurements between the base stations and the transponders [1]–[3]. Linear approximations are not always reliable due to noise and nonlinear sensor constraints. For this reason, nonlinear optimization algorithms are the method of choice. The main disadvantage of nonlinear optimization algorithms is the possible convergence to a local minimum if the initial estimates are not close to the global minimum [6]. The effect of degrees of freedom on the probability of convergence to local minima during the self-calibrated time of arrival by nonlinear least square optimization is the main aspect of this work. In [17] we demonstrated that an additional degree of freedom can transform the local minimum of the squared TOA objective function with known base station positions to a saddle point. Our approach was inspired by dimension lifting [18], [19]. Dimension lifting introduces an additional dimension to solve a specific problem. The only other known publication that dealt with the effect of degrees of freedom and self-calibration was [20]. In contrast to our work, the topic was about the difference in dimension between the affine subspaces spanned by the relative positions of base stations and transponders. Our approach is to increase the dimensions of the original model by an additional degree of freedom for every unknown base station and tag. We show that the lifted objective functions perform better than the general objective function. The test scenarios are based on real measurements and synthetic data.

This paper is organized as follows. The first section of this article introduces the TOA self-calibration problem, followed by the second section previous work. In the third section of this article our dimension lifting approach is presented. The fourth section is dedicated to the implementation of the modified objective function for the self-calibration problem. The fifth and sixth section demonstrate the performance of our approach by experiments with synthetic and real measurements performed. The results of the experiments are discussed in detail in the last section. The notations used in this article are presented in Tables 1 and 2.

The associate editor coordinating the review of this manuscript and approving it for publication was Jenny Mahoney.

TABLE 1. Notation used in the text and in equations.

Notations	Definition
B_i	Base stations, $1 \leq i \leq N$
D	Number of dimensions
M	Number of independent measurements T_j
N	Number of base stations B_i
Ra	Number of equations / Number of unknowns
T_j	Tags, $1 \leq j \leq M$

TABLE 2. Notations used in the equations.

Notations	Definition	State
$\mathbf{b}_i = (a_i, b_i, c_i)^\intercal$	Position of base station B_i	Unknown
$\mathbf{t}_j = (x_j, y_j, z_j)^\intercal$	Position of transponder T_j	Unknown
$d_{i,j}$	Distance between B_i and T_j	Known
$\tilde{\lambda}_i$	Additional dimension of B_i	Unknown
λ_j	Additional dimension of T_j	Unknown

A. CONTRIBUTION

This article presents a method to transform the objective function of the TOA in order to reduce the risk of becoming trapped in a local minimum during a nonlinear optimization. In [17], we have proven for time-of-arrival (TOA) that if the positions of the reference stations are known, the dimension lifting transforms the local minimum into a saddle point. This article aims to adopt this approach for the TOA self-calibration with unknown reference station positions. The presented approach is analyzed with synthetic and real TOA measurements, respectively. To our knowledge, no previous researchers have done this before; nor was the linear variable estimation applied inside the nonlinear optimization iteration step for the TOA self-calibration in this article, the so-called partially analytical method.

II. RELATED WORK

In [4] it was shown that the minimum number of base stations (N) and transponders (M) for the TOA self-calibration in the two-dimensional space are ($M = 3, N = 3$) and for the three-dimensional space ($M = 4, N = 6$), ($M = 5, N = 5$) and ($M = 6, N = 4$) [4]. The roles of the base stations and the transponders are interchangeable; hence it does not matter if six base stations and four transponders are used or vice versa. The number of transponders (M) could refer either to a number of seperate physical transponders in fixed locations, or a single physical device that moves to M different locations, or some combination. In [7] and [8] it was proposed to use semidefinite programming (SDP) as an initialization for the maximum likelihood (ML) estimator. Alternatively, non-iterative methods can be used. A two-dimensional non-iterative method was proposed for the case with three transponders and three receivers in [9]. The solution for the three-dimensional case was the subject of the investigation in [10], [11]. The authors provided a non-iterative solution for ($M = 5, N = 5$), ($M = 6, N = 4$)($M = 10, N = 4$). In the case of one base station position coinciding with one of the transponders, a closed-form solution was described in [12], [13]. The publication [14] presented non-iterative methods for self-calibration with the minimum configuration using the Groebner basis method and Macaulay2 software. A solution less sensitive to noise is presented based on the use of only low-degree monomials in contrast to methods like the Groebner basis [15]. On the other hand, this method requires a higher number of stations than the minimum number (M = 4, N = 7). Other linear solutions require constraints, like that the distances between the base stations and the transponders are considerably larger than between the base stations [16].

Regarding dimension lifting, our group has previously applied that approach to other aspects of TOA positioning. In [17], we demonstrated that an additional degree of freedom transforms the local minimum of the squared TOA objective function with known and stationary base stations positions to a saddle point. Furthermore, no other local minima appear for non-trivial constellations. This hypothesis was also numerically verified for the TOA objective function [17]. In [23] we showed that in the presence of noise, it is advisable to use the objective function with an additional dimension to provide initial estimates and to use the general objective function Equation without the additional dimension in the next step. The objective function with the additional dimension reduces the risk to converge to a local minimum and the general objective function minimizes the effect of noise, due to the higher ratio between the number of equations to unknown variables.

A. LIMITATIONS OF THE PREVIOUS WORK

The previous work about the TOA self-calibration is limited to specific conditions like the minimum number of base stations [10], [11], [14] or the requirement that one base station position coinciding with one of the transponders [12], [13]. In [16] the limiting factor is the distance between the base stations. However, with nonlinear constraints are the most approximation methods not applicable. Our dimension lifting approach can be applied on any TOA self-calibration problem, without the need of additional modifications [17].

III. TIME OF ARRIVAL MEASUREMENT MODEL

The time-of-arrival (TOA) measurement technique provides distance measurements between base stations and transponders. Customarily, the positions of the base stations are known and the positions of the transponders have to be estimated by triangulation. Self-calibration is concerned with the case where the positions of the base stations are unknown and only the distance measurements between the base stations and the transponders are available. Figure 1 shows three base stations B_i and three transponders T_j in unknown positions. The distances $d_{i,j}$ between base stations B_i and transponders T_j are determined through distance measurements. Distances between the base stations B_i are unknown. The aim of

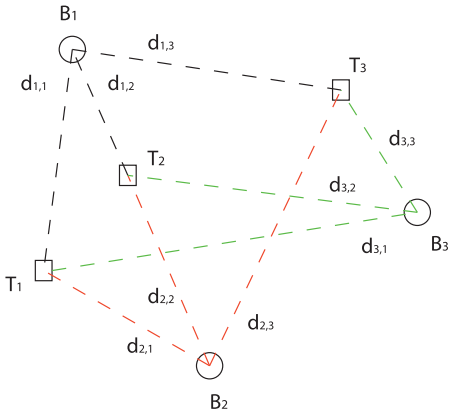

FIGURE 1. The figure shown three base stations B_i and three transponders T_j as circles and squares, respectively. The distance measurements are only possible between the base stations and the transponders. Distance measurements from one specific base station to one specific transponder are represented by black, green and red dashed lines.

self-calibration is to obtain the relative coordinates between all base stations.

A. MATHEMATICAL FORMULATION

The l_2 norm in the usual objective function is extended by an additional coordinate $\tilde{\lambda}_i$ for the base stations and λ_j for the tags. This means that if the problem is two-dimensional (the tag and the base stations are located on a two-dimensional plane), the objective function is expanded by a third dimension. The approach can be illustrated geometrically by imaging two circles. The both intersection points are the minima, one of them the local minimum and the other the global optimum. If the optimization algorithm starts close to the local minimum and it remains in the two-dimensional plane, it is not able find an alternative path. With the additional dimension, the optimization algorithm is able to move along the intersection line of the spheres from the local minimum to the global optimum. The self-calibration will only use the changing tag position to estimate the unchanging position of the base stations. Every position change of the tag increases the number of equations as well as the number of unknowns x_j, y_j and z_j. Since the positions of the base stations are unknown, the constellation can only be determined up to rotation and translation.

Classic approach:

$$\mathbf{t}_j = \begin{pmatrix} x_j \\ y_j \\ z_j \end{pmatrix} \quad \mathbf{b}_i = \begin{pmatrix} a_i \\ b_i \\ c_i \end{pmatrix}$$

Our lifted approach:

$$\mathbf{t}_j = \begin{pmatrix} x_j \\ y_j \\ z_j \\ \lambda_j \end{pmatrix} \quad \mathbf{b}_i = \begin{pmatrix} a_i \\ b_i \\ c_i \\ \tilde{\lambda}_i \end{pmatrix}$$

IV. SELF-CALIBRATION WITH DIMENSION LIFTING

The TOA self-calibration deals with the case that the positions of the base stations and the transponders are both unknown.

In presence of noise and nonlinear constraints the nonlinear optimization is the solution of choice. The relative coordinates between all base stations can be obtained by minimizing the objective function (equation 1) with non-convex optimization algorithms. It is necessary to keep in mind that the lambda coordinate of the start values must not be zero.

The measurements $d_{i,j}$ are defined as a set of Euclidean distances obtained through two-way ranging between the base stations B_i and the transponders T_j. With the classic approach, it is very likely that the optimization converges to a local minimum if the initial estimates are far away from the global optimum [6].

It is assumed that the additional dimension of the base stations and the transponders, reduces the risk to converge to a local minimum especially if the initial values for the base station or transponder positions are close to the correct geometrical constellations. The additional dimension is also part of the analytical position estimation in the partially analytical method.

$$\operatorname{argmin} \left(\sum_{i=1}^{N} \sum_{j=1}^{M} \left[\left\| T_j - B_i \right\| - d_{i,j} \right]^2 \right). \tag{1}$$

A. FULLY NUMERICAL METHOD

The first method uses the objective function (1) for the self-calibration. Equation (2) describes the ratio between the number of equations and the unknown dimensions. The ratio must be at least one. The ratio is approaching $\frac{N}{D}$ with $M \to \infty$. At a certain number of transponders, the change of the ratio becomes very small.

$$Ra = \frac{N \cdot M}{D\,(N + M)} \tag{2}$$

B. PARTIALLY ANALYTICAL METHOD

Equivalent to the fully numerical method, the aim of the partially analytical method is to obtain the relative coordinates of the base stations B_i. The main difference to the fully numerical method is that now only the base station positions are obtained by nonlinear optimization. The transponder positions are estimated analytically in every iteration step. The analytical solution is obtained by a linear least squares approach [22].

The ratio eq. (3) Ra linearly increases with M. With this method, the ratio increases indefinitely with the number of measurements.

$$Ra = \frac{M}{D} \tag{3}$$

Figure 2 shows the ratio Ra for the fully numerical method and the partially analytical method. It can be observed that the second method leads to a higher ratio Ra than

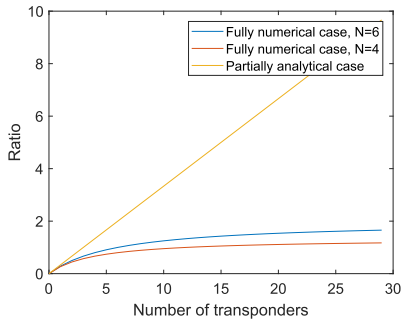

FIGURE 2. Ratio of the fully numerical and the partially analytical method with increasing number of transponders. The yellow line represent the partially analytical method the red line the fully numerical method with four base stations and the blue line the fully numerical method with six base stations.

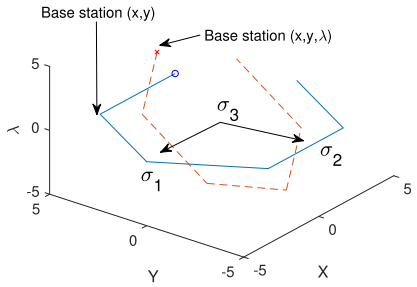

FIGURE 3. The red corners are the base station positions provided by the optimization algorithm. The blue corners are the base station positions after the back transformation in the coordinate system with $\lambda = 0$. σ_1 to σ_3 are the singular values of the SVD, with σ_3 too small to be drawn as an arrow.

the first method. With increasing number of base stations is also the ratio Ra higher for the fully numerical method.

C. BACK TRANSFORMATION

The lifted objective function for the self-calibration provides the result in the coordinate system with the additional dimension. The back-transformation rotates the result into the original subspace $\lambda = 0$. In Figure 3, a possible result of the self-calibration in $\mathbb{R}^3$ space can be observed. The red corners are the positions of the base stations in the coordinate system with the additional dimension λ.

1) BACK TRANSFORMATION BY SVD

The singular value decomposition (SVD) can be used for the back-transformation to the same dimensional space in which the measurements were obtained. In the following, we show how to perform a back transformation from $\mathbb{R}^3$ to $\mathbb{R}^2$. In the first step of the back transformation the matrix Z it is filled with the coordinates relative to the center-of-mass coordinates of the base stations $\bar{a}$, $\bar{b}$ and $\bar{\lambda}$.

$$Z = \begin{bmatrix} (a_1 - \bar{a}) & (b_1 - \bar{b}) & (\lambda_1 - \bar{\lambda}) \\ (a_2 - \bar{a}) & (b_2 - \bar{b}) & (\lambda_2 - \bar{\lambda}) \\ \vdots & \vdots & \vdots \\ (a_N - \bar{a}) & (b_N - \bar{b}) & (\lambda_N - \bar{\lambda}) \end{bmatrix} \tag{4}$$

the next step, the matrix Z is factorized of the form $U\Sigma V^* = Z$. With U as a unitary matrix, Σ as a rectangular diagonal matrix with non-negative real numbers on the diagonal and V an unitary matrix. The diagonal entries of Σ are known as the singular values σ of Z. Figure 3 shows the singular values σ_1, σ_2 and σ_3. If all base stations are located on a plane, then the singular value σ_3 is close to zero. A multiplication between the matrix U and Σ leads to a position matrix, where the additional dimension λ is close to zero. The disadvantage of the SVD is that it is computationally expensive and not able to deal with missing data. Therefore, we present a back transformation approach based on optimization in the next section.

2) BACK TRANSFORMATION BY OPTIMIZATION

We denote rotation matrices by the coordinate directions of the planes in which they act. In $\mathbb{R}^3$ with (X, Y, λ) the planes are $(XY, X\lambda, Y\lambda)$. With the overall rotation matrix $R = R_{XY}(\alpha) \cdot R_{X\lambda}(\beta) \cdot R_{Y\lambda}(\gamma)$ and the position vector $\mathbf{b}_i$ the minimization objective function for the rotation becomes:

$$\sum_{i=1}^{N} \left[\mathbf{b}_i^T \cdot R \cdot e\right]^2 \rightarrow \text{argmin} \quad \mathbf{b}_i = \begin{pmatrix} a_i \\ b_i \\ \lambda_i \end{pmatrix} \quad e = \begin{pmatrix} 0 \\ 0 \\ 1 \end{pmatrix}$$

In the $\mathbb{R}^4$ space we have the dimensions (X, Y, Z, λ) and the overall rotation matrix changes to $R = R_{XY}(\alpha) \cdot R_{XZ}(\beta) \cdot R_{X\lambda}(\gamma) \cdot R_{YZ}(\delta) \cdot R_{Y\lambda}(\epsilon) \cdot R_{Z\lambda}(\eta)$.

The position vector $\mathbf{b}_i$ become:

$$\mathbf{b}_i = \begin{pmatrix} a_i \\ b_i \\ c_i \\ \lambda_i \end{pmatrix} \qquad e = \begin{pmatrix} 0 \\ 0 \\ 0 \\ 1 \end{pmatrix}$$

V. RESULTS WITH SYNTHETIC DATA

The tests were carried out with the MATLAB Levenberg-Marquardt algorithm without noise and bias. The base stations B_i, the transponder T_j and the initial estimates were randomly generated in a $10 \times 10 \times 10$ cube. For each N and M, 10,000 constellations were created. The evaluation of the dimension-lifting methods are done by the mean square error between all objects provided by the optimization and the ground truth distances. The evaluation of the improved function has to take the additional dimension λ into account.

A. TWO-DIMENSIONAL POSITIONING

Table 3 shows the number of false results for the different methods. With more transponders, the number of equations and the number of unknowns increases. More measurements

TABLE 3. False convergence rates for a 2-D model with synthetic data. The false results represent an RMS error larger than 0.1 m.

	$N = 4, M = 12$	$N = 4, M = 24$	$N = 4, M = 36$
Ra: Fully numerical	1	1.14	1.2
Ra: Partially analytical	4	8	12
False results: Fully numerical [%]	65.27	75.56	80.93
False results: Partially analytical [%]	26.74	22.40	21.27
False results: Lifted fully numerical [%]	20.65	14.11	13.43
False results: Lifted partially analytical [%]	0.09	0.04	0.06

TABLE 4. False convergence rates for a 3-D model with synthetic data. The false results represent an RMS error larger than 0.1 m.

	$N = 5, M = 20$	$N = 5, M = 40$	$N = 5, M = 60$
Ra: Fully numerical	1	1.11	1.15
Ra: Partially analytical	5	10	15
False results: Fully numerical [%]	57.29	69.72	76.21
False results: Partially analytical [%]	11.69	15.76	17.20
False results: Lifted fully numerical [%]	51.52	41.04	37.21
False results: Lifted partially analytical [%]	0.14	0.20	0.10

increase the number of equations but also the number of unknown dimensions ($a_i, b_i, c_i, x_j, y_i, z_j, \tilde{\lambda}_i, \lambda_j$). The opposite occurs in the partially analytical method. The number of unknown variables does not increase but the ratio *Ra* increases. Therefore, the results improve with more transponders. The methods with the additional dimension behave differently. The additional dimension has the effect that the number of false results decreases for the lifted partially analytical and the lifted fully numerical method.

B. THREE-DIMENSIONAL POSITIONING

In Table 4, it can be seen that for the three-dimensional model, the results have the same characteristics as with two dimensions. The only difference to the two-dimensional example is the higher false rate for the lifted methods. It is likely due to the higher number of unkown variables.

VI. RESULTS WITH REAL MEASUREMENT DATA

The following section deals with the previously presented methods applied to real distance measurements. The selected hardware is the EVB1000 system from DecaWave. This system is based on ultra-wideband and complies with the IEEE802.15.4-2011 standard [24]. It supports six frequency bands with center frequencies from 3.5 GHz to 6.5 GHz and data rates of up to 6.8 Mb/s. The bandwidth varies with the selected center frequencies, ranging from 500 up to 1000 MHz. This system is able to operate in time-of-arrival and in time-difference-of-arrival mode. In our case, the time of arrival measurement technique is used with the restriction that measurements of distances between base stations are not performed. Table 5 and Figure 4 show the constellations of the base stations with the identification numbers one to four. The base stations are not changing their positions, only the tag. Distance measurements of the DecaWave transceiver are affected mainly by three parameters, namely the clock drift, the signal power and the antenna delay. The antenna delay can be obtained by self-calibration or with the knowledge

TABLE 5. Coordinates of the stations.

Station ID	X-Axis [m]	Y-Axis [m]	Z-Axis [m]
1	0	0	0
2	0	1.613	0
3	1.028	1.710	0
4	1.055	0.017	0

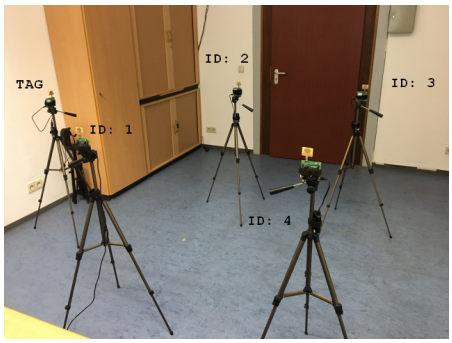

FIGURE 4. Experimental setup with Decawave UWB. The four UWB base stations with the identification number one to four are mounted on a tripod. The tag is located on the left side in the picture.

about the ground truth distance. This article deals with the effect of an additional dimension on the TOA self-calibration and the following example should be as simple as possible. Therefore, the antenna delay and the other erros have been already corrected for the distance measurements. The ground truth distances have been obtained by a laser distance sensor.

In the first test scenario, the position of the transponder changes 23 times. Every distance measurement is based on the mean of 2000 measurements in one position. The standard deviation is around 0.0185 m. Figure 5 shows the constellation of the base stations and the transponder positions. The optimization is repeated 10,000 times, with random initial estimates and the random selection of 12 measurements out

TABLE 6. False convergence rates for real 2-D measurements with a stationary transponder. The false results represent an RMS error larger than 0.1 m.

	$N = 4, M = 12$	$N = 4, M = 23$
Ra: Fully numerical	1	1.14
Ra: Partially analytical	4	7.7
False results: Fully numerical [%]	25.85	42.04
False results: Partially analytical [%]	21.86	21.06
False results: Lifted fully numerical [%]	0.11	0
False results: Lifted partially analytical [%]	0.41	0.52

TABLE 7. False convergence rates for synthetic 2-D distance measurements with noise. The constellation of the base stations and transponders is equal to the table 6. The false results represent an RMS error larger than 0.1 m.

$N = 4, M = 12$			
	$\sigma = 0$ m	$\sigma = 0.0259$ m	$\sigma = 0.05$ m
False results: Fully numerical [%]	27.13	24.07	24.12
False results: Partially analytical [%]	12.44	9.33	10.30
False results: Lifted fully numerical [%]	0	0	0
False results: Lifted partially analytical [%]	0.08	0.41	2.61

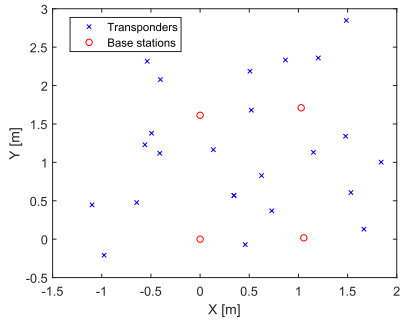

FIGURE 5. Constellation of the real base stations and stationary transponders represented by red circles and by blue crosses, respectively.

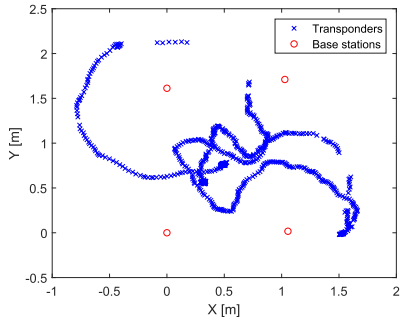

FIGURE 6. Constellation of the real base stations and one moving transponder represented by red circles and by blue crosses, respectively.

of the 23 available measurements, without selecting the same set of measurements twice. In the next test $N = 4$ and $M = 23$, all of the 23 available measurements are used for the optimization. The results of the optimization of both test cases are presented in table 6. Similar to the synthetic data, the results of the lifted objective function are better than those of the regular objective function. The false rate is much smaller compared to the synthetic data. The reason is probably that the constellation of the base stations is well suited for self-calibration. It can be observed that similarly to the synthetic data, the number of false results increases with more measurements for the fully numerical method, but decreases for the partially analytical method. The false rate with the regular objective function is about 30 percent and for the lifted objective function is 0.1 percent. In contrast to the synthetic data, the lifted fully numerical method is better than the lifted partially analytical method. This could be due to the fact that the analytical solution is more affected by noise compared to the fully numerical solution. This assumptions is checked by repeating the self-calibration with synthetic distances for the same station configuration and random initial estimates. Table 7 shows the results of the optimization with $N = 4$ and $M = 12$ with increasing Gaussian noise. It can be observed that the results of the fully numerical and the lifted fully numerical method without noise comes very close to the real measurements, most likely due to the good geometrical constellation. The false result rate of the lifted partially analytical method increases with noise. The noise of the real measurements has a standard deviation of 0.0259 m. Optimizations performed with real and synthetic measurements have similar false rates close to this deviation. For both of the non-lifted methods, a slight improvement can be seen as the noise increases. This could be due to the extra noise "lubricating" the iterative/gradient-descent optimization process.

The number of measurements can be significantly increased by using a moving transponder. This requires a good data filter and outlier detection. Figure 6 shows the path of the transponder in our experiment. In some areas the data is missing due to outlier removal.

Generally, it is advised to filter the raw data before the trilateration. Otherwise, it is possible that the nonlinear process transforms the Gaussian noise to non-Gaussian [25]. The outlier effect has been reduced by pre-filtering of the data. In order to remove outliers was in the first filtering step, a moving average filter with a time frame of 100 measurements used. Every raw measurement with a distance greater than 10 cm from the moving average has been assumed to be

TABLE 8. False convergence rates for real 2-D measurements with a moving transponder. The false results represent an RMS error larger than 0.1 m.

	$N = 4, M = 12$	$N = 4, M = 23$
Ra: Fully numerical	1	1.14
Ra: Partially analytical	4	7.7
False results: Fully numerical [%]	47.20	58.09
False results: Partially analytical [%]	37.50	37.88
False results: Lifted fully numerical [%]	2.81	0
False results: Lifted partially analytical [%]	0.39	0.40

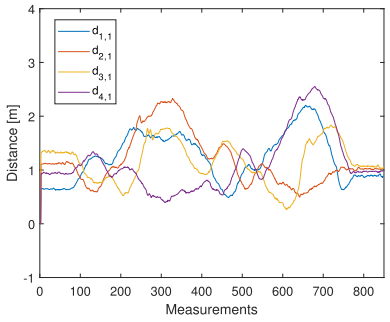

FIGURE 7. Filtered distance measurements $d_{i,j}$ between the base stations and transponders. The different colors stands for base stations with the ID one to four.

an outlier. After the outlier elimination, the remaining raw data was filtered with a moving average filter with a width of 5 values. The higher size of measurements was selected to make the filter less dynamic for the outlier detection. The second filtering was performed with a smaller window size to reduce the risk of over smoothing.

The results can be seen in Figure 7. After filtering, the measurement data was split into different path sections. The number of path sections is equal to the number of transponder positions M. In every optimization test, one measurement of the filtered data from each of the path sections was randomly selected for the optimization.

The results of 10,000 tests can be seen in Table 8. The lifted objective function performed much better than the regular objective function.

The optimization time depends on the hardware / software environment. With a higher number of dimensions, the computing time also increases. With an Intel Core i7-6600U 2.60 GHz, 16 GB RAM and 80 unknown variables, the optimization with the lifted approach took up to half a second longer. The time difference between the two approaches can be further reduced by parallel optimization.

VII. CONCLUSION

In this paper, we have presented a dimension lifting approach to the non-linear optimization for solving the self-calibration problem in time-of-arrival positioning. The objective function has been extended with an additional coordinate for all position vectors. It has been compared to the unmodified objective function with two different optimization methods: using a numerical method to optimize all unknown parameters (fully numerical), and only applying it to the base station positions and determining the tag positions analytically (partially analytical). The lifted objective function has been evaluated with both methods for both synthetically generated random geometrical constellations and real measurements using an ultra-wideband positioning system. The evaluation criterion was the percentage of non-convergence to the known correct solution under varying initial estimates.

In all cases the modified objective function performed better than the conventional one. For synthetic data with arbitrary random geometry, the partially analytical method was superior, with an improvement of a factor between 83 and 560 compared to the unmodified objective function. For noisy measurement data with a reasonable base station constellation, the fully numerical method converged correctly for any initial estimate for a sufficient number of measurements. With the partially analytical method, the improvement compared to the unmodified objective function was between 40 and 96. We conclude that our dimensional lifting approach to TOA self-calibration improves the convergence properties of the objective function considerably. Combined with the partially analytical optimization method, this advantage persists for arbitrary geometrical constellations of base stations, while the fully numerical method can be more robust to noise for reasonable constellations. This approach has already been applied to positioning itself and is worth considering for other non-linear optimization problems that do not lend themselves to linear approximations.

REFERENCES

[1] I. McCowan, M. Lincoln, and I. Himawan, "Microphone array shape calibration in diffuse noise fields," *IEEE Trans. Audio, Speech, Language Process.*, vol. 16, no. 3, pp. 666–670, Mar. 2008.

[2] N. Ono, H. Kohno, N. Ito, and S. Sagayama, "Blind alignment of asynchronously recorded signals for distributed microphone array," in *Proc. IEEE Workshop Appl. Signal Process. Audio Acoust.*, Oct. 2009, pp. 161–164.

[3] Z. Liu, Z. Zhang, L.-W. He, and P. Chou, "Energy-based sound source localization and gain normalization for ad hoc microphone arrays," in *Proc. IEEE Int. Conf. Acoust., Speech Signal Process. (ICASSP)*, vol. 2, Apr. 2007, pp. 761–764.

[4] E. Bolker and B. Roth, "When is a bipartite graph a rigid framework?" *Pacific J. Math.*, vol. 90, no. 1, pp. 27–44, Sep. 1980.

[5] K. Batstone, M. Oskarsson, and K. Åström, "Robust time-of-arrival self calibration with missing data and outliers," in *Proc. 24th Eur. Signal Process. Conf. (EUSIPCO)*, Aug. 2016, pp. 2370–2374.

[6] V. C. Raykar, I. V. Kozintsev, and R. Lienhart, "Position calibration of microphones and loudspeakers in distributed computing platforms," *IEEE Trans. Speech Audio Process.*, vol. 13, no. 1, pp. 70–83, Jan. 2005.

[7] Z. W. Mekonnen and A. Wittneben, "Self-calibration method for TOA based localization systems with generic synchronization requirement," in *Proc. IEEE Int. Conf. Commun. (ICC)*, Jun. 2015, pp. 4618–4623.

[8] P. Biswas, T.-C. Lian, T.-C. Wang, and Y. Ye, "Semidefinite programming based algorithms for sensor network localization," *ACM Trans. Sensor Netw.*, vol. 2, no. 2, pp. 188–220, May 2006.
[9] H. Stewénius, "Gröbner basis methods for minimal problems in computer-vision," Ph.D. dissertation, Dept. Math. Sci., Lund Univ., Lund, Sweden, Apr. 2005.
[10] Y. Kuang, S. Burgess, A. Torstensson, and K. Astrom, "A complete characterization and solution to the microphone position self-calibration problem," in *Proc. IEEE Int. Conf. Acoust., Speech Signal Process.*, May 2013, pp. 3875–3879.
[11] M. Pollefeys and D. Nister, "Direct computation of sound and microphone locations from time-difference-of-arrival data," in *Proc. IEEE Int. Conf. Acoust., Speech Signal Process.*, Mar. 2008, pp. 2445–2448.
[12] M. Crocco, A. Del Bue, and V. Murino, "A bilinear approach to the position self-calibration of multiple sensors," *IEEE Trans. Signal Process.*, vol. 60, no. 2, pp. 660–673, Feb. 2012.
[13] M. Crocco, A. Del Bue, M. Bustreo, and V. Murino, "A closed form solution to the microphone position self-calibration problem," in *Proc. IEEE Int. Conf. Acoust., Speech Signal Process. (ICASSP)*, Mar. 2012, pp. 2597–2600.
[14] S. Zhayida, S. Burgess, Y. Kuang, and K. Åström, "Minimal solutions for dual microphone rig self-calibration," in *Proc. 22nd Eur. Signal Process. Conf. (EUSIPCO)*, Sep. 2014, pp. 2260–2264.
[15] T.-K. Le and N. Ono, "Closed-form and near closed-form solutions for TOA-based joint source and sensor localization," *IEEE Trans. Signal Process.*, vol. 64, no. 18, pp. 4751–4766, Sep. 2016.
[16] S. Burgess, Y. Kuang, E. Ask, and K. Åström, "Understanding TOA and TDOA network calibration using farfield approximation as initial estimate," in *Proc. Int. Conf. Pattern Recognit. Appl. Methods*, 2012, pp. 1–7.
[17] J. Sidorenko, V. Schatz, L. Doktorski, N. Scherer-Negenborn, M. Arens, and U. Hugentobler, "Improved time of arrival measurement model for non-convex optimization," *Navigation*, vol. 66, no. 1, pp. 117–128, Jan. 2019.
[18] E. Balas, "Projection, lifting and extended formulation in integer and combinatorial optimization," *Ann. Operations Res.*, vol. 140, no. 1, pp. 125–161, Nov. 2005.
[19] A. E. Cetin, A. Bozkurt, O. Gunay, Y. H. Habiboglu, K. Kose, I. Onaran, M. Tofighi, and R. A. Sevimli, "Projections onto convex sets (POCS) based optimization by lifting," in *Proc. IEEE Global Conf. Signal Inf. Process.*, Dec. 2013, p. 623.
[20] S. Burgess, Y. Kuang, and K. Åström, "TOA sensor network calibration for receiver and transmitter spaces with difference in dimension," in *Proc. 21st Eur. Signal Process. Conf. (EUSIPCO)*, Sep. 2013, pp. 1–5.
[21] J. J. Moré, "The Levenberg-Marquardt algorithm: Implementation and theory," in *Numerical Analysis* (Lecture Notes in Mathematics), vol. 630, G. A. Watson, Ed. Berlin, Germany: Springer, 1978.
[22] R. Zekavat and R. M. Buehrer, *Handbook of Position Location: Theory, Practice and Advances*, 1st ed. Hoboken, NJ, USA: Wiley, 2011.
[23] J. Sidorenko, V. Schatz, N. Scherer-Negenborn, M. Arens, and U. Hugentobler, "Improved time of arrival measurement model for non-convex optimization with noisy data," in *Proc. Int. Conf. Indoor Positioning Indoor Navigat. (IPIN)*, Sep. 2018, pp. 206–212.
[24] M. Haluza and J. Vesely, "Analysis of signals from the DecaWave TREK1000 wideband positioning system using AKRS system," in *Proc. Int. Conf. Mil. Technol. (ICMT)*, May 2017, pp. 424–429.
[25] J. Sidorenko, N. Scherer-Negenborn, M. Arens, and E. Michaelsen, "Improved linear direct solution for asynchronous radio network localization (RNL)," in *Proc. ION Pacific PNT Meeting*, Jun. 2017, pp. 376–382.

JURI SIDORENKO received the Diploma degree in mechanical engineering from the Technical University Braunschweig, Germany, and the Masters of Science degree from the Cranfield University, U.K. in 2012 and 2014, respectively. He is currently pursuing the Ph.D. degree in engineering with the Technical University of Munich. He is also a Research Assistant with the Fraunhofer Institute of Optronics, System Technologies, and Image Exploitation IOSB. His research interests include the localization and self-calibration of sensor networks.

VOLKER SCHATZ received the Diploma degree in physics from Ruperto Carola University, Heidelberg, Germany, in 2000, and the Ph.D. degree in theoretical particle physics from Heidelberg University, in 2003. During his diploma degree, he was developing trigger circuits for high-energy physics experiments. After a year of Postdoctoral Research of theoretical geophysics, he started work at FGAN/FOM, Ettlingen, Germany, in 2005. In 2009, FGAN/FOM was incorporated into the Fraunhofergesellschaft of German research centres, and became part of Fraunhofer IOSB, in 2010. His current research interests include developing multisensor data acquisition systems, synchronizing imaging sensors for sensor fusion applications, and measuring the timing behaviour of commercial cameras.

DIMITRI BULATOV received the degree in mathematics from the University of Würzburg, Germany, in 2004, and the Ph.D. degree in textured 3D reconstruction from UAV-borne video sequences, in 2011. Since 2005, he has been a Senior Scientist with the Department of Scene Analysis, Fraunhofer Institute of Optronics, System Technologies, and Image Exploitation. Besides, he is affiliated with the Curtin University, Perth, Australia. His research interests include structure-from-motion, dense 3D-reconstruction algorithms, and semantic scene representation.

NORBERT SCHERER-NEGENBORN received the diploma and Ph.D. degrees in physics from the University of Freiburg, Germany, in 1996 and 2000, respectively. He is currently the Group Leader of the Tracking and Tracking Assessment Group, Department of the Object Recognition (OBJ), Fraunhofer Institute for Optronics, System Technology, and Image Exploitation IOSB.

MICHAEL ARENS received the Diploma degree in computer science and the Ph.D. degree (Dr.rer.nat.) from the University of Karlsruhe, in 2001 and 2004, respectively. He is currently the Head of the Department of the Object Recognition (OBJ), Fraunhofer Institute for Optronics, System Technology, and Image Exploitation IOSB.

URS HUGENTOBLER received the degree in theoretical physics and the Ph.D. degree in astronomy from the University of Bern, in 1997. After working as a Postdoctoral Researcher with the European Space Agency (ESA), he joined the University of Bern, as the Head of the GPS Research Group, in 1999. He has been headed the TUM's Department of Space Geodesy and TUM's Space Geodesy Research Unit, since 2006. He is currently a Secretary General of the Project Geodesy (DGK) of the Bavarian Academy of Science.

4.9. P-IX: Self-Calibration for the Time Difference of Arrival Positioning

Authors

Juri Sidorenko, Volker Schatz, Dimitri Bulatov, Norbert Scherer-Negenborn, Michael Arens, Urs Hugentobler

Journal paper

Sensors 2020, 20, 2079, DOI: 10.3390/s20072079.

Introduction

In the publication P-VIII a method was presented for the TOA self-calibration. These publications investigate whether it is possible to use the developed approaches also for the TDOA position self-calibration Q^4_{Self}. The effect of dimension lifting on the TDOA self-calibration is verified by experiments with synthetic and real measurements. In both cases, self-calibration is performed for two very common and often combined localization systems, the DecaWave Ultra-Wideband (UWB) and the Abatec Local Position Measurement (LPM) system. The measurement algorithms of both systems are explained in detail in P-III and P-I. Equivalent to publication P-VIII also next to the usual numerical optimization a partially-analytical method is suggested.

Summary

The number of false results of the self-calibration for the Decawave UWB with synthetic data increases with more measurements for the regular objective function, but decreases or remains the same for the partially analytical optimization. The result for the lifted UWB objective functions is exactly the opposite. Overall, the lifted function works best, as shown in Table 5.
The number of false results differs for the real measurements compared to the synthetic data. This aspect is due to the geometric constellation of the base stations and transponders, as shown in Table 7 and Table 8. The difference between the Decawave UWB and the LPM equation is that, for TDOA measurement technology, only the LPM system is affected by the offset. The elimination of the offset can be obtained by subtracting one measurement equation from all the others as shown in Table 9 or by taking a pairwise difference of measurement equations as shown in Table 10. The results without the offset are slightly better, but at higher computational costs for the filtering.

Conclusions and outlook

In conclusion it can be said that the lifted partially analytical optimization is more affected by outliers and noise; and with a higher amount of measurements it makes sense to use the lifted fully numerical method Q^7_{Self}. The results of the LPM are much worse, compared to the UWB system, which is due to the additional unknown offset and the higher noise. In case of the UWB system the lifted solution is superior to the conventional objective function for real and synthetic measurements Q^4_{Self} . In contrast to the synthetic measurements the results with real LPM measurements are too noisy to gain an advantage from the lifted optimization Q^6_{Self}. This requirement leads to the need to develop better pre-filtering.

Declaration of own contribution

The first author came up with the idea for the additional dimension for the TDOA self-calibration. The co-authors improved the paper through their comments and corrections about the layout, content and the obtained results. **The overall own contribution is estimated at 88 %.**

Criteria	Estimated own contribution
Paper concept	80 %
Computations and software development	100 %
Data analysis and interpretation of results	90 %
Design and creation of figures	90 %
Manuscript structure and writing	80 %

Table 4.9.: Apportionment of own contributions for P-IX

sensors

MDPI

Article

Self-Calibration for the Time Difference of Arrival Positioning

Juri Sidorenko [1,2,*,†], Volker Schatz [1], Dimitri Bulatov [1], Norbert Scherer-Negenborn [1], Michael Arens [1] and Urs Hugentobler [2]

[1] Fraunhofer Institute of Optronics, System Technologies and Image Exploitation IOSB, 76275 Ettlingen, Germany; volker.schatz@iosb.fraunhofer.de (V.S.); dimitri.bulatov@iosb.fraunhofer.de (D.B.); norbert.scherer-negenborn@iosb.fraunhofer.de (N.S.-N.); michael.arens@iosb.fraunhofer.de (M.A.)

[2] Institute of Astronomical and Physical Geodesy, Technical University of Munich, 80333 München, Germany; urs.hugentobler@tum.de

* Correspondence: juri.sidorenko@iosb.fraunhofer.de

† Current address: Object Recognition (OBJ), Gutleuthausstraße 1, 76275 Ettlingen, Germany.

Received: 13 February 2020; Accepted: 2 April 2020; Published: 7 April 2020

check for updates

Abstract: The time-difference-of-arrival (TDOA) self-calibration is an important topic for many applications, such as indoor navigation. One of the most common methods is to perform nonlinear optimization. Unfortunately, optimization often gets stuck in a local minimum. Here, we propose a method of dimension lifting by adding an additional variable into the l^2 norm of the objective function. Next to the usual numerical optimization, a partially-analytical method is suggested, which overdetermines the system of equations proportionally to the number of measurements. The effect of dimension lifting on the TDOA self-calibration is verified by experiments with synthetic and real measurements. In both cases, self-calibration is performed for two very common and often combined localization systems, the DecaWave Ultra-Wideband (UWB) and the Abatec Local Position Measurement (LPM) system. The results show that our approach significantly reduces the risk of becoming trapped in a local minimum.

Keywords: dimension lifting; self-calibration; time-difference-of-arrival (TDOA)

1. Introduction

Localization requires knowledge about the reference system, such as worldwide navigation satellites. The position of the satellites is well known, and it is unlikely that one satellite will disappear and reappear in a completely different orbit. This is different for most ground localization systems. If our own position is observed with respect to the reference system, it is necessary to know the coordinates of the reference system at any time. These coordinates can be obtained by external measurement equipment or by the system itself. The second case is also known as self-calibration. Self-calibration has the advantage that no additional measurement equipment is required, only the distance measurements between the reference stations and the changing tag position. Autonomous driving is a fascinating, albeit fiercely discussed, paradigm shift in today's world of science. Contrary to other research fields of machine vision [1], it has already been established that the performance of automatic methods outperforms that of a human operator. However, while driving, humans are understandably reluctant to relinquish control. The crucial reason is that the problem of automatic self-localization in GPS-denied areas, such as urban canyons, has not yet been solved to a satisfying level, and much less so in dynamic environments where vehicles must consider not only static obstacles, but also each other. Signal-based self-localization has increasingly gained popularity. Two very

common and often combined systems are the DecaWave Ultra-Wideband (UWB) and the Abatec Local Position Measurement (LPM) system. The DecaWave UWB system is less affected by reflections, but is, due to regulations, limited in its transmitting power. The LPM system faces the opposite problem. However, here, the problem of self-localization becomes problematic, where neither the positions of the transmitters nor the receivers are known. This is analogous to the microphone-speaker problem, where systems of (sometimes redundant or self-contradicting) quadratic equations must be solved, sometimes resulting in zero and sometimes resulting in dozens of solutions for the minimum cases (see Chapter 10 in [2]). In the few related works outlined below, it is therefore commonplace to find overdetermined systems of equations. From a reliable solution and a suitable optimizer, these systems are developed to converge to the global minimum and thus successfully self-localize the sensors.

The notations used in the text and in the equations are shown in Tables 1 and 2.

Table 1. Notations used in the text and in the equations.

Notations	Definition
B_i	Base stations, $1 \leq i \leq N$
D	Number of dimensions
N	Number of base stations B_i
M	Number of independent measurements T_j
Ra	Number of equations/number of unknowns
T_j	Tags, $1 \leq j \leq M$

Table 2. Notations used in the equations.

Notations	Definition	Status
$\mathbf{b}_i = (a_i, b_i, c_i)^T$	Position of base station B_i	Unknown
$\mathbf{t}_j = \left(x_j, y_j, z_j\right)^T$	Position of transponder T_j	Unknown
$d_{i,j}$	Distance measurements between B_i and T_j	Known
O_i	Local Position Measurement (LPM) time offset	Unknown
$\tilde{\lambda}_i$	Additional dimension of B_i	Unknown
λ_j	Additional dimension of T_j	Unknown
r	Distance between the base and reference station	Unknown

2. Related Work

The most common approach for self-calibration is to perform nonlinear optimization [3]. This solution has the disadvantage that if the initial estimates are unfavorable, the optimization becomes stuck in a local minimum [4]. Different approximation strategies have been developed to reduce this risk. Wendeberg et al. [5,6] used an iterative cone alignment algorithm for the iterative solving of a nonlinear TDOA optimization problem through a physical spring-mass simulation. In [7], this problem was re-formulated by a linear rank constraint on the matrix, and the unknown variables were estimated by minimizing the cost function using nuclear norm minimization. A non-iterative algorithm with rank constraints was presented in [8,9]. In [10,11], Semidefinite Programming (SDP) was proposed as an initialization for the Maximum Likelihood (ML) estimator. As an alternative to iterative approaches, closed-form solutions have also been developed. Closed-form solutions were presented in [12], which used time-of-arrival information recovery and time-of-arrival-based joint source and sensor localization. Time-of-arrival self-calibration closed-form solutions were the subject of the investigation in [13–15].

However, approximations of the nonlinear model have different disadvantages. For example, Semidefinite Programming (SDP) [10,11] requires high computational power, and linear solutions are only valid for small measurement noise due to the need to square the nonlinear measurement equations [9]. Moreover, it is possible that sensor specifications will lead to nonlinear constraints, which will make it difficult to obtain a linear approximation. In the field of TDOA self-calibration, there are many other different methods, each dealing with a different aspect, such as the occurrence of an additional time offset [16]. None of these approaches, however, employ lifting of the objective function, which, as we show later, can always be applied to time-of-flight measurements.

2.1. Localization Systems

Dimension lifting has been tested with two different localization systems, the DecaWave Ultra-Wideband (UWB) and the Abatec Local Position Measurement (LPM) system. Both systems have a slightly different objective function. Figures 1 and 2 illustrate the communication between the stations. The reference station and the tag emit a signal. The Base Stations (BS) obtain the difference between the arrival times of the two signals, which is also the reason why this technique is called the Time-Difference-Of-Arrival (TDOA). In contrast to the LPM system, the UWB system allows using the information about the flight time between the reference station and the tag. Moreover, the Abatec LPM objective function has an unknown offset O_j for every emitted transmitter signal.

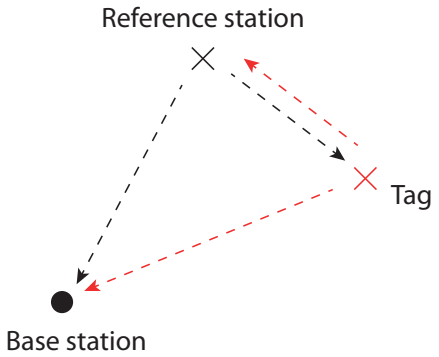

Figure 1. Transmitted messages with the DecaWave UWB system are represented by the dashed lines. The black circle is the base station, the black cross the reference station, and the red cross the tag.

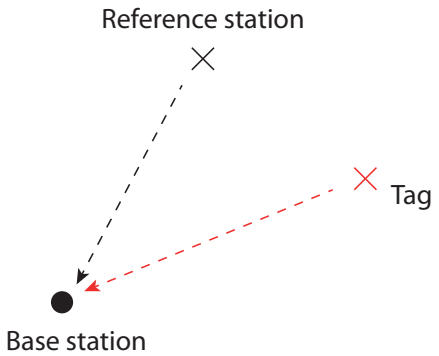

Figure 2. The messages transmitted with the Abatec Local Position Measurement (LPM) system are represented by the dashed lines. The black circle is the base station, the black cross the reference station, and the red cross the tag.

2.2. Mathematical Formulation

The regular objective functions are expanded by $\tilde{\lambda}_i$ for the base stations and tag λ_j for the tags in the l_2 norm. This means that if the model is two-dimensional (i.e., the tag and the base stations are located on a two-dimensional plane), the objective function is expanded by a third dimension. This approach can be illustrated geometrically by imagining two circles. Both intersection points are the minima: one of them is the local minimum, and the other is the global optimum. If the optimization algorithm starts close to the local minimum and remains in the two-dimensional plane, it is not able to find an alternative path. With the additional dimension, the optimization algorithm is able to move along the intersection line of the spheres from the local minimum to the global optimum. The self-calibration will only use the change of the tag position to estimate the unchanging position of the reference station and base stations. Every position change of the tag increases the number of equations, as well as the number of the unknown x_j, y_j, and z_j coordinates of the tag and the time offsets O_i for the LPM system. Since the positions of the base stations are unknown, the constellation can only be determined up to rotation and translation. It is necessary to keep in mind that the initial estimates should not be the same as or equal to zero.

The following two paragraphs show the coordinates of the transponder and the base stations for the classic approach and our lifted approach. Here, the only differences are the additional dimensions $\tilde{\lambda}_i$ and λ_j.

Classic approach:

$$\mathbf{t}_j = \begin{pmatrix} x_j \\ y_j \\ z_j \end{pmatrix} \qquad \mathbf{b}_i = \begin{pmatrix} a_i \\ b_i \\ c_i \end{pmatrix}$$

Our lifted approach:

$$\mathbf{t}_j = \begin{pmatrix} x_j \\ y_j \\ z_j \\ \lambda_j \end{pmatrix} \qquad \mathbf{b}_i = \begin{pmatrix} a_i \\ b_i \\ c_i \\ \tilde{\lambda}_i \end{pmatrix}$$

3. TDOA Localization

In [17], we demonstrated that if the base station positions are known and only the tag positions have to be estimated, an additional dimension in the l^2 norm of the TOA objective function transforms the local minimum to a saddle point. This fact has been proven analytically for the squared objective function and empirically for the general TOA objective function through more than 10,000 test scenarios with different constellations and initial estimates. The test scenarios were repeated for the general TDOA equation. Table 3 shows the results of 10,000 nonlinear optimizations with the presented TDOA measurements. In contrast to the self-calibration, the results in Table 3 are provided with known base station positions. The optimization was performed with four base stations for the UWB objective function and with five base stations for the LPM objective function. The lifted UWB objective function did not converge at a single time to the local minimum instead of the correct global minimum. On the other hand, this did not apply for the LPM equation. The difference was that the offset also needed to be estimated for the LPM equation. This led to the lifted LPM optimization being inferior to the lifted UWB optimization. The same applied if one LPM measurement was subtracted from another LPM measurement with the aim of eliminating the offset. The results of the subtracted optimization are presented in the final column of Table 3.

Table 3. The self-localization results are based on a 2D model with synthetic data and known reference stations positions. The identified false optimizations have an error larger than 0.1.

False Result Rate (%)	UWB	LPM with Offset	LPM (Subtracted)
General TDOA	13.19	6.99	9.88
Lifted TDOA	0	0.10	0.08

4. TDOA Self-Calibration

In the previous section, the positions of the base and reference station were known. In this section and the following section, the base and reference station positions are unknown. The self-calibration presented for the UWB and LPM system was based on measurements between the base stations, the reference station, and the tag. Since the base stations were passive, the distance measurements between the base stations were unknown. An important factor to determine for self-calibration is how many measurements should be used for optimization. Usually, the answer is as many as possible, as using more measurements reduces noise. In contrast to the fully-numerical method, the number of unknown variables does not increase with more measurements for the partially-analytical method. Table 4 shows the ratio between the number of equations and the unknown variables. The ratio of the partially-analytical method increased indefinitely with the number of measurements. In contrast to the LPM objective function, the UWB objective function was the reference station portion of the base stations. In the presence of noise and nonlinear constraints, nonlinear optimization was the solution of choice. The results were determined with the MATLAB Levenberg–Marquardt algorithm.

Table 4. Ratio between the number of equations and the number of unknown variables.

	UWB	LPM
Ra Fully-Numerical	$\frac{N \cdot M}{D \cdot (N+M)}$	$\frac{N \cdot M}{D \cdot (N+M+1)+M}$
Ra Partially-Analytical	$\frac{M}{D}$	$\frac{N \cdot M}{D \cdot (N+1)}$

4.1. Objective Functions

The DecaWave UWB minimization of the objective function is:

$$\operatorname{argmin} \left(\sum_{i=1}^{N} \sum_{j=1}^{M} \left[\left\| T_j - B_i \right\| - \left\| B_1 - B_i \right\| - d_{i,j} \right]^2 \right) \tag{1}$$

Abatec LPM minimization of the objective function is:

$$\operatorname{argmin} \left(\sum_{i=2}^{N} \sum_{j=1}^{M} \left[\left\| T_j - B_i \right\| - \left\| B_1 - B_i \right\| + O_j - d_{i,j} \right]^2 \right) \tag{2}$$

4.2. Fully-Numerical Method

In the first method, the objective functions from Equations (1) and (2) were used. The ratio (Table 4) approached $\frac{N}{D}$ for UWB and $\frac{N}{D+1}$ for LPM with $M \to \infty$.

4.3. Partially-Analytical Method

In this method, only the base station positions were obtained by non-linear optimization. These positions were used to obtain the tag positions analytically in every iteration step. The ratio *Ra* linearly increased with M. In contrast to the UWB, it was necessary to calculate the offset analytically

for the LPM, as well. The linear estimation that we used can be found in [18]. This linear solution was expanded by the ability to operate with the additional dimensions $\tilde{\lambda}_i, \lambda_j$ and $\bar{\lambda}$. Like with the fully-numerical method, it was necessary to keep in mind that the initial estimates should not be the same as or equal to zero.

5. TDOA with the Decawave UWB System

In the following, the two test methods are employed to UWB self-calibration with and without the additional dimension. The coordinate system was centered on the position of the reference station $a_{ref} = b_{ref} = c_{ref} = \tilde{\lambda}_{ref} = 0$.

5.1. Synthetic Data

5.1.1. Random Geometry

Table 5 shows the number of false optimizations with synthetic data. The evaluation of the optimization was undertaken using the mean squared error between all objects provided by the optimization and the ground truth distances. The base stations B_i, tag T_j, and the initial estimates were randomly generated in a $10 \times 10 \times 10$ cube. For every test case, ten-thousand constellations were created and tested with the Levenberg–Marquardt algorithm.

Table 5. The UWB self-calibration results are based on a 2D model with synthetic data. The identified false optimizations have an error larger than 0.1.

	$N = 4$, $T = 23$	$N = 5$, $T = 9$	$N = 5$, $T = 18$	$N = 5$, $T = 27$
Ratio *Ra*: fully-numerical	1.14	1.07	1.30	1.41
Ratio *Ra*: partially-analytical	7.6	3	6	9
False results: fully-numerical (%)	70.91	51.09	57.61	61.44
False results: partially-analytical (%)	48.75	55.97	55.41	55.76
False results: lifted fully-numerical (%)	7.71	5.46	2.73	2.03
False results: lifted partially-analytical (%)	8.13	11.68	10.28	10.64

The number of false results increased with more measurements using the fully-numerical method, whereas it decreased or remained the same for the partially-analytical method. This did not apply for the lifted objective functions. The false rate decreased or remained the same for the partially-analytical method. This did not apply to the lifted objective functions. With more measurements, the false rate decreased with the lifted fully-numerical method in contrast to the lifted partially-analytical method. With a higher number of base stations, the false result rate between the two methods became the opposite. Put simply, with a higher number of base stations, it was recommended to use the lifted fully-numerical method or the lifted partially-analytical method.

5.1.2. Selected Geometry

The geometric constellation, which is known as the Dilution Of Precision (DOP), and the noise/outliers had a strong impact on localization. Therefore, the test was repeated using synthetic data without noise and outliers, but with the same geometric constellation as the real measurements, as shown in Table 6. Equivalent to the real measurement data was the position of the tag, which changed 23 times. The optimization was repeated 10,000 times, with random initial estimates.

5.2. Real Measurements

In this section, the previously obtained synthetic results for the UWB objective function are verified by the measurements received from the sensor data. The DecaWave transceivers were based on Ultra-Wideband (UWB) technology and complied with the IEEE802.15.4-2011 standard [19]. They supported six frequency bands, with center frequencies ranging from 3.5 GHz to 6.5 GHz and data rates of up to 6.8 Mb/s. The bandwidth varied with the selected center frequencies, from 500 to 1000 MHz. The timestamps for positioning were provided by estimating the Channel Impulse Response (CIR). The CIR estimation was obtained by correlating a known preamble sequence against the received signal and accumulating the results over a certain period of time. In contrast to narrow band signals, the UWB was more resistant to multipath fading [20]. Reflections caused an additional peak in the impulse response. The probability that two peaks interfered with each other was small. The sampling of the impulse response was performed by an internal 64 GHz chip with 15 ps event timing precision (4.496 mm). Due to general regulations, the transmission power density was limited to -41.3 dBm/MHz. These regulations were due to high bandwidth occupied by the UWB transceiver. The following experiments were performed using a DecaWave EVK1000. This board mainly was comprised of a DW1000 chip and a STM32 ARM processor. Equation (1) shows the objective function of our UWB TDOA equation. The base station with ID 1 was used as the reference station with the coordinates a_1, b_1 and c_1. In contrast to the LPM, the UWB objective function contained one additional measurement due to the distance measurement between the tag and the reference station. Table 6 and Figure 3 show the constellation of the base stations, the reference station, and the tag. The ground truth distances were obtained by a laser rangefinder. The station with ID 1 was the reference station. The position of the tag was changed 23 times. Every distance measurement was based on the mean of 2000 measurements in one position. The optimization was repeated 10,000 times with random initial estimates. Figure 4 shows a constellation of the base stations and the tag positions. The results of the optimization with real measurements can be found in Table 7. In contrast to the synthetic results, the lifted partially-analytical method performed less favorably than the non-lifted method. The best results were delivered by the lifted fully-numerical method with 23 tag measurements. This discrepancy with the synthetic measurements was due to the noise and the outliers. In Table 8, the test was repeated with synthetic data, but with the same geometric constellation of the base stations and transponders, like with the real case. The only differences between the two test cases were the noise and the outliers. It can be observed that the constellation from Table 6 required fully-numerical optimization. The performance of the partially-analytical method primarily depended on the intermediate solution provided by the linear estimator. Outliers had a much stronger influence on the linear solution than on nonlinear optimization. More information about the effects of noise on optimization with an additional dimension was provided in [21].

Table 6. Coordinates of the UWB stations.

Station ID	X (m)	Y (m)	Z (m)
1	0	0	0
2	0	1.613	0
3	1.028	1.710	0
4	1.055	0.017	0

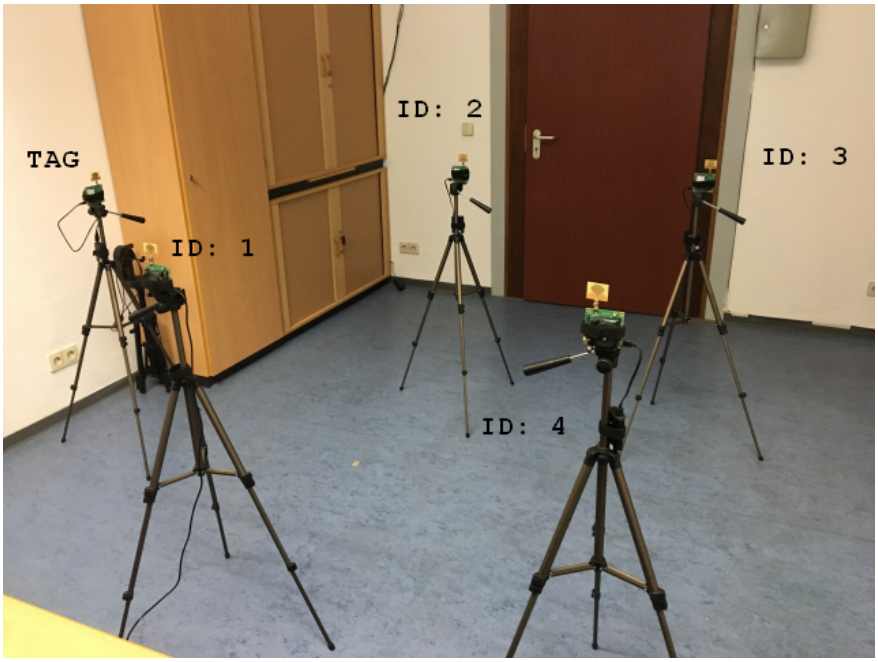

Figure 3. Experimental setup with the DecaWave UWB. The four UWB base stations with ID 1 to 4 are mounted on a tripod. The tag is located on the left side in the picture.

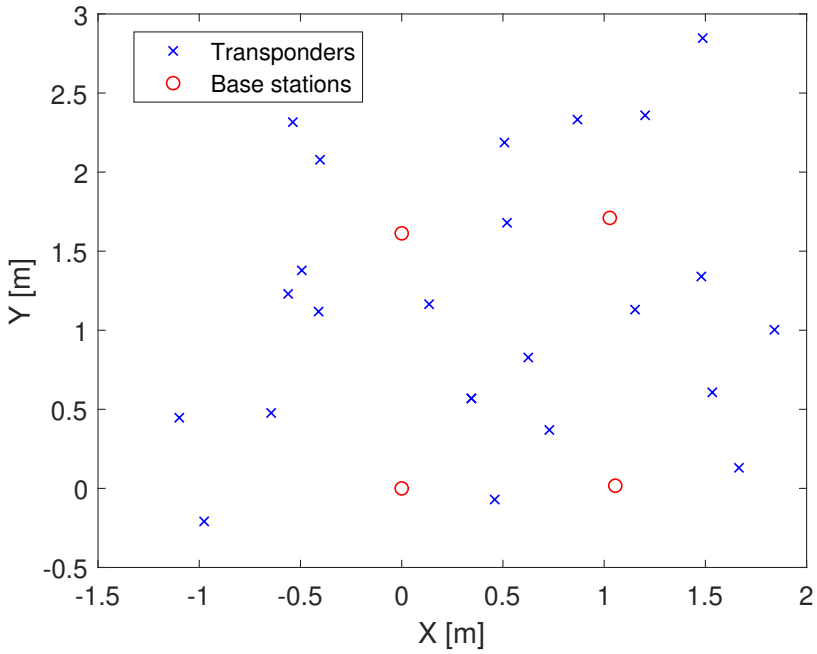

Figure 4. Constellation of the DecaWave UWB systems. The red circles are the real base stations locations, and the crosses are the tag locations.

Table 7. UWB self-calibration optimization results based on real 2D measurements. The identified false optimizations have an error larger than 0.1 m.

	$N = 4, T = 23$
Ratio *Ra*: fully-numerical	1.14
Ratio *Ra*: partially-analytical	7.6
False results: fully-numerical (%)	51.28
False results: partially-analytical (%)	55.41
False results: lifted fully-numerical (%)	20.90
False results: lifted partially-analytical (%)	99.92

Table 8. UWB self-calibration optimization results with synthetic measurements based on the same geometric constellation as the real 2D measurements. The identified false optimizations have an error larger than 0.1 m.

	$N = 4, T = 23$
Ratio *Ra*: fully-numerical	1.14
Ratio *Ra*: partially-analytical	7.6
False results: fully-numerical (%)	33.37
False results: partially-analytical (%)	54.47
False results: lifted fully-numerical (%)	6.91
False results: lifted partially-analytical (%)	0.45

6. TDOA with the Abatec LPM System

In this section, LPM self-calibration is obtained for the fully-numerical and partially-analytical method, with and without the additional dimension. The coordinate system is centered at the reference station.

6.1. Synthetic Data

The test scenarios for the synthetic data were equivalent to those for UWB optimization. The positions of the base stations B_i, tag T_j, and initial estimates were randomly generated in a $10 \times 10 \times 10$ cube. For each N and M, ten-thousand constellations were created. Table 9 shows the results of the optimization, in which the offset was eliminated by subtracting one base station from all the other base stations. The offset could also be eliminated by subtracting all the base stations from each other. This made the objective function more symmetrical. The results of this optimization can be found in Table 10. Generally, the optimization in which the offset was eliminated by subtracting all stations from each other had slightly better results. In contrast to the UWB optimization, the number of false results increased for the lifted fully-numerical method with an increasing number of measurements. However, this did not apply to the lifted partially-analytical method. Optimization with the offset was not recommended since it was not possible to pre-filter the data. Furthermore, the optimization required much more time due to the additional unknown variables.

Table 9. The self-calibration results are based on a 2D model of synthetic LPM measurements where the offset is eliminated by subtracting one measurement equation from all others. The identified false optimizations have an error larger than 0.1.

	$N = 5$, $T = 30$	$N = 5$, $T = 45$	$N = 6$, $T = 15$	$N = 6$, $T = 30$	$N = 6$, $T = 45$
Ratio *Ra*: fully-numerical	1.08	1.14	1.1	1.28	1.34
Ratio *Ra*: partially-analytical	8.3	12.5	12.86	8.57	12.86
False results: fully-numerical (%)	83.30	88.06	63.51	74.34	81.32
False results: partially-analytical (%)	88.70	89.82	74.35	77.61	79.59
False results: lifted fully-numerical (%)	57.43	60.89	32.06	33.22	39.43
False results: lifted partially-analytical (%)	85.62	86.63	43.28	38.10	38.72

Table 10. Self-calibration results are based on a 2D model of synthetic LPM measurements where the offset is eliminated by forming a pairwise difference of measurement equations. The identified false optimizations have an error larger than 0.1.

	$N = 5$, $T = 30$	$N = 5$, $T = 45$	$N = 6$, $T = 15$	$N = 6$, $T = 30$	$N = 6$, $T = 45$
Ratio *Ra*: fully-numerical	1.08	1.14	1.1	1.28	1.34
Ratio *Ra*: partially-analytical	8.3	12.5	12.86	8.57	12.86
False results: fully-numerical (%)	78.81	84.61	58.43	66.83	74.92
False results: partially-analytical (%)	84.57	86.08	68.85	71.80	74.95
False results: lifted fully-numerical (%)	55.84	60.31	31.99	33.14	40.55
False results: lifted partially-analytical (%)	82.78	83.30	37.78	31.01	30.11

6.2. Real Measurements

The real LPM measurements are the subject of the investigation in this section. Figure 5 shows the constellation of the base stations, the reference station, and the tag path. In contrast to the UWB measurement, the LPM measurements were now obtained while moving the tag. On the one hand, this approach was more practical because it allowed obtaining more measurements more quickly. On the other hand, more intelligent filters required were now needed to reduce noise and eliminate outliers. Additionally, it had to be taken into account that the tag was carried by hand; thus, it was not possible to provide a perfect two-dimensional plane. The Local Position Measurement system (LPM) by Abatec was strongly inspired by the Frequency-Modulated Continuous Wave radar (FMCW). This radar system generates an increasing frequency chirp, which is sent in a certain direction. In the next step, the reflected signal was compared with the internal chirp. The frequency difference between these chirps represented the range with respect to the slope of the chirp. Generally, the frequency differences were obtained by additive or multiplicative mixers. The LPM used the same principle; however, in contrast to the FMCW radar, the sent chirp of the tag was mixed with the internal chirp of the base station. The chirp itself had a bandwidth of 150 MHz and a ramp duration of 500 us, with an update rate of 1000 measurements per second [22]. If the starting times of the tag and the base station were synchronous, the result would be equivalent to that of the FMCW radar, although the range would be 50% shorter. The frequency difference represented the flight time, with the assumption that electromagnetic waves propagated with the speed of light and that we could obtain the relative range. Unfortunately, the base stations did not have the same starting times; hence, they were not

synchronous, which led to a time offset. The Abatec LPM system used a reference station in a known fixed position. The position of the tag could be estimated for every measurement if we had four base stations and one reference station in known positions. Knowledge about the base station and reference station positions could be obtained from several measurements by changing the position of the tag. Accordingly, there was no need for further hardware to calibrate the system. The Abatec LPM system was described in detail in [22,23]. Previous publications on the Abatec LPM have been mainly concerned with the measurement principles [22,23] and how the sensor data can be fused and filtered to detect an outlier [24] and obtain the most accurate position [25]. The most recent publications on LPM have focused on the numerical solver. Generally, the LPM uses a Bancroft algorithm [26–28] to estimate the position of the tag. At this time, no work has been conducted on LPM self-calibration. In contrast to the DecaWave UWB, the LPM objective function (2) had an additional offset O_j, which was higher than the distance measurement by a factor of 1000. Figure 6 shows the raw LPM measurements, G_i, Equation (3).

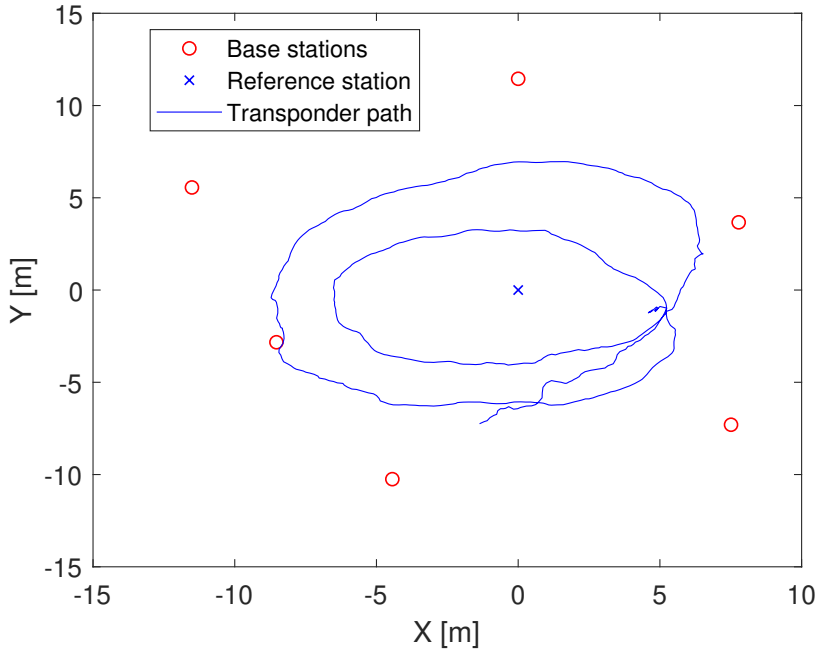

Figure 5. Constellation of the LPM system. Red circles are the base stations, the blue cross the reference station, and the blue line the tag path.

$$G_i = \left(\left\|T_j - B_i\right\| - \left\|B_r - B_i\right\| + O_j\right) \tag{3}$$

The only changing value was T_j, due to the moving tag, with the index i as the ID of the base station, index r as the used reference station ($r \neq i$), and j as the tag position.

$$\begin{aligned} G^S_{1,i} = &\left(\left\|T_j - B_1\right\| - \left\|B_r - B_1\right\|\right) \\ &- \left(\left\|T_j - B_i\right\| - \left\|B_r - B_i\right\|\right) \end{aligned} \tag{4}$$

The plot of Figure 7 shows the measurements, $G^S_{1,i}$, Equation (4), after subtracting one station from another to eliminate the offset.

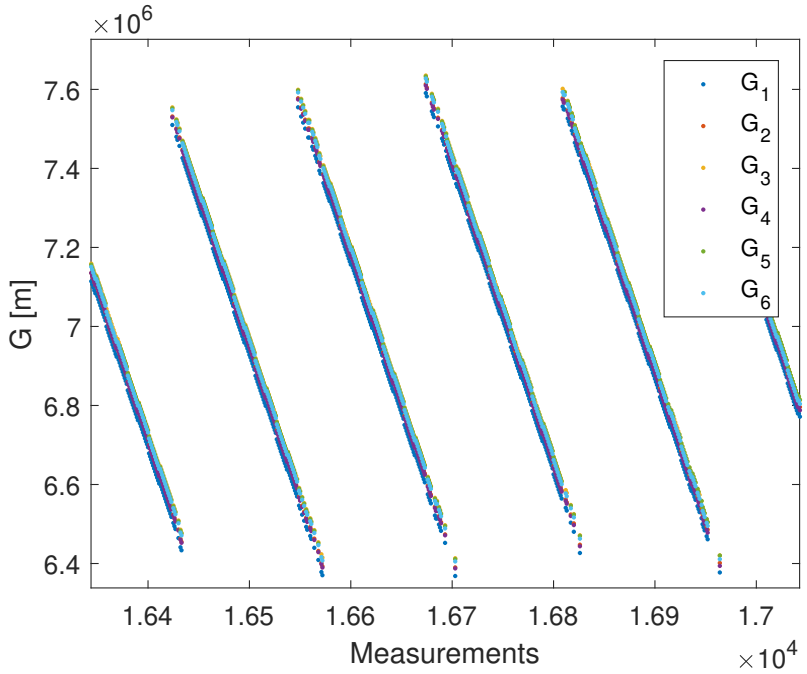

Figure 6. Zoom-in of the raw LPM measurements. The different colors represent the outcomes of the raw measurements before every station is subtracted from Station 1.

The LPM system was more suitable for long-range measurements, although it was more strongly affected by reflections and fading [29]. This made it difficult to differentiate between the moving path and the measurement errors. After filtering, the measurement data were split into different subsets. The number of subsets equated to the number of tag positions T. In every optimization test, one measurement of the filtered data from every subset was randomly selected for optimization. Table 11 shows the results of 10,000 tests. The number of false results was much higher than that of the UWB TDOA self-calibration. The lifted partially-analytical method was thus not usable. The best results were provided by the fully-numerical method with six base stations and only fifteen measurements. With an increasing number of measurements, the possibility of false results also increased. In contrast to the synthetic data, the results of the lifted fully-numerical method were better than those of the general method, with a higher number of tags in some constellations. More measurements also had the advantage of reducing Gaussian noise. This would be the ideal method; however, in reality, there are always outliers. In practice, we recommend using the RANSAC algorithm [30]. The important disadvantage of the LPM equation was that all data were strongly affected by the offset O_j, which changed from one measurement to the next. In [18], we showed that subtracting one measurement from another eliminated the offset and had some significant advantages for data filtering. In contrast to the UWB, it was also necessary to calculate the offset analytically for the LPM. The linear estimation that we used can be found in [18]. This linear solution was expanded by the ability to operate with the additional dimensions, $\tilde{\lambda}_i$ and λ_j.

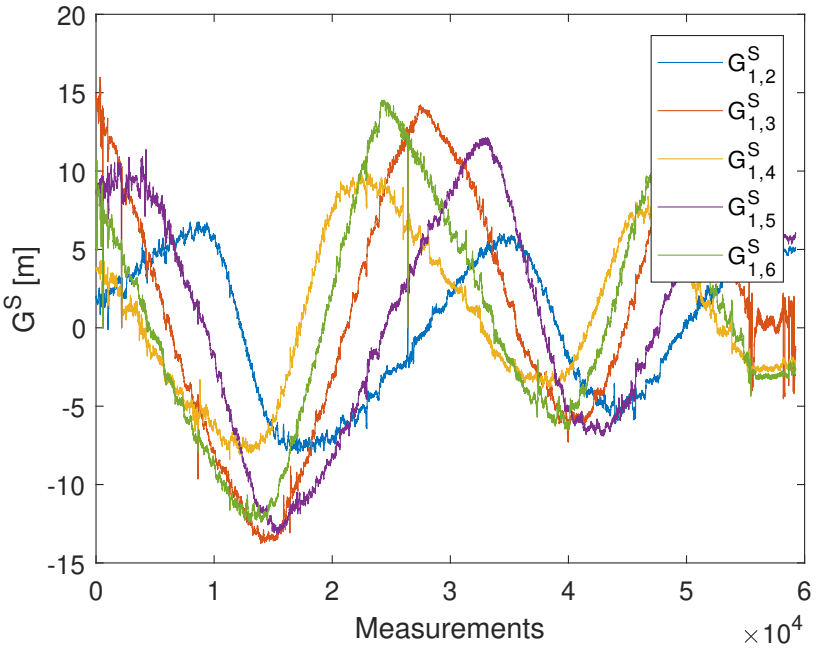

Figure 7. LPM measurement differences. The different colors represent the outcome of the filtered measurements, after every station is subtracted from Station 1.

Table 11. Self-calibration results of the real LPM measurements. The identified false optimizations have errors larger than 0.1 m.

	$N = 6, T = 15$	$N = 6, T = 30$	$N = 6, T = 45$
Ratio *Ra*: fully-numerical	1.1	1.28	1.34
Ratio *Ra*: partially-analytical	4.29	8.57	12.86
False results: fully-numerical (%)	79.49	92.21	96.41
False results: partially-analytical (%)	93.17	96.47	98.73
False results: lifted fully-numerical (%)	89.30	87.12	91.13
False results: lifted partially-analytical (%)	99.81	99.98	100

7. Conclusions

This paper presented a dimension-lifting approach to reduce the risk of converging to a local minimum during nonlinear optimization. The impact of the additional dimension in the l^2 norm on self-calibration was shown by synthetic and real measurements. Optimization was carried out using two different methods. In the fully-numerical method, all of the unknown parameters were optimized. In the partially-analytical method, the optimization handled only the base station position estimation, while the other unknown parameters were obtained analytically in each iteration step. The methods were evaluated by synthetic data and real measurements for the DecaWave UWB and Abatec LPM systems. The lifted TDOA method provided the best results for optimization with Gaussian noise and a sufficient quantity of base stations to compensate for the additional dimension. The additional dimension increased the number of unknown variables; therefore, it was necessary

to obtain more measurements for an exactly determined or an overdetermined system. This did not apply to measurements with outliers; hence, it was required to pre-filter the real measurements before self-calibration.

Author Contributions: The idea for the dimension lifting was developed by the first author, J.S. The co-authors V.S. and D.B. improved the paper through their comments and corrections about the layout, content, and the obtained results. Conceptualization, methodology, software, validation, visualization, formal analysis, investigation, and writing, original draft preparation, were done by the first author, J.S. Supervision and project administration were done by N.S.-N. and U.H. Funding acquisition was done by M.A. All authors have read and agreed to the published version of the manuscript.

Funding: This research was funded by the Fraunhofer Institute of Optronics, System Technologies and Image Exploitation IOSB.

Conflicts of Interest: The authors declare no conflict of interest.

References

1. Kheradpisheh, S.R.; Ghodrati, M.; Ganjtabesh, M.; Masquelier, T. Deep Networks Can Resemble Human Feed-Forward Vision in Invariant Object Recognition. *Sci. Rep.* **2016**, *6*, 32672. [CrossRef] [PubMed]
2. Stewénius, H. Gröbner Basis Methods for Minimal Problems in Computer Vision. Ph.D. Thesis, Centre for Mathematical Sciences, Lund University, Lund, Sweden, 2005.
3. Batstone, K.; Oskarsson, M.; Åström, K. Robust time-of-arrival selfcalibration with missing data and outliers. In Proceedings of the 24th European Signal Processing Conference (EUSIPCO), Budapest, Hungary, 29 August–2 September 2016; pp. 2370–2374.
4. Ono, N.; Kohno, H.; Ito, N.; Sagayama, S. Blind alignment of asynchronously recorded signals for distributed microphone array. In Proceedings of the IEEE Workshop on Applications of Signal Processing to Audio and Acoustics, New Paltz, NY, USA, 18–21 October 2009; pp. 161–164.
5. Wendeberg, J.; Höflinger, F.; Schindelhauer, C.; Reindl, L. Anchor-free TDOA self-localization. In Proceedings of the International Conference on Indoor Positioning and Indoor Navigation, Guimarães, Portugal, 21–23 September 2011; pp. 1–10.
6. Wendeberg, J.; Höflinger, F.; Schindelhauer, C.; Reindl, L. Calibration-free tdoa self-localisation. *J. Locat. Based Serv.* **2013**, *7*, 121–144. [CrossRef]
7. Jiang, F.; Kuang, Y.; Åström, K. Time delay estimation for TDOA selfcalibration using truncated nuclear norm regularization. In Proceedings of the IEEE International Conference on Acoustics, Speech and Signal Processing, Vancouver, BC, Canada, 26–31 May 2013; pp. 3885–3889.
8. Kuang, Y.; Åström, K. Stratified sensor network self-calibration from TDOA measurements. In Proceedings of the 21st European Signal Processing Conference (EU-SIPCO 2013), Marrakech, Morocco, 9–13 September 2013; pp. 1–5.
9. Zou, Y.; Wan, Q.; Liu, H. Semidefinite Programming for Tdoa Localization with Locally Synchronized Anchor Nodes. In Proceedings of the IEEE International Conference on Acoustics, Speech and Signal Processing (ICASSP), Calgary, AB, Canada, 15–20 April 2018; pp. 3524–3528.
10. Mekonnen, Z.W.; Wittneben, A. Self-calibration method for TOA based localization systems with generic synchronization requirement. In Proceedings of the IEEE International Conference on Communications (ICC), London, UK, 8–12 June 2015; pp. 4618–4623.
11. Biswas, P.; Lian, T.; Wang, T.; Ye, Y. Semidefinite programming based algorithms for sensor network localization. *ACM Trans. Sens. Netw.* **2006**, *2*, 188–220. [CrossRef]
12. Le, T.; Ono, N. Closed-form solution for TDOA-based joint source and sensor localization in two-dimensional space. In Proceedings of the 24th European Signal Processing Conference (EUSIPCO), Budapest, Hungary, 28 August–2 September 2016; pp. 1373–1377.
13. Kuang, Y.; Burgess, S.; Torstensson, A.; Åström, K. A complete characterization and solution to the microphone position self-calibration problem. In Proceedings of the 2013 IEEE International Conference on Acoustics, Speech and Signal Processing, Vancouver, BC, Canada, 26–31 May 2013; pp. 3875–3879.
14. Le, T.; Ono, N. Closed-Form and Near Closed-Form Solutions for TOA-Based Joint Source and Sensor Localization. *IEEE Trans. Signal Process.* **2016**, *64*, 4751–4766. [CrossRef]

15. Crocco, M.; Del Bue, A.; Bustreo, M.; Murino, V. A closed form solution to the microphone position self-calibration problem. In Proceedings of the IEEE International Conference on Acoustics, Speech and Signal Processing (ICASSP), Kyoto, Japan, 25–30 March 2012; pp. 2597–2600.
16. Wang, L.; Hon, T.-K.; Reiss, J.D.; Cavallaro, A. Self-localization of ad-hoc arrays using time difference of arrivals. *IEEE Trans. Signal Process.* **2015**, *64*, 1018–1033. [CrossRef]
17. Sidorenko, J.; Schatz, V.; Doktorski, L.; Scherer-Negenborn, N.; Arens, M.; Hugentobler, U. Improved time of arrival measurement model for non-convex optimization. *Navigation* **2019**, *66*, 117–128. [CrossRef]
18. Sidorenko, J.; Scherer-Negenborn, N.; Arens, M.; Michaelsen, E. Improved Linear Direct Solution for Asynchronous Radio Network Localization (RNL). In Proceedings of the ION 2017 Pacific PNT Meeting, Honolulu, HI, USA, 1–4 May 2017; pp. 376–382.
19. Haluza, M.; Vesely, J. Analysis of signals from the decawave trek1000 wideband positioning system using akrs system. In Proceedings of the International Conference on Military Technologies (ICMT), Brno, Czech Republic, 31 May–2 June 2017; pp. 424–429.
20. Zwick, T.; Wiesbeck, W.; Timmermann, J.; Adamiuk, G. *Ultra-Wideband RF System Engineering (EuMA High Frequency Technologies Series*; Cambridge University Press: Cambridge, UK, 2013.
21. Sidorenko, J.; Schatz, V.; Scherer-Negenborn, N.; Arens, M.; Hugentobler, U. Improved time of arrival measurement model for non-convex optimization with noisy data. In Proceedings of the International Conference on Indoor Positioning and Indoor Navigation (IPIN), Nantes, France, 24–27 Sepember 2018; pp. 206–212.
22. Resch, A.; Pfeil, R.; Wegener, M.; Stelzer, A. Review of the LPM local positioning measurement system. In Proceedings of the International Conference on Localization and GNSS (ICL-GNSS), Starnberg, Germany, 25–27 June 2012; pp. 1–5.
23. Pourvoyeur, K.; Stelzer, A.; Fischer, A.; Gassenbauer, G. Adaptation of a 3-D local position measurement system for 1-D applications. In Proceedings of the Radar Conference EURAD, Paris, France, 3–4 October 2005; pp. 343–346.
24. Pfeil, R.; Pourvoyeur, K.; Stelzer, A.; Stelzhammer, G. Distributed fault detection for precise and robust local positioning. In Proceedings of the 13th IAIN World Congress and Exhibition, Stockholm, Sweden, 27–30 October 2009.
25. Pourvoyeur, K.; Stelzer, A.; Gahleitner, T.; Schuster, S.; Gassenbauer, G. Effects of motion models and sensor data on the accuracy of the LPM positioning system. In Proceedings of the 9th International Conference on Information Fusion, Florence, Italy, 10–13 July 2006; pp. 1–7.
26. Pourvoyeur, K.; Stelzer, A.; Gassenbauer, G. Position estimation techniques for the local position measurement system LPM. In Proceedings of the Microwave Conference APMC, Yokohama, Japan, 12–15 December 2006; pp. 1509–1514.
27. Stelzer, A.; Pourvoyeur, K.; Fischer, A. Concept and application of lpm- a novel 3-d local position measurement system. *IEEE Trans. Microw. Theory Tech.* **2004**, *52*, 2664–2669. [CrossRef]
28. Pfeil, R.; Schuster, S.; Scherz, P.; Stelzer, A.; Stelzhammer, G. A robust position estimation algorithm for a local positioning measurement system. In Proceedings of the IEEE MTT-S International Microwave Workshop in Local Positioning and RFID, IMWS2009, Cavtat, Croatia, 24–25 September 2009; pp. 1–4.
29. Güvenc, I.; Sahinoglu, Z.; Gezici, S. *Ultra-Wideband Positioning Systems Theoretical Limits, Ranging Algorithms, and Protocols*; Cambridge University Press: Cambridge, UK, 2008.
30. Zhu, W.; Sun, W.; Wang, Y.; Liu, S.; Xu, K. An improved ransac algorithm based on similar structure constraints. In Proceedings of the International Conference on Robots Intelligent System (ICRIS), Zhangjiajie, China, 27–28 August 2016; pp. 94–98.

5. Conclusions and outlook

Every publication was a piece of the puzzle, fitting into each other to draw the picture of the topic. The developed theoretical concepts are supported by real measurements. It was shown, that it is not possible to address one problem like the occurrence of the local minima without taking into consideration the objective function and the filtering.

5.1. Conclusions

The development of the self-calibration should start with the question of how to pre-filter the measurements. In contrast to the Decawave UWB (Section 3.2) the LPM system (Section 3.1) requires a transformation for the pre-filtering. The publication P-I describes the transformation of the general LPM objective function and presents a linear solution, which is able to use the pre-filtered data. This linear solution applies for the case that the base station positions are known and that the filtering was performed with respect to one specific station. Therefore this solution is not symmetrical. This problem was addressed in P-II and a symmetrical linear solution was presented.
The Decawave UWB system has more possibilities to interact with the hardware and to develop an own TOA and TDOA technique. Before that, it was obligatory to address two main issues of this system, which affects the precision significantly. The first error is caused by the signal power on the timestamp. This issue is usually solved with additional measurement equipment.

In P-III and P-IV a method is presented to perform a self-calibration to obtain the power correction curve. The clock drift was also the topic of the same publication. It was proposed to use the time stamp differences between three messages instead of the integrator of the PLL due to the fact, that the later is affected by the signal power. The developed correction methods were used later on in TOA and TDOA techniques, presented in P-V.

After the preparation of the hardware and the definition of the objective function the next step was to address an important problem of nonlinear optimizations, the probability to converge into a local minimum. It was observed that a smaller number of dimensions not automatically provide better results for the nonlinear optimization. Therefore, the opposite was applied, by implementation of an addition dimension into a l_2 norm. It was surprising that during the test case with known base

station positions the optimization algorithm never converged into a local minimum. Hence, it was assumed that the additional dimension transforms the local minimum into a saddle point. The analytical prove of this hypothesis was provided in P-VI.

Least square minimization reduces the effect of Gaussian noise with increasing number of equations. With more dimensions the noise reduction is lower. This problem was addressed in P-VII and the proposed solution was to use the lifted objective function at the beginning to avoid local minima and afterwards the regular objective function close to the global minimum to reduce the noise.

The final two publications P-VIII and P-IX are combining the methods delivered in P-I to P-VI, with the aim to perform a position self-calibration. In addition to the lifted objective function, also a partitally analytical optimization was presented. In this method the linear solution is used to provide the position of the transponder during every iteration step, as well as the symmetrical linear solution from P-II. The lifted objective function for the self-calibration requires, in contrast to the lifted objective function with known base stations, a back transformation, which is described in detail in P-VIII. The self-calibration with the lifted objective function has still local minima but the risk to get trapped into one is much lower. Depending on the noise and the measurement technique the lifted objective function or the lifted partitally analytical is the solution of choice. The only disadvantage of the lifted case is that one more station is required to compensate the additional dimension. In any case is it also possible to adapt the presented solution for other nonlinear optimization problems, especially for the cases where no linear solution exists to provide initial estimates.

This flexibility enables the integration of localization systems into everyday life without the user having to deal with technical subtleties. During operation, the system can adapt to a new or changing environment in order to provide the best possible position estimates. An example of this would be the presented LPM system. This requires well trained staff to set it up. The self-calibration with automatic prefiltering enables even laypeople to set up and dismantle the LPM system anywhere. This additional feature enables further applications without the manufacturer having to change anything in the hardware. With the UWB system presented, a self-calibration can be carried out in addition to the position determination in order to calculate hardware-specific dependencies. Here, too, the self-calibration reduces the risk of incorrect handling by the user and increases the accuracy of the system.

5.2. Open questions

As with any scientific work, new questions arise during research that want to be answered. It was possible for us to prove analytically that for the squared lifted objective function the local minimum becomes a saddle point, but not for the non-squared form. This question remains open. In this work, we mainly limited ourselves

to working with TOA and TDOA. An investigation of the self-calibration for angle of arrival (AoA) would provide further interesting results. The last question that remains open is whether there is a way to transform the objective function for self-calibration so that there are no more local minima. This would mean that, even with unfavorable starting values, the self-calibration would always deliver the best result with a non-linear optimization.

5.3. Further work

The presented methods could be applied for the hardware delay self-calibration and wall thickness estimation with the Decawave UWB. Thereby, the self-calibration would be equivalent to the one presented in P-VIII, but additionally the unknown hardware and wall delay could be estimated. Due to the ability of the Decawave system to use different channels, it could be possible to estimate the wall thickness. Decawave company has already announced that they are working on a chip with the ability to provide angle of arrival measurements. This information could highly improve the self-calibration and also reduce the number of required base stations.

Acknowledgments

At this point, I would like to thank Prof. Urs Hugentobler for giving me the opportunity to pursuing the doctorate under his supervision.

I thank all the co-authors for their contribution and comments to improve the publications. I greatly appreciate the patience and time of Dr. Norbert Scherer-Negenborn and Dr. Michael Arens invested in discussing the ideas and concepts.

I would like to express my sincere gratitude to Prof. Uwe Stilla for the professional and personal support during my doctorate. I would like to extend my sincere thanks to Prof. Dr. Christian Schindelhauer and Prof. Dr. Johann Dambeck for the review.

I also appreciate the help of Dr. Volker Schatz and Dr. Dimitri Bulatov for comments on mathematical concepts. Both scientists provided constructive feedback and thus helped to improve the quality of my publications.

I am very thankful for the possibility to work at the Fraunhofer IOSB in a very professional environment with many interesting and intelligent people. I was able to grow academically and personally during this time.

Last but not least, I want to thank my wife for her never ending support, patience and love.

A. Appendix

A.1. GUI of the Local Position Measurement (LPM)

In addition to the main software called “Self Calibration and Position Estimation” (SCAPE) also a simulation software was developed. This simulation software is shown in Figure A.1. It emulates the TCP packets sent from the LPM system to test the synchronization algorithm. The main window of the simulation software shows the position of the base stations one to six, with a reference station in the origin of the coordinate system. The blue circle represents the path of the tag. Any position of the stations can be set using the tree widget located at the right hand side of the panel, also the path can be modified. The spin box at the bottom is used to set a delay between the messages.

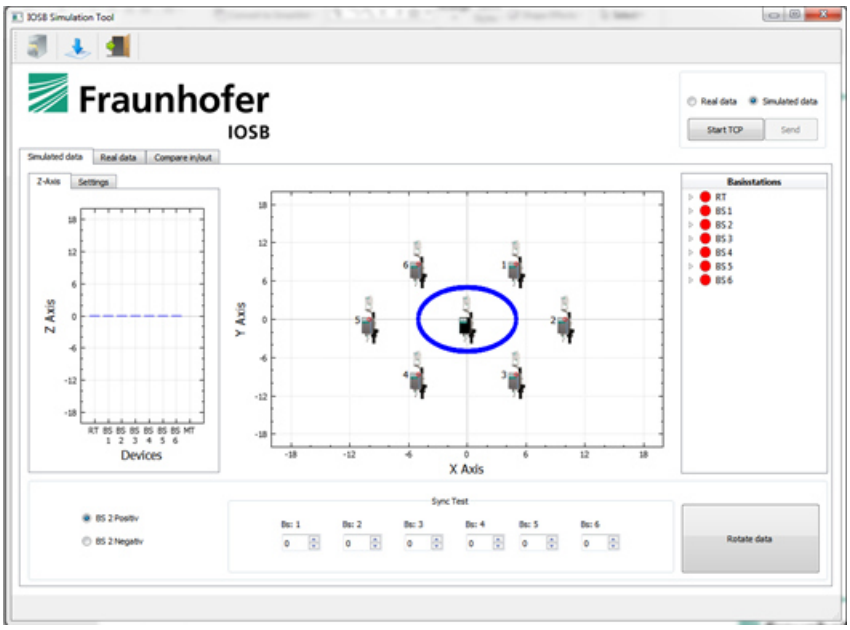

Figure A.1.: LPM simulation software

The interface of the software SCAPE is presented in Figure A.2. It has the same layout as the simulation tool but in addition to the two dimensional view it also offers a visualization of the base stations in the three dimensional space. For SCAPE it

does it not make a difference whether the information is provided by the LPM system or by the simulation tool.

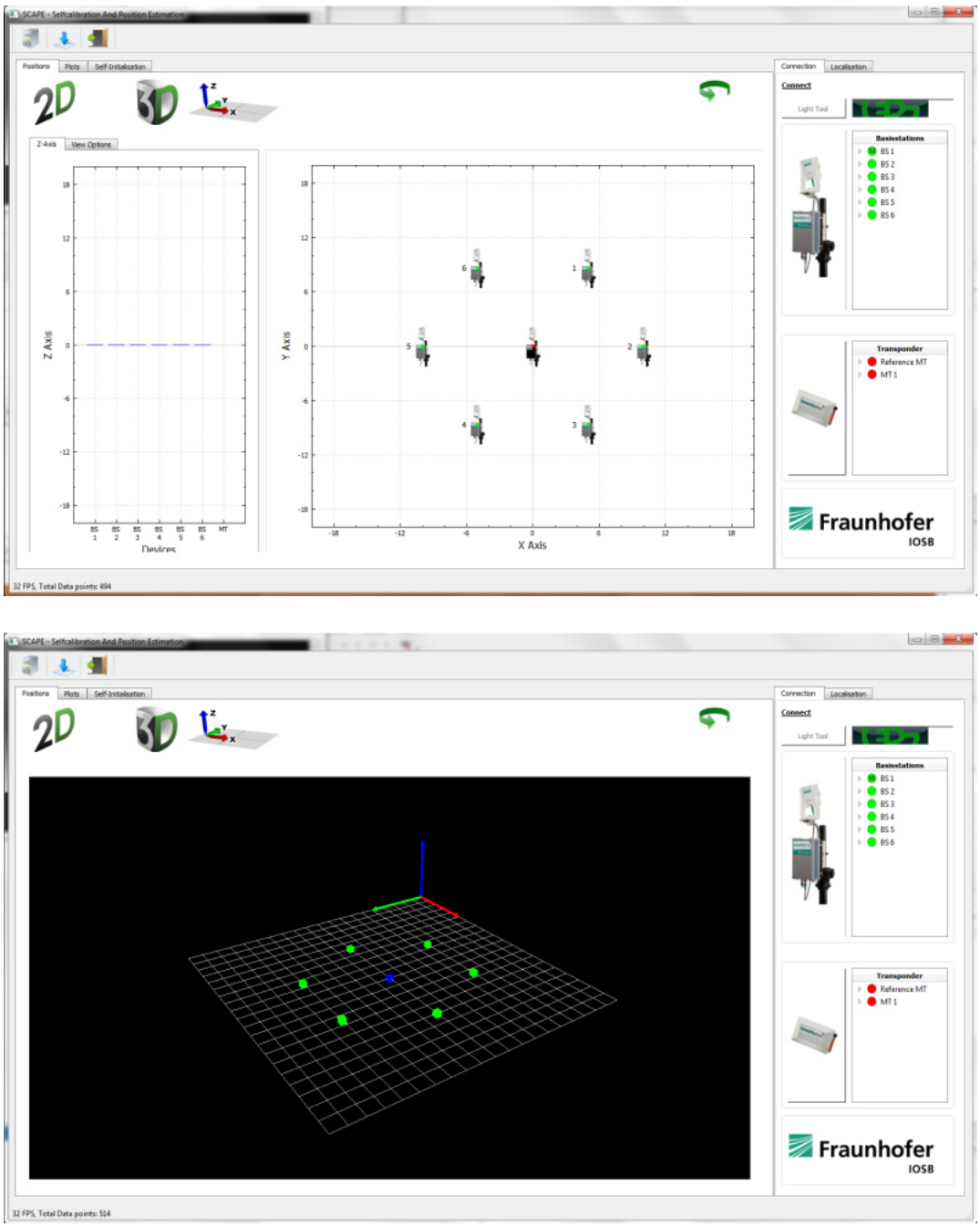

Figure A.2.: Self-calibration and position estimation software (SCAPE)

The pre-filtering of the data requires a transformation to eliminate the offset. More details about the transformation and the closed-form solution which is able to use the filtered data are presented in the papers P-I and P-II. Figure A.3 shows the

transformed measurements and the filtered measurements. The top plot represents the real time filtering of the distance measurements without the offset and the bottom plot the history of the data, necessary for the self-calibration. The table at the bottom of the window shows the signal power, update rate, telemetry and the shift between data vectors with respect to the master station. The last information is provided by the synchronization algorithm.

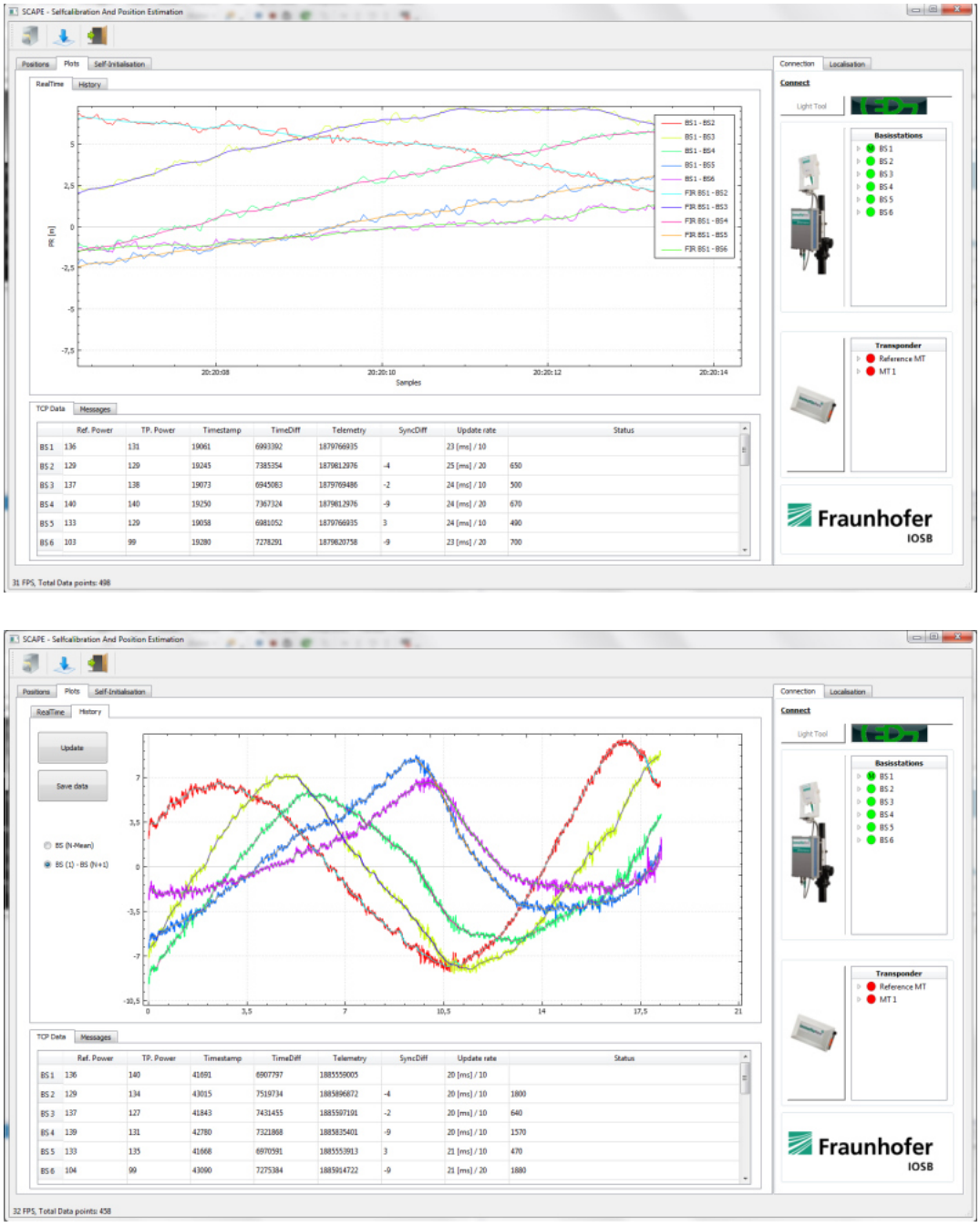

Figure A.3.: SCAPE real time data filtering

The measurements saved in the history, can be used for the self-calibration as it can be seen in the top plot of figure A.4. The algorithm is selecting a random set of measurements (red dots) and provides a self-calibration. The bottom plot shows the result for one dimension after the coordinate transformation into a reference coordinate system. The green line represent the residuals after the optimization, in some cases the residuals are low but the output differs from the mean of all results. This problem is most likely due to the convergence to a local minimum. All the different results can be fused together by using the mean value, median, RANSAC or Bayes.

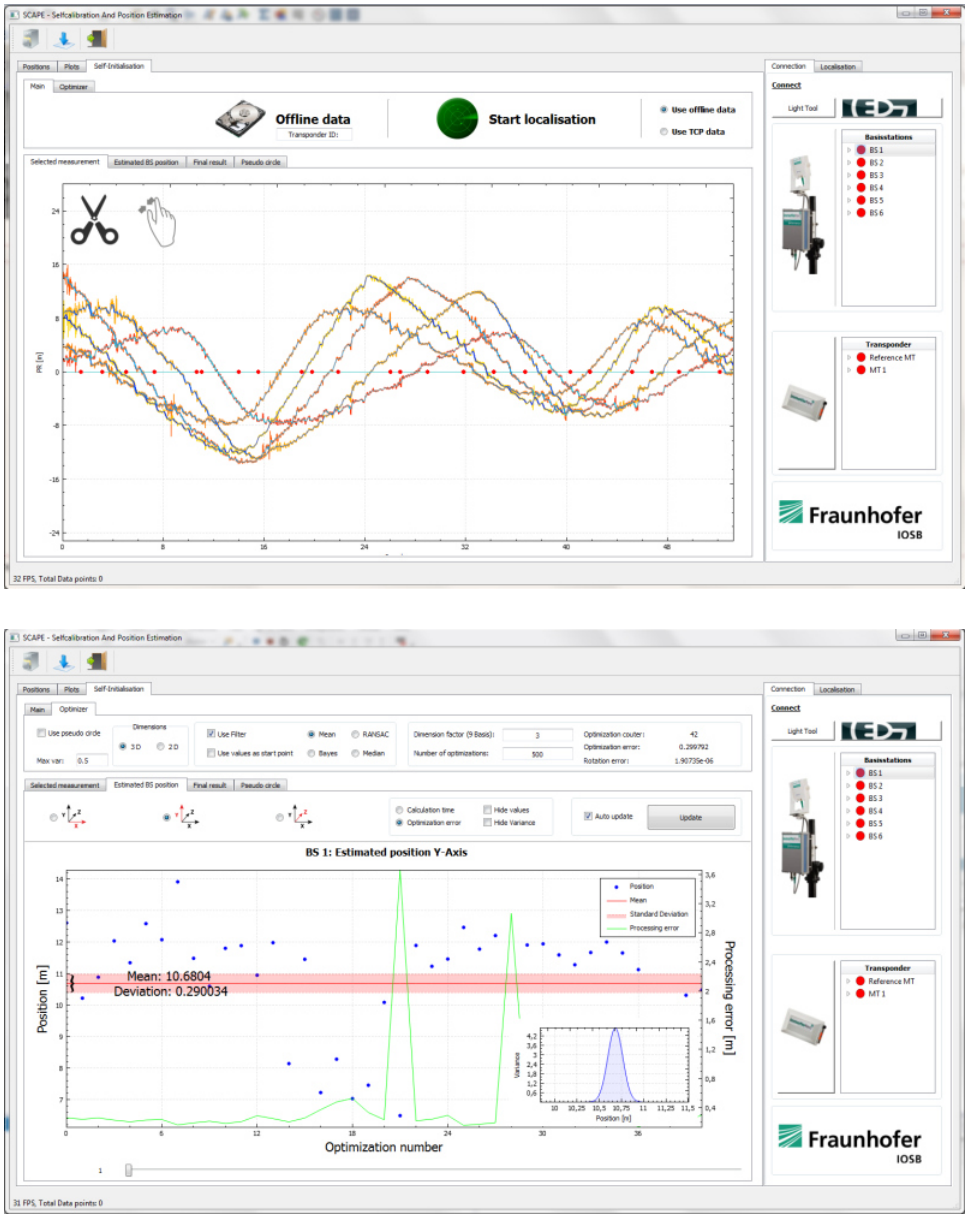

Figure A.4.: SCAPE self-calibration

A.2. GUI of the Decawave UWB

The developed Graphical User Interface for the Decawave UWB software is presented in Figure A.5.

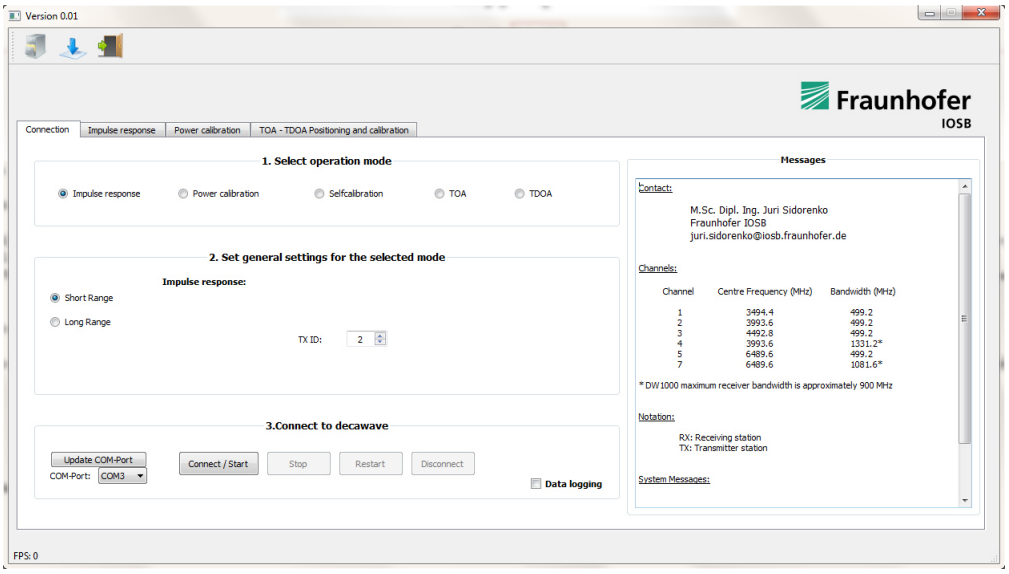

Figure A.5.: UWB GUI: Main window

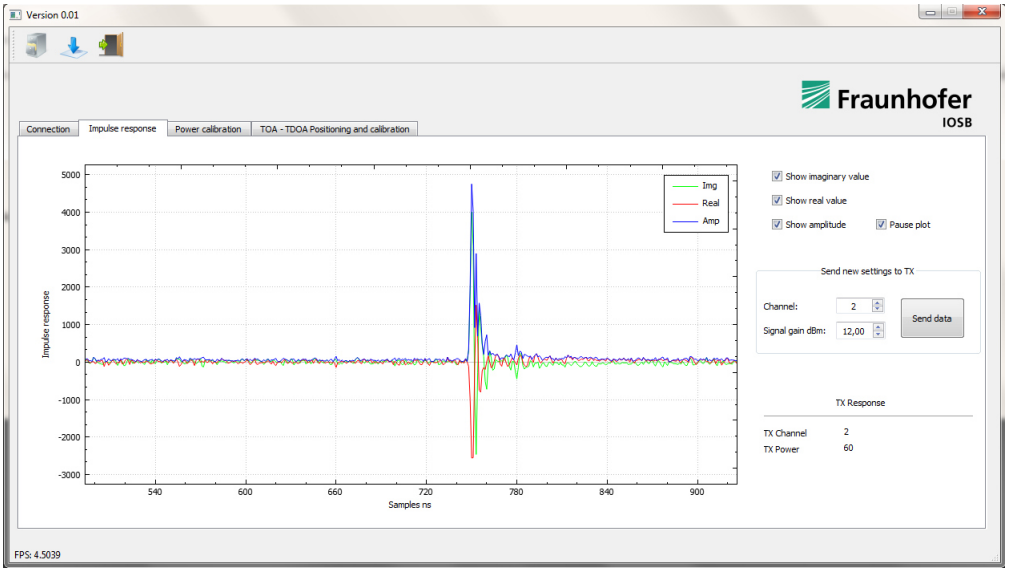

Figure A.6.: UWB GUI: Impulse response

The first selectable operation mode is the impulse response presented in Figure A.6. The first peak with an amplitude higher than a certain threshold corresponds to

the measured timestamp. This assumption is correct if the signal is received under line-of-sight conditions. Other peaks are caused by reflections from the environment. The developed GUI offers the selection of different channels and signal strengths.

In P-III a method is presented to obtain the signal power dependency. The GUI allows to perform this self-calibration for different channels for specific stations (TX and RX), even if the RX station is not the master station. In this case, the data of every measurement is sent to the master station and after a short delay to the ground station. The top plot of Figure A.7 shows the options for this operation. Next to the channel settings it is possible to set the number of iterations and restarts. Every point in the bottom of Figure A.7 is based on the mean of a certain amount of measurements (in this example 20). With increasing number of measurements the curve is getting smoother. To reduce the possibility to obtain outliers, caused by external sources, restarts are used. In P-III it is shown that the curves are deterministic, therefore it is possible to restart the calibration and obtain the median between the different curves.

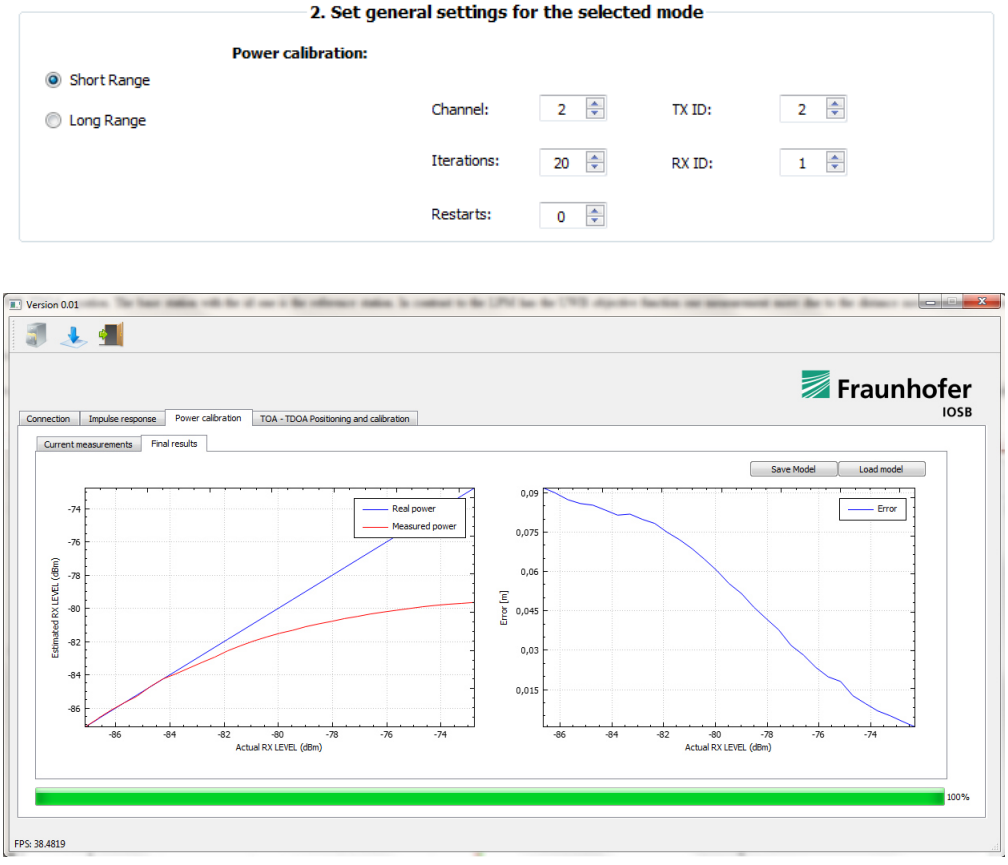

Figure A.7.: UWB GUI: Power calibration

The results of the self-calibration using TOA and TDOA positioning are illustrated in the same window. The top plot of Figure A.8 shows the options for these three

operation modes.

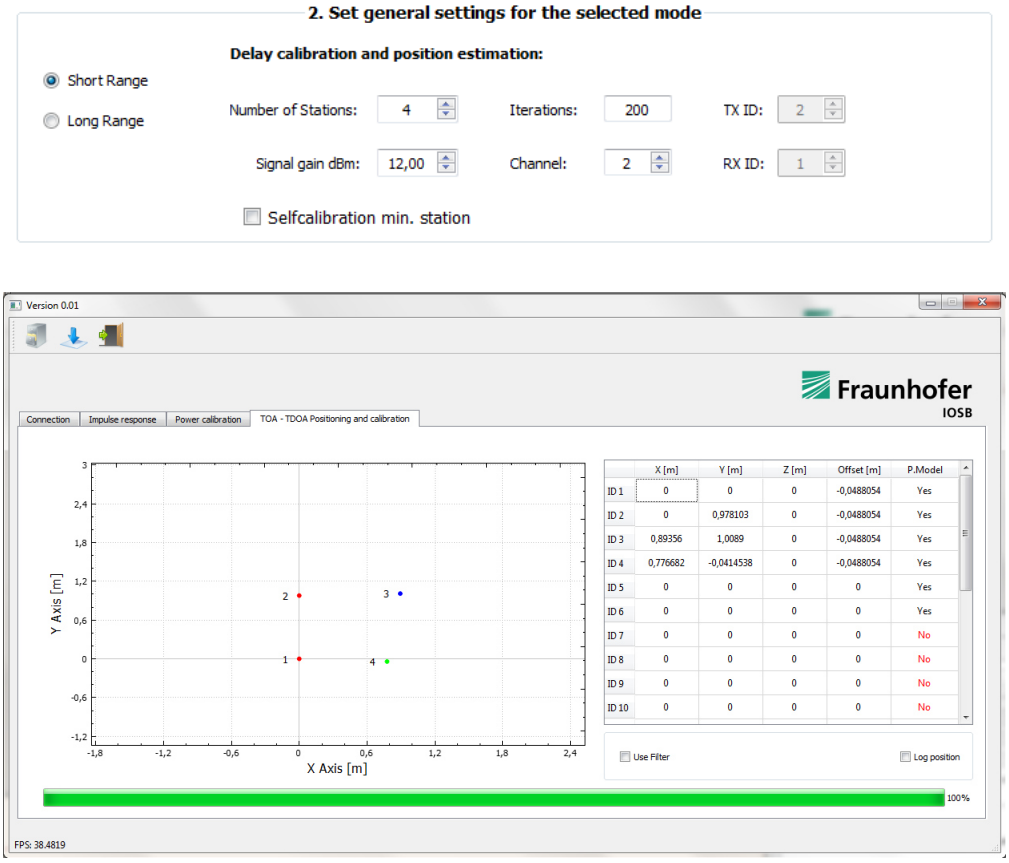

Figure A.8.: UWB GUI: TOA and TDOA

The self-calibration of the base stations and the offset is obtained by TOA measurements between every station. Therefore is it not possible to select the TX or RX station. The check box 'Selfcalibration min.station' allows to change the position of one station, to perform a self-calibration with one moving transponder. The bottom plot of Figure A.8 shows the obtained coordinates of every station with its identification number. Equivalent to the power calibration the number of iterations define how many measurement are used to compute the mean result (in this example 200). The colors of the dots stands for the role of the stations. Red dots indicate the passive nodes, green the reference station and blue the tag. Operation modes for TOA position estimation requires to set the identification number of the tag station (TX). It is not possible to specify the reference station (RX) for this operation mode, because every position estimation with TWR requires the distance measurement between every station with respect to the tag. Thus, every station except the tag has to take the role of the reference station once. The changing of the station role requires time and with more tags this time is increasing. The developed TDOA measurement technique presented in P-V is much faster due to the fact that it does

not require to change the role of the station. Only the reference station and the tag station need to be chosen. The other stations are taking automatically the role of the passive node. The label 'P. Model' located in the right column of the bottom Figure A.8, gives information about the availability of the power correction curve for the ID.

Bibliography

[1] Don Douglass. GPS instant navigation : A practical guide from basics to advanced techniques by kevin monahan. *Fine Edge Productions, Reanne Hemingway Douglass*, 1998.

[2] RB Thompson. Global positioning system: the mathematics of GPS receivers. *Mathematics magazine, pages 260-269*, 1998.

[3] T. K. Kumar and P. K. Kumar. UWB impulse radar for three dimensional through-the-wall radar imaging. In *2011 IEEE International Conference on Microwaves, Communications, Antennas and Electronic Systems (COMCAS 2011)*, pages 1–5, Nov 2011.

[4] J. F. M. Gerrits, J. R. Farserotu, and J. R. Long. Multipath behavior of FM-UWB signals. In *2007 IEEE International Conference on Ultra-Wideband*, pages 162–167, Sept 2007.

[5] R. A. Saeed, S. Khatun, B. M. Ali, and M. A. Khazani. Ultra-wideband (UWB) geolocation in NLOS multipath fading environments. In *2005 13th IEEE International Conference on Networks Jointly held with the 2005 IEEE 7th Malaysia International Conf on Communic*, volume 2, page 6, Nov 2005.

[6] I. Dotlic, A. Connell, H. Ma, J. Clancy, and M. McLaughlin. Angle of arrival estimation using decawave DW1000 integrated circuits. In *2017 14th Workshop on Positioning, Navigation and Communications (WPNC)*, pages 1–6, Oct 2017.

[7] Xiaolong Shen, Shengqi Yang, Jian He, and Zhangqin Huang. Improved localization algorithm based on RSSI in low power bluetooth network. In *2016 2nd International Conference on Cloud Computing and Internet of Things (CCIOT)*, pages 134–137, Oct 2016.

[8] J. Y. Zhu, J. Xu, A. X. Zheng, J. He, C. Wu, and V. O. K. Li. WIFI fingerprinting indoor localization system based on spatio-temporal (s-t) metrics. In *2014 International Conference on Indoor Positioning and Indoor Navigation (IPIN)*, pages 611–614, Oct 2014.

[9] B. Barua, N. Kandil, and N. Hakem. On performance study of TWR UWB ranging in underground mine. In *2018 Sixth International Conference on Digital Information, Networking, and Wireless Communications (DINWC)*, pages 28–31, April 2018.

[10] A. Resch, R. Pfeil, M. Wegener, and A. Stelzer. Review of the LPM local positioning measurement system. In *2012 International Conference on Localization and GNSS*, pages 1–5, June 2012.

[11] Xinxin Pei, Zhigang Huang, Yanbo Zhu, and Wei Liu. Research on the relationship between DOP and the number of stations for multilateration system. In *Information Theory and Information Security (ICITIS), 2010 IEEE International Conference on*, pages 786–789, Dec 2010.

[12] K. Batstone, M. Oskarsson, and K. Astrom. Robust time-of-arrival self calibration with missing data and outliers. In *2016 24th European Signal Processing Conference (EUSIPCO)*, pages 2370–2374, Aug 2016.

[13] S. T. Birchfield and A. Subramanya. Microphone array position calibration by basis-point classical multidimensional scaling. *IEEE Transactions on Speech and Audio Processing*, 13(5):1025–1034, Sept 2005.

[14] V. C. Raykar, I. V. Kozintsev, and R. Lienhart. Position calibration of microphones and loudspeakers in distributed computing platforms. *IEEE Transactions on Speech and Audio Processing*, 13(1):70–83, Jan 2005.

[15] J. Prieto, A. Bahillo, S. Mazuelas, P. Fernandez, R. M. Lorenzo, and E. J. Abril. Self-calibration of TOA/distance relationship for wireless localization in harsh environments. In *2012 IEEE International Conference on Communications (ICC)*, pages 571–575, June 2012.

[16] N. Ono, H. Kohno, N. Ito, and S. Sagayama. Blind alignment of asynchronously recorded signals for distributed microphone array. In *2009 IEEE Workshop on Applications of Signal Processing to Audio and Acoustics*, pages 161–164, Oct 2009.

[17] A. Resch, R. Pfeil, M. Wegener, and A. Stelzer. Review of the LPM local positioning measurement system. In *Localization and GNSS (ICL-GNSS), 2012 International Conference on*, pages 1–5, June 2012.

[18] K. Pourvoyeur, A. Stelzer, Alexander Fischer, and G. Gassenbauer. Adaptation of a 3-D local position measurement system for 1-D applications. In *Radar Conference, 2005. EURAD 2005. European*, pages 343–346, Oct 2005.

[19] R. Pfeil et al. Distributed fault detection for precise and robust local positioning. In *In Proceedings of the 13th IAIN World Congress and Exhibition*, 2009.

[20] K. Pourvoyeur, A. Stelzer, T. Gahleitner, S. Schuster, and G. Gassenbauer. Effects of motion models and sensor data on the accuracy of the LPM positioning system. In *Information Fusion, 2006 9th International Conference on*, pages 1–7, July 2006.

[21] K. Pourvoyeur, A. Stelzer, and G. Gassenbauer. Position estimation techniques for the local position measurement system LPM. In *Microwave Conference, 2006. APMC 2006. Asia-Pacific*, pages 1509–1514, Dec 2006.

[22] M. Haluza and J. Vesely. Analysis of signals from the decawave TREK1000 wideband positioning system using AKRS system. In *2017 International Conference on Military Technologies (ICMT)*, pages 424–429, May 2017.

[23] J. Wendeberg, F. Hï¿œflinger, C. Schindelhauer, and L. Reindl. Anchor-free TDOA self-localization. In *2011 International Conference on Indoor Positioning and Indoor Navigation*, pages 1–10, Sep. 2011.

[24] Johannes Wendeberg, Fabian Hï¿œflinger, Christian Schindelhauer, and Leonhard Reindl. Calibration-free TDOA self-localisation. *Journal of Location Based Services*, 7(2):121–144, 2013.

[25] G. C. Calafiore, L. Carlone, and M. Wei. A distributed gauss-newton approach for range-based localization of multi agent formations. In *2010 IEEE International Symposium on Computer-Aided Control System Design*, pages 1152–1157, Sep. 2010.

[26] Z. W. Mekonnen and A. Wittneben. Self-calibration method for TOA based localization systems with generic synchronization requirement. In *2015 IEEE International Conference on Communications (ICC)*, pages 4618–4623, June 2015.

[27] R. Biswas and S. Thrun. A passive approach to sensor network localization. In *In Proceedings of the International Conference on Intelligent Robots and Systems (IROS)*, 2004.

[28] Yubin Kuang, Erik Ask, Simon Burgess, and Kalle Åström. Understanding TOA and TDOA network calibration using far field approximation as initial estimate. In *International Conference on Pattern Recognition Applications and Methods*, 2012.

[29] M. Crocco, A. Del Bue, and V. Murino. A bilinear approach to the position self-calibration of multiple sensors. *IEEE Transactions on Signal Processing*, 60(2):660–673, Feb 2012.

[30] M. Crocco, A. Del Bue, M. Bustreo, and V. Murino. A closed form solution to the microphone position self-calibration problem. In *2012 IEEE International Conference on Acoustics, Speech and Signal Processing (ICASSP)*, pages 2597–2600, March 2012.

[31] Pratik Biswas, Tzu-Chen Lian, Ta-Chung Wang, and Yinyu Ye. Semidefinite programming based algorithms for sensor network localization. *ACM Trans. Sen. Netw.*, 2(2):188–220, May 2006.

[32] F. Jiang, Y. Kuang, and 3. K. Astrom. Time delay estimation for TDOA self-calibration using truncated nuclear norm regularization. In *2013 IEEE International Conference on Acoustics, Speech and Signal Processing*, pages 3885–3889, May 2013.

[33] Y. Kuang and K. Astrom. Stratified sensor network self-calibration from TDOA measurements. In *21st European Signal Processing Conference (EUSIPCO 2013)*, pages 1–5, Sep. 2013.

[34] Dong-Ho Shin and Tae-Kyung Sung. Comparisons of error characteristics between TOA and TDOA positioning. *Aerospace and Electronic Systems, IEEE Transactions on*, 38(1):307–311, Jan 2002.

[35] Warren S. Torgerson. Multidimensional scaling: I. theory and method. *Psychometrika*, 17(4):401–419, Dec 1952.

[36] Y. Kuang, S. Burgess, A. Torstensson, and K. Astrom. A complete characterization and solution to the microphone position self-calibration problem. In *2013 IEEE International Conference on Acoustics, Speech and Signal Processing*, pages 3875–3879, May 2013.

[37] T. Le and N. Ono. Closed-form and near closed-form solutions for TOA-based joint source and sensor localization. *IEEE Transactions on Signal Processing*, 64(18):4751–4766, Sept 2016.

[38] Y. Kuang, S. Burgess, A. Torstensson, and K. Astrom. A complete characterization and solution to the microphone position self-calibration problem. In *2013 IEEE International Conference on Acoustics, Speech and Signal Processing*, pages 3875–3879, May 2013.

[39] M. Pollefeys and D. Nister. Direct computation of sound and microphone locations from time-difference-of-arrival data. In *2008 IEEE International Conference on Acoustics, Speech and Signal Processing*, pages 2445–2448, March 2008.

[40] Y. Kuang, S. Burgess, A. Torstensson, and K. Astrom. A complete characterization and solution to the microphone position self-calibration problem. In *2013 IEEE International Conference on Acoustics, Speech and Signal Processing*, pages 3875–3879, May 2013.

[41] S. Zhayida, S. Burgess, Y. Kuang, and K. Astrom. Minimal solutions for dual microphone rig self-calibration. In *2014 22nd European Signal Processing Conference (EUSIPCO)*, pages 2260–2264, Sept 2014.

[42] P. Loustaunau W. Adams. An introduction to groebner bases. In *USA:American Math. Society*, 1994.

[43] *D. Grayson, M. Stillman, Macaulay2, [online] Available: http://www.math.uiuc.edu/Macaulay2/.*

[44] Y. Zou, Q. Wan, and H. Liu. Semidefinite programming for tdoa localization with locally synchronized anchor nodes. In *2018 IEEE International Conference on Acoustics, Speech and Signal Processing (ICASSP)*, pages 3524–3528, April 2018.

[45] Egon Balas. Projection, lifting and extended formulation in integer and combinatorial optimization. *Annals of Operations Research*, 140(1):125, 2005.

[46] A. E. Cetin, A. Bozkurt, O. Gunay, Y. H. Habiboglu, K. Kose, I. Onaran, M. Tofighi, and R. A. Sevimli. Projections onto convex sets (POCS) based

optimization by lifting. In *2013 IEEE Global Conference on Signal and Information Processing*, pages 623–623, Dec 2013.

[47] H. Fawzi et al. Equivariant semidefinite lifts of regular polygons. In *DOI: 10.1287/moor.2016.0813*, 2014.

[48] S. Burgess, Y. Kuang, and K. Astrom. TOA sensor network calibration for receiver and transmitter spaces with difference in dimension. In *21st European Signal Processing Conference (EUSIPCO 2013)*, pages 1–5, Sept 2013.

[49] Wozniak B. and Dera J. *Light Absorption in Sea Water*. New York: Springer, 2007.